Final Report

Flying Through Urban Turbulence: A Weather-Rugged Vehicle for Urban Air Mobility

AE3200: Design Synthesis Exercise

Group 5

Delft University of Technology

TU Delft Delft University of Technology

"You may say I'm a dreamer, but I'm not the only one.
I hope someday you'll join us.
And the world will live as one."
John Lennon

Final Report

Flying Through Urban Turbulence: A Weather-Rugged Vehicle for Urban Air Mobility

by

Group 5

on

Tuesday 21st June, 2022

Student Name	Student Number
Korneel Van den Berghe	5022878
Tobias Evers	5060761
Ronald Hagman	4670027
Stijn Koelemaij	5089344
Oleksandr Krochak	5015529
Ole de Koning	4822870
Mitchell Lubout	4652932
Jonatan Valk	5028817
Omkar Vaidya	4865081
Jonathan Robert van Zyl	5039738

Instructors:	Prof. Dr. F. Scarano and Dr. A.K. Doan
Coaches:	V. Poorte and W. Qu
Project Duration:	19/04/2022 - 24/06/2022
Faculty:	Faculty of Aerospace Engineering, TU Delft

Nomenclature

Roman symbols

Table 1: A table of Latin symbols used.

Symbol	Definition	Unit
a	Acceleration	[m/s^2]
a_s	Speed of sound	[m/s], [ft/s]
b	Blades per rotor	[−]
A_b	Rotor blade area	[m^2], [ft^2]
A_{prop}	Rotor disk area	[m^2]
A	Area	[m^2]
B	Boom area	[m^2]
c_b	Main rotor blade chord length	[m]
c_{def}	Deflector chord length	[m]
C_D	Drag coefficient	[−]
C_l	Airfoil lift coefficient	[−]
C_F	Friction drag coefficient	[−]
$C.G.$	centre of gravity	[m]
C_H	specific heat constant	[J/kgK]
C_L	Lift coefficient	[−]
C_{m_p}	Pitch coefficient	[−]
C_{m_q}	Roll coefficient	[−]
C_{m_r}	Yaw coefficient	[−]
C_p	Center of pressure	[−]
C_T	Thrust coefficient	[−]
C_X	Aerodynamic coefficient in the x-axis	[−]
C_Y	Aerodynamic coefficient in the y-axis	[−]
C_Z	Aerodynamic coefficient in the z-axis	[−]
D	Aerodynamic drag	[N]
DoD	Depth of Discharge	[−]
E_{cr}	Energy consumed in cruise	[J]
E_{LD}	Energy consumed in landing	[J]
E_{TO}	Energy consumed in take-off	[J]
f	Fuselage fineness ratio	[−]
F_{control}	Control force	[N]
F_{side}	Side force acting upon vehicle	[N]
g	Gravitational acceleration	[m/s^2]
h_{cr}	Cruise altitude	[m]
H	Angular momentum	[kg $\cdot$ m^{2}2/s]
I	Mass moment of inertia	[kg m^2]
I_{xx}	Area moment of inertia in xx-plane	[m^4]
I_{yy}	Area moment of inertia in yy-plane	[m^4]
I_{zz}	Mass moment of inertia in zz-plane	[kg m^2]
J	Cost function	[−]
m	Mass	[kg]
m	Harmonic number	[−]
m_{gradient}	Gradient	[−]
M_x	Bending Moment in x-direction	[N m]
M_y	Bending Moment in y-direction	[N m]
n_{ult}	Load factor	[−]
N_{prop}	Number of propellers	[−]
p	pressure	[Pa]
$P_{\text{req,TO}}$	Take-off power required	[W]
q	Dynamic pressure	[Pa]
$\bar{q}$	Shear flow	[Pa m]

Table 1: A table of Latin symbols used.

Symbol	Definition	Unit
Q	Torque	[Nm]
r	Radius	[m]
r_{dev}	Position deviation	[m]
R	Range	[km]
R_t	Tip radius of main rotors	[m]
R_{eff}	Effective blade radius	[m]
ROI	rate of interest	[−]
ΔS	Distance between the vehicle and the observer	[m]
S_{def}	Deflector flap surface area	[m^2]
S_{front}	Fuselage frontal projected area	[m^2]
S_{side}	Side area	[m^2]
S_{wing}	Wing area	[m^2]
S_W	Wet area	[m^2]
t	Time	[s]
T	Thrust	[N]
$\mathbb{T}$	Transformation matrix	[−]
t	Thickness	[m]
t_b	Thickness of main rotor blade	[m]
t_{D}	Design thickness	[m]
T_{TO}	Thrust at take-off	[N]
T_z	Torque around z-axis	[Nm]
$Temp$	Temperature	[K]
V	Velocity	[m/s]
V_a	Relative air velocity	[m/s]
V_b	Blade element velocity due to rotation	[m/s], [ft/s]
V_{cr}	Cruise velocity	[m/s]
V_{gust}	Gust velocity	[m/s]
V_{i}	Induced velocity	[m/s]
V_{side}	Side velocity of UAM	[m/s]
V_{TO}	Take-off velocity	[m/s]
V_∞	Free stream velocity	[m/s]
$V_{\infty,x}$	Horizontal component of the free stream velocity in body reference system	[m/s], [ft/s]
$V_{\infty,z}$	Vertical component of the free stream velocity in body reference system	[m/s], [ft/s]
V_x	Shear Force in x-direction	[N]
V_y	Shear Force in y-direction	[N]
x	x position	[m]
y	y position	[m]
z	z position	[m]

Greek symbols

Table 2: A table of Greek symbols used.

Symbol	Definition	Unit
α	Angle of attack	[rad]
α_{local}	Local angle of attack of a blade element	[deg]
α_s	Spherical angle of attack	[°]
β	Side-slip angle	[rad]
β_s	Spherical side-slip angle	[°]
τ	Time constant	[s]
θ	X angle between the trajectory and disturbed reference frame	[rad]
θ_c	Pitch angle of control propeller blades	[deg]
θ_{obs}	Angle between negative z-axis and observer	[rad]

Table 2: A table of Greek symbols used.

Symbol	Definition	Unit
θ_l	Linear blade twist of main rotor blade	[deg]
θ_{local}	Local pitch angle of a blade element	[deg]
θ_t	Tip pitch angle of the main rotor blade	[deg]
$\theta_{\text{risk}}(p)$	Catastrophic risk for path p	[-]
μ	Mean	[-]
μ_{shard}	Shard angle	[rad]
μ_{air}	ISA air kinematic viscosity	[Pa]
ρ	Air density	[kg/m^3]
σ	Standard deviation	[-]
σ_s	Solidity ratio	[−]
$\overline{\sigma}$	X angle between vertiport and trajectory reference fram	[rad]
$\bar{\sigma}$	Stress	[Pa]
$\bar{\sigma}_y$	Yield strength	[Pa]
$\bar{\sigma}_t$	Tensile strength	[Pa]
$\bar{\sigma}_b$	Buckling strength	[Pa]
$\bar{\tau}$	Shear stress	[Pa]
τ	Time delay	[s]
$\overline{\tau}$	Y angle between vertiport and trajectory reference fram	[rad]
ω	Angular velocity	[rad/s]
ω_s	Angular velocity of the propeller's shaft	[rad/s]
ϕ	Y angle between the trajectory and disturbed reference frame	[rad]
ψ	Z angle between the trajectory and disturbed reference frame	[rad]
$\overline{\upsilon}$	Z angle between the trajectory and disturbed reference frame	[rad]

Summary

With an increasing demand for fast and sustainable modes of transportation within cities, new technologies on land and even on water emerge on a regular basis. The urban airspace, however, remains relatively unused, therefore, a growing interest in Urban Air Mobility (UAM) can be seen in cities across the world. One promising technology is an electrical vertical takeoff and landing vehicle (eVTOL). The design presented here, is not just another version of the concepts on the market today. A new vehicle, using cutting edge materials, a high performance electric propulsion system, a highly optimized aerodynamic shape and an innovative autonomous control system is developed in this report. The vehicle is called the Veatle. This new vehicle promises a way of transport that is available and affordable for the public. The UAM vehicle poses a more quiet, sustainable and affordable option than helicopters. The design of such a vehicle not only entails the technical design of the vehicle itself, but also the operational aspects, certification aspects, business aspects and more. The Veatle is different from competitors in various aspects. The design was led by comfort and weather ruggedness considerations. Thanks to how the subsystems were designed, every part from the propeller to the resistor in the central computing system works together in perfect harmony to ensure that the vehicle stays within one meter from the trajectory while ensuring a comfortable experience, even in heavy turbulence.

The design phase consisted of four main parts, namely the aerodynamic design, the control system design, the propulsion and power system design and the structural design. For the aerodynamic design, the vehicle was simulated using the OpenFoam simulation platform. The optimisation of the shape led to a drag area during cruise of roughly 1.1 m^2. The propulsion system consists of eight electric engines powered by lithium-ion battery packs. This allows for zero-emission flight within cities, with a generous nominal range of 20 kilometres and 5 kilometres reserve. The structural design utilises mainly carbon fibre, which has a high specific strength and offers a stiff structure which protects and houses the payload and electronic components during operation. Lastly, the autonomous control system is designed. The control system uses three propellers which can operate in the sideways direction. Since three points allow you to define a plane, a sideways disturbance can be rejected by pure translation. The control propellers are spinning constantly during flight with a zero angle of attack, which allows the propeller to react quickly by rotating the blades around its axis, which it can do in both directions. The design of this propeller is shown in Figure 1. The response of the vehicle to disturbances has a frequency of more than 0.5Hz and a magnitude of less than 0.325 $m\,s^2$ to maximise passenger comfort. All of this together leads to a vehicle which weighs around 900kg and costs less than 500,000 euros.

The vehicle can be operated by private customers or by companies which aim at the airborne taxi sector thanks to its swappable batteries and quick charging opportunities. This allows to keep the downtime at a minimal. An example case is worked out from Heathrow Airport to the centre of London. With only 10 flights a day, a revenue of around 180k euros every year can be expected for every vehicle. Considering the vehicle is designed to have a lifespan of 15 years, a revenue of 2.7 million euros can be expected. However, with proper maintenance, the lifetime can potentially be much longer if the batteries are swapped for new ones every 5 years.

To conclude, the designed vehicle allows for fully autonomous flight within the urban turbulence under windy conditions and safely perform its mission with an accuracy of within one metre. The comfort of the passenger is

Table 3: Specifications of the Veatle

Parameter	Value	Unit
Range	20	km
Payload	250	kg
MTOW	932	kg
Cruise speed	180	km/h
Climb speed	6	m/s
Cruise altitude	450	m
Power (in cruise)	115	kW
Power (in T/O)	385	kW
Costs	478,000	EUR
Outer dimensions	6 x 5 x 2	m^3
Noise emission during cruise	51	dBA
Mission duration	<10	min

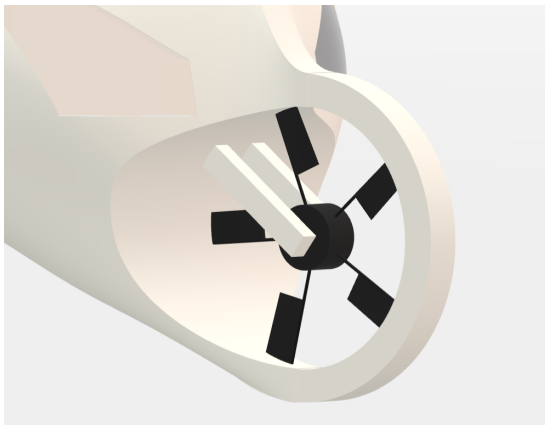

Figure 1: The front control propeller of the Veatle.

guaranteed by reducing the accelerations and altering the frequencies of the responses to disturbances, which is important when flying in the urban environment. Future recommendations to increase the acceptance of these vehicles with the public, more research should be done to analyse the noise footprint more accurately. Next to that, an increase in the number of UAM vehicles in a city would require precise path planning and smart obstacle avoidance algorithms to take over when dangerous situations between two or more vehicles take place. Bird proofing is also a point which could be researched more in the future.

The front view of the Veatle

The side view of the veatle

Contents

1. Introduction

As automobiles crowd the streets and emissions continue to rise, it becomes imperative to develop new sustainable methods of swiftly traversing the urban landscape. Traditional approaches to solving this growing problem have been to build more bicycle paths, or to raise the capacity of existing public transport. However, these options may not be able to keep pace with future demand for urban transportation. Several futuristic solutions have also been proposed, such as the hyperloop concept[1], or the use of high-speed autonomous automobiles. Evidently, a solution to this problem would satisfy the needs of existing key stakeholders, as well as provide bountiful economic opportunities for any firm able to meet this demand. The contribution proposed in this project is Urban Air Mobility (UAM). UAM vehicles are usually small flying vehicles that operate at low altitudes in the urban environment. There are many possible avenues for such a technology, for example in law enforcement, or in emergency medical services (EMS). However, initially, it is expected that these vehicles would be used as a point to point passenger transport service in urban centres. To this end, this project aims to create a design concept for a UAM vehicle, with a focus on passenger transport and comfort. The vehicle will be called the Veatle: the Vertical Electric Air Taxi Looking Excellent.

Based on the previous report**midterm** and summarised **??**, the multi rotor design option was selected. The main aim of this report is to complete the conceptual design for the Veatle UAM vehicle. To do this, the vehicle would need to be analysed in greater detail for each subsystem. First, a basic analysis was completed for each subsystem to identify the relevant design parameters. Next, the relevant input and output parameters from each subgroup were summarized in an N2 diagram. This diagram was used to guide the design process, and improve coordination between the subsystems. From the initial values of the budgets for power and mass, an iterative design process was used to optimize the design. In order to perform iterations efficiently, it is important to create the necessary programs, which are both verified and validated. Finally, after sufficient analysis and weighing design options, a final conceptual design can be presented. In addition to the final design, it is also important to reiterate, or summarize tasks from previous reports, such as the risk analysis, market analysis, and the production plan.

The report is structured in the following order. The executive overview is presented in Chapter 2. Chapter 3 explains the current market and what it is expected to be in the future. The system engineering is described in Chapter 4. Chapter 5 describes the process of the aerodynamic design of the vehicle. Chapter 6 comprises the final propulsion and power design. In Chapter 7 the control system design of the UAM vehicle is reported. The structural design is presented in Chapter 8. Chapter 9 gives an overview of the iterated design parameters and weight breakdown. Chapter 10 presents the verification of the assumptions used, and verification of all design tools used, while Chapter 11 explains how validation was performed. Chapter 12 is a summary of all the operations performed by the UAM vehicle during its lifetime. The manufacturing, assembly and integration plan is presented in Chapter 13. The block diagrams of the instrumentation on the vehicle are shown in Chapter 14. Furthermore, a sustainability analysis is given in Chapter 16, together with an ethics analysis in Chapter 15. A conclusion of the project is written in Chapter 17. In appendix A and B the V&V plan and project Gantt chart are given respectively, preceded by the references

[1] *https://builtin.com/transportation-tech/what-is-hyperloop[Cited 15/06/2022]*

2. Executive Overview

This executive summary creates an overview of the overall contents of this report concisely. Through a set of hypothetical questions posed in Section 2.1, the process of finding a solution is documented, a solution to a gripping problem that most of us deal with on a daily basis. Following that, Section 2.2 contains a description of what autonomous flight is exactly and what considerations must take into account. Section 2.3 explains the concept of urban turbulence, which is the environment in which the aircraft will operate. The proposed solution is presented in Section 2.4, and the chapter ends with the presented business case in Section 2.5.

2.1. Defining the problem

Any entrepreneur would confirm that step one in creating a business is identifying a problem, and making sure that people want this problem solved. The exact problem and the importance of finding a solution are described below.

What exactly is the problem?

With the world's population increasing, an ever-increasing number of people are moving into urban areas. More often than not, the important city centres, where the bulk of the population works, are not designed to facilitate such an influx in movement of people on a daily basis. This can be seen clearly when looking at what the city centre of Paris looks like during rush hours. Parisian's drivers are stuck in traffic an average of 140 hours every year[1] (almost 6 full days), and this problem will only get worse. Cars are stuck in traffic for hours every day, polluting the air and making it difficult to arrive to a destination efficiently. A solution to this problem is the concept of UAM.

What is UAM?

UAM entails exactly the following: short range flights above or around the residential and office buildings of a city. These types of flights do not reach high altitudes or high cruise speeds; since they are solely aimed at transporting people or goods within one urban area. Vehicles capable of performing such flights follow the implicit rule of having vertical take-off and landing capabilities. Vehicles with this trait can take off virtually everywhere, as long as there is enough space to accommodate the vehicle. There is not really a 'typical' UAM vehicle as the characteristics may differ greatly based on the specific mission of the vehicle, but an impression of such vehicle is displayed in Figure 2.1.

Figure 2.1: Possible UAM vehicle

Why is UAM important?

Mainly due to the congestion reasons mentioned before, there is a clear need for advancements in UAM. It is expected that by 2030 UAM will have a market valued at $15.2 billion[2]. The reason for such a big potential is rather straightforward: many people live busy lives, where time is scarce, and travel time should be minimized. Especially the business world, as it is a fast moving world where timing and being on time can mean the difference between a big opportunity being taken or missed. CEOs or representatives often move from city to city to speak at events, attend meetings or arrive at important appointments. When travelling between two business centres of different cities, it often happens that the travel inside the city takes up a significant part of the whole journey, sometimes even more (think of a journey from Paris to London). This time can be very costly, but with current technology there is no sufficient solution to this problem. Also for the public, UAM vehicles could offer a green mode of transport within cities as an alternative to taxis.

[1] *https://www.londonworld.com/news/traffic-and-travel/londons-traffic-ranked-as-the-worst-in-world-paris-new-york-and-moscow-15/06/2022]*

[2] *https://www.urbanairmobilitynews.com/market-analysis/uam-market-will-hit-usd15-2bn-by-2030-research/*[Cited: 12/05/2022]

Why is there need for change?

The alternatives that are currently available do not sufficiently solve the problem faced. Conventional cars or taxis will inevitably run into traffic along important routes, resulting in an uncomfortable journey in loud stop-start traffic, often suffering delays exceeding 30 minutes (depending on the distance). Public transport can sometimes allow swift travel between main travel hubs, such as airports and main train stations, and important city centres or financial districts. Still problems remain: firstly, public transport often is uncomfortable, especially during rush hour. Secondly, also in public transport, unexpected delays are a common occurrence. The only aerial alternative that exists is a helicopter. The problem with helicopters is that they could never be implemented on a large scale for UAM, because of their high levels of pollution and noise. A single helicopter flying by can sometimes already make it impossible to continue a conversation. The generated noise, together with high fuel consumption and emissions, make helicopters an infeasible option.

How can UAM be realised properly?

A solution to the problem must thus adhere to some standards: the form of transport must be fast (faster than cars and trains), flexible (agile), quiet, reliable (safe and punctual), and comfortable. For long-term success of the concept, sustainability must also be taken into account. Even if noise is ignored, helicopters are too polluting to implement at a large scale for UAM, and they cost more since a pilot is needed. The emissions will have negative effects on the air quality of the city, along with other negative effects on the planet as a whole. That is why a viable UAM solution should at least operate emission-free, and possibly be made of recyclable materials that are manufactured sustainably. For any UAM, the noise and safety are especially important since the urban environment houses much more people that can be affected by the noise, and a catastrophic failure is more likely to cause expensive damage or even (fatal) casualties in urban areas. The other standards are mostly to allow for a profitable business model.

2.2. Autonomous flight

One of the challenges and main choices UAM companies run into is if they want to have pilots or will use control systems for autonomous flight.

What is autonomous flight?

Just as there is a demand for self-driving cars, new technology will give a chance for self flying vehicles as well. Of course, normally a pilot is flying an aircraft, drone technology is already ground controlled, and some drones are already flying autonomously using sensors. Autonomous flying could be the new standard for small vehicles such as the UAM vehicles, since this technology is rapidly improving in this day and age.

Why is autonomous flight important?

If all UAM vehicles were piloted, there would be a need for a lot of pilots who all need to do a different typewriting or a whole generation of new pilots, trained to fly VTOLs in urban areas. Additionally, these pilots need to work in shifts and are vulnerable to sickness or might get tired of flying the same route every day. With autonomous flight, no pilots are needed. This means that with a good control and path planning system, the same level of comfort can be reached without having to train pilots. This of course saves large amounts of money, and there will be no wages that need to be paid, which will save even more. With autonomous flight, not only will there be fewer costs, it can also return more revenues. Without a pilot, the vehicle can operate non-stop as long as it does not need maintenance, which means that it can have a lot more flights and thus gain more profit.

What are the risks of autonomous flight?

Of course, just as with self-driving cars, autonomous vehicles are tied to certain risks as well. Since there is no pilot involved in the process, people will be sceptical of the safety of flying. The most common problem people have with autonomous flight is that the vehicle will not have survival instinct in case of an emergency, which a pilot would have. The main risks will be when there are piloted and autonomous vehicles flying in the same airspace. Where autonomous vehicles will be programmed to fly in different parts, piloted vehicles could be unpredictable for the autonomous vehicle and this can create problems.

How can these risks be managed to have safe autonomous flight?

When autonomous flight will get implemented it is very important to have a safe flight, and maybe just as important, give the passengers a comfortable feeling, so they feel safe as well. Things like turbulence and sudden movement will tend to be more frightening when in an autonomous vehicle, where there is no pilot that can be trusted to handle these conditions. The first thing for a safe flight will be that there should be a path planning before take-off. This can be done in communication with the air traffic control of the airspace. This

route will then be claimed, and other vehicles can not be at the same position or same route at the time the first vehicle has planned to be there. Of course this needs some margins where the air traffic controllers have certain rules for. To deal with the increased risk of piloted vehicles and autonomous vehicles on the same path, some air spaces could be claimed for piloted vehicles only and other spaces can be claimed by autonomous vehicles only. This is easier to do with VTOL aircraft since take-off and landing is done vertically and do not have to have the same flight path to a runway. Lastly, it is important that all autonomous vehicles should be equipped with high quality sensors in case of an emergency that will be used to detect other objects in their path.

2.3. Urban turbulence

A big difference with regular flight is that the turbulence in cities is unpredictable and severe. The urban canopy can cause gusts to develop and disturb aircraft.

What is Urban turbulence?

Urban turbulence is best explained as the weather and gusts you encounter while going through the urban environment, such as cities with high buildings. A way to imagine urban turbulence is as follows: It is a quite windy day, and you walk next to a big, tall building. Due to the building, you will not feel any wind. At the moment you are passed the building, You are suddenly exposed to a strong wind.

For vehicles, this gust will create a force, which then will cause a displacement. While flying, especially in the city, this can be very dangerous. When a gust hits a vehicle while flying in between buildings, and it does not respond quick enough, a second gust can take it even further from its trajectory and might even lead to scraping or flying into a building. Of course, this should be avoided at all costs.

Why is designing for urban turbulence important?

As described above, urban turbulence can cause dangerous situations. For VTOL vehicles, the most critical cases will be encountered during the take-off and landing. This is because they are between the most buildings and need the most power from their rotors to make sure they will generate the needed lift. Since changing RPM of the propellers, which normally could be an option to handle gusts, might decrease the lift. This could be dangerous, and a special design will be needed. Either the rotor sizing should take it into account that they will never spin to generate the maximum lift, but this will not be very efficient. This loss in efficiency, however, is compensated by the improved noise levels. To make sure the UAM vehicles will really be able to fly in the urban environment, a design also incorporating urban turbulence should be a main consideration.

2.4. The solution

The problems described above may all need their own technology and solutions, but by implementing all kind of different technologies in the correct way, a vehicle can be designed that overcomes all of these problems.

A weather rugged vehicle for urban air mobility

A vehicle which can solve the problem of urban turbulence while being very safe will on its own be a huge step forward for the UAM sector. For general implementation of UAM vehicles, it is important that it should be a weather-rugged vehicle. This means that the vehicles should be able to operate in almost all kinds of weather conditions.

The Veatle

The Veatle will be designed as an autonomous urban air mobility vehicle which will be focused on flying through urban turbulence. Just like other UAM vehicles, the Veatle will be able to fly a set range depending on some requirements, however the Veatle will be autonomous. This will give all the benefits described in Section 2.2 such as that it will be able to be ready to fly almost 24/7 without having the costs of training and paying a pilot. Next to this, the Veatle will have a main focus on controls for gusts and turbulence in the city. Due to this, the Veatle will be able to stay within one meter of the predefined trajectory with wind speeds up to 8 Beaufort. This makes the Veatle more weather rugged than a general aviation aircraft.

Specifications of the Veatle

The main specifications of the Veatle can be seen in Table 2.1

Table 2.1: Specifications of the Veatle

Parameter	Value	Unit
Range	37	km
Payload	250	kg
MTOW	932	kg
Cruise speed	180	km/h
Climb speed	6	m/s
Cruise altitude	450	m
Power (in cruise)	115	kW
Power (in T/O)	385	kW
Costs	478,000	€
Outer dimensions	6 x 5 x 2	m^3
Noise emission during cruise	51	dBA
Mission duration	<10	min

2.5. The business case

As can be read later in Section 3.1, London is one of the cities which can be an attractive market entry point. Due to the fact that the Veatle is focused on urban turbulence, the final business case will be from London Heathrow airport to the Guy's hospital next to the Shard building. London is also attractive since the UK has shown that they are willing to accept UAM, having built world's first vertiport in Coventry

This will combine the focus on a big city with loads of business traffic as well as the urban turbulence due to the huge Shard building. This case will take a bit more than an hour by taxi, so it is also a great opportunity to safe time to get into the city centre. This business case is also taken since the Shard building is the highest building in western Europe. This will thus be one of the most extreme cases of urban turbulence for flying. When designing for this extreme business case, the vehicle should be able to operate in all the other environments in the other places in London such as the London City Airport to the business district.

3. Market Analysis

This chapter discusses the market analysis. First, the current market is described in Section 3.1. The potential alternatives, possible changes of the market and our main competitors are being described in Section 3.2, Section 3.3 and Section 3.4 After this a Swot analysis is performed in Section 3.5. This is followed by a description of the market share and the market entry in Section 3.6 and Section 3.8. Lastly, the costs and financial plan are presented in Section 3.9 and Section 3.10

3.1. Current market for UAM vehicles

To start the market analysis, first the market sector must be identified. For our UAM vehicles, we would like to focus on operations between the airports and business districts or city centres of cities (ideally those with high traffic). Some key aspects about why this mission profile was chosen is listed below.

- *Flying over areas of high traffic*: this will increase the utility of the "air-taxi", due to shortened travel times. Many cities with a big and important business centre have roads that are incredibly congested. The average speed of inner London traffic, which is not even just central London, is estimated to be as low as 18.5 km/h [1], which is much slower than desired. A 25 km journey from Paris Orly airport to the business district of la Défense already takes 40 minutes in moderate traffic, while a 10 km trip from London City airport to the City of London business district takes the same time. It is evident that UAM vehicles could easily cut this time in half, if not perform even better.
- *Operating from transport hubs*: travel hubs like airports have thousands of passengers move through them each day, and they often require a transfer to reach any final destination; the Veatle aims to become an option for a faster, more comfortable transfer. This UAM vehicle allows the customer to have one simple connecting journey from place to place, while offering better comfort than a car stuck in busy and noisy stop-start traffic. While some cities are developing fast public transport connections from main travel hubs to the best of their abilities, many cities do not have such infrastructure at all. One such city is Los

[1] *https://www.london.gov.uk/questions/2019/19767*

Angeles, which happens to be a city where on average, each driver stands still in traffic for 82 hours each year[2].

- *Flying to business districts*: due to only fitting two passengers and operating from large transport hubs, business-people provide the best market; due to their short term business trips, they are paid expensively per hour and thus quicker travel may save their employers' money. Secondly, focusing on a single market allows for the exclusivity appeal of the brand to grow. More attention can be given to ensure passenger comfort and interaction with the customer. This avoids the issue where components are chosen purely because they are of low cost, even though they are the lesser performing option.
- *Short-distance flights*: as the range of the UAM vehicle is 20 km. However, if demand is as high as expected, an extended range model can be developed to further increase functionality, being able to fly more routes in bigger cities and possibly flying intercity trips.

To model the entry market, five cases are presented below:

1. London City Airport to the City of London business district. The City of London is where the Bank of England is located, together with multiple stock exchanges. It is the undisputed financial centre of the UK, and London is the city with the 5th highest GDP in the world. Although this will be the main route, other important locations such as Southwark and Shoreditch can also be easily and rapidly reached from London City Airport. Getting around London by car is not as fast, as it is known for its highly congested roads, especially in peak hours. The City of London is connected directly via public transport, so in theory this is optimised, but still it takes almost 30 minutes, about 3 times as much as it will take with the Veatle, and it will not be nearly as comfortable because the passenger must travel via chaotic and busy public transport stations.
2. Paris Orly Airport to the business district of La défense. This route is chosen largely for the same reasons as the main case. It is a connection between the airport of a highly congested city to its business district. Paris also follows London directly in the ranking of cities with the highest GDP, which is important since this service will initially be more expensive than other ways of transport. A secondary consideration for the city of Paris can be from Le Bourget airport to la défense. This Airport is much smaller than Orly, however it is the 3rd busiest private flight airport in the world, and its route to La défense is longer than from Orly since it passes right through the centre of Paris. Despite this, the straight line distance between the two points, which is basically the route that would be flown by this aircraft, is smaller than from Orly, allowing the fly time to be 3 times shorter than by car (and public transport takes a full hour).
3. Another route that undoubtedly will spark demand is from JFK Airport to the New York City (NYC) financial district (around Wall Street). This location was chosen since NYC has the 2nd highest GDP in the world, only behind Tokyo: which has almost twice the number of inhabitants. NYC is known to be incredibly hard to get around in the car, and the public transport has a terrible reputation as well when it comes to comfort. Besides this, both by car and public transport, the trip takes more than an hour, which is about 4 times as much as it is expected to take with this UAM vehicle.
4. Although the general idea for the mission is travel between large travel hubs and business centres, another flight route that can be interesting is from Nice airport to the centre of Monaco. Where Le Bourget was the 3rd busiest private flight airport, Nice Airport is 4th, and considering that Monaco does not have its own airport, but plenty of heliports, this is an area where there could be high demand. Despite the route taking around 35 minutes by car, which is not terrible, but in this part of the world practicality and efficiency are not the only important thing. Monaco is a place filled with luxury houses, cars and restaurants, where the harbour is filled with yachts and the streets filled with high-class boutiques. It is a place where people come to enjoy and show off their wealth, and what better way to do just this than taking a private UAM vehicle straight from the airport to the harbour, while flying comfortably and enjoying the coastal views of southern France. Besides this, other expensive tourist destinations such as Nice itself and Cannes are also in the area.
5. Another possible implementation is using it as an ultra nimble air ambulance in an area such as a ski resort. Even though the vehicle is designed for an urban environment, the windy conditions of mountainous areas should not be too much for the aircraft to fly. Due to its excellent controllability, it can reach people who are injured or trapped under snow in the most difficult areas. The limited range of the aircraft would be a bigger constraint, however. This also caters more to the corporate social responsibility climate in the current business world.

(Note that each of these options has been checked to be inside the operating range of the aircraft.)

[2] *https://tripnet.org/wp-content/uploads/2018/08/CA_Los_Angeles_Transportation_by_the_Numbers_TRIP_Report_Aug_2018.pdf [Cited: 10/05/2022]*

Another smaller market would be the tourism market, this will be alike to helicopter tours around cities. The vehicle can be bought by luxury hotels or resorts to offer their customer a comfortable and fast trip from the airport to the hotel/resort. Yet another market could be to sell the vehicle to private users. However, for simplicity of the business, we will focus on transporting business-people from airports to the business centres of the close-by cities.

To better understand the potential of the business, imagine the following possible scenario:

You are a business person and have just taken a flight from Paris to London City Airport. Your company pays you €800 an hour. You chose London City Airport because it is supposed to offer a rapid connection to the financial district, but it is rush hour and the taxi driver estimates that getting from the airport to the City of London financial district would take 40 minutes to an hour. This way, your company already pays €533 plus a taxi fare in expenses. On the other hand, a 10-minute flight with a nice view could take you there potentially cheaper, more comfortably and faster. This way, you waste less time in transit and can get to business quicker, while evading a tiring traffic jam or a hectic and uncomfortable public transport journey. This scenario would be just as critical in cities like Paris and New York City, arguably even more, since their airports are further away from their financial districts.

3.2. Potential alternatives

Aside from the routes which are being planned to have a business for, also the competitive alternatives should be analysed. Looking at daily transport from airports to business districts, a couple of services are immediately seen as rivals for the UAM industry. Public transport and taxis are often used for transferring from one place to another. For crossing rivers, ferries could also be used. For more luxurious transport, more expensive taxis as well as limousines and even helicopters are in the field of transport, which UAM vehicles should be able to compete with.

Public transport

The UAM vehicles will not be able to compete with public transport in terms of price. This is because public transport is always one of the cheapest ways of travelling, since you are sharing the costs with many other people. However, for the target clients this is often not the preferred option. Public transport is lacking in many aspects, however. The level of comfort of public transport is rather low. Passengers must travel through busy and noisy stations, and even the availability of a seat is not guaranteed. Furthermore, if a seat is available, it is often close to a stranger. This is not a comfortable experience for people who are trying to get to work or a meeting. Next to that, public transport often faces delays. Even though operators make a large effort to combat this, delays often happen in public transport. They can vary from only a couple of minutes to half an hour. The Docklands Light Railway (public transport that serves the same route as the proposed business case in London) normally works only around 75% of the time[3], with most issues of course occurring in rush hour times. The passenger is often left in the dark about what is causing the delay and whether it will increase, which creates frustration. The business world is a fast moving world, where arriving at places on time can be of critical importance. This means that people need a fully reliable way of transport, which public transport is not; due to the aforementioned delays and possible closing of certain routes at unexpected times.

Taxis

As said before, another method of urban transport are taxis. Regular and more luxurious taxis are used often, and the most expensive taxis will probably still be cheaper than the UAM vehicles. However, it could be possible to compete with luxurious car taxis in terms of costs. However, it should be taken into account that the unit cost of a UAM is around €478k (explained in Section 3.9), so this would be more in line with expensive automobiles; which are not commonly used as taxis. Therefore, the expectation is that the UAM vehicles for transport will be more expensive. However, this extra cost can be worth the investment since taxis must use public roads to get from A to B, which also makes it an unreliable service. Not in terms of vehicle reliability, but in terms of the traffic that is encountered along the way. A perfectly smooth journey on the roads of cities like London and New York is something that has proven to be practically impossible throughout most of the day. This is not an issue for aerial travel.

Helicopters

Currently, the only existing type of vehicle operating in the UAM segment is the helicopter, but helicopters experience difficulties as well. Firstly, they produce a large amount of noise, which is not only uncomfortable for citizens, but also for the passengers inside the aircraft. They also produce vibrations which are often felt throughout the cockpit. If the UAM market experiences the expected growth, the sky will be a layer of continuous loud and irregular noise if no better alternative than a helicopter is made. The noise that many

[3] *https://tubestatus.net/line/dlr [Cited: 11/05/2022]*

helicopters produce while taking off or flying by would create an unsustainable living environment. Additionally, helicopters are inefficient machines that require large amounts of fuel to operate. Worse yet, the burning of all of this fuel causes severe pollution which can affect the air quality and is in general not sustainable either. The UAM design proposed will not nearly be as noisy due to the smaller propellers and will not generate any emissions, without losing any functionality compared to helicopters. This makes it a viable UAM option, even if there will be a very large number of them flying around.

3.3. Predicting changes to the market

This section contains a prediction of the future market. A couple of the main UAM competitors will quickly be mentioned, since there are more companies working on UAM vehicles, which may enter the market in the future.

The UAM market is part of the general people transport market, which is a market that has been growing steadily throughout modern times. This is because of the rapid globalisation that the world has seen in recent generations. Furthermore, the world's population keeps growing, in particular population in urban areas, as increasing urbanization is a trend that has been seen for more than half a century. This means that the future need for urban mobility is expected to increase in multiple ways.

The first change in the future market will be the introduction of robot taxis or driverless cars. This implies that the driver cost aspect that the competitors deal with will vanish and even more competitive prices could be offered. For this reason, the designers of UAM vehicles should try to keep improving on costs as well. The plan is to enlarge the operation from an airport shuttle or an air metro (fixed routes), to an air taxi service. Another possibility is to enlarge the range to be able to travel on intercity routes and build an intercity network of UAM vehicles.

Furthermore, when UAM vehicles are proven to be safe on their own and later in traffic as well, another expected change is the adjustment of existing laws and restrictions. For now the number of aircraft allowed over a certain area is rather limited and to realistically make urban air mobility available for everyone, there should be leniency in the rules to have more aircraft flying in one airspace, as long as there are proper regulations on assigning airspace. The current rules have been made long before concepts such as the proposed design, so it is expected that the rules could be adjusted or special rules for UAM vehicles (excluding helicopters) could be written to enable those vehicles to function. It is expected that regulatory organisations will cooperate when the safety is proven. The reason for cooperation will be because UAM vehicles such as the Veatle are a more sustainable form of transport, considering a push towards renewable energy than (gas powered) cars and helicopters, and they are less noisy. This change would be beneficial since it would allow more operations, but it will likely also increase the competition.

3.4. Competitor analysis

The main competitors for the future are other UAM designers. There are already multiple eVTOL designers who all try to be the first to get their product on the market. It can already be seen that the vehicles in development differ largely from each other. Some do not have wings, some have tilting engines or wings, some have their propellers on top of their wings. In short, it seems like the designs are very mission specific, meaning that they will work the best only for a certain niche. This decreases the strength of the competition, since each design is best for its own purpose. It is not expected that a new competitor will enter this market segment with a finished product in the near future, since all current efforts have proven that the design and certification of these types of aircraft is really a long term project, taking at least 10 years. The strongest competitors that match the mission objective are Volocopter, Wisk, Airbus and Ehang. These are seen as the strongest competitors because they have manufactured vehicles already and have proven that they are functional. A quick overview of each competitor's strengths and weaknesses can be found in Table 3.1.

Table 3.1: Strengths and weaknesses of competitors

Competitor	Strong point(s)	Weakness(es)	Expected market entry
Airbus (CityAirbus)	High payload	Very loud Heavy Low range	2025
Volocopter (Volocity)	Quiet Far in development Safe Quick battery swap	Large structure	2024
Ehang (216)	Far in development Redundancy of systems Cheap	Short range	2023
Wisk (Cora)	Efficient in cruise Safety features Many demonstrated flight hours	Very heavy Inefficient take-off	2024

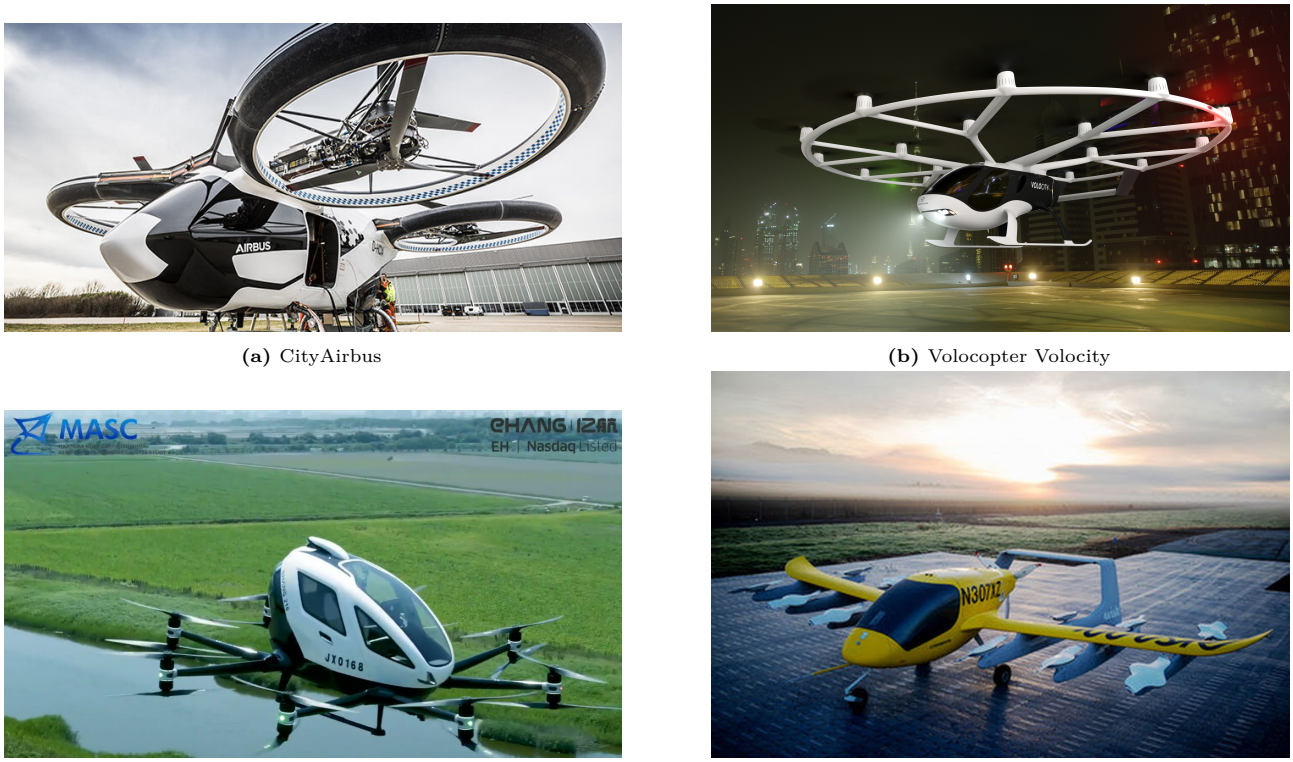

(a) CityAirbus

(b) Volocopter Volocity

(c) Ehang 216

(d) Wisk Cora

Figure 3.1: Main competitors at the UAM industry

The CityAirbus had flight time, but it had too many weak points to be successful, which is why Airbus even stopped development on the model. However, they learned from their flaws and are designing a second generation model. This model is not far in development, so it cannot be considered. On the other hand, the Cora is a strong competitor, but it is a winged aircraft, which means that it is more likely to be deployed for longer range applications. Besides this, the wing makes it heavier and takes up more space. The Ehang is a serious competitor in theory, but it is likely that its range is not sufficient. Ehang itself claims a range of 35 km, but the longest range it has ever flown is only 8.8 km[4]; which would make it rather impractical. However, they are of course still improving as well and are a team to take into account into the future. The main serious competitor is the Volocity from Volocopter. The company has almost identical ideas for usage, and the aircraft performance numbers closely resemble the high level requirements. It also has a claimed range of 35 km, but this has not been proven yet. However, the company is already close to getting the aircraft certified for flight, and the aircraft also absolutely excels in noise emissions, as the noise it generates is even lower than normal

[4] *https://evtol.news/ehang-216/ [Cited: 10/05/2022]*

street noise of busy cities[5].

3.5. Performing a SWOT analysis

In this section, a first breakdown of the strengths, weaknesses, opportunities and threats of the UAM vehicle with regard to the business perspective is given in the so-called SWOT (Strength, Weaknesses, Opportunities and Threats) analysis, which can be seen in Table 3.2.

Table 3.2: The SWOT analysis

Strengths	**Weaknesses**
Faster transport than current city vehicles. No extra delays due to traffic jams. More direct transport. More quiet and comfortable than helicopters. Relatively low unit costs compared to helicopters. No emissions. Accurate controllability.	Higher operating cost than cars, metros and trams. Very limited capacity per transport. Higher maintenance costs. More air traffic control is needed. Failure is more likely to be catastrophic for both passengers inside and people or buildings on the ground below the vehicles. People will be scared for autonomous flight, just as with self-driving cars. Vertiports might be needed in a lot of places, which will take valuable place in the city centres.
Opportunities	**Threats**
The UAM will be more quiet and environmentally friendly than it's only air traffic competitor, the helicopter. Possible future use cases such as cargo delivery or emergency services. Improvement in battery technology could enable much longer range flights to be possible and will make the flights a lot cheaper.	Alternative cheaper air taxi options Civilians might have a negative opinion of the UAM vehicles since the sky would be crowded in urban areas, or jobs of luxurious taxi drivers or helicopter pilots might disappear since UAM can have autonomous flight. Other transport's low prices can be hard to compete with due to the high unit costs of the vehicles. Privacy concerns for UAM vehicles flying over houses, just as with filming drones.

3.6. Market share

With a million dollar design project like this, it is important to have an idea of the market share and the possible revenues which are achievable. Following studies on UAM by Hader et al. **Roland_Berger**, around 160,000 UAM passenger transport vehicles will be used in 2050. They expect that a total revenue of around 90 billion dollars will be generated on a yearly basis, where half of the revenues will come from the airport taxis. A simple calculation gives that on average, a single UAM vehicle will generate around 560,000$ a year. Their estimation is that a single UAM will fly around 117,000 km a year, which is higher than the annual mileage of a car taxi right now with 90,000 km a year. This can be achieved because no pilot is involved; it can operate almost 24/7 and traffic jams will not delay the transport process. The estimated revenue of an air taxi will thus be around 5$ per km. This should be taken into account when designing for the market price and operational cost.

3.7. Other markets for UAM

Next to passenger transport, there are a lot of possibilities for UAM vehicles to expand to other markets as well. Of course, not only passenger transport has problems in the city, also regular package transport might be a lot more efficient due to UAM transport. Transportation companies do not have to get the packages from the airport to their storage where the couriers need to pick up the packages and deliver them to the person in the middle of a city, while waiting in traffic jams for a long time. Instead, the UAM vehicles can just take the packages straight from the airport and deliver them, especially for the air taxis that will be able to land in any specific place on parking spots, this will be a great market to conquer.

[5] *file:///C:/Users/stijn/Downloads/20210324_Volocopter_WhitePaper_Roadmap_to_scalable_UAM_m-1.pdf [Cited: 10/05/2022]*

The next market where UAM vehicles can take a share in is the emergency help sector. At this moment, the police and ambulances are using helicopters to search for people or get to a busy place in a short time when they really need to hurry. UAM vehicles can be an option to reduce the use of helicopters in this section, especially for ambulances, since it is more comfortable to be in a UAM vehicle than in a helicopter. Also, for firefighters, UAM vehicles can be used to get people out of tall burning buildings. Maybe with some more focus, the autonomous vehicles can even be used to fight the fire at most critical points instead of trying to extinguish it from the ground or even go inside the burning building.

Tourists often pay a lot of money for helicopter tours over tourist attractions such as the Grand Canyon. With UAM vehicles, a more comfortable, more sustainable and less noisy experience for less money can be offered. This will be one of the main markets UAM vehicles can gain a lot of ground on helicopters since many people want to try these entertaining flights, but with a helicopter it is often just too expensive.

The last markets which UAM vehicle can be used for are other markets in which the helicopter operates in right now. Such as going to oil platforms or the top of windmills.

3.8. Market entry

At the moment, there are many companies working on UAM vehicle designs, trying to be one of the early birds in the market. This makes sense, of course, since the company that enters the market first will have virtually no competition and the technology will still be new and interesting, as opposed to just being practical. For this design project, the same holds: it is desired to enter the market as early as possible. However, development time should not be cut down just to enter the market early for a number of reasons, the first one being that obviously a better, safer design is more important than an earlier market entry. Secondly, the technology behind some important subsystems of the aircraft, like the batteries, is still improving steadily, so waiting a bit longer may result in better performance. Finally, most competitors are also still far from ready to start flying. Only Joby, who started development in 2009, is planning to enter commercial service as early as late 2023. Archer Aviation hopes to enter the market late 2024 along with Lilium, while Airbus and EVE are not planning to enter before 2025. Main competitor Volocopter also aims to put their vehicles into service in 2024, but with new concepts like these, delays often happen. Volocopter has already made many advancements and is far into the certification process, so entering the market at the same time as them would be too ambitious. A good goal to aim for is to enter the market in late 2028. Research done by KPMG suggests that steady, almost linear growth of the market will continue after 2028 **marketprediction**. After 2030 it is even expected to start growing exponentially, so entering late 2028 is not considered too late.

As with any new concept, the start will be slow in terms of production numbers. Especially since this concept will serve a more luxurious market segment, even compared to other air taxis, it is not necessary to directly produce in large numbers, as this takes away the premium appeal. EVE plans to produce 75 units in its first year of production in 2026, while Lilium and Volocopter are planning only 10-20. Ehang has reported a pre-order of 100 vehicles by Prestige Aviation, but Ehang is not focused on luxury and comfort as much. This concept will be produced in numbers similar to the Volocopter. The idea is to, just as Ehang does, sell the product to transportation services as Uber or other interested companies. It could also become available for private use in later developments, but then free planning of routes and vertiports will not be ready at market entry. The initial plan is to start with 15 units, all deployed in London. The next year, 30 units, some additional ones for London, but mostly for another city will be put in operation. Since KPMG concluded that the US are more ready for air taxis, the second city to get the vehicles will be New York City. Singapore is also an attractive option, but this is the main market for Volocopter, so other cities are preferred since there will be less direct competition. After this, more expansion is possible. It is not expected that more than 30 units are necessary per city. Throughout Europe, Australia, the US and Asia around 25 cities seem to have a potentially large demand, making the total estimated production series 750 units, ideally over a time period of 5 years. Which cities will receive service depends mostly on regulations and competition, but the main planned cities besides the ones already named are: Paris, Milan, Los Angeles, Hong Kong, Moscow, Toronto, Melbourne, Seoul, Sydney, Tokyo, Tel Aviv, Kiev, Osaka, Dubai and Nice, in no particular order.

3.9. Costs

The main cost component considered is the unit cost of one vehicle. In the calculations, the unit cost is split up in the following components: engineering costs, battery, motors, power management system, propellers, materials, tooling, manufacturing, development support, flight testing, quality control, avionics, retracting system landing gear and a product liability. According to the high level requirements, the unit cost must be below €500k. A parametric cost estimation is used, which includes formulas for all the cost components. An example for the

engineering costs is given in Equation 3.1 [6]. In this formula, W_{struct} is the weight of the empty structure, V_{cr} is the cruise speed, N_{ps} is the amount of vehicles made in the product series, CPI is the consumer price index and exrate is the exchange rate between euros and dollars.

$$C_{\text{eng}} = 0.083 \cdot W_{\text{struct}}^{0.791} \cdot (V_{\text{cr}} \cdot 1.96)^{1.521} \cdot N_{\text{ps}}^{0.183} \cdot 1.6 \cdot 1.66 \cdot 92 \cdot CPI \cdot \text{exrate} \tag{3.1}$$

Using multiple parametric formulas, the costs for the components are calculated, which are listed in Table 3.3. The unit cost of a vehicle is estimated to be approximately 475k €. This is compliant with the cost requirement.

Table 3.3: Cost breakdown

Component	**Cost [€]**
Per production series	
Engineering	20 000 000
Development support	500 000
Flight testing	200 000
Per vehicle	
Motors	70 000
Power system	62 500
Propellers	120 000
Materials	13 250
Tooling	12 500
Manufacturing	92 500
Quality control	350
Avionics	13 500
Product liability	75 000

3.10. Financial plan

To make sure the design of an eVTOL is actually a good investment, a financial plan is constructed. In this plan, the costs and revenues will be made clear and an expected Return On Investment (ROI) will be calculated. The costs calculated in Section 3.9 are used for this financial plan.

As explained in Section 3.6, literature estimates the revenues per vehicle to be around $560k per year. However, the range needs to adjusted for this. Assuming 10 flights of 15 km per day for 350 days a year (maintenance included), a total range of 37,500 km will be flown. Scaling this yields a revenue of $180k. The estimated energy consumption per flight is approximately 15.5 kWh. The average price of energy in 2021 Europe is $0.213 per kWh. Thus, the energy cost per year is $350 \cdot 10 \cdot 15.5 \cdot 0.213 = \$11,555$. Maintenance is estimated at an average of $100 per operating day. The profit then becomes around $133k. An important advantage over helicopters is that pilot costs are not included, as the vehicle is autonomous.

The ROI will be calculated over the 15 years as if only 15 vehicles will be flying in this period of time. The total ROI will then be $133000 \cdot 15 \cdot 15 - (478000 \cdot 15) = 22755000$ \$. So the total profit would be around 20 million dollars in 15 years. The actual ROI will then be $\frac{22{,}755{,}000}{478{,}000 \cdot 15} \cdot 100\% = 318\%$.

[6] *Engineeringhttps://www.researchgate.net/profile/Falk-Goetten/publication/337757069_Cost_Estimation_Methods_for_Hybrid-Electric_General_Aviation_Aircraft/links/5de87703299bf10bc3405695/Cost-Estimation-Methods-for-Hybrid-Electric-General-Aviation-Aircraft.pdf*

4. Systems Engineering

In order to complete a complex project like this, it is of uttermost importance to organise efficiently and have clear communication in the team. Various system engineering tools help realising a project efficiently. First and foremost, the project objectives are laid down in Section 4.1. Secondly, the ways of communication within the team, with external specialists and within departments are discussed in Section 4.2. Then, the requirements are listed and compliance is indicated in Section 4.3. Another essential part in successfully finishing a design is to account for all possible risks and design to mitigate these. This is explained in Section 4.4. A reliability, availability, maintainability and safety (RAMS) analysis is performed in Section 4.5. The chapter is concluded with a summary of the trade-off performed by the team in an earlier phase of the design **midterm**, in Section 4.6.

4.1. Project objectives

When starting a design process, one of the principal steps is to clearly define the mission to be performed by the product. In this phase, clear communication with the customer is key. Often, it happens that the customer and engineer unintentionally misunderstand each other and the product does not fully meet expectations. This chapter gives a clear description of the mission in Section 4.1.1 and Section 4.1.2.

4.1.1. Statements

To create an immediate rough idea of what exactly this project is about, it is useful to formulate a Mission Need Statement and a Project Objective Statement, both of which are stated below:

Mission Need Statement

"The mission of this project is to perform the design selection and preliminary design of a short-range sustainable urban flying vehicle with Vertical Take-Off and Landing capabilities."

Project Objective Statement

"To design an eVTOL vehicle with high flight accuracy and stability in urban environment, by 10 students in 10 weeks"

4.1.2. Mission description

The product shall be an aerial vehicle, aimed at safely transporting 2 passengers through the air over a short distance. In addition to this, the control system has been predetermined to be autonomous, meaning that the aircraft will be given a trajectory, and it will follow this to a high degree of accuracy. Another special consideration is that the aircraft should be weather rugged, implying that harsh conditions such as heavy precipitation, high and low temperatures and windy weather can not interfere with the performance and safety of the aircraft. As this vehicle will essentially be an air-taxi, it shall be comfortable for the passenger(s) by not causing excessive cabin noise and shaking during flight, even in the aforementioned harsh weather conditions. Furthermore, the vehicle shall not generate too much noise outside of the cabin, as this might negatively affect the public acceptance of the product. In addition, the aircraft shall perform its operations in an emission-free fashion: all propulsion will be generated with electric power and not with any type of fuel. Lastly, the aircraft must fly at relatively high velocity. The velocity is specified in Table 4.1.

4.2. Systems engineering organisation

Systems engineering is an integral part of any successful aerospace design project. In order to successfully facilitate effective systems engineering in this DSE, a number of measures were taken:

- **Scheduled and effective intra-group communication.** In order to enable effective concurrent engineering, short daily meetings were held inside the group twice a day - once in the morning and once at the end of the day. This made sure that each department contributes effectively to the overall product, and also allows for effective planning, as the Gantt chart was always updated at the end of the day.
- **Communication with the client and external specialists.** Even the best technical design may not see the light of day if it does not meet any social need. For this reason, detailed research has been made into economical feasibility of eVTOL vehicles. This was also supplemented with both business and technical experts in the field from EVE Air Mobility, Fusion Engineering, as well as the TU Delft professors with experience in control theory, vehicle design, acoustics and micro-air vehicle design. Weekly meetings

were held with the tutors who have valuable knowledge of control theory and urban turbulence, and more frequent informal meetings with the coaches. The OSSAs TAs made sure we had no questions during the DSE.

- **N2 Chart and Systems Integration.** In order to keep track of system interfaces and manage delays that can happen due to inter-system dependencies, weekly SE meetings were organized. These meetings were chaired by the systems engineer, and each department was represented by the department chief. The N2 Chart was updated during those meetings and the most significant threats to the progress of the design were identified and mitigation measures were planned. For example, the aerodynamics department needed knowledge of the external fuselage geometry to estimate the aerodynamic performance of the vehicle. However, this was only finalized in the final weeks. As a mitigation measure, first runs were performed with preliminary fuselage designs, which were later updated.

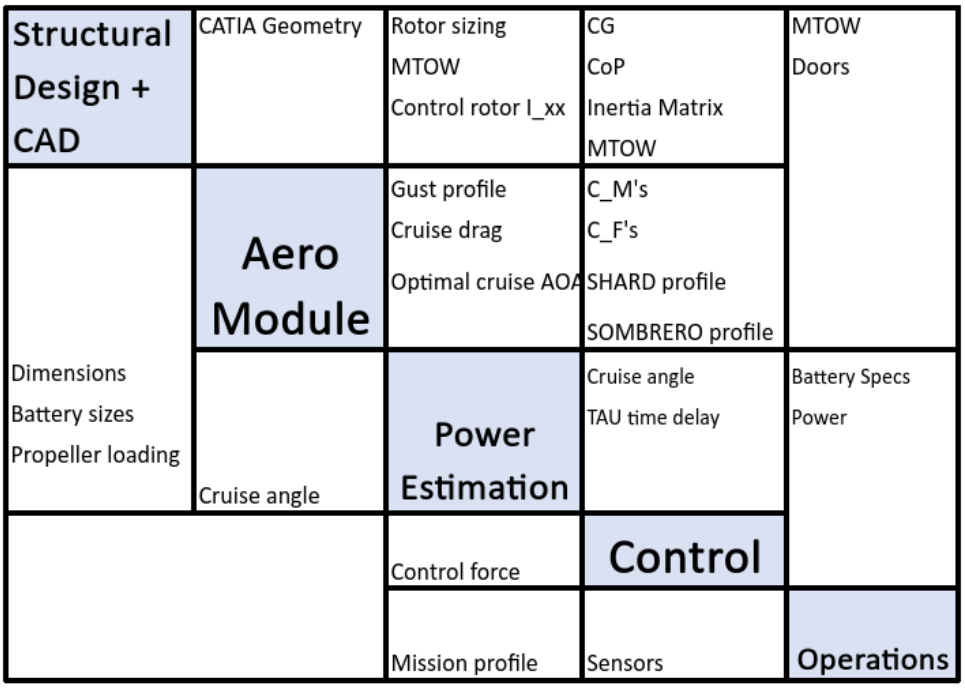

Figure 4.1: N2 chart

4.3. Requirements and compliance

The following section presents the requirements that were used to guide the design. As some requirements were changed or removed, the chapter starts with the changelog of the altered requirements:

- REQ-STAB-VIB-01 (”The maximum vibrational frequency shall be <TBD> Hz.”) has been removed, as there is only a bound on the minimum.
- REQ-CON-FT-04 was changed to: ”The state of the vehicle shall be updated at a rate of at least 20 Hz.”; as it would give a maximum time delay contribution of 0.05 seconds. As a result, REQ-CON-ATT-01 (”The vehicle shall detect its current attitude at least a 20 Hz rate.”) has been removed; due to their overlapping content. Also, REQ-CON-ATT-03 (”The vehicle shall know its desired attitude at all times.”) has been changed and encompassed in the new REQ-CON-FT-04. Therefore, the numbering of REQ-CON-ATT have been remade.
- REQ-OPS-FE-02 was deleted, because high enough frequencies for vibrations are filtered out by the human body.

Table 4.1: List of high level requirements

High-Level		
Identifier	Requirement	Met?
REQ-HL-01	The vehicle shall be able to carry a payload of at least 250 kg.	Yes
REQ-HL-02	The vehicle shall have a cruise speed of at least 100 km/h.	Yes
REQ-HL-03 **(DRIVING)**	The vehicle shall not deviate more than 1 m from the nominal trajectory.	Yes
REQ-HL-04	The vehicle shall have a lower vibrational magnitude than 0.315 m/s^2.	Yes
REQ-HL-05	The vehicle shall respect European noise emissions regulations.	Yes
REQ-HL-06	The vehicle shall have power autonomy for 20 km + a reserve of 5 km.	Yes
REQ-HL-07	The vehicle shall be able to fly according to daytime safety standards overnight.	Yes
REQ-HL-8	The vehicle shall be able to safely operate at a distance of 5 m from people.	Yes
REQ-HL-9	The vehicle shall be able to safely operate at a distance of 3 m from objects.	Yes
REQ-HL-10	The vehicle shall be able to fly during rainy weather.	Yes
REQ-HL-11	The vehicle shall be able to fly in winds under 8 Beaufort (17.2-20.7 m/s).	Yes
REQ-HL-12	The vehicle's propulsive system shall be able to operate at 75% capacity.	Yes
REQ-HL-13	The vehicle propulsive system shall be redundant.	Yes
REQ-HL-14	The vehicle shall respect aeroacoustic regulations over urban areas.	Yes
REQ-HL-15	The vehicle shall have a maximum level of cabin noise of 60 dBA.	Yes
REQ-HL-16	The vehicle noise emission shall not exceed 60 dB.	Yes
REQ-HL-17	The vehicle shall not emit pollutants.	Yes
REQ-HL-18	The vehicle's electric power supply shall be replaceable after 5 years of operation.	Yes
REQ-HL-19	The vehicle's main structure shall be replaceable after 10 years.	Yes
REQ-HL-20	The vehicle shall have modular design.	Yes
REQ-HL-21	The vehicle's main structure shall be recyclable for 75% after EOL.	Yes
REQ-HL-22	The vehicle cost shall not exceed €500,000.	Yes
REQ-HL-23	The vehicle mass shall be lower than 3175 kg.	Yes

Table 4.2: List of stability and control requirements

Identifier	Requirement	Met?
Stability		
REQ-STAB-GUS-01 (**KEY**)	The control mechanisms shall keep the vehicle stable at all flight conditions within the manoeuvre load diagram.	Yes
REQ-STAB-GUS-02 (**KEY**)	The control mechanisms shall keep the vehicle stable at all flight conditions within the gust load diagram.	Yes
REQ-STAB-VIB-02	The minimum vibrational frequency shall be more than 0.5 Hz.	No
REQ-STAB-LEV-01 (**KEY**)	The vehicle shall have moment equilibrium in steady flight.	Yes
REQ-STAB-LAT-02	The vehicle shall have directional stability on the ground.	Yes
REQ-STAB-ALT-01	The vehicle shall be able to maintain its altitude, up to 500 m.	Yes
REQ-STAB-TIP-01	The vehicle shall be stable in all configurations of passenger loading.	Yes
Control		
REQ-CON-FT-01	If necessary, the vehicle shall be able to deviate from its flight trajectory.	Yes
REQ-CON-FT-02	The vehicle shall be assigned a trajectory throughout the entire flight.	Yes
REQ-CON-FT-03	The vehicle shall be assigned a new trajectory if the current trajectory is no longer usable.	Yes
REQ-CON-FT-04	The state of the vehicle shall be updated at a rate of at least 20 Hz.	Yes
REQ-CON-FT-05 (**KEY**)	The vehicle shall be able to follow its assigned trajectory.	Yes
REQ-CON-COL-01	The vehicle shall be able to detect surrounding objects up to 90 m away.	Yes
REQ-CON-COL-02	The vehicle shall be able to change course according to commands from the ground station.	Yes
REQ-CON-COL-03	The vehicle shall be visible in foggy weather up to 10 m.	Yes
REQ-CON-COL-04	The control system shall have a time delay of less than 0.3 s.	Yes
REQ-CON-PTO-01	The vehicle shall be able to perform take-off safely.	Yes
REQ-CON-PTO-02	The vehicle shall be able to perform take-off vertically.	Yes
REQ-CON-PLA-01	The vehicle shall be able to perform landing safely.	Yes
REQ-CON-PLA-02	The vehicle shall be able to perform landing vertically.	Yes
REQ-CON-PLA-03	The vehicle shall have a landing accuracy of 1 m.	Yes
REQ-CON-ATT-01	The signal-to-noise ratio of the detection signal shall be above 20 dB.	Yes
REQ-CON-ATT-02	The vehicle shall be able to correct its attitude at all times.	Yes
REQ-CON-COS-01 (**KEY**)	The control system performance shall comply with airworthiness regulations.	Yes
REQ-CON-WEA-01	The control system shall be functional from temperatures of 230 to 330 K.	Yes
REQ-CON-WEA-02	The control system shall be functional from 10% to 100% levels of humidity.	Yes
REQ-CON-WEA-03	The control system shall be functional from wind speeds of 0 to 20.7 m/s.	Yes
REQ-CON-WEA-04	The control system shall be functional when struck by lightning.	Yes
REQ-CON-WEA-05	The control system shall be functional if the vehicle has ice cover.	Yes
REQ-CON-BAT-01	The battery management system shall be able to sense the temperatures of the batteries.	Yes
REQ-CON-BAT-02	The battery management system shall be able to monitor the voltages of the batteries.	Yes
REQ-CON-BAT-03	The battery management system shall be able to provide commands to lower/raise the battery's voltage.	Yes
REQ-CON-BAT-04	The battery power transmission system shall be able to provide sufficient current isolation from the passengers and rest of the vehicle.	Yes

Table 4.3: List of operational, aerodynamic and propulsive requirements

Identifier	Requirement	Met?
Operations		
REQ-OPS-LUG-01	The vehicle shall allocate a space of 150 litres to accommodate luggage of the passengers.	Yes
REQ-OPS-LUG-02	The temperature in the luggage department shall be between 1 and 25 °C.	Yes
REQ-OPS-PAX-01	The temperature in the passenger cabin shall be able to set the temperature by climate control.	Yes
REQ-OPS-PAX-02	The vehicle shall protect the passengers from weather conditions (rain, lightning and wind).	Yes
REQ-OPS-PAX-03	The passengers shall be able to access the vehicle comfortably.	Yes
REQ-OPS-PAX-04 **(KEY)**	The vehicle shall not experience accelerations due to gusts above 0.5 g.	Yes
REQ-OPS-TO-01 **(KEY)**	The maximum acceleration during take-off should be kept below 1.5 g.	Yes
REQ-OPS-FE-01	The vehicle shall have a flight ceiling of 2134 m.	Yes
REQ-OPS-FE-02	The vehicle shall have a maximum speed of 350 km/h.	Yes
REQ-OPS-FE-03 **(KEY)**	The vehicle shall attain a minimum climb rate of 3 m/s .	Yes
REQ-OPS-FE-04	The vehicle shall attain a minimum climb angle of 5° during the TO manoeuvre.	Yes
REQ-OPS-GR-01	The vehicle shall have a maximum downtime of 30 minutes.	Yes
Aerodynamics		
REQ-AERO-DRA-01 **(KEY)**	The ratio of lift over drag during cruise shall be at least <TBD>.	TBD
REQ-AERO-NOI-01	The maximum velocity of the airflow over the lift generating devices should be lower than Mach 1.	Yes
REQ-AERO-SUR-01	Fuselage surface roughness shall be below 20 microns.	TBD
Propulsion		
REQ-PROP-THR-01 **(KEY)**	The propulsion system shall be able to provide sufficient thrust force at take-off, in order to obtain vertical acceleration while taking unexpected gusts into account ($1.1 \cdot 1.5 MTOW g$).	Yes
REQ-PROP-THR-02	The propulsion system shall be able to provide the same thrust force during landing as during take-off.	Yes
REQ-PROP-THR-03 **(KEY)**	The propulsion system shall provide <TBD> N of thrust force to accelerate to cruise speed.	TBD
REQ-PROP-THR-04	The propulsion system shall provide <TBD> N of thrust force to maintain a cruise speed of 100 km/h.	Yes
REQ-PROP-THR-05	The propulsion system shall provide <TBD> N of thrust force for control manoeuvres.	TBD
REQ-PROP-NOI-01	The propulsion system shall not emit more than 75 dB of noise at a distance of 100 m.	Yes
REQ-PROP-NOI-02 **(KEY)**	The propulsion system shall comply with all European noise emission regulations.	Yes
REQ-PROP-OPS-01	The propulsion system shall be able to start remotely.	Yes
REQ-PROP-OPS-02	The propulsion system shall be able to shut off remotely.	Yes
REQ-PROP-OPS-03	The propulsion system shall not lose functionality during unexpected weather conditions.	Yes
REQ-PROP-OPS-04 **(KEY)**	The propulsion system shall be able to provide the required power to reach 20 km of range plus a reserve of 5 km.	Yes
REQ-PROP-OPS-04	The auxiliary battery shall be able to keep communication and navigation systems connected for at least 30 min.	Yes
REQ-PROP-OPS-05	The main battery shall be swappable within 15 min.	Yes
REQ-PROP-MNT-01	All components of the propulsion system shall be accessible for maintenance.	Yes
REQ-PROP-MNT-02	The rotor blades shall be replaceable.	Yes
REQ-PROP-SFT-01	Rotor blade failure shall not cause serious injury to passengers.	Yes
REQ-PROP-SFT-02	All possible fire hazards shall not pose a fire risk towards the passengers.	Yes

Table 4.4: List of structural and RAMS requirements

Identifier	Requirement	Met?
Structures		
REQ-STRUCT-INT-01 **(KEY)**	The structure shall not fail under limit loads.	Yes
REQ-STRUCT-INT-02 **(KEY)**	The structure shall not fail due to fatigue within its lifespan.	Yes
REQ-STRUCT-INT-03	The structure shall damp out vibrations in <TBD> s.	TBD
REQ-STRUCT-INT-04	Corrosion shall not cause the structure to fail during lifetime.	Yes
REQ-STRUCT-INT-05	The structure shall provide structural integrity for the servo element.	Yes
REQ-STRUCT-INT-06 **(KEY)**	The structure shall not fail under ultimate loads applied for 3 seconds.	Yes
REQ-STRUCT-SUS-01	75% of the materials shall be recycled for at least 1 more lifetime in a new application.	Yes
REQ-STRUCT-SUS-02	The CO2-emissions when manufacturing the materials shall not exceed <5> t.	Yes
REQ-STRUCT-SUS-03	The CO2-emissions when manufacturing the structure shall not exceed <TBD> t.	TBD
REQ-STRUCT-SUS-04	The total embodied energy of the vehicle must be less than <TBD> MJ.	TBD
REQ-STRUCT-SFT-01	The structure shall damp external noise during operation below <50> dB.	Yes
REQ-STRUCT-SFT-02	The structure shall keep the passengers safe from fire for 30 s.	Yes
REQ-STRUCT-SFT-03	The structure shall have no failure from degradation throughout its lifespan.	Yes
REQ-STRUCT-SFT-04	The structure shall not have sharp elements on accessible places.	Yes
REQ-STRUCT-PL-01	The structure shall provide space of at least 2 m^3 for payload on board.	Yes
REQ-STRUCT-PL-02	The total cost of the materials, structures and the manufacturing shall not exceed <500,000> EUR.	Yes
REQ-STRUCT-PL-03	Passengers shall be able to enter the cabin through a door.	Yes
REQ-STRUCT-PL-04	The cabin shall provide space for at least 2 passengers on board.	Yes
REQ-STRUCT-PL-05	The luggage compartment shall have a separate door to access it.	Yes
REQ-STRUCT-MNT-01	The subsystem compartments shall be accessible for maintenance workers.	Yes
REQ-STRUCT-MNT-02	Structural parts which are susceptible to fatigue shall be accessible for maintenance workers.	Yes
REQ-STRUCT-CSH-01	Deformable zones shall protect passengers during impact of energies up to 25 kJ.	TBD
REQ-STRUCT-CSH-02	Seats will remain fixed during impact of energy up to 5kJ.	TBD
REQ-STRUCT-CSH-03	Seatbelts will restrain the passengers during impact with a maximum force of 400 N.	TBD
RAMS		
REQ-RAMS-MNT-01	Small failures that do not directly lead to loss of operability shall be fixed within 24 hours.	Yes
REQ-RAMS-MNT-02	Large failures that lead to loss of operability shall be fixed or replaced within 7 days.	Yes
REQ-RAMS-MNT-03	Large failures that lead to loss of operability shall not occur more than once per 10000 flight hours.	TBD
REQ-RAMS-AVL-01	The full availability of the air vehicle shall be above 90%.	Yes
REQ-RAMS-SFT-01	The probability of catastrophic failure shall be below 1 per 10000 flight hours.	TBD
REQ-RAMS-SFT-02	The propulsive unit failure rate shall be below 1 per 10000 flight hours.	TBD
REQ-RAMS-SFT-03	The autonomous controller for the vehicle shall be at least double redundant.	Yes

4.4. Technical risk management

In this section, the technical risk management is documented. Technical risks are risks related to the failure of meeting the requirements for performance, operability, producibility, testability, integration and environmental protection, that originate from occurrences in the design phase. There are several steps involved in the risk management of a project. The first step is documented in Section 4.4.1, and includes identifying the sources and consequences of possible risks, and plotting these risks in a risk map. Furthermore, mitigations are generated that can be implemented during the design phase. The risks after implementation of the mitigations are plotted in a second risk map. Both the risk maps are displayed in Section 4.4.2.

4.4.1. Performing technical risk assessment

The technical risks for the project are shown in Table 4.5, and are identified as follows. Of all risks that came up during the brainstorm session, risks with a severity or likelihood index of 1 were discarded. Including these risks in the table below would decrease the clarity of the overview and would not add any real value to the risk assessment. Because the design of the vehicle is finished at this stage of the project, the risks for the production and testing phases will be considered. The mitigation column is modified from the Midterm report based on the actual used mitigation methods. However, risks R-PROP-03, R-CERT-01 and all production risks (with the tag PROD) are not mitigated yet. Also, R-STRUC-04 is removed and substituted with a broader risk of supply chain problems (R-PROD-06).

Both the severity and likelihood of a risk are defined as: very low, low, medium, high and very high. For severity, very low means that a risk is negligible, and low means that the risk may be noticeable but not cause any major setbacks in the project. Medium means that a part of the project has to be redone, and high means the same for a large part of the project, or even that it needs to be restarted from scratch. Very high means that people's lives have been endangered. The likelihood ranges from "probably never going to occur", to "will most definitely occur at some point in the project".

Table 4.5: Technical risk mitigation table

Risk	Consequence	Mitigation
R-CON-01: A bug could occur during the coding process.	Time is needed to revise the code. Residual errors that the team is unaware of could still be present after debugging.	The functionality of the code is regularly checked, in order to discover bugs right after they occur, reducing the severity of the risk. Also, the code is extensively verified and validated.
R-PROP-01: The rotor design is ineffective at the RPM at which the aircraft flies.	The rotor design must be revised, causing a possible change in RPM and/or the size could change, leading to reiterations of other design aspects.	The rotors are designed based on the different flight phases. The models used for these are validated and verified.
R-PROP-02: Degradation of the energy storage system is inaccurately estimated in the design phase.	This leads to it having a shorter lifetime than expected, severely increasing the maintenance costs of the product.	The batteries are designed to be swappable. Also, the battery health will be closely monitored.
R-PROP-03: The thrust vectoring mechanism of the control propellers turned out to be more complex than initially anticipated.	Some parts of it might need to be redesigned, and the production process will take longer. So this could mainly cause delay.	First a working prototype will be designed before producing and integrating all control propellers. This will decrease the likelihood of the risk.
P-PROP-04: The required reserve energy is underestimated during the design phase.	The vehicle is not capable of flying to alternate landing locations in case of emergency, and could crash with fatal consequences.	Emergency landings are incorporated into the case study in order to take the required reserve energy into account, reducing the likelihood of the risk.
R-AERO-01: The control system of the aircraft malfunctions due to wrongly estimated aerodynamic parameters.	Some more precise aerodynamic simulations or experimental tests need to be done. This will cause delays and increase costs.	For the estimation of the aerodynamic parameters, different verification and validation tests are performed.

R-STRUC-01: The centre of gravity position might be wrongly estimated, negatively impacting the controllability or stability.	When discovered during the final design phase, this risk would set the project back to the preliminary phase, causing a great time delay and increase in costs.	As with the other parameter estimation scripts, a significant amount of verification and validation is done, which decreased the likelihood of the risk.
R-STRUC-02: With the materials chosen for the design, it is not possible to meet the recyclability requirement.	Other materials should be used which drive the total weight up or have another negative impact on the product. The cost could increase due to the need of more special materials.	The sustainability engineer kept track of the advances made in the structures department and made sure that the recyclability requirements are met.
R-STRUC-03: Another department wants to shift a heavy element, a servo element, or wants to make a gap in the structure.	The structure should be revised for the new critical load cases, causing more costs and time delays.	Due to good interfacing between departments, the structures department knew in time where gaps needed to be in the structure.
R-STRUC-05: Passengers are insufficiently protected from possible battery fires.	If this risk is not found during testing, passengers can be endangered during flight, possibly resulting in fatalities.	Safety systems design was done by the structures department.
R-CERT-01: Certification standards are chosen that are not applicable to the vehicle that is designed.	This leads to a do-over of the certification process and possible reiterations of the design, causing an increase in time and costs.	Discuss certification standards with an external expert. This will reduce the likelihood of the risk.
R-GEN-01: Flawed communication between the design group and client.	This can lead to a final product that does not correspond to the client's wishes.	This can lead to a variety of problems that can set back the project several times. Regular meetings with the tutors and the external contact were set up in order to know if the project is heading in the right direction.
R-GEN-02: Later on, it is found that an infeasible design option is chosen.	This could mean that a significant amount of design steps need to be redone. So, a significant amount of additional time will be needed.	Due to frequent communication with the tutors, the likelihood of this risk was lowered.
R-PROD-01: Supply chain problems.	This will cause delay and can increase the cost.	It has to be made sure that multiple subcontractors are used for components with a higher risk of supply chain problems. This will decrease the impact of the risk.
R-PROD-02: Inexperience of production crew.	The crew turned out to be less experienced than initially anticipated. More material could be wasted, and more time will be spent.	The crew needs to be properly trained. Also, hire workers which have experience with certain production processes.
R-PROD-03: There are not enough manufacturing facilities available.	Facility costs will increase and there will be more delay.	The manufacturing processes need to be known in time. Then, the manufacturing facilities can be built/rent relatively early in the development process. This will limit time delays from these risks, so the risk will have less impact.
R-PROD-04: Another virus outbreak happens.	The production process has to be stopped. This will mostly cause delay and might increase costs.	Production facilities can be built in places where virus outbreak regulations are not that strict. This decreases the impact of the risk.

4.4.2. Risk maps

The risks elaborated upon in the previous subsection are divided into groups based on impact and likelihood of occurrence. The risk map in Figure 4.2a shows this division. Applying the mitigations explained in Table 4.5 results in a different risk map, with a decreased impact and likelihood of the risks. This new risk map is shown in Figure 4.2b.

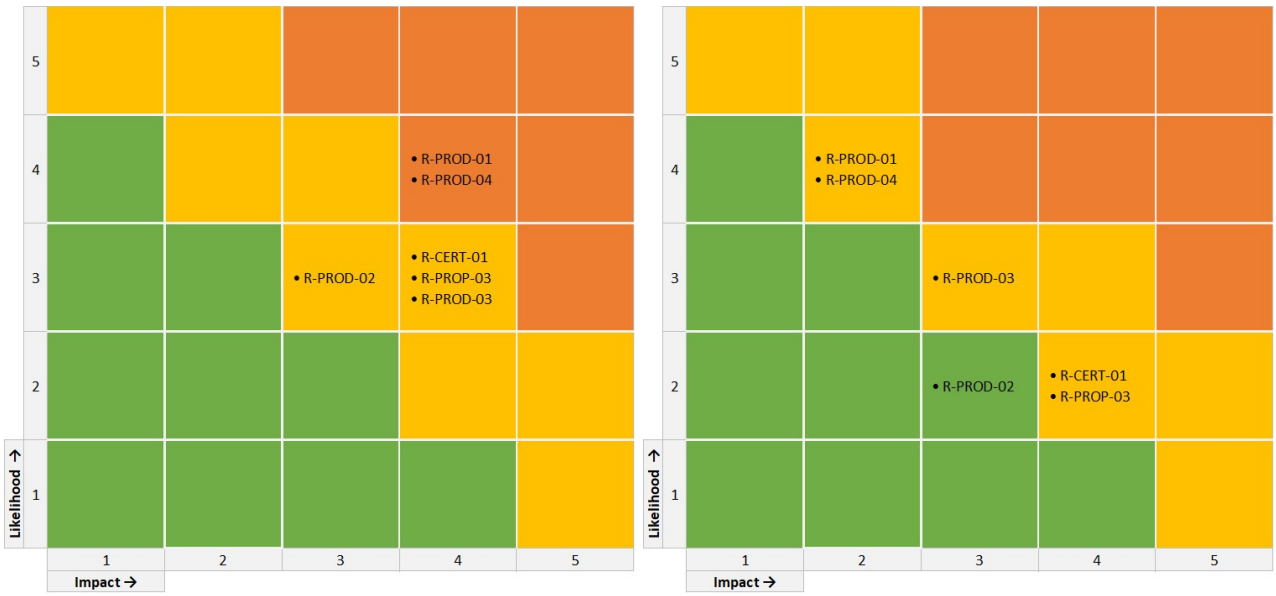

(a) Initial technical risk map

(b) Technical risk map after mitigation

Figure 4.2: Technical Risk maps

4.5. RAMS analysis

Reliability, Availability, Maintainability and Safety (RAMS) analysis is an integral part of the modern aerospace design process. NASA has contracted the Boeing company to conduct an extensive FMECA (Failure Modes Effects and Criticality Analysis) on 4 various eVTOL concepts, including the multirotor. The FMECA is presented in **FMECAnasa**. The most critical failure rates were adjusted for the Veatle and are given below. Other statistics were taken from **BirdStrike**, **EASA_Safety**.

Table 4.6: Reliability Statistics

Failure Mode	**Failure Rate per 10^6 flight hours**
Electric Motor	9.24
Heat exchanger	8.08
Driveshaft + propeller failure	8.01
Damaging Bird Strike	35.0 (est.)
Total	60.3

Of course, there are many more possible risk events. The most critical events and possible mitigation measures are given below.

Table 4.7: Events and Mitigation

Event	**Mitigation**
Bird Strike, rotor damaged	Continue flight with 7 rotors, seek emergency landing.
Heat exchanger not functional	Lower battery voltage, seek emergency landing.
Driveshaft / propeller not functional	Continue flight with 7 rotors, seek emergency landing
Electric motor failure	Continue flight with 7 rotors, seek emergency landing.
Battery cell damage	Lower the voltage, you may proceed with the flight.

Because of improved safety characteristics of the Veatle, even the most critical events during operation such as a bird strike or generator failure will not result in serious injury or loss of life. The vehicle has been designed

in such a way that a loss of 2 rotors still leaves it in an operational state, and the battery system is distributed in parallel to reduce the severity of the cell damage, which can happen in Li-ion battery.

Maintainability is also a strong suit of the vehicle. Because of the modular design, the beams that support the propellers can be easily taken on and off. In case of the propeller fault or a bird strike, it can be quickly replaced by a working part from storage and repaired in the meantime, thus improving the availability. The battery packs are designed to be swappable, so an ageing or faulty battery can be quickly replaced as well. The Veatle uses commercially available batteries. An overview of the RAMS characteristics can be found in Table 4.8.

Table 4.8: RAMS analysis

Reliability	**Customer Comfort** - Reliability deals with the satisfactory functioning of the product. If the customer experiences too much noise or large perturbation due to an incoming gust, they will not be satisfied with the product. **Malfunctioning components** - Furthermore, minimizing the chance of components malfunctioning will increase the reliability of the vehicle. The reliability needs to be maximised in order to prevent operation delays. So this is also an important factor for the customers.
Availability	**Battery** - Most chemical based batteries have low capacity, especially when used for aerospace vehicles. They would need recharging, leading to potentially reduced availability. Their low energy density also limits the range of the aircraft.
Maintainability	**Battery** - Batteries have a limited life-cycle and fast performance degradation, so it is likely they are to be replaced/maintained numerous times during its life-cycle.
Safety	**Rotor Safety** - If the propulsion system uses a rotor, there is a risk of it coming off and damaging the structure/user. **Incoming Turbulence** - The vehicle has to follow a nominal trajectory accurately due to incoming gusts, in order to prevent collisions. **Traffic** - due to operating in a busy urban environment, there is a high risk of collision due to cars, other flying vehicles, etc. Therefore, the autopilot system should be able to effectively avoid possible collisions with other objects.

4.6. Trade-off summary

For the midterm deadline of the project, a trade-off between multiple design options has been performed. The trade-off consisted of two stages: the initial trade-off reducing the options from 10 to 3 and the final trade-off reducing the options from 3 to 1. In this section, both trade-offs are briefly explained and elaborated.

In the initial trade-off, 10 design options were considered. The following trade-off criteria were used: cost, weight, energy, control safety and comfort. Each project member graded all 10 concepts in these areas. A sensitivity analysis was included. Three design options scored the highest in the initial trade-off. Firstly, the wingless, non ducted contra-rotating multirotor concept was considered good mostly on the aspects of cost weight and control. Then, the vector tilted thrust design scored well on the comfort and energy criteria. Thirdly, the lift and cruise with tail option scored well on energy, safety and comfort. These three designs were analysed quantitatively in the second trade-off.

The goal of the second trade-off was to determine the best parts of the design options and combine them to obtain the best possible design for the problem at hand. For this, multiple 'sub trade-offs' were performed. First, the three configurations of the initial trade-off were analysed based on cost, weight and energy. For this, developed tools were used to obtain values for the three criteria. The multirotor concept won this trade-off. The second trade-off supported the material choice. The criteria were cost recyclability, strength, stiffness, corrosion and weight. Multiple materials were chosen: carbon fibres, aluminium and steel. Then, the landing gear configuration was chosen to be skids. Furthermore, a trade-off of the cabin form was performed: seats abreast appeared to be favourable over seats in a row. Finally, one of the most important trade-offs was made to distinguish the design from existing concepts: how to counteract disturbances? Options considered were vector thrust, deflectors, pre-tilted rotors or in plane rotors. The trade-off criteria considered were time-delay, weight, power required and control force. The results of this sub trade-off was the in plane rotor configuration, that scored well on time-delay and power required.

The overall result of the trade-off was the following design. A multirotor VTOL made out of carbon fibres, steel and aluminium and with skids, seats abreast and in plane rotors to counteract disturbances and minimise the deviation from the trajectory. This design has been further elaborated in the final design phase.

5. Final Aerodynamic Analysis

During the design of the vehicle, the main focus was put on the rejection of disturbances caused by gusts in the urban environment. Thus, extensive analysis of the aerodynamic response of the vehicle to gusts is beneficial. However, since the field of urban air mobility is still young, it is difficult to properly estimate the aerodynamic forces and moments on the fuselage body from the literature. For this reason, the decision was made to run simple coarse CFD studies on the external geometry of the UAM vehicle. A brief overview of assumptions associated with the model presented in this section is given in Section 10.1. Extensive verification and validation of the model is done in Section 10.2 and Section 11.1, respectively. It should also be noted that OpenFOAM is an open-source software, meaning its code can be reviewed by anyone. Furthermore, it is widely used in scientific research.

5.1. Solver

OpenFOAM v.9.0 simpleFoam solver was used, which solves the continuity and momentum equation assuming incompressible flow [1]:

$$\nabla \cdot \mathbf{u} = 0 \tag{5.1}$$

$$\nabla(\mathbf{u} \otimes \mathbf{u}) - \nabla \times \mathbf{R} = -\nabla p + \mathbf{S} \tag{5.2}$$

Where $\mathbf{u}$ is the velocity, $\mathbf{R}$ is the stress tensor, and $\mathbf{S}$ is the momentum source. A shear stress transport $k - \omega$ model was employed to simulate turbulence [2]. As a convergence criterion, pressure residual of 0.005 and velocity residual of 0.005 was used for more refined cruise cases and 0.01 pressure / velocity residual was used for coarse gust cases. For the divergence calculation, `bounded Gauss upwind` was used (the velocity was usually oriented in negative CATIA frame X direction), and for the gradient calculation `Gauss linear` was employed. For the pressure field, `GAMG` solver was employed, and for the other fields `smoothSolver`.

5.2. General setup

First, a CAD model of the fuselage body and the beams (without the rotors) is imported into the software and the enclosure is defined. The used fuselage is not the final version, because the fuselage was not finalised when the aerodynamic parameters had to be estimated. However, the largest contribution to the aerodynamic forces acting on the body is likely to be from the beams and the fuselage. For most runs the domain limits are $[-20, 10] \times [-10, 10] \times [-8, 8]$ (m) in the XYZ CATIA reference frame, this is set in the `blockMeshDict` dictionary file.

5.2.1. Generation of the mesh

After that, the mesh in the enclosure was generated with the `blockMesh` utility. Then, with the `snappyHexMesh` utility, the mesh around the geometry is refined and the mesh in the geometry is removed. After that, it adds additional cell layers in regions of interest (so around the surface of the vehicle). In Figure 5.1, the result of this process is given.

[1] `https://www.openfoam.com/documentation/guides/latest/doc/guide-applications-solvers-incompressible-simpleFoam.html`

[2] `https://www.cfd-online.com/Wiki/SST_k-omega_model`

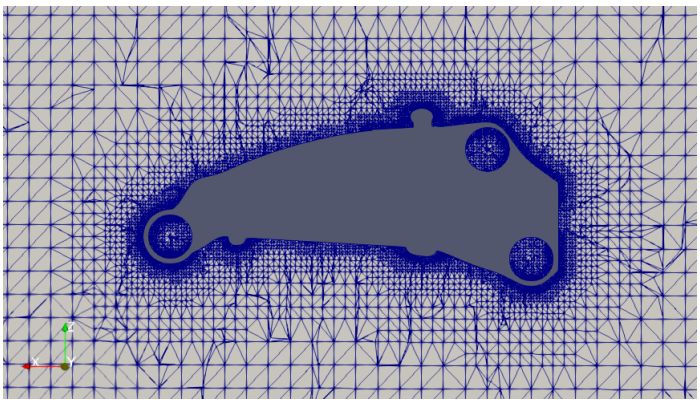

Figure 5.1: Slice of the $X_B Z_B$-plane of the used fuselage mesh

5.2.2. Setting up the boundary conditions

With the mesh generated, the initial and boundary conditions are set up. For the pressure, a zero gradient boundary condition is applied on every wall, and kinematic pressure $p_{\text{kin}} = p_\infty/\rho = 82714\ \text{m}^2/\text{s}^2$ ($p_\infty = 101325\text{Pa}$). The velocity boundary condition V_{boun} depends on the considered case and was enforced on each wall. It should be noted that the peak gust velocity was considered for the gust cases, as this is the greatest force experienced. For other gust velocities, the force can be calculated assuming a quadratic relationship between force and velocity, e.g., $F \propto V^2$. At the surface of the vehicle, a zero velocity boundary condition is applied due to the no-slip physical phenomenon.

As an initial condition, kinematic pressure of $p_{\text{kin}} = 82714\ \text{m}^2/\text{s}^2$ was prescribed over the whole field. For the velocity field, it was found that using $V_{\text{in}} = V_{\text{boun}}/3$ prevented the solution from diverging. The $k-\omega$ turbulence model fields (turbulent kinetic energy `k`, specific dissipation rate `omega`, turbulent viscosity `nut`) are prescribed according to OpenFOAM internal wall functions or guides found online. [3]:

5.3. Aerodynamic parameter determination

For each case, three force coefficients and three moment coefficients are determined. These coefficients are given in the body reference frame of the vehicle. The determination of these coefficients was done with the `forceCoeffs` post-processing function. In this function, several parameters need to be specified: the directions of the desired force and moment coefficients (as vectors), a reference area and length to normalise the aerodynamic forces and moments and some general free stream flow conditions. For all cases, a reference area of 1 m^2 and length of 1 m have been used respectively. Because this coefficient is relatively constant for varying air speeds (Section 10.2.3), it can be used to model the controls in different gust velocities.

5.4. Analysed cases

For each case, a different relevant airflow condition is simulated. The airflow conditions were not given in the regular aerodynamic axis system (with the airspeed magnitude, angle of attack and sideslip angle relative to the body axis system). However, the flow conditions were given spherically by an airspeed magnitude, the angle between the air velocity vector and the $X_B Y_B$-plane (α_s) and the angle between the projection of the air velocity vector on the $X_B Y_B$-plane and the X_B-axis (β_s). These are shown visually in Figure 5.2.

[3] `https://curiosityfluids.com/2019/02/11/basic-komega-sst-boundary-conditions/`

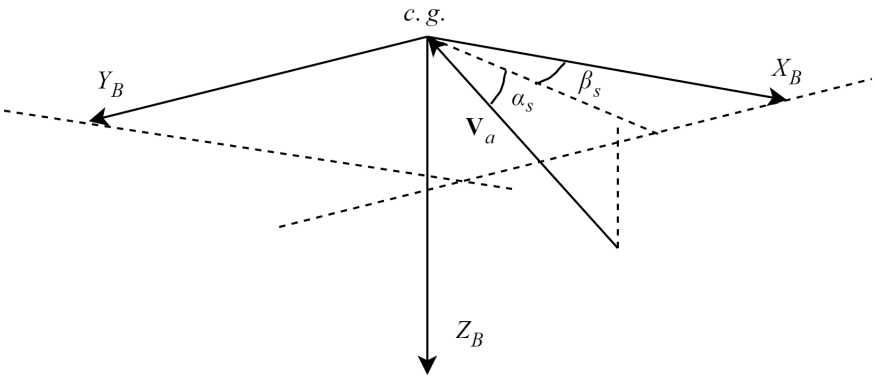

Figure 5.2: The defined angles with respect to the body axis system

The cases are listed in Table 5.1. As can be seen, most cases use an airspeed of 20.7 m/s. These cases are run in order to provide an accurate estimation of aerodynamic forces during the peak gust velocity. This will then be an implicit constraint for the control department. The cases with an airspeed of 50 m/s (cruise velocity) are done in order to give the propulsion department a good estimate of the parasite drag for the fuselage. This allows to estimate the tilt angle during cruise. The cases at the other airspeeds are used in the sensitivity analysis. For most cases, the correct incidence of the airflow was achieved by changing the boundary conditions. However, for some cases, the body was rotated for convenience. In order to reduce the computational time, some converged cases were used as an initial condition for relatively similar cases.

Besides the aerodynamic analysis of the vehicle, one extra case was run in order to investigate the implications of the urban turbulence on the operation of the vehicle. London's largest skyscraper, the Shard, was used for a case study of the flow around the tall building and also to study the implications of the vehicle moving in a wake of the building. The methodology employed is similar to other fuselage cases, and the results are given in Section 12.2.1.

Table 5.1: The analysed aerodynamic cases

Case name	α_s [°]	β_s [°]	V_a [m/s]
FrontGust	0	0	20.7
Front_30	0	0	30
Front_10	0	0	10
SideGust_15	0	15	20.7
SideGust_45	0	45	20.7
SideGust_90	0	90	20.7
SideGust_135	0	135	20.7
RearGust	0	180	20.7
PitchGust_15	15	0	20.7
PitchGust_-15	-15	0	20.7
RollSideGust_15	15	90	20.7
RollSideGust_30	30	90	20.7
RollSideGust_-15	-15	90	20.7
FrontCruise	0	0	50
PitchupCruise_7.5	7.5	0	50
PitchupCruise_15	15	0	50
BottomGust	90	0	20.7
TopGust	-90	0	20.7

5.5. Results

The results of these cases are summarised in Table 5.2. In order to get the force and moment coefficients for a case between the measured values, the coefficients are interpolated. This will be elaborated in Chapter 7.

For visualisation, in Figure 5.3 a pressure and velocity distribution of the FrontCruise case are given from the ParaView post-processing software. The free stream flow points in the negative X_B direction. As expected, a large high pressure region is found on the front of the vehicle and some smaller high pressure regions are found

at the front of the beams connecting to the rotors. In Figure 5.3b, it can also be seen that the flow behind the front control propeller and the beams is separated. The flow at the back of the vehicle also looks detached.

Table 5.2: Results of the analysed aerodynamic cases

Case name	$C_X[-]$	$C_Y[-]$	$C_Z[-]$	$C_{m_Y}[-]$	$C_{m_X}[-]$	$C_{m_Z}[-]$
FrontGust	-1.32	0	-0.23	$-1.10 \cdot 10^{-2}$	0	0
Front_30	-1.31	0	-0.22	$-2.80 \cdot 10^{-3}$	0	0
Front_10	-1.34	0	-0.19	$-3.50 \cdot 10^{-2}$	0	0
SideGust_15	-1.46	0.57	-0.476	$5.66 \cdot 10^{-3}$	-0.223	0.56
SideGust_45	-1.15	1.95	-0.68	-0.21	-0.75	1.24
SideGust_90	0.29	2.7	-0.65	-0.17	-0.86	0.83
SideGust_135	1.29	2.19	-1.04	0.47	-0.83	-0.085
RearGust	1.29	0	0.2	0.072	0	0
PitchGust_15	-1.33	0	0.55	-1.14	0	0
PitchGust_-15	-1.48	0	-1.23	1.2	0	0
RollSideGust_15	0.3	2.85	0.51	-0.79	-1.35	0.68
RollSideGust_30	0.32	2.76	1.45	-1.22	-1.76	0.49
RollSideGust_-15	0.32	2.69	-1.4	0.29	-0.6	0.88
FrontCruise	-1.16	0	$-8.70 \cdot 10^{-2}$	$1.45 \cdot 10^{-2}$	0	0
PitchupCruise_7.5	-1.26	0	-0.3	-0.51	0	0
PitchupCruise_15	-1.4	0	-0.13	-1.04	0	0
BottomGust	0.136	0	3.48	-1.57	0	0
TopGust	-0.214	0	-3.12	1.38	0	0

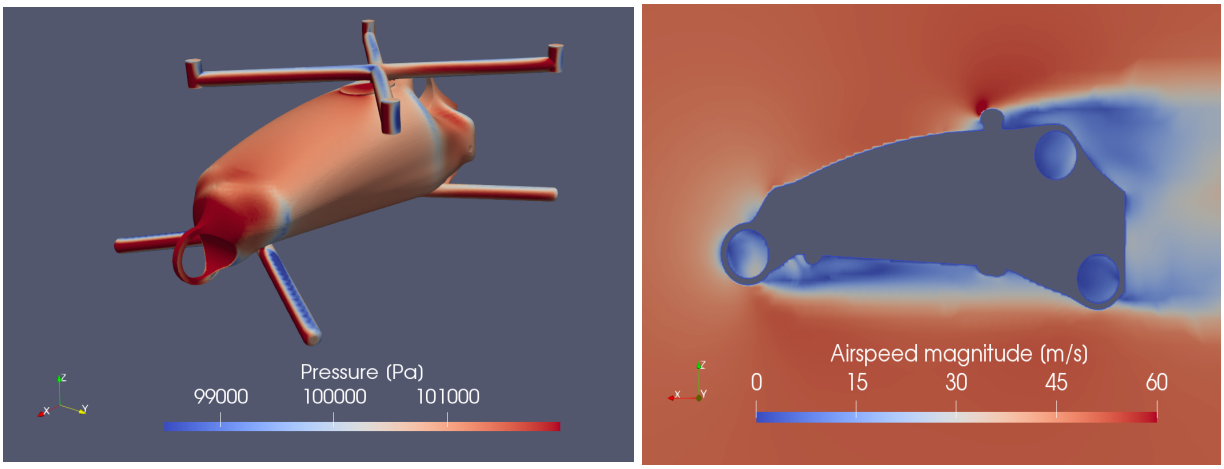

(a) Static pressure field on the fuselage surface for the FrontCruise case

(b) Slice of the $X_B Z_B$-plane around the fuselage with the airspeed distribution colored

Figure 5.3: Visualised flow conditions around the fuselage for the FrontCruise case

5.6. Cruise drag final design

As mentioned previously, for most cases an earlier design is used. However, in order to have a final drag coefficient value during cruise (airspeed of 50m/s and α_s is roughly -10 °), one OpenFoam run with the final design without the rotors is done. The setup was similar to the previously described cases. The static pressure distribution at the surface of the vehicle, the streamlines and the velocity distribution at the $X_B Y_B$-plane are given in Figure 5.4. In this case, the drag coefficient (in the direction of the flow) is 1.09.

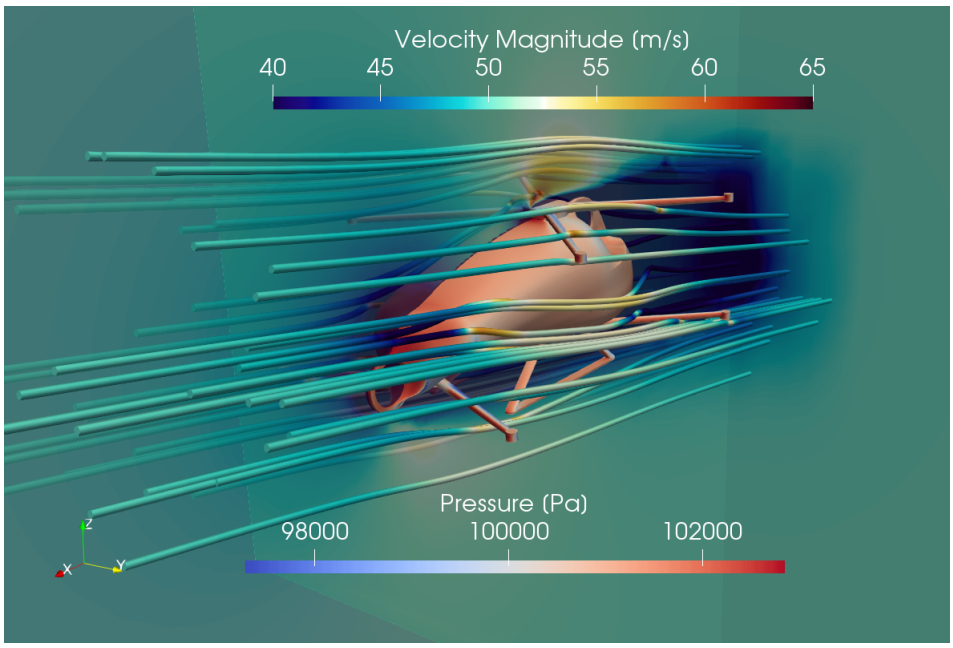

Figure 5.4: Static pressure distribution, streamlines and velocity distributions around the final design of the fuselage together with the landing gear and support beams

6. Final Propulsion and Power Design

This chapter describes the process of the propulsion system design. The propulsion system in multirotors is of high importance because it determines lifting performance, cruise performance and at the same time it is the main control system as well, as opposed to control surfaces of the conventional aircraft. This chapter is subdivided into 2 parts: a propulsion system part in Section 6.1 and a power storage system part in Section 6.2.

6.1. Propulsion

Section 6.1.1 explains how the rotors were sized, Section 6.1.2 documents the search for the optimal cruise speed. Next, Section 6.1.3 shows how the detailed design of the actual rotor blade was performed, while Section 6.1.4 concludes the analysis of the main rotors. Finally, Section 6.1.5 explains how the control propeller was designed.

6.1.1. Rotor sizing

The rotor blade length and amount of rotors are parameters that have an influence on almost all aspects of the design, which is why they were analysed first. The old concept had 6 contra-rotating propellers (so 12 in total), which was chosen because contra-rotating propeller have an increased efficiency and redundancy, and they also make efficient use of space. However, it was also found that they generate a large amount of noise **CRnietgoed**, which is not acceptable for the business case of the Veatle. Close spacing and increased rotor RPM significantly increase noise, and an increased blade length has the same effect. A 2019 study even concluded that contra-rotating propellers produce up to 20 dB more noise than single propellers of the same size **MCKAY2021107850**. For this reason, the contra-rotating option was forced to be discarded, leading to the need for a new design. The design approach for the iteration was based mostly on efficiency, since a power efficient system would decrease the battery weight, and any decrease in weight is beneficial for aircraft design. It was assumed that any consequent increase in the propulsion system weight would be considerably smaller than the reduction in the battery weight. It was found that increasing the disk area leads to a lower power required, and thus it was chosen to focus on maximising the disk area. The main limiting factor in this case was the requirement regarding the allowed dimensions of the vehicle (further referred to as "the box", 4 x 6 x 2 m^3).

Since the contra-rotating propeller option was ruled out, the propellers were not allowed to be stacked closely on top of each other. This makes it more complex to efficiently obtain a large disk area while staying in the box. For this reason, it was chosen to change the configuration to an 8 rotor design, divided into 2 levels. 4 per level were chosen because this is the optimal number to occupy as much space as possible in the box with circular shapes. A minimum horizontal spacing between the rotor blades was set at 20 cm. The diameter of the disks was then maximised inside the box, which yielded a result for blade length. When this value was used for the power required and battery weight, it was found that the resulting power required and battery weight were far too high. Since the given dimensions of the box were an 'indicative' size, it was decided with permission of the customers to increase the dimensions of the box. The width was increased by 1 m, resulting in a 5 x 6 m^2 box. The maximum radius was then found with the same approach, resulting in a blade length of 1.2 m, and a disk area of 36.2 m^2.

The 2 levels were chosen in order to maximize the vertical spacing between the rotors, thus minimizing the noise generating interference effects between the propellers. The placement was chosen to be simply as far away from the fuselage as possible, to minimise overlap between the fuselage and rotor blades. The 2 forward rotors of the top layer are mounted as far back as possible, while still satisfying the 20 cm spacing. This was done to decrease the necessary beam length and thus beam weight. There is overlap between fuselage and rotors, which will have effects on the airflow and thus performance, however the fuselage will be placed such that this is minimised. The choice of two layers of rotors is expected to cause a decrease in efficiency of the bottom aft rotors, as they have to deal with the induced drag caused by the rotors above them. This decrease in efficiency is not quantifiable without running tests that simulate this effect, and is therefore not taken into account in the calculations for the propulsion system. It is recommended that tests are run to quantify the decrease in efficiency and that these numbers are integrated into the calculations in later stages of the research into this concept.

The number of blades per rotor was chosen to be 3. Most multirotor eVTOLs only have 2 blades per propeller (EHang, Volocopter, Boeing NeXt, Wisk Cora), which is most likely because 2 bladed rotors produce lift in the most efficient way and possibly to reduce weight (fewer blades means less weight of course). However, there are

more things to consider, such as noise and stability. Especially the noise aspect led to the decision to increase the blade number. Where 2 bladed propellers produce only 2 noise peaks per revolution, the magnitude of these peaks is larger than for 3 bladed ones[1]. Besides this, propellers with more blades allow for a more stable flight. For this reason, 3 blades is considered to be an option that delivers well-balanced performance when it comes to stability, efficiency and noise[2], which are all important factors for this design. It was not chosen to implement even more blades, since this would increase weight to a level deemed not worth the benefit in performance. An illustration of the final design can be found in the technical drawings of Figure 9.3.

6.1.2. Determining optimal cruise speed

Since a dominant component of the total mass of the vehicle will be the battery, an analysis should be performed to minimise its mass, while still fulfilling all requirements. The main independent parameter that decides the battery mass is the cruise speed. The higher the cruise speed, the higher the power required (after a certain velocity). However, flying faster also means that this power is supplied for a shorter time, reducing the total energy required for flight. This implies that somewhere in the range of possible cruise speeds, there is an optimal speed to be found.

Since the contra-rotating propeller option has been dropped as explained in Section 6.1.1, the new propulsion system can be described as follows: 8 main propellers of 2.4 m diameter (4 above and 4 below the fuselage). The method used up to this point for finding the power required during cruise was using the equation (6.1):

$$P_{req,cruise} = T \cdot V_{\infty\perp} + \kappa \cdot T \left(-\frac{V_{\infty\perp}}{2} + \sqrt{\frac{V_{\infty\perp}^2}{4} + \frac{T}{2 \cdot \rho_\infty \cdot A_{\text{disk}}}} \right) \tag{6.1}$$

With this P_{req} estimate, along with other assumptions stated earlier about cruise speed, range and take-off & landing parameters, an estimate for battery weight can be made. The results of this can be plotted for a range of cruise speeds to see what the theoretical optimal speed will be. Cruise speeds from 80 to 250 km/hr were considered. The result can be seen in Figure 6.1.

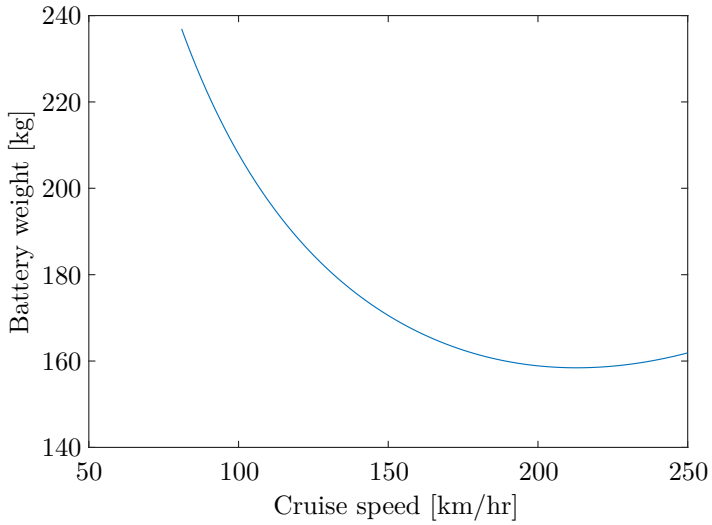

Figure 6.1: Cruise speed vs battery weight

The figure suggests that the optimal speed lies just above 200 km/hr, however, since equation (6.1) was derived based on momentum theory where drag is not explicitly taken into account **cruiseProtor**, it was decided to also analyse the power required based on a different approach which is more based on drag.

The method used was taken from **HeliPower**, and it divides the drag experienced by the aircraft in 3 contributors: induced drag, profile drag and parasite drag. The induced drag is caused by the tip vortices of the rotor blades inducing a downwash of the flow behind them. This causes the effective airflow to be pointed slightly down, which means that the lift vector is tilted a bit more to the rear. The component of this lift to the back

[1] *https://hartzellprop.com/are-more-propeller-blades-better/[Cited 30/05/2022]*

[2] *https://dronesgator.com/how-many-blades-for-a-drone-propeller/#:~:text=2%20blades%20are%20best%20for,since%20they%20provide%20a%20balance.[Cited 30/05/2022]*

is the induced drag. This drag actually decreases when flight speed increases. The power required to overcome this drag can be calculated by first calculating the induced drag power coefficient C_{P_i}:

$$C_{P_i} = \frac{\kappa C_T}{2 \cdot \mu} \tag{6.2}$$

where $\kappa = 1.15$**HeliPower** and C_T and μ are calculated as seen below:

$$C_T = \frac{T}{\rho A_{disk}(\Omega R)^2} \tag{6.3}$$

$$\mu = \frac{V_{cruise}}{\Omega \cdot R} \tag{6.4}$$

This coefficient is then multiplied by a factor of $\rho A \cdot (\Omega R)^3$ to obtain the actual power required. This factor can be seen as a 'dimensionalising' factor that yields an actual P_{req} value in W as opposed to having a coefficient**HeliPower**. This factor is also used to obtain the P_{req} values from the other drag coefficients, which are explained below.

The profile drag is related to the drag that the rotor blades create, in the same way that airfoils of wings do. The profile drag coefficient is obtained using the following relation:

$$C_{P_0} = \frac{\sigma C_{d_0}}{8} \cdot (1 + K\mu^2) \tag{6.5}$$

Where K can be set at 4.65 for forward flight**HeliPower** and σ is the solidity, the ratio between the actual blades' surface area and the disk area, or:

$$\sigma = \frac{N_{\text{blades}} \cdot R_{\text{blade}} c_{\text{blades}}}{\pi R^2_{\text{blade}}}$$

The chord length was assumed to be 20 cm since most similar vehicles have length to chord ratios of around 5-6. The C_{d_0} was assumed to be 0.008.

Finally, the parasitic power, required to overcome effects of viscous shear and pressure drag, was analysed. The parasitic drag coefficient is calculated by means of the following equation:

$$C_{P_P} = \frac{1}{2} \cdot \left(\frac{f}{A_{\text{disk}}} \right) \cdot \mu^3 \tag{6.6}$$

where f is known as the equivalent wetted area and is calculated with $\sum C_{D_f} \cdot S_{ref}$, or the drag coefficient of each component's surface times its surface area.

Component	**Drag area (f)**
Landing gear	0.02 m^2
Fuselage and beams	1.16 m^2

Table 6.1: Components of the vehicle with their parasitic drag areas

The final results of P_{req} is then the summation of all of these components. This result is still final, since efficiencies and redundancies have not been taken into account. Due to REQ-HL-12 it must be divided by 0.75, and several efficiencies must be taken into account. What effiencies have been taken into account and their values can be found in Table 6.2.

Table 6.2: Efficiencies of different components **efficiencies**

Component	**Value**
Rotor	0.8 **rotorEFF**
Electric motor	0.95
Power transfer	0.97
Battery	0.95

As stated, these coefficients are then multiplied with the dimensionalising factor seen above to obtain actual values. The total sum is the required power during cruise. In Section 6.2 it is explained how the battery mass is obtained based on these P_{req} estimates. The new cruise speed vs battery weight curve is shown in Figure 6.2.

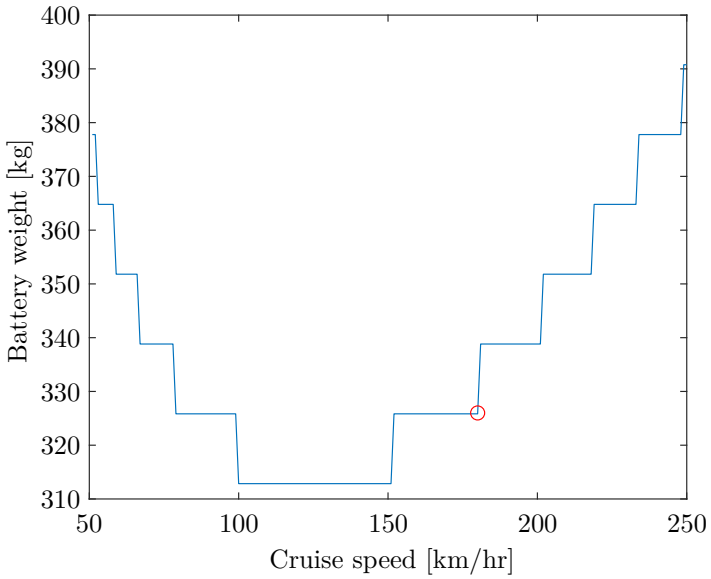

Figure 6.2: Cruise speed vs battery weight new method

Note: the large differences between the 2 plots can be explained as follows: Figure 6.2 was generated with more recent weight estimates (≈930 kg *as opposed to the ≈600* kg *used for Figure 6.1), an updated P_{req} method and an updated battery mass algorithm based on P_{req}, which explains the fact that it is a discontinuous graph (see Section 6.2.2)*

This method suggests that the optimal cruise speed lies in the 100-150 km/hr region, however it is also important to take depth of discharge into account. The weight saved by taking a low cruise speed is around 13 kg (4.0%), while the required depth of discharge of the cruise battery decreases from 91% to 55.3% when V_{cr} is increased from 130 km/hr to 180 km/hr. For this reason, a V_{cr} of 180 km/hr is chosen. The EASA does not explicitly state any speed limits below a certain altitude, and the FAA has set a speed limit of 200 knots below 2500 ft (≈ 750 m)**FAArules**. 200 knots is approximately equal to 370 km/hr, so the calculated cruise speed fits well within the regulations.

6.1.3. Rotor design

The rotor sizing in Section 6.1.1 and the calculation of the final value for the maximum take-off weight allows for the in-depth design of the rotors. The optimal blade geometry with regard to airfoil shape, linear twist and tip angle is calculated first, after which the rotational velocity in RPM is calculated for each stage of flight during normal operations.

The airfoil used for the final design is the NACA 23012 airfoil, and was chosen based on the analysis by Prouty **prouty1995helicopter**. This analysis firstly shows that this airfoil has a high lift coefficient for low Mach numbers. As the final design should produce as little noise as possible, the rotational velocity and thus the tip Mach number of the rotors are expected to be small. This is thus a beneficial property for this vehicle. Secondly, the NACA 23012 airfoil has a pitching moment coefficient close to 0 for most angles of attack. As the magnitude of this coefficient is usually high for cambered airfoils, they are not often used in rotors. However, the forward camber of the NACA 23012 airfoil resolves this problem, especially at the low Mach numbers at which the final rotor is expected to rotate. This is beneficial, as high pitching moments can cause the blade to twist unexpectedly, sometimes with catastrophic consequences.

The linear twist and the tip pitch angle are also determined using theory presented by Prouty **prouty1995helicopter**. The calculation is based on the imperial system. The linear twist and tip pitch angle were decided to be optimised for take-off conditions, as this flight stage requires far more power than cruise, and is closest to the ground, which means it has a big impact on the noise levels as observed by the public. Linear twist in this report is defined as the twist from the start of the effective part of the rotor blade to the tip. The effective rotor blade starts at 19 cm from the centre of the tip, which is the hub radius plus a value of 9 cm, taken from reference rotor designs. The first step in the calculation is to determine the thrust coefficient based on effective blade area:

$$C_T/\sigma = \frac{T}{\rho A_b (\Omega R_t)^2} \tag{6.7}$$

Where T is the thrust per rotor lbf, ρ is the air density at sea level slug/ft^3, A_b is the effective blade area, Ω is the angular velocity in rad/s, and R is the tip radius of the rotor in ft. The tip pitch angle θ_t is then calculated as follows:

$$\theta_t = 57.3\left(\frac{4}{a_s}C_T/\sigma + \sqrt{\frac{\sigma C_T/\sigma}{2}}\right)\mathrm{deg} \tag{6.8}$$

Here, a_s is the speed of sound ft/s and σ is the ratio of the blade area over the total disk area of the rotor A_b/A_disk. The optimal pitch angle at the tip of the blade for take-off was found to be 10 degrees.

A program was written to iterate the required RPM over several values of linear twist of the rotor blades, given the optimal tip pitch angle. This iteration was performed using the blade element theory. For each considered value of the linear twist, the local pitch angle at each blade element was calculated as follows:

$$\theta_\mathrm{local} = \theta_t - \frac{1 - R_\mathrm{eff}}{R_\mathrm{eff}}\theta_l \tag{6.9}$$

Where R_eff is the effective blade radius in m, as described previously in this section. The angle of attack per blade element is then:

$$\alpha_\mathrm{local} = \theta_\mathrm{local} - \tan^{-1}\left(\frac{V_{\infty,z} + V_i}{V_b}\right) \tag{6.10}$$

Here, $V_{\infty,z}$ is the vertical component of the free-stream velocity in ft/s, V_b is the local velocity of the blade element due to the rotational velocity of the rotor in ft/s, and V_i is the induced velocity in ft/s, calculated by:

$$V_i = \sqrt{\frac{T}{2\rho\pi R_t^2}} \tag{6.11}$$

The calculated value of α_local can be used to find the lift coefficient of the considered blade element. For this, the lift curve of the NACA 23012 is used as presented by Abbott et al. **abbott2012theory**. Using this lift coefficient, the lift produced by the rotor for the given blade geometry is calculated as follows:

$$L = \sum_{i=1}^{n}\left(\frac{1}{2}C_l\rho\left(\sqrt{(V_{\infty,z} + V_i)^2 + V_b^2}\right)^2 c_b\ dr\right)b \tag{6.12}$$

With C_l is the local lift coefficient, c_b is the chord length in ft, dr is the width of the blade element in ft, and b is the number of blades per rotor. This value for the produced lift is compared to the required thrust, and once the RPM is reached for which L exceeds T, this RPM is chosen for the used linear twist. In the end, the rotational velocities for all considered values of the linear twist are compared, and the optimal linear twist for take-off is chosen. Finally, the rotational velocities for landing and cruise are also calculated for this blade geometry.

In order to calculate this performance characteristic for cruise, however, the factor of free stream velocity in x-direction must be added for increased accuracy. This is done by replacing V_b in Equation 6.10 and Equation 6.12 by $V_b + V_{\infty,x}$, and calculating the generated lift for each segment of the rotation of the rotor.

The value of linear twist for which the required RPM during take-off is minimal is -38 deg. Hence, the rotor blade has a pitch angle of 48 deg at the start of the effective part of the blade. For this blade geometry, the rotational velocities required for take-off, landing and cruise are 900 RPM, 900 RPM, and 600 RPM, respectively.

With this information, an overview can be given of the characteristics of the main rotor. The design is shown in Figure 6.3, and the characteristics are presented in Table 6.3.

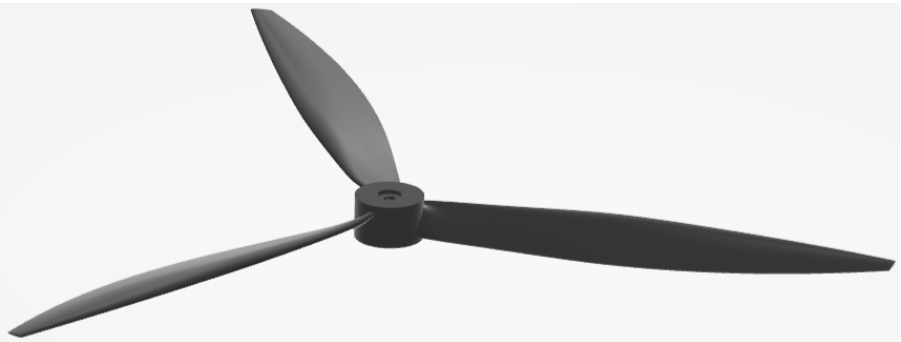

Figure 6.3: Final design of main rotor

Table 6.3: Main rotors characteristics

Characteristic	Value	Unit
Main rotor specifications		
Number of blades per rotor	3	-
Tip radius	1.2	m
Hub radius	0.1	m
Chord length	0.2	m
Effective blade length	1.0	m
Tip pitch angle	10.0	deg
Linear twist of effective blade	-38	deg
Airfoil	NACA 23012	-
Rotational velocity for take-off	900	RPM
Rotational velocity for landing	900	RPM
Rotational velocity for cruise	600	RPM
Cruise power per rotor	11.2	kW
take-off power per rotor	35.9	kW

In the table above, the values for power in the table above represent normal operation conditions. The power required for cruise is taken at its optimal cruise velocity of 180 km/h, whereas the power required for take-off is taken at normal take-off conditions with the corresponding safety factors taken into account, such that a thrust of $T = 1.1 \cdot 1.5MTOWg$ is generated.

The motors, however, were designed for emergency conditions. The requirement REQ-HL-12 states that the vehicle shall provide safe flight with only 75% of the propulsive system active. For the Veatle, this comes down to failure of two of the eight rotors. For each of the eight rotors, the critical case was analysed with regard to which rotor failures would require the rotor in question to use the most power. As this is a very extreme emergency condition, the factor of 1.5 was removed from the required thrust, as the only thing that matters in this case is to land safely as quickly as possible. An overview of the required power per motor is shown in Table 6.4. These powers are calculated by ensuring that enough lift is still produced to counteract the gravitational force, while making sure that the moment around the centre of gravity remains zero.

Table 6.4: Maximum required powers per rotor for emergency conditions

Rotors	Maximum power required per rotor
Front, bottom rotors	40 kW
Front, top rotors	22 kW
Back rotors	32 kW

To conserve the rotational momentum, the direction in which the rotors spin must be kept in mind. It is possible to have the directions perfectly mirrored with respect to the symmetry plane, or to have the same amount of clockwise spinning rotors as counter-clockwise spinning rotors on each side of the symmetry plane. For reasons of noise generation, it is not desired to have two adjacent rotors spinning in the same direction, as vortices would be projected onto incoming rotor blades. For this reason, the latter of the options mentioned before will be chosen. This applies for the top and bottom rotors. The direction of the top and bottom rotors with respect to each other is another point of debate. Since the space between both levels is ≈ 1.4 m, the beneficial effect of contra rotating rotors is not present any more. Once more, to reduce the effects of vortices being 'thrown' onto other rotor blades (vortices that move downwards relative to the vehicle), each lower rotor will spin in the same direction as the one located above it. This results in the configuration seen in Figure 6.4.

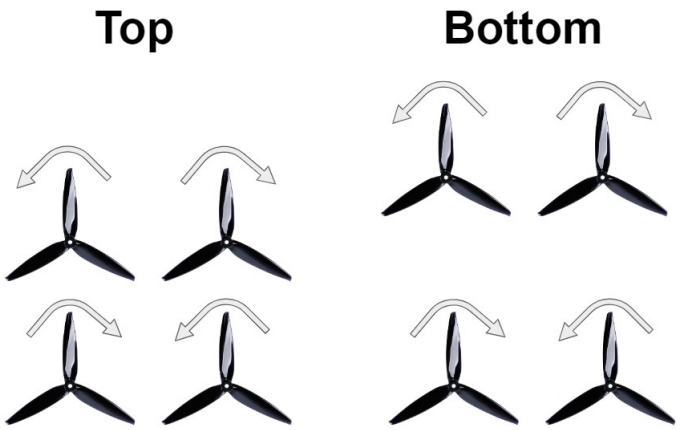

Figure 6.4: Spinning direction of rotors

6.1.4. Noise analysis

Following the final design of the rotor blades and the calculation of the required power during normal operations, a calculation can be made of the noise produced by the vehicle. These calculations are necessary to show compliance with several requirements, and to ensure that the noise levels are low enough for public acceptance of the Veatle. The noise produced by a rotorcraft can be roughly divided into three categories: blade slap, rotational noise and vortex noise.

Blade slap noise

Blade slap is said to occur either due to high Mach numbers at the blade tips, stall occurring at parts of the blade, or vortex interactions **brown2018vehicle leverton1966helicopter**. Blade slap due to shock waves is non-existent for the Veatle as the rotors are designed specifically for low Mach numbers at the tips.

Blade slap due to stall could be an issue, as some parts of the rotor blades stall during cruise. This can be seen in the lift distribution graph in Figure 6.5.

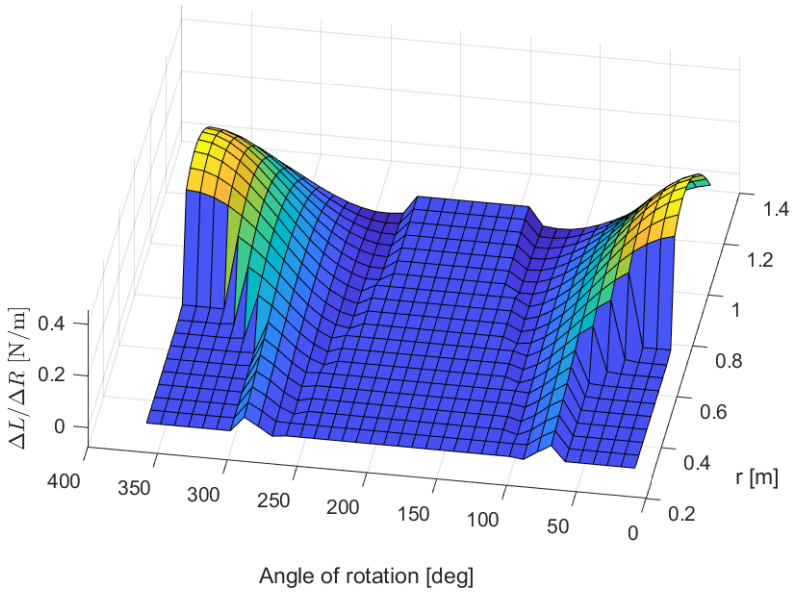

Figure 6.5: Visualisation of the lift distribution over the blade at several angles of the rotor rotation

The large part of the rotor disk where stall occurs is due to the low rotational velocity of the rotor blades in combination with the high cruise velocity, and due to the fact that the rotors are designed for take-off conditions as mentioned previously in this section. A lower linear twist of the rotors would yield a more evenly distributed lift along the rotor blade. Numerical models are still to be presented for the exact calculation of this form of noise production, which makes an accurate analysis of this type of blade slap impossible at this moment.

As the lift distribution over the blades for take-off and landing does not suffer from the high cruise velocity, there is little to no stall in these flight phases. In Figure 6.6, the distribution of the lift over each rotor blade is shown per rotational velocity. For both take-off and landing, shown in Figure 6.6a and Figure 6.6b respectively, stall starts occurring at 1150 RPM. This stall is the result of an increasing horizontal velocity component of the blade elements, in combination with a high pitch angle at the start of the blade. This RPM value is also above the required value for take-off and landing, which is at 900 RPM for both flight phases. The difference in velocity in z-direction between take-off and landing does not have a significant effect on its stalling characteristics, according to the shown lift distribution.

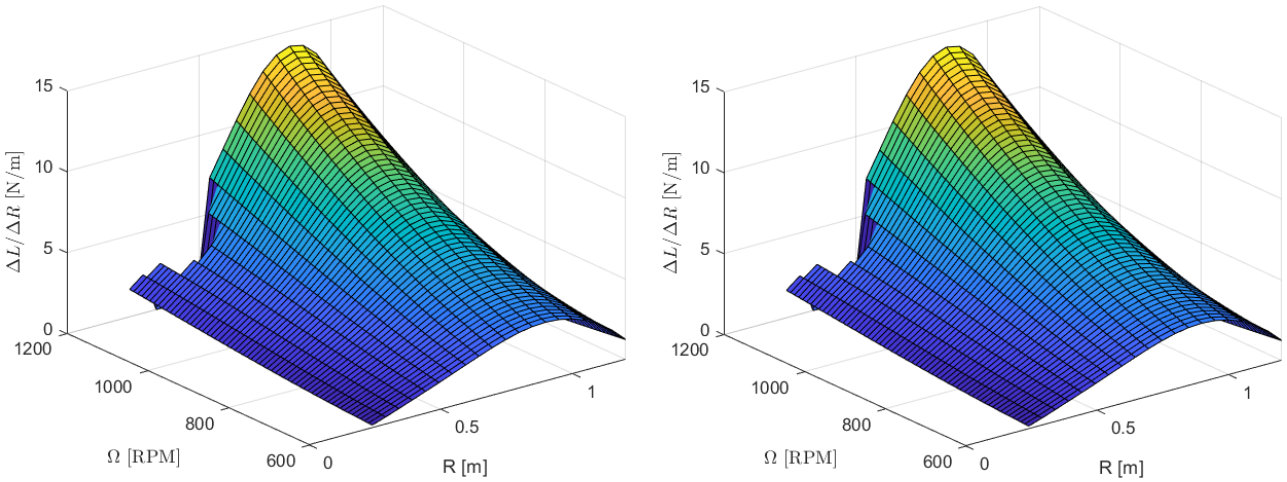

(a) Lift distribution for take-off.

(b) Lift distribution for landing.

Figure 6.6: Distribution of lift over the rotor blade for different stages of normal operation

The final form of blade slap, namely due to blade-vortex interactions, is also expected to be a problem that should be further investigated. The rotors are turning in an optimal direction relatively to the surrounding rotors to minimise this form of noise production, as described Section 6.1.3, but it is still expected to be present. Again, it is hard to quantify the contribution of this type of blade slap through calculations. To research the impact of this noise to the overall noise spectrum, tests must be run with several rotors in the same configuration as in the final design of the Veatle. Only then can an accurate analysis be made of the effect of the blade-vortex interactions of a rotor in its own wake, and in the wake of the surrounding rotors. Therefore, this type of blade slap is also not taken into account in the numerical analysis of the noise spectrum of the Veatle.

As calculations on the effect of blade slap are difficult to perform, it is advised that tests are run specifically for the effect of blade slap on the sound pressure level of the Veatle. For the blade slap due to stall, the rotor of the Veatle should be placed in a wind tunnel while rotating around its axis. The increase of the sound pressure level with regard to the calculated value will mostly be due to this form of blade slap, which can then be calculated. The effect of the configuration of rotors as shown in Figure 6.4 on the sound pressure level should also be tested, to assert the effect of blade slap due to blade-vortex interactions.

Rotational noise

The rotational noise, contrary to blade slap, is quantifiable through numerical analysis. The rotational noise can be calculated with the following sequence of equations, taken from **brown2018vehicle**. Rotational noise can be divided into two components: loading noise and thickness noise. These are caused by thrust generation and finite blade thickness, respectively. The pressures that cause these noises are shown in Equation 6.13 for loading noise, and Equation 6.14 for thickness noise.

$$p_{mL} = \frac{mb\Omega}{2\sqrt{2}\pi a(\Delta S)}\left(T\cos\theta_{\text{obs}} - Q\frac{a_s}{\Omega R_{\text{eff}}^2}\right)J_{mb}\left(\frac{mb\Omega}{a_s}R_{\text{eff}}\sin\theta_{\text{obs}}\right) \tag{6.13}$$

$$p_{mT} = \frac{-\rho(mb\Omega)^2 B}{3\sqrt{2}\pi(\Delta S)}c_b t_b R_{\text{eff}} J_{mb}\left(\frac{mb\Omega}{a_s}R_{\text{eff}}\sin\theta_{\text{obs}}\right) \tag{6.14}$$

In these equations, m is the harmonic number, b the number of blades per rotor, Ω the angular velocity in rad/s, a_s the speed of sound in m/s, T the thrust in N, Q the torque in N/m, R_{eff} the effective blade radius in m, θ_{obs} the angle from the negative z-axis to the observer in rad, ρ the air density in kg/m^3, ΔS the distance from the vehicle to the observer in m, c_b the blade chord length, t_b the blade thickness, and J_{mB} a Bessel function of the

order mB. With these sound pressures, the total sound pressure level due to rotor rotation can be calculated as follows:

$$SPL_r = 10\log_{10}\left(N\frac{p_{mL}^2 + p_{mT}^2}{p_{\text{ref}}^2}\right) \tag{6.15}$$

Where N is the number of rotors, and p_{ref} is the reference pressure level, defined as $2 \cdot 10^5$Pa.

Vortex noise

The final way in which sound is generated is through vortices. The sound pressure level for this manner of noise production is:

$$SPL_v = 20\log_{10}\left(K_2\frac{R\Omega}{\rho(\Delta S)}\sqrt{\frac{NT}{s}\frac{T}{A_{\text{disk}}}}\right) \tag{6.16}$$

K_2 is a constant defined as $0.426\text{s}^3/\text{m}^3$.

A-weighting factor

The final factor that should be taken into account for the noise analysis is the A-weighting factor, as described by Clarke et al. in **clarke2021evaluating**. This factor is applied to take the perception of noise by the human ear into account, and can be calculated through the following two equations:

$$\begin{aligned} R_A(f) &= \frac{12194^2 f^4}{(f^2+20.6^2)\sqrt{(f^2+107.7^2)(f^2+737.9^2)}(f^2+12194^2} \\ A(f) &= 20\log_{10}(R_A(f)) - 20\log_{10}(R_A(1000)) \end{aligned} \tag{6.17}$$

Where f is the frequency of the rotor rotation, calculated by:

$$f = 2\pi m\Omega b \tag{6.18}$$

The A-weighting factor is added to the individually calculated SPL_r for each harmonic, and to SPL_v. The total sound pressure level of the vehicle then becomes:

$$SPL_{\text{tot}} = 10\log_{10}\left(10^{\frac{SPL_v+A(f)}{10}} + \sum_{m=1}^{20} 10^{\frac{SPL_r(m)+A(f)}{10}}\right) \tag{6.19}$$

Both the calculation of the rotational noise and the A-weighting factor take the first twenty harmonics into account, in order to get a complete overview of the noise spectrum produced by the vehicle. The first three harmonics have positive A-weighting factors, which is not desired as it increases the noise as perceived by people.

The calculations described in this section yield the results as presented in Table 6.5. The noise is analysed at two positions for observers. One is directly under the vehicle at its cruise altitude, which is 450 m. The other position is at an angle of 45 deg with respect to the vehicle's positive z-axis (straight into the ground) at a height of 50 m.

Table 6.5: Noise observed at certain distances and angles from the Veatle

Flight phase	**Distance to observer** m	**Angle to observer** deg	**Sound pressure level** dBA
Cruise	450	0	51
Take-off	50	45	68

The presented sound exposure levels are similar to those of classroom chatter and urban environment noise for take-off and cruise, respectively [3]. These results are promising, as the most critical case does not exceed harmful noise levels, and the noise produced during cruise is at the same level as normal urban background noise.

6.1.5. Control propeller detailed design

Control propellers are distributed throughout the fuselage of the vehicle. Their key function is to provide sufficiently high control forces in extremely short periods of time in order to maintain the desired attitude and stay within 1 m of the nominal trajectory (see **REQ-HL-03**).
The propeller must be able to provide control thrust in both directions. As a result, a variable pitch propeller with 0 twist shall be used. Due to high thrust that needs to be generated in combination with very low disk

[3] *https://www.osha.gov/otm[Cited 13/06/2022]*

area of the propeller, the induced velocity in the rotor plane will achieve high values. The actual velocity through the plane will be a combination of the induced velocity due to thrust plus the gust velocity, see Equation 6.20 **prouty1995helicopter**. This will change the effective angle of attack on the rotor blade element by $\phi = \arctan\left(V_i/\Omega r\right)$, as can be seen from Equation 6.21.

$$V_i = V_{gust} + \sqrt{\frac{T}{2\rho A}} \tag{6.20}$$

$$\alpha_{eff} = \theta_c - \arctan\left(V_i/\Omega r\right) \tag{6.21}$$

This significantly complicates the design of the rotor by analytical methods, thus a blade-element method (BEM) code was written, which will predict the lift and torque of the propeller. A NACA 0012 airfoil is used, and the following equations serve as the foundation for the code **prouty1995helicopter**:

$$L = b\frac{\rho}{2}\int_{R_{\text{root}}}^{R_{\text{tip}}} c\left(r\right)\left(\Omega r\right)^2 C_l\left(\alpha_{\text{eff}}\right) dr \tag{6.22}$$

$$Q = b\frac{\rho}{2}\int_{R_{\text{root}}}^{R_{\text{tip}}} c(r)\left(\Omega r\right)^2 \left[C_l(\alpha_{\text{eff}})\phi + C_d(\alpha_{\text{eff}})\right] dr \tag{6.23}$$

Where L is the total lift produced by the propeller and Q is the total torque exerted on it. Power required is then simply $P_{\text{req}} = \Omega Q$. It was found that at low values of radial distance r the effective angle of attack α_{eff} would reach negative values, producing negative lift. This is due to the large values of induced velocity at the rotor plane. As a mitigation measure, R_{root} value is chosen to be approximately half of R_{tip} to eliminate this undesired effect. In order to sustain the low reaction time of this system, the rotor will be continuously spinning at $\theta_c = 0°$ pitch setting throughout the flight. When there is a gust coming and a reaction force is needed, the variable collective pitch system changes the pitch angle to a needed negative or positive value. At the same time, the main motor provides higher power in order to sustain the surge in power required due to an increase in both α_{eff} and ϕ during the gust duration, see Equation 6.1.5. Because for the most part of the cruise, the propeller power will only be limited to the profile drag from the airfoil $C_d(0)$ for such a small diameter, its impact on the total battery budget is confirmed to be negligible. For the finalized design, the power consumption in cruise when no control force F_c is needed is only 2.4 kW. The design of control propellers is inspired by the Airbus Helicopters' Fenestron system, which allows for a greater performance at smaller diameter and reduces the noise[4].

A new actuator model is proposed in order to move most of the driving elements of the control propeller in the fuselage and keep the propeller section relatively clean for aerodynamic and visual reasons. The main motor will be housed inside the fuselage and connected to the propeller via a gear system, labelled in orange, see Table 6.8. On the other side of the propeller, a small control motor will be connected to a magnetic gear, (cyan and blue), which allows exerting a moment on the gear inside the propeller hub (blue gear) without the physical connection. The blue gear will then adjust the collective propeller pitch as needed. Of course, if this mechanism doesn't prove to be feasible, an existing collective pitch control mechanism can be taken from the helicopter tail rotors.

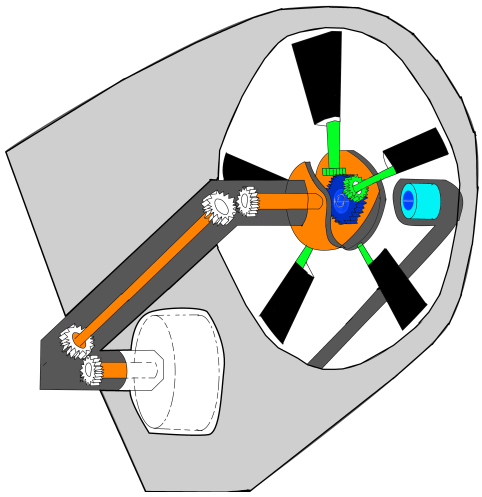

Figure 6.7: Control propeller actuator mechanism

During the design, it was found that the control propeller needs to produce approx. 300-350 N per rotor to counteract the most critical gusts. This has led to the propeller design with the specifications found in Table 6.6.

[4] *https://www.airbus.com/en/newsroom/press-releases/2018-04-50th-anniversary-of-the-trademark-fenestron[Cited 31/05/2022]*

Table 6.6: Control propeller characteristics

Control Propeller Specifications	
Chord	5 cm
Root radius	10 cm
Tip radius	20 cm
Hub radius	20.5 cm
Chord length	5 cm
Hub length	5 cm
Airfoil	NACA 0012
RPM	10000
P_{cruise}	2.4 kW
P_{gust}	31.8 kW
T_{max}	473 N
$\theta_{T_{\text{max}}}$	27 deg

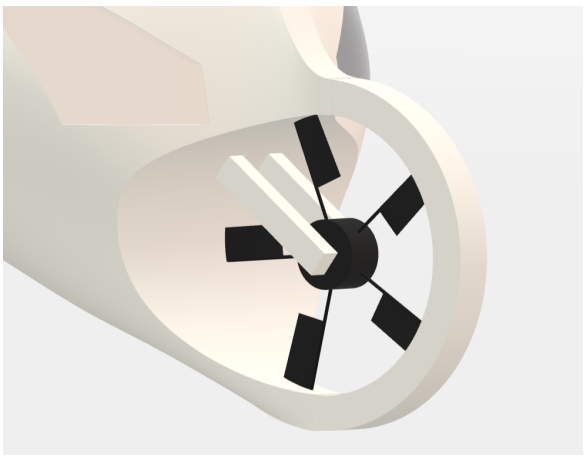

Figure 6.8: CAD drawing of the control propeller

6.2. Power storage and distribution

This section describes how the initial sizing of the battery performed in Section 6.2.1, together with how the battery type was selected. The more detailed sizing is displayed Section 6.2.2, in which the exact battery layout is generated. Finally, Section 6.2.3 explains how the temperatures are kept at an acceptable level.

6.2.1. Required capacity

The battery weight can be estimated based on the energy required, which in turn is estimated by evaluating the power required per flight stage and the duration of these stages. When assuming a take-off height, vertical speed, cruise range and cruise speed, the total energy can be calculated. In this case, the take-off height was set at 450 m, such that the aircraft does not fly in between buildings during cruise. As the vertical flight phases are the most power-intensive, it is desired to reach cruise altitude quickly, however the assumption must be taken cautiously, as drag effects are ignored for the vertical flight analysis. Reaching 450 m in 1 minute would mean a required vertical speed of 7.5 m/s, and taking acceleration and deceleration roughly into account, a vertical speed of 6 m/s was assumed. In most cases, the cruise phase can start at much lower altitudes, but the vehicle is designed for the worst case scenario where the 450 m vertical flight is necessary before starting cruise.

Cruise speed was assumed to be 180 km/hr as explained in Section 6.1.2, while cruise range was assumed to be 20 km, plus an additional 5 km diversion range. All necessary parameters are now known to estimate the required energy for the batteries. This quantity decides the weight that a battery will have to meet a certain energy requirement. A high specific energy is desired and should be the main criterion for battery selection, along with cycle life. It is widely known that with readily available technology, Li-ion batteries are the best option for 'low weight' energy storage. Furthermore, they are able to provide high amounts of power, are maintenance free and do not demonstrate the memory effect[5].

There are other types of batteries that have a better specific energy than Li-ion, such as so called 'solid-state' batteries, often also making use of Lithium. These batteries can also perform better on voltage and safety[6] and thus seem like the best option. However, at this point, the technology readiness level is simply too low to implement this battery type in an aircraft. This battery type still has not been fully mastered yet, and they often display chemically unstable behaviour, which is not tolerable for aircraft. Once this technology is sufficiently developed, it will undoubtedly outperform Li-ion batteries.

Another technology that is worth considering is the so called 'Licerion' batteries, developed by a company called Sion Power. The company describes it as a "hybrid between today's lithium-ion and tomorrow's solid-

[5] *https://www.cei.washington.edu/education/science-of-solar/battery-technology/[Cited 31/05/2022]*

[6] *https://cosmosmagazine.com/technology/energy/are-solid-state-batteries-safer-than-lithium-ion/#:~:text=The%20key%20difference%20is%20what,efficient%20than%20normal%20lithium%20batteries.[Cited 31/05/2022]*

state batteries.[7]" They state that for aerospace applications the battery can achieve a specific energy of 490 Wh/kg and that the batteries are readily available. Additionally, they state that battery packs with integrated safety features are available and that they have tested it to 2500 cycles, where it maintained 70% of its capacity[8]. However, none of these statistics have been verified by an independent party, and the company stated in 2018 that they would start production at the end of that year[7], but this still has not happened for undisclosed reasons. Besides this, the performance the company promises would make every electric car manufacturer want to use Licerion cells, but still not one real life application has been shown. For these reasons, this battery was not deemed a viable option.

It was decided to stick with the Li-ion battery option, more specifically the NMC type as opposed to LFP type. This option was chosen since it offers superior energy density and does not have any major drawbacks compared to other types[9].

6.2.2. Sizing and weight

The required power output of the battery system is sized for emergency conditions. For this, the power for cruise is divided by a factor of 0.75 to account for two of the eight propellers failing. During take-off and landing, the aircraft then demands the highest power output, which is approximately 385 kW. This figure is comparable to the power output of the Porsche Taycan 4 (350 kW), which is a fully electric car by Porsche that has proven to possess a well working and reliable battery system. Through sophisticated thermal management, the battery operates at a voltage of 800 V. A higher voltage is beneficial for charging time and for power delivery, so even though many electric car batteries run at 400 V, the Veatle battery will operate at 800 V like the Taycan (723 V nominal[10]). Using the fact that $P = U \cdot I$, the calculated current required is 532.9 A. Since the power required during take-off is so much higher than for cruise, it was decided to split the battery into 2 packs: one for cruise and one for take-off and landing. The cells for take-off were selected by prioritising the discharge current and low weight. The best option was found to be the Sony VTC5A 18650 Battery. For cruise, the current was given slightly less priority, and the best option was found to be the Sony VTC6 18650. Some key parameters of both cells can be found in Table 6.7.

Table 6.7: Battery cell parameters

	VTC6 18650 (cruise)	**VTC5A 18650 (take-off)**
Nominal voltage	3.6 V	3.6 V
Max. continuous discharge current	20 A	35 A
Max. energy stored	10.8 Wh	9.36 Wh
Max. discharge power	72 W	126 W
Weight	45.5 g	48.6 g

To meet the voltage requirement, $723/3.6 \approx 201$ (rounded up) cells are needed in series. The current needed is obtained by dividing P_{req} (per phase) by the (nominal) voltage and then dividing it by the max continuous discharge current. This way, the necessary amount of cells in parallel and in series can be calculated for each pack. To take into account the mass of the battery management system, cooling systems and wiring, the mass of the cells alone should be multiplied by a factor of roughly 1.42 **celltopack** to obtain a mass estimate. The results are displayed in Table 6.8. Note that no extra redundancies/safety factors were used in these calculations, since efficiencies, safety factors and DoD have already been taken into account for the P_{req} estimations.

Table 6.8: Battery pack parameters

	Cruise battery	**Take-off battery**
#Cells in series	201	201
#Cells in parallel	8	16
Total nr. of cells	1608	3216
Capacity	17.4 kWh	30.1 kWh
Weight	103.9 kg	221.9 kg
DoD	0.55	0.40

[7] *https://sionpower.com/files/Company-Brochure-21B.pdf[Cited 31/05/2022]*

[8] *https://www.autoevolution.com/news/sion-power-s-promising-licerion-cells-reach-more-than-2500-cycles-183652.html[Cited 31/05/2022]*

[9] *https://lghomebatteryblog.eu/en/this-is-why-ncm-is-the-preferable-cathode-material-for-li-ion-batteries/#comparison[Cited 02/06/2022]*

[10] *https://jalopnik.com/an-extremely-detailed-look-at-the-porsche-taycans-engin-1837802533[Cited 02/06/2022]*

The battery packs will be divided into modules for safety and redundancy purposes. Both batteries will be divided into 8 modules wired in series. The cruise battery will have 7 modules in 25s8p (25 cells in series, 8 in parallel) configuration, and 1 module with 1 extra cell wired in series per channel (26s8p). The take-off battery will have 7 25s16p modules and 1 26s16p module. This way, each battery produces the required amount of voltage and current. Each module will also have a bypass channel such that current can keep flowing through the rest of the modules in case of failure for one of the modules.

The volumetric energy density (in Wh/L) of Li-ion batteries is currently around 450 [Wh/L][11], which gives a volume estimate of 105.5 L.

Aside from the main batteries, there will also be a very small auxiliary battery present to keep systems such as the flight computer, infotainment system and GPS system active during battery swapping. This is done to avoid the need for a complete vehicle reboot every battery swap. This battery will be recharged when the main battery is in place again. The desired capacity was estimated to be comparable to a high performance laptop battery. The chosen battery was the MacBook Pro 14 battery (95 Wh). The weight is negligible compared to the main battery's weight. The Apple A1494 battery[12] is a Li-Po battery with a 94.6 Wh capacity, which is considered sufficient.

Performing an accurate estimation of the charge time is rather complicated since it depends on many factors like charge level (a battery charges faster at 50% charge level than 95% for example), depth of discharge and temperature. As stated, the battery voltage was set high to reduce charging time. The Porsche Taycan battery can be charged from 5% to 80% in 22.5 minutes[13], and since the DoD of the worst case mission is only around 50%, charging is not expected to take more than 30 minutes.

6.2.3. Thermal management

When discharging, it is inevitable that heat is generated by the batteries. This can lead to a decrease in performance or even failure and/or fires. The desired cooling option would be air cooling, since this is the most lightweight option. The heat power generated per cell is equal to $I^2 \cdot R$, where R is the resistance in Ω, calculated with $R = \frac{U}{I}$ (U is the voltage in V). The total heat power generated is then a summation of this value over all cells in the battery. Take-off is once again the critical case since the mass flow of air is lower while I is higher. The heat power that can be taken away by air can be calculated as follows:

$$P = \dot{m} \cdot C_H \cdot \Delta Temp \tag{6.24}$$

Assuming an air temperature of 20°C, $\Delta Temp$ can be set at 40K since the maximum working temperature of the cells is 60°C. C_H of air is 1005J/kgK [14], $\dot{m} = \rho \cdot A \cdot V$, where V is the speed of the airflow. Because the battery will be placed in the structure directly below the rear rotors, the airflow will be greatly accelerated to $2 \cdot V_{ind} + V_{TO}$ [15] (see Section 6.1.3 for a definition of V_{ind}). The necessary inlet area for complete air cooling of the battery is then calculated to be 0.085 m^2. The vents will be placed on the fuselage below the rear main rotors. Required cooling during cruise is much less than during take-off, since heat power scales with the square of I. Additionally, the speed of the airflow around the body is higher than during take-off, so the cooling system is assumed to be sufficient for cruise as well. It must be noted that the V_{ind} assumption has a rather large impact in favour of the design, and one must thus be sceptical. However, several aspects like natural aerodynamic cooling and the ability of heat absorption of the structure are ignored as well. At this point it can not be verified whether any one of these effects is much stronger than the other, however a first analysis suggests that cooling using the airflow will be sufficient. This is most likely due to the high battery voltage, which decreases the required current and thus the generated heat.

[11] https://www.energy.gov/eere/vehicles/articles/fotw-1234-april-18-2022-volumetric-energy-density-lithium-ion-batteries#: :text=In%202008%2C%20lithium%2Dion%20batteries,450%20watt%2Dhours%20per%20liter

[12] *https://www.123accu.nl/Apple-A1494-accu-11-26-V-8400-mAh-123accu-huismerk-i27716.html?mkwid=sD8HZOkok_dc%7Cpcrid%7C452696066597%7Cpkw%7C%7Cpmt%7C%7Cslid%7C%7Cprid%7Cpf_AAP00292_4894128108115_A1494&pgrid=104917626469&ptaid=pla-930691817025&gclid=CjOKCQjwhqaVBhCxARIsAHK1tiMdyNJzQZD_hvD-rdNbbel9OupnpHC1MpkTitV3iX1BEPAO1Yq62GEaAqn8EALw_wcB[Cited 15/06/2022]*

[13] *https://media.porsche.com/mediakit/taycan/en/porsche-taycan/das-laden[Cited 10/06/2022]*

[14] *https://www.ohio.edu/mechanical/thermo/property_tables/air/air_Cp_Cv.html#\protect\protect\leavevmode@ifvmode\kern+.2222em\relax~:textT\char"0304\relaxhe%20nominal%20values%20used%20for,v%20%3D%200.718%20kJ%2Fkg. [Cited 10/06/2022]*

[15] *https://brightspace.tudelft.nl/d2l/le/content/397992/viewContent/2238599/View[Cited 10/06/2022]*

7. Final Control Design

Without a good control system, an autonomous vehicle has no chance of operating safely and properly. Considering the strict requirements on accuracy during flight, the control system is paramount in performing safe and accurate flight within the urban environment. The control was analysed by designing and testing a simulator for two distinct cases: a wind gust and flying past a building wake. First the method behind the simulation is explained in Section 7.1, followed by the results being displayed, analysed and evaluated in Section 7.2.

7.1. The method behind generating the control simulation

This section aims to provide the reader with the knowledge of the workings of the simulator. The simulator may be seen as many interlinked blocks, taking inputs and outputs from other blocks. For ease of understanding, the software block diagram showing the overview of the control simulation is first shown in Figure 7.1, where each block is a simulation module, while the output and inputs are shown by the arrows. The external constant parameters are not given as they are constant throughout the simulation, these parameters are summarised in Table 7.1.

Table 7.1: Values of the constant parameters used.

Constant Parameter	Value [Unit]
Inertia	$\begin{bmatrix} 411.61 & 1.15676 & 33.1961 \\ 0 & 1090.74 & -0.287697 \\ 0 & 0 & 1251.05 \end{bmatrix}$
Mass	941.102 [kg] [1]
Time delay	0.1 [s]
Initial angles	0 [°]
Air density	1.225 $[kg \cdot m^{-3}]$
Geometry	CATIA generated [2]
Maximum control propeller thrust	300 [N]
Maximum top front rotor thrust	5600 [N]
Maximum bottom front rotor thrust	2600 [N]
Maximum top back rotor thrust	3200 [N]
Maximum bottom back rotor thrust	3200 [N]
Aerodynamic interpolants	**fig:force_coeffs**
C_D	1.6 [-]
S_{side}	3.6 $[m^2]$ [3]

For this model, four sensors are simulated, and all give readings in 3 axes: a GPS, accelerometer, gyroscope and a magnetometer. For obstacle avoidance: Radars, LIDARs and cameras are also used, but obstacle avoidance modelling is currently outside the scope of the project. These sensors are first discussed in Section 7.1.1. Following this the wind case is explained in Section 7.1.2; here two options are presented: first a wind gust profile and secondly a wake from the Shard. Afterwards the method behind the aerodynamic module is laid out in Section 7.1.3; where the results from the aerodynamic's body runs are implemented into the model. Followed by the transformation module's explanation in Section 7.1.4. The explanation of the linear dynamics model and its Kalman filter is provided in Section 7.1.5 and Section 7.1.6, respectively. Likewise for the angular model in Section 7.1.7 and Section 7.1.8. Finally, the propulsion module is explained in Section 7.1.9; where the acceleration of the propellers and control allocation of the rotors and propellers is described.

[1] The old mass generated from the first iteration of the CATIA model was used for the simulation.

[2] Several dimensions were given from the geometry, mainly the CATIA reference frame's origin to the centre of mass, and the centre of mass to the propeller's and rotor's centres.

[3] This was a estimate generated in the Midterm.

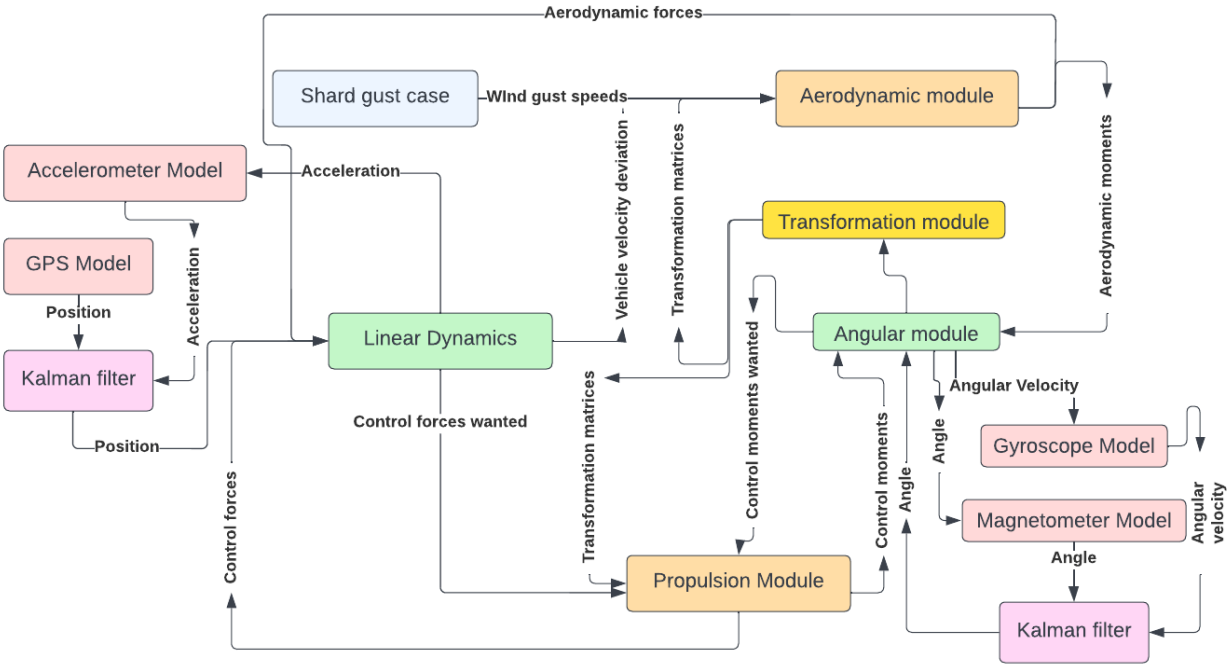

Figure 7.1: Software block diagram for the control simulation.

7.1.1. Sensors used for autonomous flight

The next section elaborates on the sensors used for the autonomous flight of the vehicle. This includes attitude and position determination sensors and sensors that can be used for obstacle avoidance.

Inertial sensors

To measure the attitude and change in attitude of the vehicle, inertial sensors are installed. Two types of inertial sensors are used: a gyroscope and an accelerometer. The gyroscope measures the angular velocities of the vehicle, whereas the accelerometer monitors the translational accelerations. Combining the measurements yields the attitude of the vehicle. For both the sensors, the mechanisms are briefly explained and biases are elaborated on.

Gyroscopes are in essence spinning disks that resist a change in attitude. The rotating object possesses angular momentum which should be conserved. Using these gyroscopic phenomena, the angular velocities of the vehicle can be measured. The vehicle will use CRH02 Gyroscope Silicon Sensing Sensors [4]. A data sheet containing the specifics of this sensor is used to model the sensors in Matlab. To be able to model the sensors in a realistic way, the biases that are introduced need to be included in the Matlab model. Multiple types of bias are considered. Firstly, a bias instability is incorporated, which essentially means how stable the bias is over a specific amount of time. Secondly, the angular random walk is modelled for. This is the bias due to integrating values that also contain a certain bias. The integration can introduce drifts from the real value. Next, a bias due to temperature changes is included. Lastly, the sensor produces noise which is accounted for. The biases and their respective values for the CRH02 Gyroscope are listed in Table 7.2.

Table 7.2: Biases of the gyroscope

Bias	Value
Bias instability	0.12 °/hr
Angular random walk	0.017 °/$\sqrt{\text{hr}}$
Temperature bias	0.25 rad/s
Noise	0.15 rad/s

Accelerometers measure the translational acceleration of the vehicle. The type of accelerometer chosen is the CAS290 dual-axis accelerometer also produced by Silicon Sensing. The linear acceleration sensing is achieved

[4] `https://www.siliconsensing.com/home/`[Cited 14/06/2022]

by the detector forming an orthogonal pair of sprung masses. Each mass provides the moving plate of a variable capacitance. A change in capacitance is then directly related to the acceleration and is measured by demodulation of the square wave excitation. For the accelerometer, also several types of biases are taken into account. These include the bias instability, bias due to temperature changes and bias due to noise of the signal. The biases and their respective values for this type of sensor are listed in Table 7.3.

Table 7.3: Biases of the accelerometer

Bias	Value
Bias instability	7.5 mg
Temperature bias	50 µg
Noise	150 µg

Both inertial sensors are modelled in Matlab. Using IMU simulation models, the biases of the specific types of sensors are included in the model. Eventually, the sensor models are implemented in the six degrees of freedom model to simulate reality. The sensor models take angular velocity and acceleration in x, y and z-directions as input. The output are the same velocities and accelerations, but modelled with the biases and noise.

GPS and magnetometer

For the positioning of the aircraft, the Global Positioning System (GPS) is used. The GPS sensor chosen has an accuracy of approximately 0.3 m. To model the sensor, a normal distribution is created with a standard deviation of 0.15 m. In that way, 95% is in the range between -0.3 m and 0.3 m. A random number of the distribution is added to the x, y and z coordinates of the position. In that way, the inaccuracies are modelled.

To determine the heading of the vehicle, a magnetometer is used. It is assumed that at cruise altitude, the interference of the city is negligible.

This section elaborates upon the obstacle avoidance sensors. These are important to be able to react to unexpected circumstances. These may include another vehicle passing by or flying close to buildings, for instance.

Lidar Lidar sensors operate by transmitting a laser beam and measuring the time it takes for this beam to reflect back to the sensor. Lidar has several advantages over other sensors that can be used for a similar purpose. One of those is that it has a high sampling frequency. This means that the vehicle can very quickly respond to objects that may inflict with its trajectory. A big disadvantage is that the laser beam can reflect on water droplets. Therefore, weather conditions such as rain or fog may negatively affect the readings of this sensor. For the Veatle, Velodyne Puck Lidar sensors are selected for the design. The range of this sensor is 100 m with an accuracy of approximately 0.03 m [5].

Radar Similarly to Lidar sensors, radar sensors also operate by transmitting a signal and measuring the time for the signal to reflect back to the sensor. Unlike Lidar, a radar uses radio waves instead of light waves. The advantage of using radio waves is that it works in any weather condition or lighting condition. This makes it more reliable than the Lidar sensor. However, the accuracy is usually lower. Two main types of radar sensors exist. Namely, an impulse radar sensor and a frequency modulated continuous wave radar. The latter is most commonly used in autonomous vehicles. One big advantage of radar sensors is that they can be used to estimate the velocity of a detected object. Due to the Doppler effect, relative motion of an obstacle can be estimated. For the Veatle, Baumer RR30 radar sensors are used. This type of sensor has a range of 80 m. The linearity error of this sensor is 10 mm and the temperature drift is another 10 mm [6].

In order to increase the safety of the passengers and support the functioning of the vehicle, redundancy of the sensors is built in. For each sensor type, multiple sensors are installed in the vehicle to prevent the vehicle from failing in case of a sensor misfunctioning.

Camera Next to Lidar and radar sensors, the vehicle shall also be equipped with a camera system. A camera system is required to recognize objects. As the Veatle should not come closer than 3 m to buildings and 5 m from humans, making a distinction between humans and other objects is mandatory. Stereo cameras also allow estimating distances and can therefore add to the accuracy of the overall control system.

[5] *https://velodynelidar.com/products/puck/[Cited 14/06/2022]*
[6] *https://www.baumer.com/ca/en/product-overview/distance-measurement/radar-sensors/c/291[Cited 14/06/2022]*

7.1.2. Disturbance simulation environment

To simulate the conditions outside of the vehicle, two cases have been posed. First a generic gust profile taken from literature. Followed by one more aligned with our business case; the wake acting from the Shard building. Both these profiles will be simulated with the control system; in order to validate the vehicle's design.

Primary gust profile During the baseline report, a gust profile was found. It is shown by Equation 7.1 and has a time constant of 10.5 seconds. Figure 7.2 shows this gust profile, giving a maximum speed at 21.4 m/s. The problem with this gust is that it is independent of nominal vehicle speed; so one can't conclude the effect of the vehicle's cruise speed on the controllability of the vehicle. However, it can give a good indication if the design of the vehicle is good enough to meet the requirements.

$$V_{gust}(t) = 12.4 - 4.5 \sin\left(\frac{3\pi t}{\tau}\right)\left(1 - \cos\left(\frac{2\pi t}{\tau}\right)\right) \tag{7.1}$$

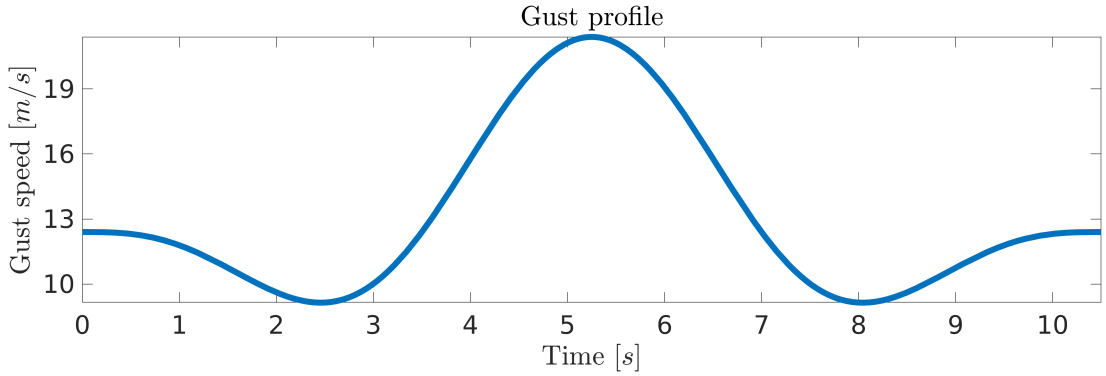

Figure 7.2: Gust profile

Shard gust profile

After the simulation has been run with a primary gust profile, a case more relevant to our business case of London was wanted. As a result, the aerodynamics department simulated the wake behind the Shard building. Then the wind speed was measured behind the building. Furthermore, a vehicle speed of 100 km/hr was taken, so the wind gust could be modelled with respect to time rather than position. Equation 7.2 calculates the velocities of the vehicle in the Shard reference frame. From interpolating the data from the Shard case, one can find the gust speeds at any position. The position is found from the time, by $t = \frac{s}{v}$ (with s as distance).

$$\begin{aligned} m_{gradient} &= \frac{|max(z)| + |min(z)|}{|max(y)| + |min(y)|} \\ \mu_{shard} &= tan^{-1}(m_{gradient}) \\ v_x &= 0 \\ v_y &= |V_{shard}| cos(\mu_{shard}) \\ v_z &= |V_{shard}| sin(\mu_{shard}) \end{aligned} \tag{7.2}$$

After finding the wind speeds in the Shard reference frame, they must be transformed into the vertiport reference frame; this can be done via Equation 7.3. These transformations are developed through the knowledge that the reference frame of the Shard model has X is in the direction of vertiport's Y, Y in the direction of vertiport's X, and Z in the direction of the vertiport's negative Z. The culmination of all these steps within the software is shown in Figure 7.3.

$$\mathbb{T}_{VS} = \begin{bmatrix} cos(\frac{pi}{2}) & -sin(\frac{pi}{2}) & 0 \\ sin(\frac{pi}{2}) & cos(\frac{pi}{2}) & 0 \\ 0 & 0 & 1 \end{bmatrix} \cdot \begin{bmatrix} 1 & 0 & 0 \\ 0 & cos(\pi) & -sin(\pi) \\ 0 & sin(\pi) & cos(\pi) \end{bmatrix} \tag{7.3}$$

The resulting velocity profile from the Shard case is shown in **??**.

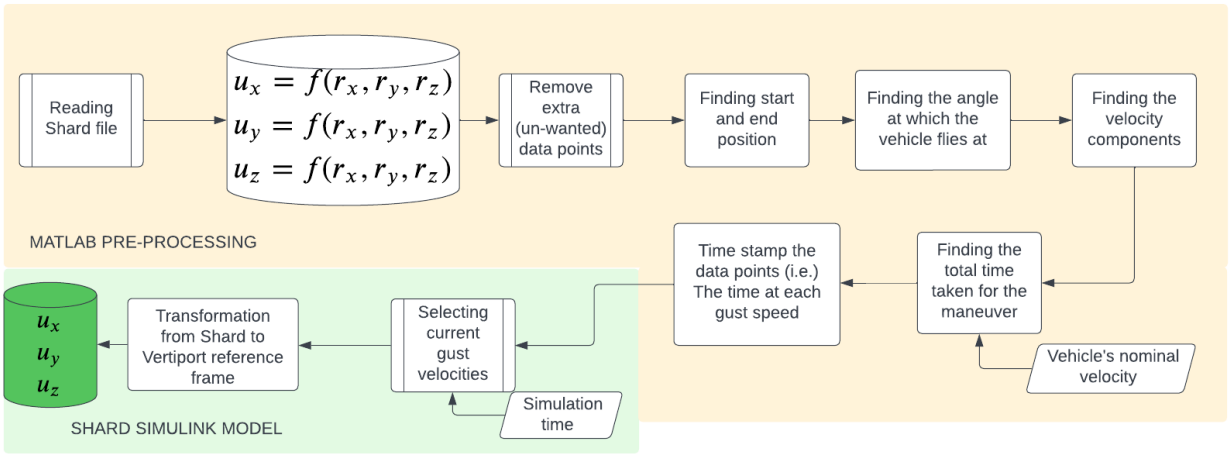

Figure 7.3: The software block diagram for the Shard case.

7.1.3. Aerodynamic module

Two aerodynamic modules were built, first a simple one under the assumptions of uniform sections, and then a more complicated one resulting from CFD. The primary model was used in sizing tests, to give departments a better idea of design parameters including geometry, propulsion types and aerodynamic importance.

Modelling the vehicle's drag.

The first drag model used equation Equation 7.4 to generate the drag acting upon the vehicle. This was a function of the time-delay, density, area, vehicle speed, gust speed and drag coefficients. This model allowed for the importance of design parameters to be estimated, when combined with the later linear dynamic model.

$$F_{side} = F_{control_{t-\tau}} + \frac{1}{2}\rho S_{side} C_D (V_{gust} - V_{side})^2 \tag{7.4}$$

Modelling the vehicle's aerodynamic coefficients

To better understand the vehicles' response to aerodynamic disturbances, and to model it in the angular frame; the aerodynamic coefficients of the vehicle should be taken into the control simulation. Here the aerodynamic department's CFD resulted in force and moment coefficient, however they were provided in the CATIA reference frame, and as such had to be first rotated by 180° around x to align to the body reference frame, also a translation for the forces must be made.

$$\mathbb{T}_{cg-CATIA} = \begin{bmatrix} 1 & 0 & 0 \\ 0 & -1 & 0 \\ 0 & 0 & -1 \end{bmatrix} \tag{7.5}$$

The force and moments can be calculated in the body frame by Equation 7.6. Note that, the second term in the moment equation is due to the forces acting on the CATIA reference frame's origin being translated into moments around the body frame's origin (the centre of mass).

$$\begin{aligned} \begin{bmatrix} F_x \\ F_y \\ F_z \end{bmatrix} &= q \cdot \begin{bmatrix} 1 & 0 & 0 \\ 0 & -1 & 0 \\ 0 & 0 & -1 \end{bmatrix} \cdot \begin{bmatrix} C_X \\ C_Y \\ C_Z \end{bmatrix} \\ \begin{bmatrix} M_x \\ M_y \\ M_z \end{bmatrix} &= q \cdot \begin{bmatrix} 1 & 0 & 0 \\ 0 & -1 & 0 \\ 0 & 0 & -1 \end{bmatrix} \cdot \begin{bmatrix} C_{m_p} \\ C_{m_q} \\ C_{m_r} \end{bmatrix} + \begin{bmatrix} x_{cg-CATIA} \\ y_{cg-CATIA} \\ z_{cg-CATIA} \end{bmatrix} \times \left(q \cdot \begin{bmatrix} 1 & 0 & 0 \\ 0 & -1 & 0 \\ 0 & 0 & -1 \end{bmatrix} \cdot \begin{bmatrix} C_X \\ C_Y \\ C_Z \end{bmatrix} \right) \end{aligned} \tag{7.6}$$

The aerodynamic department ran their CFD in terms of angles α_s and β_s (Figure 5.2), for example, $C_X = f(\alpha_s, \beta_s)$ etc. As a result these angles must be found. They were derived with respect to a Cartesian to spherical coordinate transformation, and can be shown in Equation 7.7.

$$\begin{aligned} \alpha_s =& sin^{-1}\left(\frac{v_{z,gust}}{|V_{gust}|}\right) \\ \beta_s =& sin^{-1}\left(\frac{v_{y,gust}}{|V_{gust}| \cdot cos(\alpha_s)}\right) \end{aligned} \tag{7.7}$$

To find the dynamic pressure to put into Equation 7.6, Equation 7.8 can be used. First, the magnitude of the gust and vehicle velocity must be found, before one can finally calculate the dynamic pressure.

$$\begin{aligned} |\vec{U}_{gust}| =& \left(\sqrt{v_x^2 + v_y^2 + v_z^2}\right)_{gust} \\ |\vec{V}_{vehicle}| =& \left(\sqrt{v_x^2 + v_y^2 + v_z^2}\right)_{vehicle} \\ q =& \frac{1}{2}\rho(|\vec{U}_{gust} - \vec{V}_{vehicle}|)^2 \end{aligned} \tag{7.8}$$

From the CFD results, interpolations were made to find the aerodynamic coefficients at multiple values of α_s and β_s. For simplicity, they were done linearly. Once, the coefficients have been found, the procedure of Equation 7.6 can provide the force and moments in the vertiport reference frame. Note that, the graphs for the aerodynamic coefficients are shown in Figure 7.4.

The software block diagram is clearly presented in Figure 7.5. This offers an explanation into how the procedure was carried out.

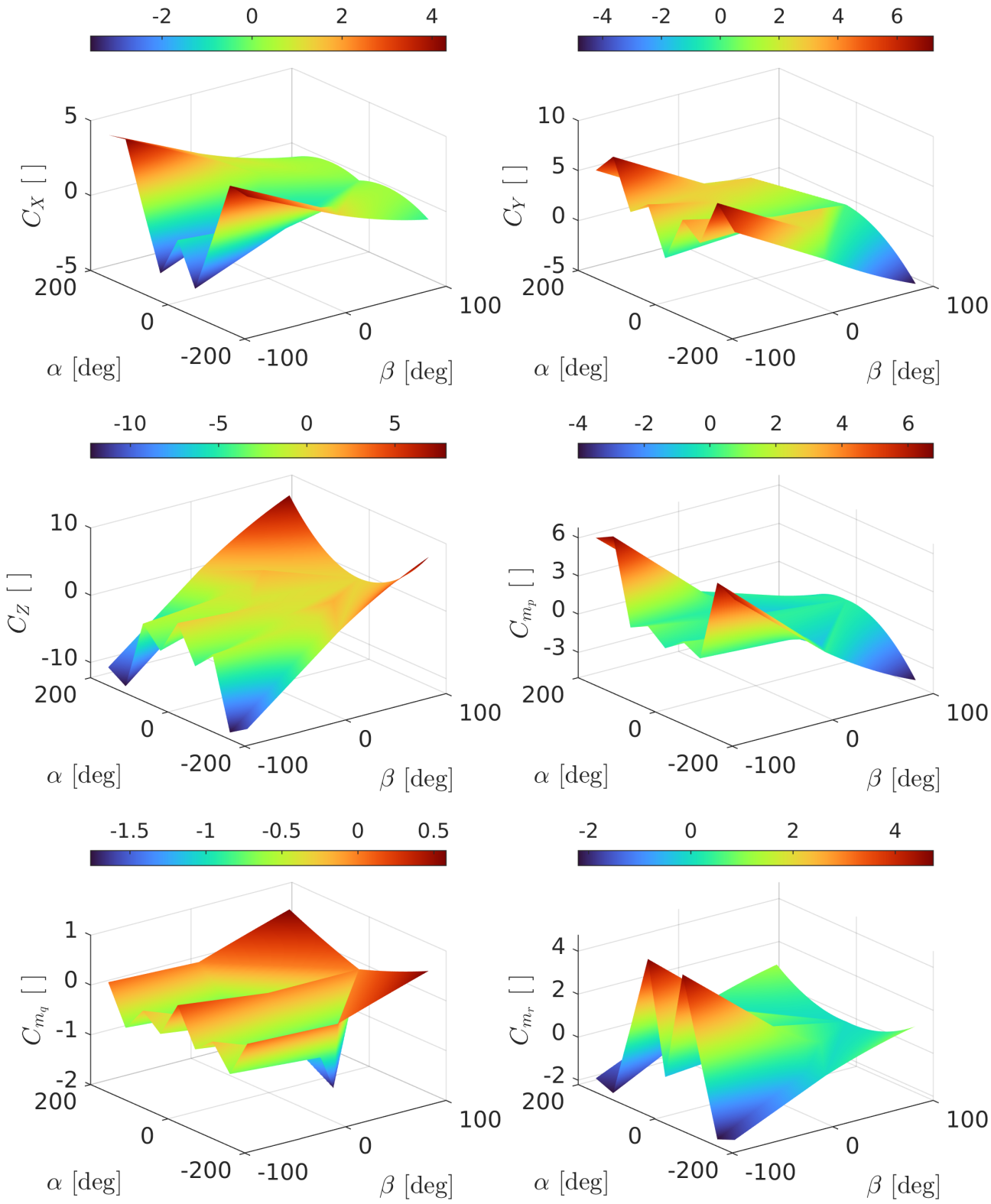

Figure 7.4: Surface maps of interpolated aerodynamic coefficients

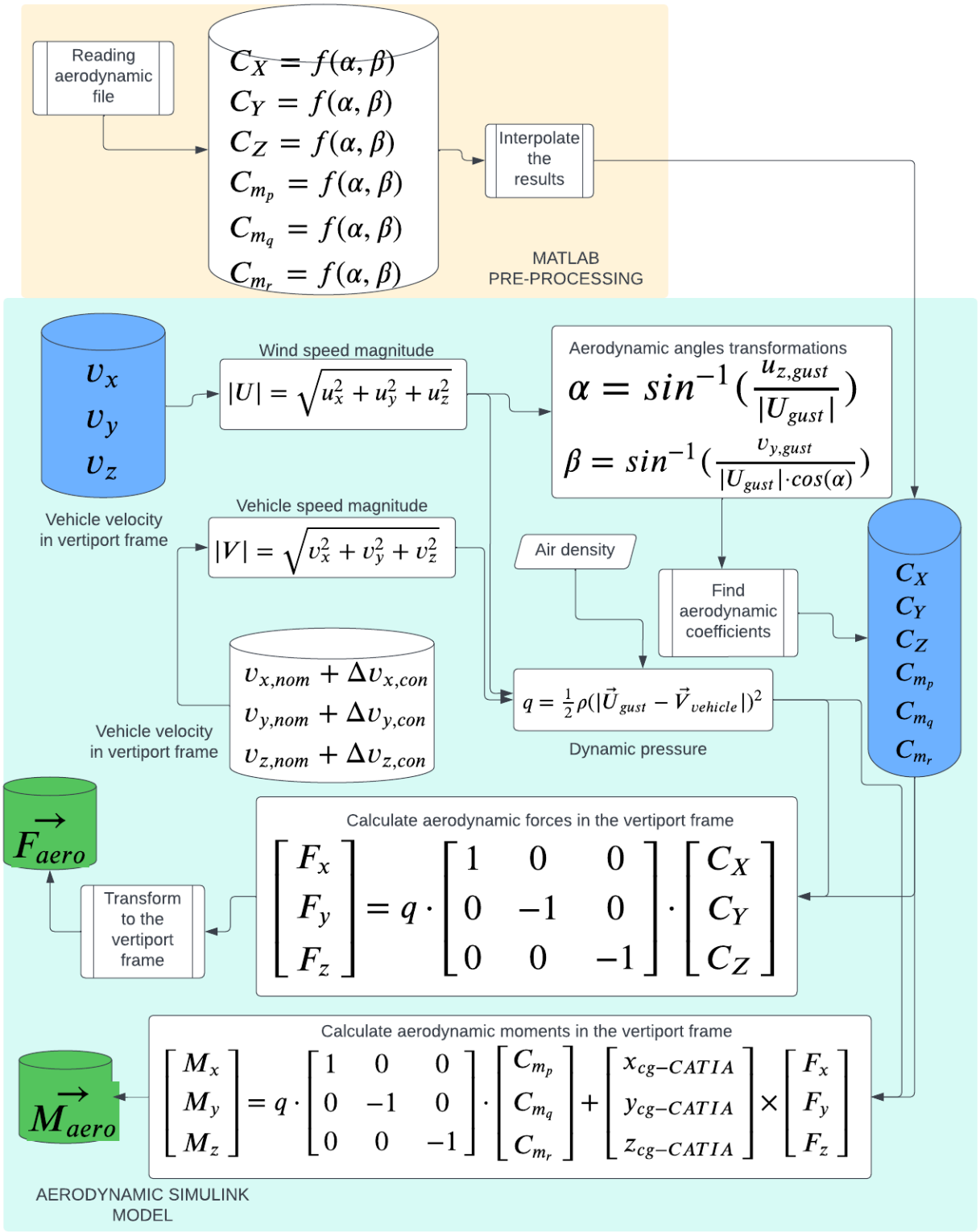

Figure 7.5: Software block diagram for the aerodynamic module

7.1.4. Transformations function

Before an engineering mechanics problem is tackled, reference frames must always be found. In this model three reference frames are used: fixed-vertiport frame, inertial-trajectory frame and the disturbance frame.

- Fixed-vertiport frame $\mathcal{F}^V$ - This frame is fixed at the take-off location; with the Z axis pointing into the ground, the X axis pointing through the nose, and the Y axis pointing through the right side of the vehicle, perpendicular to X and Z. Note that the origin is in the centre of gravity.
- Inertial-trajectory frame $\mathcal{F}^t$ - This frame models the pre-planned trajectory, with its distance and orientation computed pre-flight, or updated due to objects in its path. Here the XYZ directions are the same as $\mathcal{F}^V$ frame, however the frame moves as time goes on. This frame has θ, ϕ, ψ rotation angles to $\mathcal{F}^V$ in x, y and z respectively.
- Disturbance frame $\mathcal{F}^d$ - This is reference frame is with respect to the vehicle's actual position. This frame has $\overline{\sigma}, \overline{\tau}, \overline{\upsilon}$ rotation angles to $\mathcal{F}^t$ in x, y and z respectively.

Once defining the reference frames, transformation matrices can be created to transform x,y,z column vectors shown in Equation 7.9, Equation 7.10 and Equation 7.11.

$$
\begin{aligned}
\mathbb{T}_{dt} &= F_x(\theta)F_y(\phi)F_z(\psi) \\
\mathbb{T}_{dt} &= \begin{bmatrix} 1 & 0 & 0 \\ 0 & cos(\theta) & sin(\theta) \\ 0 & -sin(\theta) & cos(\theta) \end{bmatrix} \cdot \begin{bmatrix} cos(\phi) & 0 & -sin(\phi) \\ 0 & 1 & 0 \\ sin(\phi) & 0 & cos(\phi) \end{bmatrix} \cdot \begin{bmatrix} cos(\psi) & sin(\psi) & 0 \\ -sin(\psi) & cos(\psi) & 0 \\ 0 & 0 & 1 \end{bmatrix} \\
\mathbb{T}_{dt} &= \begin{bmatrix} cos(\theta)cos(\psi) & cos(\theta)sin(\psi) & -sin(\theta) \\ sin(\phi)sin(\theta)cos(\psi) - cos(\phi)sin(\psi) & sin(\phi)sin(\theta)sin(\psi) + cos(\phi)cos(\psi) & sin(\phi)cos(\theta) \\ cos(\phi)sin(\theta)cos(\psi) + sin(\phi)sin(\psi) & cos(\phi)sin(\theta)sin(\psi) - sin(\phi)cos(\psi) & cos(\phi)cos(\theta) \end{bmatrix}
\end{aligned} \tag{7.9}
$$

$$
\begin{aligned}
\mathbb{T}_{tV} &= F_x(\overline{\sigma})F_y(\overline{\tau})F_z(\overline{\upsilon}) \\
\mathbb{T}_{tV} &= \begin{bmatrix} cos(\overline{\sigma})cos(\overline{\upsilon}) & cos(\overline{\sigma})sin(\overline{\upsilon}) & -sin(\overline{\sigma}) \\ sin(\overline{\tau})sin(\overline{\sigma})cos(\overline{\upsilon}) - cos(\overline{\tau}) \cdot sin(\overline{\upsilon}) & sin(\overline{\tau})sin(\overline{\sigma})sin(\overline{\upsilon}) + cos(\overline{\tau})cos(\overline{\upsilon}) & sin(\overline{\tau})cos(\overline{\sigma}) \\ cos(\overline{\tau})sin(\overline{\sigma})cos(\overline{\upsilon}) + sin(\overline{\tau})sin(\overline{\upsilon}) & cos(\overline{\tau})sin(\overline{\sigma})sin(\overline{\upsilon}) - sin(\overline{\tau})cos(\overline{\upsilon}) & cos(\overline{\tau})cos(\overline{\sigma}) \end{bmatrix}
\end{aligned} \tag{7.10}
$$

$$
\begin{aligned}
\mathbb{T}_{tV}^{\mathcal{T}} &= \mathbb{T}_{Vt} \\
\mathbb{T}_{dt}^{\mathcal{T}} &= \mathbb{T}_{td} \\
\mathbb{T}_{dV} &= \mathbb{T}_{dt}\mathbb{T}_{tV} \\
\mathbb{T}_{Vd} &= \mathbb{T}_{dV}^{\mathcal{T}}
\end{aligned} \tag{7.11}
$$

The software block diagram for this procedure is shown in Figure 7.6.

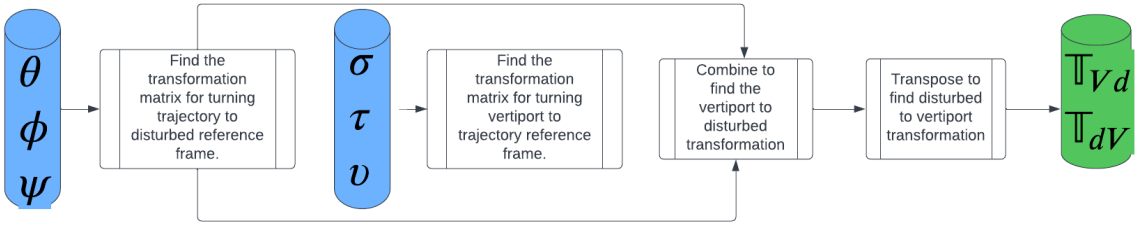

Figure 7.6: Software block diagram for the transformation function.

7.1.5. Linear dynamics model

The point mass model from **midterm** has been adapted to model all three axes of linear motion. The linear dynamics model takes in the aerodynamic force vector, the position vectors showing the displacement from $\mathcal{F}^d$ to $\mathcal{F}^t$, the accelerometer adjusted acceleration and the propulsion force. From this model the linear accelerations,

velocities and positions can be calculated. As the directions can be decoupled, three PID (Proportional-Integral-Definitive) controllers are used to provide control force commands to the position deviation; these control forces are modelled with a time delay of 0.1 seconds **midterm**. The linear dynamics equations revolve around Equation 7.12.

$$a = \frac{F}{m} \tag{7.12}$$

As will be explained in a later section, several sensors are used in the model, although the Kalman filters aim to smooth them, they are never 100% perfect; this causes resulting noise and bias. If this noise was allowed in the model, it would make the PID think that the vehicle is not in its desired position when it is, and so there would be control forces continually acting. As a result a threshold is given for control forces from the linear model, in this model it is 0.1 m deviation, before the control model acts. One interesting thing to note about this model is that it outputs desired control forces, these are fed into the propulsion module, which outputs feasible control forces when combined with the angular model's demands. These control forces are fed back into this model. This is shown more clearly in Figure 7.7.

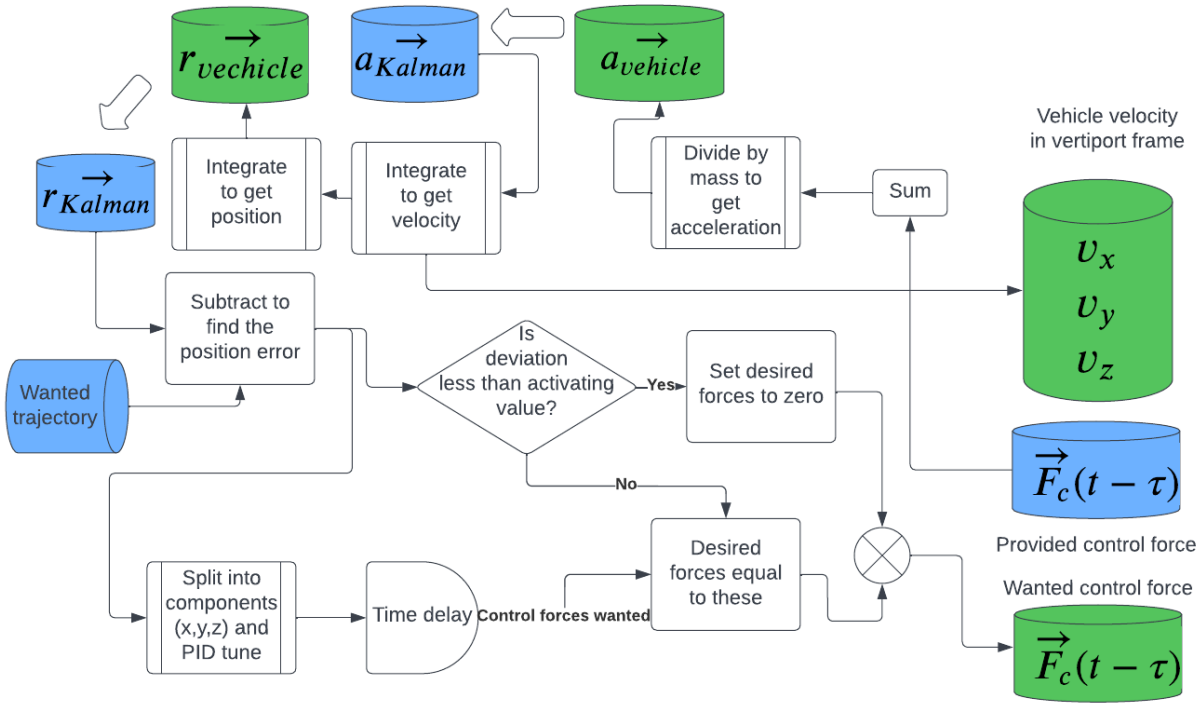

Figure 7.7: Software block diagram for linear dynamics

7.1.6. Kalman filtering for the linear model

The Kalman filter is used to combine the accelerometer and GPS measurements, such that a position reading is given. This method is called sensor fusion and can reduce random walk from the accelerometer. The Kalman filter block from Simulink is used, this takes $\vec{x}$ and $\vec{u}$ as inputs, the state space matrices A, B, C and D as parameters, and $\dot{\vec{x}}$ as an output. The accelerometer reading is converted to a velocity reading through integration; note that this causes an error propagation, which can be reduced through the use of a Kalman filter. The software block diagram for this is shown below in Figure 7.8.

The state space equations for this model are given below in Equation 7.13 and Equation 7.14. Where the GPS gives the r_x, r_y and r_z measurements, and the accelerometer integrated gives the v_x, v_y and v_z measurements.

$$
\begin{aligned}
\dot{\vec{x}} =& \underline{A}\vec{x} + \underline{B}\vec{u} \\
\begin{bmatrix} \dot{r_x} \\ \dot{r_y} \\ \dot{r_z} \\ \dot{v_x} \\ \dot{v_y} \\ \dot{v_z} \end{bmatrix} =& \begin{bmatrix} 0 & 0 & 0 & 1 & 0 & 0 \\ 0 & 0 & 0 & 0 & 1 & 0 \\ 0 & 0 & 0 & 0 & 0 & 1 \\ 0 & 0 & 0 & 0 & 0 & 0 \\ 0 & 0 & 0 & 0 & 0 & 0 \\ 0 & 0 & 0 & 0 & 0 & 0 \end{bmatrix} \cdot \begin{bmatrix} r_x \\ r_y \\ r_z \\ v_x \\ v_y \\ v_z \end{bmatrix} + \begin{bmatrix} 0 & 0 & 0 & 0 & 0 & 0 \\ 0 & 0 & 0 & 0 & 0 & 0 \\ 0 & 0 & 0 & 0 & 0 & 0 \\ 0 & 0 & 0 & \frac{1}{m} & 0 & 0 \\ 0 & 0 & 0 & 0 & \frac{1}{m} & 0 \\ 0 & 0 & 0 & 0 & 0 & \frac{1}{m} \end{bmatrix} \cdot \begin{bmatrix} \sim \\ \sim \\ \sim \\ F_x \\ F_y \\ F_z \end{bmatrix}
\end{aligned} \tag{7.13}
$$

$$
\begin{aligned}
\vec{y} =& \underline{C}\vec{x} + \underline{D}\vec{u} \\
\begin{bmatrix} r_x \\ r_y \\ r_z \\ v_x \\ v_y \\ v_z \end{bmatrix} =& \begin{bmatrix} 1 & 0 & 0 & 0 & 0 & 0 \\ 0 & 1 & 0 & 0 & 0 & 0 \\ 0 & 0 & 1 & 0 & 0 & 0 \\ 0 & 0 & 0 & 1 & 0 & 0 \\ 0 & 0 & 0 & 0 & 1 & 0 \\ 0 & 0 & 0 & 0 & 0 & 1 \end{bmatrix} \cdot \begin{bmatrix} r_x \\ r_y \\ r_z \\ v_x \\ v_y \\ v_z \end{bmatrix} + \begin{bmatrix} 0 & 0 & 0 & 0 & 0 & 0 \\ 0 & 0 & 0 & 0 & 0 & 0 \\ 0 & 0 & 0 & 0 & 0 & 0 \\ 0 & 0 & 0 & 0 & 0 & 0 \\ 0 & 0 & 0 & 0 & 0 & 0 \\ 0 & 0 & 0 & 0 & 0 & 0 \end{bmatrix} \cdot \begin{bmatrix} \sim \\ \sim \\ \sim \\ F_x \\ F_y \\ F_z \end{bmatrix}
\end{aligned} \tag{7.14}
$$

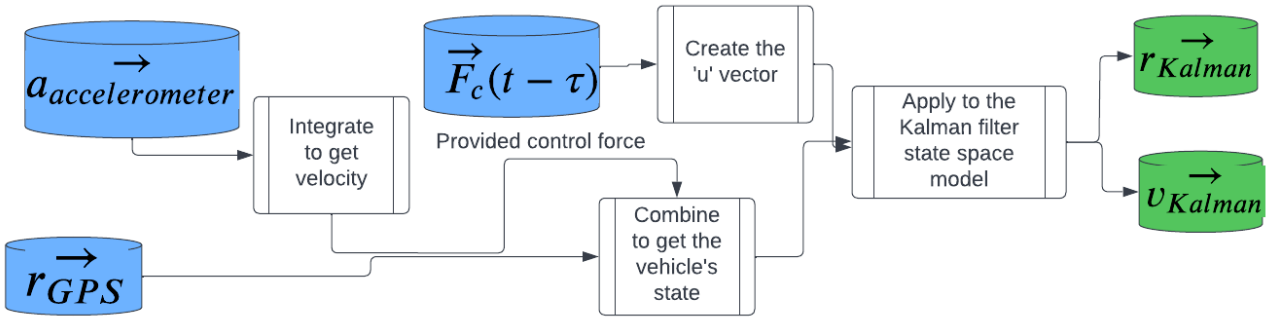

Figure 7.8: Software diagram for the linear dynamics Kalman filter.

7.1.7. Angular dynamics model

To fully model the dynamics of the vehicle, the angular frame must also be modelled. If one assumes a rigid body, then Euler's equations for rotational motion can be used; as shown in Equation 7.15. However, the Coriolis effect causes difficult problems with designing controllers, due to the coupling between the axes. During a meeting with Fusion engineering, they gave their expert reasoning to allow this force to be neglected; this resulted in Equation 7.16.

$$
\begin{aligned}
H =& I\omega \\
\dot{H} + \omega \times H =& M
\end{aligned} \tag{7.15}
$$

$$
\begin{aligned}
\dot{\omega} =& \frac{M}{I} \\
\begin{bmatrix} \dot{\omega_x} \\ \dot{\omega_y} \\ \dot{\omega_z} \end{bmatrix} =& \begin{bmatrix} I_{xx} & I_{xy} & I_{xz} \\ I_{yx} & I_{yy} & I_{yz} \\ I_{zx} & I_{zy} & I_{zz} \end{bmatrix}^{-1} \cdot \begin{bmatrix} M_x \\ M_y \\ M_z \end{bmatrix}
\end{aligned} \tag{7.16}
$$

Several controllers for the angular dynamic were trialed, first through PID controllers for turning the angle deviation into a control moment. However, due to the coupling of axes, this did not produce good results. Afterwards, a MPC (Model Predictive Controller) was trialed. However, due to the lack of knowledge within the group of non-linear control, the "Non-Linear MPC" block in Simulink proved difficult to implement. However, a normal MPC worked well for controlling the angular velocity, but it had no control for the angle, as the input of the system was the angular velocity.

Note that in this version of the model, the sensor reading for angular velocity is disconnected for verification and validation, but when it runs it will be joined. Secondly, the control moments go to the propulsion module, where the feasible control moments are returned.

The MPC needs the state space model as a parameter: they are given below in Equation 7.17 and Equation 7.18.

$$\begin{aligned} \dot{\vec{x}} &= \underline{A}\vec{x} + \underline{B}\vec{u} \\ \begin{bmatrix} \dot{\omega_x} \\ \dot{\omega_y} \\ \dot{\omega_z} \end{bmatrix} &= \begin{bmatrix} 0 & 0 & 0 \\ 0 & 0 & 0 \\ 0 & 0 & 0 \end{bmatrix} \cdot \begin{bmatrix} \omega_x \\ \omega_y \\ \omega_z \end{bmatrix} + \begin{bmatrix} - & - & - \\ - & \underline{I}^{-1} & - \\ - & - & - \end{bmatrix} \cdot \begin{bmatrix} T_x \\ T_y \\ T_z \end{bmatrix} \end{aligned} \tag{7.17}$$

$$\begin{aligned} \vec{y} &= \underline{C}\vec{x} + \underline{D}\vec{u} \\ \begin{bmatrix} \omega_x \\ \omega_y \\ \omega_z \end{bmatrix} &= \begin{bmatrix} 1 & 0 & 0 \\ 0 & 1 & 0 \\ 0 & 0 & 1 \end{bmatrix} \cdot \begin{bmatrix} \omega_x \\ \omega_y \\ \omega_z \end{bmatrix} + \begin{bmatrix} 0 & 0 & 0 \\ 0 & 0 & 0 \\ 0 & 0 & 0 \end{bmatrix} \cdot \begin{bmatrix} T_x \\ T_y \\ T_z \end{bmatrix} \end{aligned} \tag{7.18}$$

To calculate the desired angular velocity from a desired angle, the following steps are taken:

1. The error in angle is found.
2. Then the direction of the angular velocity is found. Here if the angle error is negative a negative factor is given, positive error gives a positive factor and zero error gives a zero factor.
3. The error is normalized such that all the angles are weighted evenly, then they are passed through a sigmoid function which outputs the desired angular velocity (irrespective of positive or negative angles). The sigmoid function is tuned to match with the normalized values. The sigmoid equation is shown in Equation 7.19, and the coefficients have been matched intuitively to normalized values via visual inspection of the function on *Desmos graphing calculator* [7]. Here it found that $a = 10^{-8}, b = 10, c = 1000, K = 125$ to provide a good response to multiple gust scenarios. Note that they were fine-tuned to provide a good response. It was found that (with respect to the angles) "a" controls the frequency of the oscillation, "c" controls the magnitude and "K" controls the settling time, whilst "b" was used to match the data to the sigmoid function.
4. The output of the sigmoid and the factors from Step 2 are multiplied to provide a desired angular velocity in the correct direction.

$$f(x) = K/(1 + e^{-a(bx-c)}) \tag{7.19}$$

Again, to reduce oscillations from the sensors, an activation angle error is taken as 0.5-0.1 degrees, depending on comfort. The complete angular dynamics software block diagram is shown in Figure 7.9.

[7] *https://www.desmos.com/calculator [Cited: 15/06/2022]*

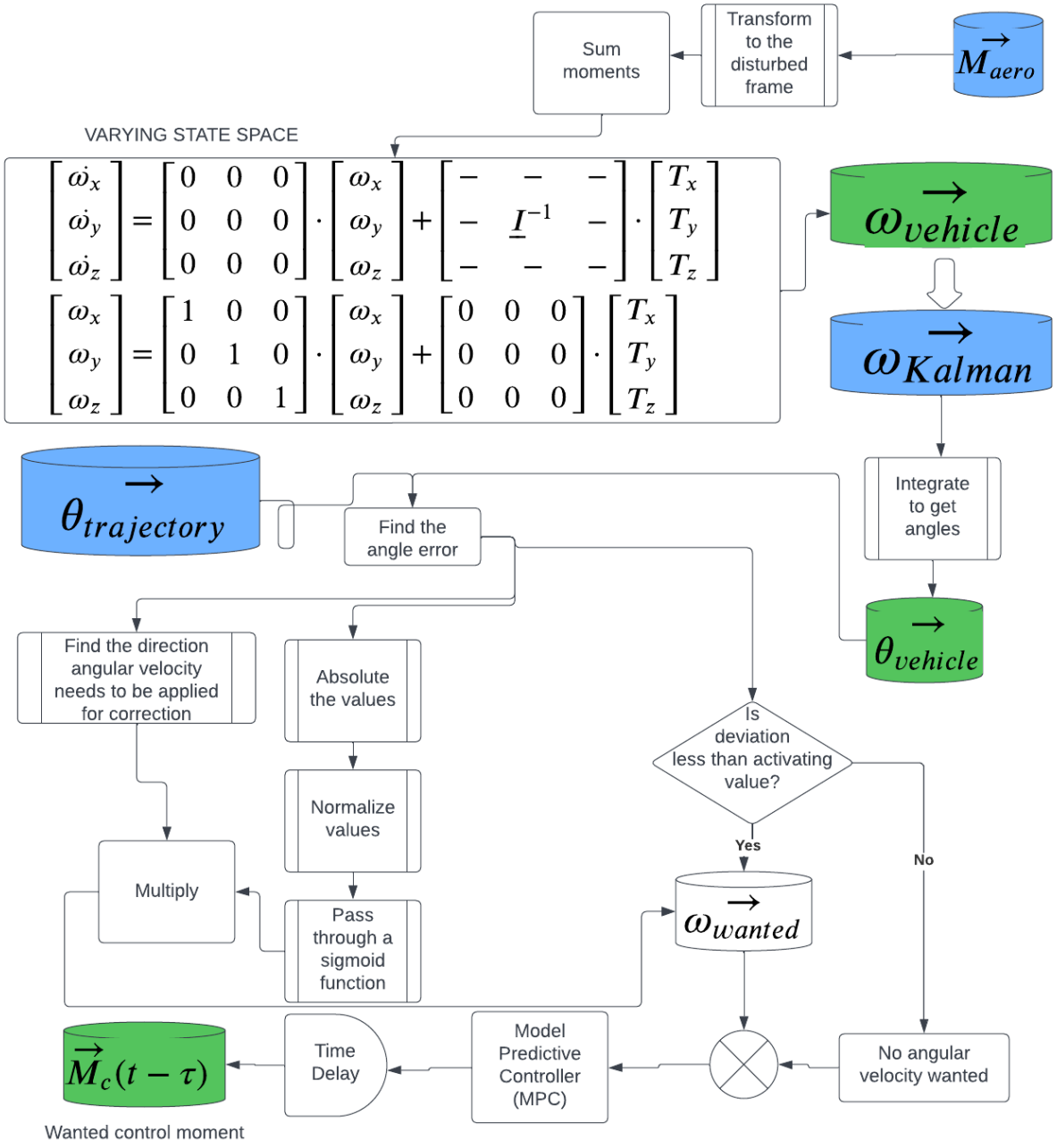

Figure 7.9: Software block diagram for the angular dynamics

7.1.8. Kalman filter for the angular model

The angular model uses a Kalman filter to fuse measurements of the angular velocities $(\omega_x, \omega_y, \omega_z)$ from the gyroscope and angle/orientation measurements from the magnetometer $(\theta_x, \theta_y, \theta_z)$. Again, this sensor fusion allows for the gyroscope propagation to be reduced. The state space used for this are shown in Equation 7.20 and Equation 7.21. The software block diagram for this process is shown in Figure 7.10.

$$\dot{\vec{x}} = \underline{A}\vec{x} + \underline{B}\vec{u}$$

$$\begin{bmatrix}\omega_x\\ \omega_y\\ \omega_z\\ \dot{\omega}_x\\ \dot{\omega}_y\\ \dot{\omega}_z\end{bmatrix} = \begin{bmatrix}0&0&0&1&0&0\\0&0&0&0&1&0\\0&0&0&0&0&1\\0&0&0&0&0&0\\0&0&0&0&0&0\\0&0&0&0&0&0\end{bmatrix}\cdot\begin{bmatrix}\theta_x\\ \theta_y\\ \theta_z\\ \omega_x\\ \omega_y\\ \omega_z\end{bmatrix} + \begin{bmatrix}0&0&0&0&0&0\\0&0&0&0&0&0\\0&0&0&0&0&0\\0&0&0&[-&-&-]\\0&0&0&|-&\underline{I}^{-1}&-|\\0&0&0&[-&-&-]\end{bmatrix}\cdot\begin{bmatrix}\sim\\ \sim\\ \sim\\ T_x\\ T_y\\ T_z\end{bmatrix} \tag{7.20}$$

$$\vec{y} = \underline{C} \cdot \vec{x} + \underline{D} \cdot \vec{u}$$

$$\begin{bmatrix} \theta_x \\ \theta_y \\ \theta_z \\ \omega_x \\ \omega_y \\ \omega_z \end{bmatrix} = \begin{bmatrix} 1 & 0 & 0 & 0 & 0 & 0 \\ 0 & 1 & 0 & 0 & 0 & 0 \\ 0 & 0 & 1 & 0 & 0 & 0 \\ 0 & 0 & 0 & 1 & 0 & 0 \\ 0 & 0 & 0 & 0 & 1 & 0 \\ 0 & 0 & 0 & 0 & 0 & 1 \end{bmatrix} \cdot \begin{bmatrix} \theta_x \\ \theta_y \\ \theta_z \\ \omega_x \\ \omega_y \\ \omega_z \end{bmatrix} + \begin{bmatrix} 0 & 0 & 0 & 0 & 0 & 0 \\ 0 & 0 & 0 & 0 & 0 & 0 \\ 0 & 0 & 0 & 0 & 0 & 0 \\ 0 & 0 & 0 & 0 & 0 & 0 \\ 0 & 0 & 0 & 0 & 0 & 0 \\ 0 & 0 & 0 & 0 & 0 & 0 \end{bmatrix} \cdot \begin{bmatrix} \sim \\ \sim \\ \sim \\ T_x \\ T_y \\ T_z \end{bmatrix} \tag{7.21}$$

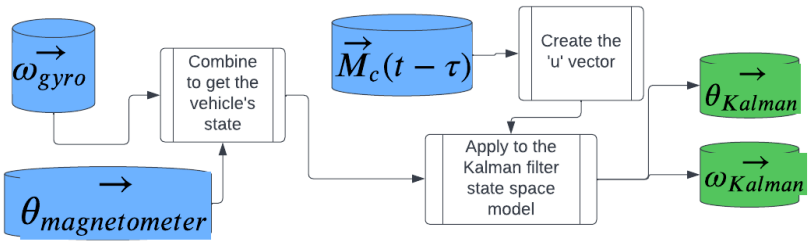

Figure 7.10: Software block diagram for the angular Kalman filter

7.1.9. Propeller module

In order to keep the control forces within reasonable limits, one should consider the control allocation problem. Smart control allocation can minimize the magnitude of the forces required from each propeller. Unfortunately, propellers cannot accelerate and decelerate instantaneously, therefore, the propeller acceleration has to be taken into account as well. This section starts by showing the software block diagram of Figure 7.11, before justifying the calculations behind it. First, the explanation of how the propeller commands are generated via solving a control allocation problem, before the justification of the propeller acceleration is present.

Figure 7.11 starts by converting the Z force and Y moment in the body frame to a factor 'a' (derived following the diagram), which shall be discussed later. This variable 'a' can be used to find the top and bottom propeller thrusts. For the control propellers, a simple matrix relation can give them their thrust commands. Following this, their thrusts are limited to the maximum and minimum thrust each propeller can provide. To model the acceleration, the thrusts are digitised to simulate the time-delay to accelerate the propellers to give their thrust. Note that a more accurate propeller acceleration model should be made in the future. Following this, the propeller thrusts are converted back to forces and moments acting around the body's centre of mass.

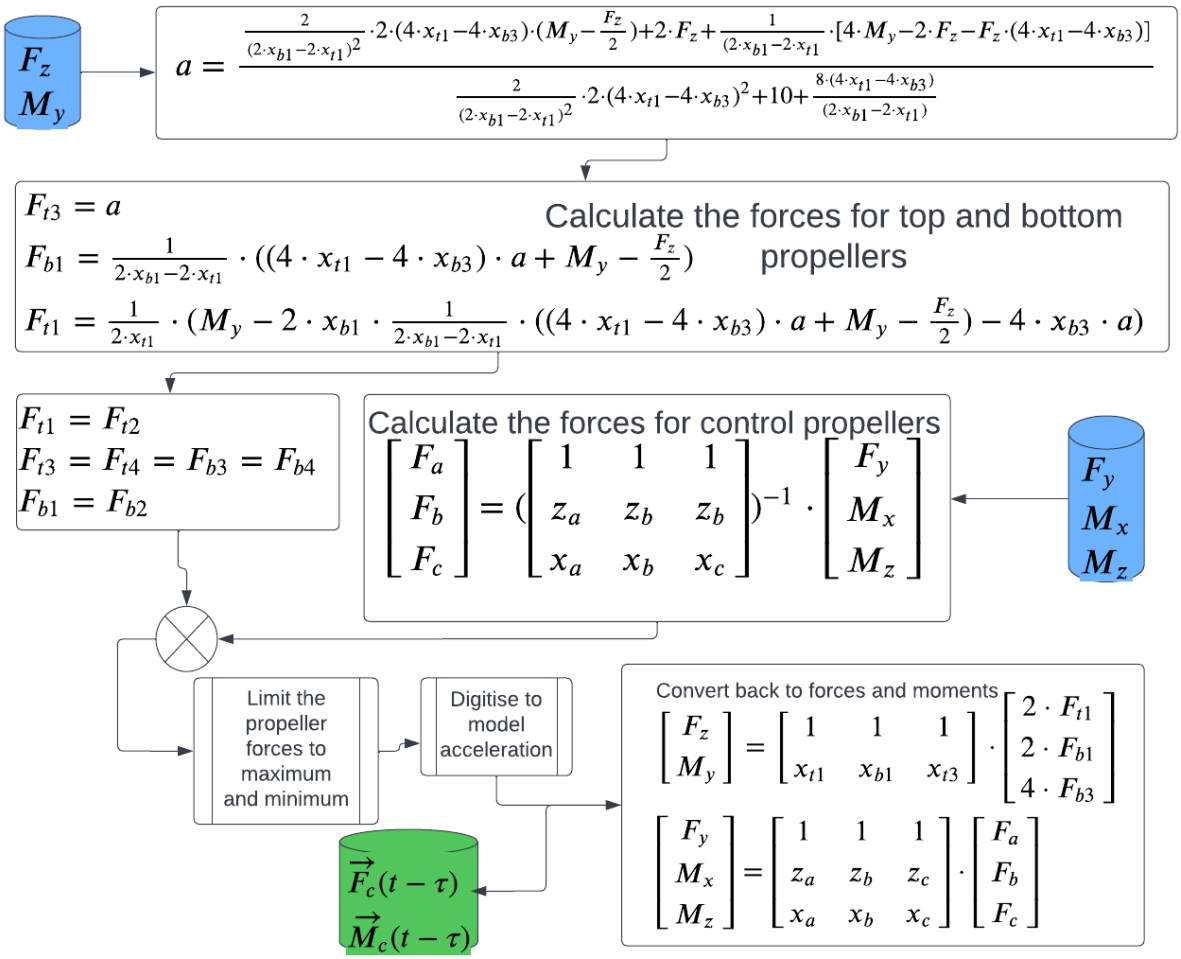

Figure 7.11: Software block diagram for the propulsion module

Control allocation justification:

The propellers are counted under the numbering scheme of:

- First letter : 'T' for top, or 'B' for bottom - this is in the Z^b axis (body frame): with 'B' having a positive value and 'T' a negative value.
- Second letter : 'F' for front, or 'B' for back - this is in the X^b axis: with the 'F' having a positive value and 'B' a negative value.
- Third letter: 'L' for left, or 'R' for right, or 'C' for control - this is in the Y^b axis: with the 'L' having a positive value and 'R' a negative value, the 'C' has a zero value.

This results in eleven propellers: TFL, BFL, TFR, BFR, TBL, BBL, TBR, TBL, TBC, BBC and BFC; as summarised by Figure 7.12. The control allocation system is designed to use the C propellers whenever possible; these can counter moments in x and z, and force in y-axis - in the body fixed frame. This leaves the L and R propellers (lifting propellers) to counteract the moments in the y-axis and force in the z axis, they can also counter moments in the x-axis, but this is not considered, nor is yaw control through differing propeller speeds. Note that, there is no propeller which can directly counter a force in the x-axis, so the vehicle will tilt until there is no force in that direction.

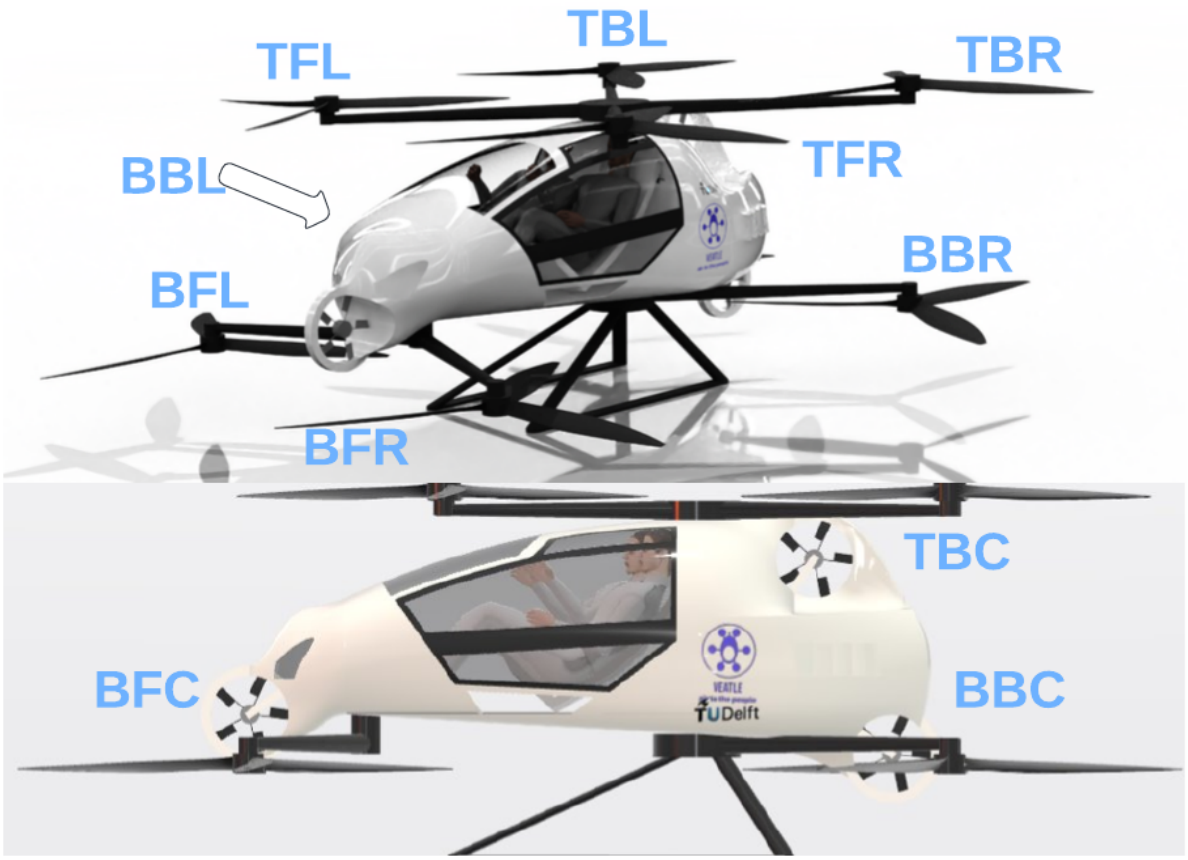

Figure 7.12: Schematic of the propeller numbering

First, the control allocation for the control propellers shall be analysed. For ease of equations, TBC is now 'a', BBC is now 'b' and FBC is now 'c'. From the positions of the propellers with respect to the centre of mass, the equilibrium equations of Equation 7.22 can be made for the control propellers. Note that $^{\ominus}$ indicates the component acting in the negative direction.

$$\begin{aligned} F_y &= F_a + F_b + F_c \\ M_x &= F_a \cdot z_a + z_b \cdot F_b^{\ominus} + z_c \cdot F_c^{\ominus} \\ M_z &= F_a \cdot x_a^{\ominus} + F_b \cdot x_b^{\ominus} + x_c \cdot F_c \end{aligned} \tag{7.22}$$

When they are converted into matrix form, they can be solved:

$$\begin{aligned} \begin{bmatrix} F_y \\ M_x \\ M_z \end{bmatrix} &= \begin{bmatrix} 1 & 1 & 1 \\ z_a & z_b & z_c \\ x_a & x_b & x_c \end{bmatrix} \cdot \begin{bmatrix} F_a \\ F_b \\ F_c \end{bmatrix} \\ \begin{bmatrix} F_a \\ F_b \\ F_c \end{bmatrix} &= \left(\begin{bmatrix} 1 & 1 & 1 \\ z_a & z_b & z_b \\ x_a & x_b & x_c \end{bmatrix} \right)^{-1} \cdot \begin{bmatrix} F_y \\ M_x \\ M_z \end{bmatrix} \end{aligned} \tag{7.23}$$

Now moving onto the lifting propellers; as mentioned before, these propellers are used to make moments in the y-axis and a force in the z-axis. Again, for ease of numbering, TFL is '1', TFR is '2', TBL is '3', TBR is '4', BTL is '1', BTR is '2', BBL is '3' and BBR is '4', with t for top and b for bottom. With all the propellers

acting in the negative z-axis, the following relation is built:

$$\begin{bmatrix} F_z \\ M_x \\ M_z \end{bmatrix} = \begin{bmatrix} 1 & 1 & 1 & 1 & 1 & 1 & 1 & 1 \\ y_{t,1} & y_{t,2} & y_{t,3} & y_{t,4} & y_{b,1} & y_{b,2} & y_{b,3} & y_{b,4} \\ x_{t,1} & x_{t,2} & x_{t,3} & x_{t,4} & x_{b,1} & x_{b,2} & x_{b,3} & x_{b,4} \end{bmatrix} \cdot \begin{bmatrix} F_{t1} \\ F_{t2} \\ F_{t3} \\ F_{t4} \\ F_{b1} \\ F_{b2} \\ F_{b3} \\ F_{b4} \end{bmatrix} \tag{7.24}$$

Due to certain moment arms being equal, the problem can be simplified to remove M_x from the equation, by setting it equal to zero: to do this $F_{t1} = F_{t2}$, $F_{t3} = F_{t4} = F_{b3} = F_{b4}$ and $F_{b1} = F_{b2}$. Resulting the following matrix, which will have 2 knowns 'F_z' and 'M_y', a constant matrix and 3 unknowns: 'F_{t1}', 'F_{b1}' and 'F_{t3}'.

$$\begin{bmatrix} F_z \\ M_y \end{bmatrix} = \begin{bmatrix} 1 & 1 & 1 \\ x_{t1} & x_{b1} & x_{t3} \end{bmatrix} \cdot \begin{bmatrix} 2 \cdot F_{t1} \\ 2 \cdot F_{b1} \\ 4 \cdot F_{b3} \end{bmatrix} \tag{7.25}$$

To solve this equation, a cost function must be made. This is aimed at minimising the total force used equally over all propellers, shown below. Note that the values are squared, so negative values don't affect it.

$$J = min(F_{t1}^2 + F_{b1}^2 + F_{b3}^2) \tag{7.26}$$

To solve this, a parametric equation is found from Equation 7.25, with now the right column vector being changed to x, y, z for ease of mathematics.

$$\begin{aligned} F_{b3} = z =& a \\ F_{b1} = y =& \frac{1}{2 \cdot x_{b1} - 2 \cdot x_{t1}} \cdot ((4 \cdot x_{t1} - 4 \cdot x_{b3}) \cdot a + M_y - \frac{F_z}{2}) \\ F_{t1} = x =& \frac{1}{2 \cdot x_{t1}} \cdot (M_y - 2 \cdot x_{b1} \cdot y - 4 \cdot x_{b3} \cdot a) \\ =& \frac{1}{2 \cdot x_{t1}} \cdot (M_y - 2 \cdot x_{b1} \cdot \frac{1}{2 \cdot x_{b1} - 2 \cdot x_{t1}} \cdot ((4 \cdot x_{t1} - 4 \cdot x_{b3}) \cdot a + M_y - \frac{F_z}{2}) - 4 \cdot x_{b3} \cdot a) \end{aligned} \tag{7.27}$$

This leads to the cost function which is aimed to be minimised.

$$\begin{aligned} J =& \frac{2}{(2 \cdot x_{b1} - 2 \cdot x_{t1})^2} \cdot [(4 \cdot x_{t1} - 4 \cdot x_{b3})^2 \cdot a^2 + M_y^2 + \frac{F_z^2}{4} + 2 \cdot (4 \cdot x_{t1} - 4 \cdot x_{b3}) \cdot M_y \cdot a \\ & - F_z \cdot (4 \cdot x_{t1} - 4 \cdot x_{b3}) \cdot a - F_z \cdot M_y] + 4 \cdot a^2 + \frac{F_z^2}{4} + 2 \cdot F_z \cdot a + a^2 \\ & + \frac{4 \cdot a - F_z}{2 \cdot x_{b1} - 2 \cdot x_{t1}} \cdot [(4 \cdot x_{t1} - 4 \cdot x_{b3}) \cdot a + M_y - \frac{F_z}{2}] \end{aligned} \tag{7.28}$$

To find the minimum of this, it must be differentiated. It can be confirmed as the minimum and not the maximum, as the maximum has the value of infinity.

$$\begin{aligned} \frac{\partial}{\partial a} J =& a \cdot [\frac{2}{(2 \cdot x_{b1} - 2 \cdot x_{t1})^2} \cdot 2 \cdot (4 \cdot x_{t1} - 4 \cdot x_{b3})^2 + 10 + \frac{8 \cdot (4 \cdot x_{t1} - 4 \cdot x_{b3})}{(2 \cdot x_{b1} - 2 \cdot x_{t1})}] + \\ & \frac{2}{(2 \cdot x_{b1} - 2 \cdot x_{t1})^2} \cdot 2 \cdot (4 \cdot x_{t1} - 4 \cdot x_{b3}) \cdot (M_y - \frac{F_z}{2}) + 2 \cdot F_z + \\ & \frac{1}{(2 \cdot x_{b1} - 2 \cdot x_{t1}} \cdot [4 \cdot M_y - 2 \cdot F_z - F_z \cdot (4 \cdot x_{t1} - 4 \cdot x_{b3}] \\ & = 0 \end{aligned} \tag{7.29}$$

When re-arranged, it leads to:

$$a = \frac{\frac{2}{(2\cdot x_{b1}-2\cdot x_{t1})^2}\cdot 2\cdot(4\cdot x_{t1}-4\cdot x_{b3})\cdot(M_y-\frac{F_z}{2})+2\cdot F_z+\frac{1}{(2\cdot x_{b1}-2\cdot x_{t1}}\cdot[4\cdot M_y-2\cdot F_z-F_z\cdot(4\cdot x_{t1}-4\cdot x_{b3})]}{\frac{2}{(2\cdot x_{b1}-2\cdot x_{t1})^2}\cdot 2\cdot(4\cdot x_{t1}-4\cdot x_{b3})^2+10+\frac{8\cdot(4\cdot x_{t1}-4\cdot x_{b3})}{(2\cdot x_{b1}-2\cdot x_{t1})}} \tag{7.30}$$

This can be used to find the thrust for each lifting propeller.

Justification of the propeller acceleration.

In order to react quickly to a gust, the control propellers need to be able to accelerate in a certain mount of time. In other words, the reaction time of the propellers needs to be sufficiently low. The reaction time of the control system is implemented in the model to check if the requirements are still met. First of all, the inertia of the control propeller needs to be calculated. This is done by the following steps. Here, it is assumed that the blade is made up of a solid cylinder rod connecting it with the blade element, which has the shape of a NACA0012 airfoil and a thickness equal to the cylinder rod diameter. Material density is assumed to be of standard carbon fibre: 2000 kg/m^3. The masses are calculated by Equation 7.31 and Equation 7.32.

$$M_{cyl} = \rho R_1 \pi (0.06c)^2 \tag{7.31}$$

$$M_{blade} = \rho A_{airfoil} c^2 (R - R_1) \tag{7.32}$$

R_1 is the hub radius, R is the outer radius, c is the chord and $A_{airfoil}$ is the dimensionalised are of the NACA0012 airfoil. The total inertia of the propeller is then calculated using Equation 7.33.

$$I = (R_1^2 M_{blade} + 0.3333(R - R_1)^2 M_{blade} + 0.3333 R_1^2 M_{cyl})b \tag{7.33}$$

Here, b is the number of blades per propeller. The motors selected for the control system can deliver a maximum torque of 90 N/m. The maximum acceleration possible can then be calculated by Equation 7.34. Using the geometry of the propeller blades and the rpm needed for the control force, it is discovered that the time delay is of acceptable value, namely around 0.03 s. The reason for this is the strong motor type combined with the low weight of the blades.

$$\alpha = \frac{T}{I} \tag{7.34}$$

To model this effect, a digital signal of frequency = $\frac{1}{0.03}$ Hz is used as the activation for a sample and hold function, before the new thrust is used within the simulation. This is a simplified version, due to a more complicated model being out of the scope of the analysis at this point.

7.2. Results, analysis and evaluation from 6DOF and 3DOF simulations

This section lays out the results from the simulation, here two cases are posed: first the full 6DOF model with the shard case taken at a nominal vehicle velocity of 60 km/hr at a 53.22° angle to keep the same angle as simulated in the aerodynamic modelling of the Shard building, described in Chapter 5. This is followed by an analysis of a method to combat the defects shown from the results. After these results, a simple gust profile acting across the body is given.

7.2.1. 6DOF Shard case results

The gust profile and Shard wake produced some interesting results, relating to the comfort of the passengers and the trajectory deviation

The PID-tuned linear dynamics system takes in the aerodynamic forces to bring around an acceleration. The results of the vehicle's linear state are shown in Figure 7.13. It can be seen that the Y deviation is the largest at just under 0.6 m, while the Z has a 0.3 m maximum deviation. The velocity graph represents the velocity difference from the nominal velocity: it shows how the velocity change is small compared to the vehicle's nominal velocity. Note that, the noise and bias of the GPS and accelerometer model and the resulting Kalman filtering can be seen in the velocity well, while the bias more in the position plot. The acceleration plot is also present.

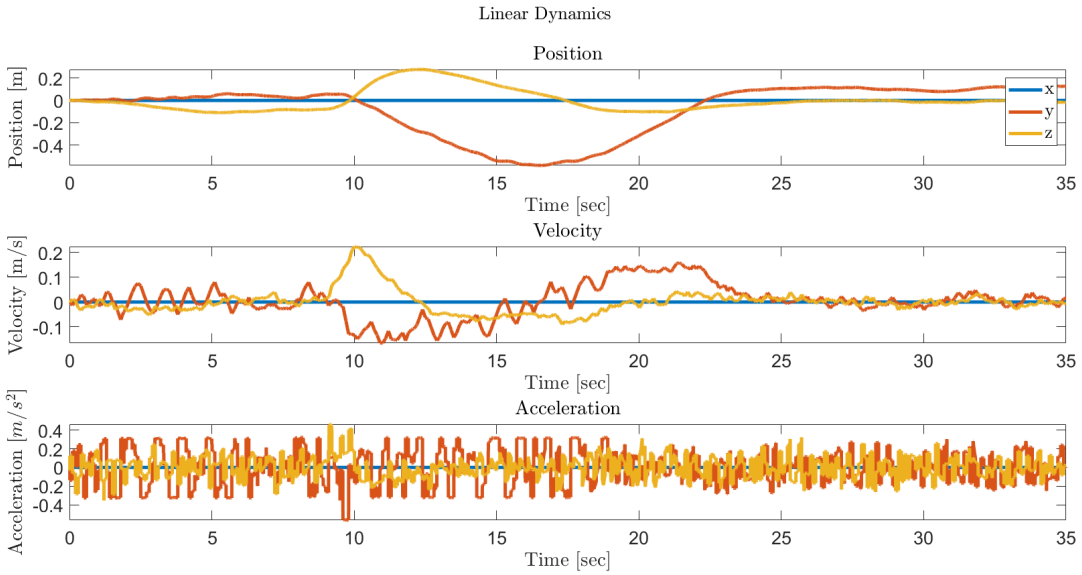

Figure 7.13: Linear dynamics results

For the angular model, a complex sigmoid-activated MPC aims to control against the disturbance. However, this control will not nullify the problem: on the final oscillation the X has an amplitude of 0.15°, Y of 0.04° and Z of 0.125°. This verifies how the controller is a good method for angular control, as these deviations are small. It is shown to decrease outside the building's wake. As the error is partially proportional to the amplitude of the angular velocity, it shows an almost linear decrease in angular velocity magnitude. The controller should aim to zero the angular velocity, as it is trying here, same as for the angular acceleration. The reduction of the angular velocity is largely due to the sigmoid activation part.

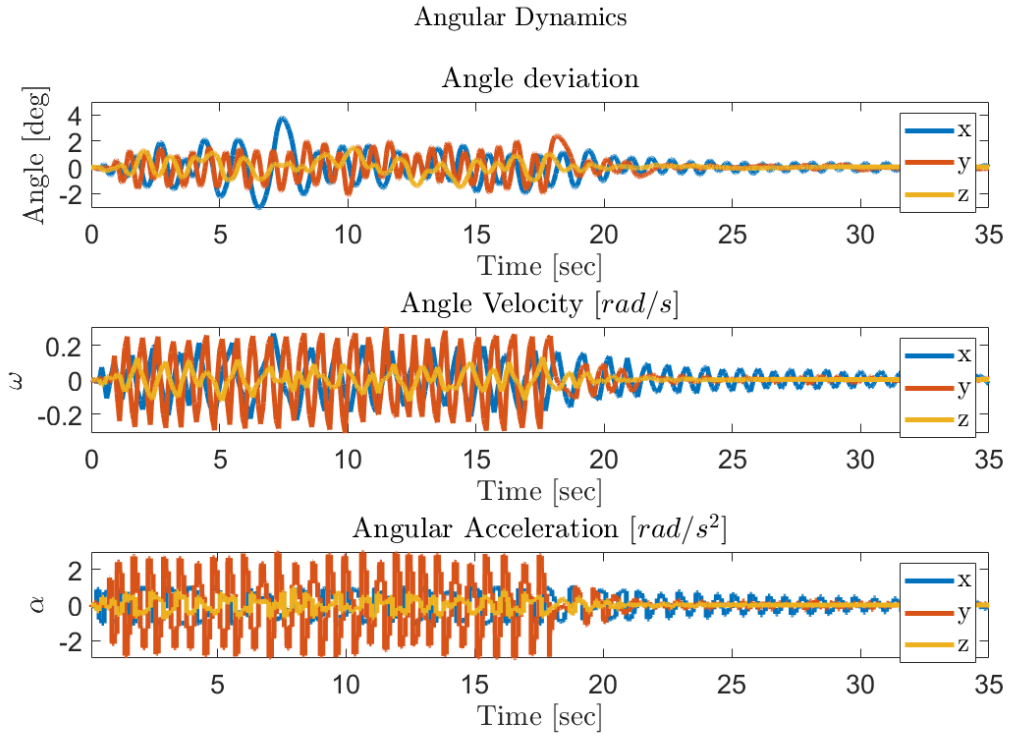

Figure 7.14: Angular dynamics results

The wanted thrusts from the system are translated into propeller thrusts, while they are limited to maximum values and the effect of propeller acceleration is taken into account. In (Figure 7.15), it can be seen that the

control forces are limited to their maximum of 300 N thrust. In fact, the system ideally wants more than the 300 N of thrust available. Here it is shown that propellers with high acceleration are important. A recommendation for a more advanced model would be to take the propeller acceleration into account for moments, but this is currently in too much depth for the current design.

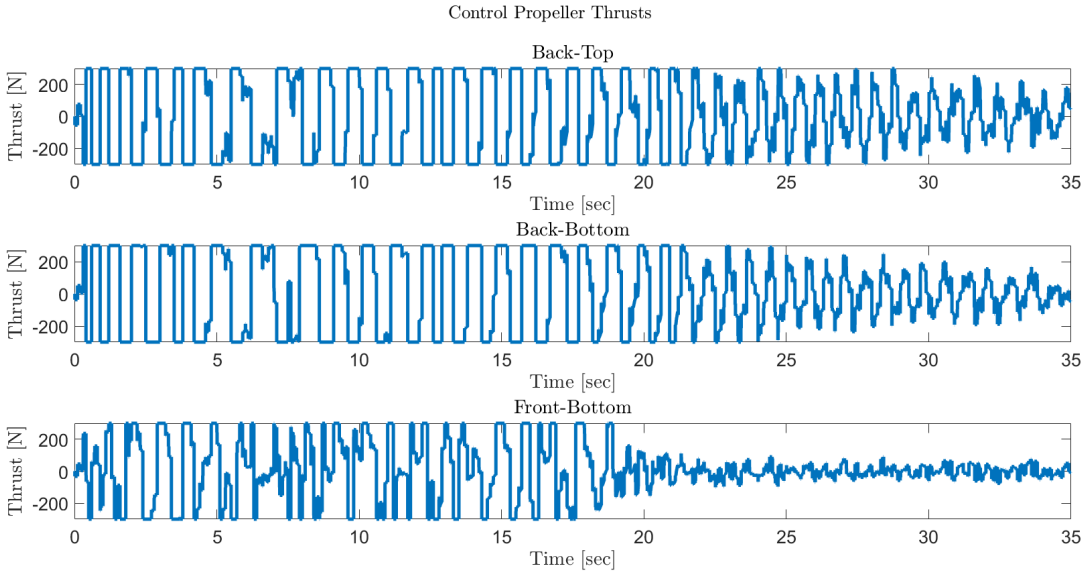

Figure 7.15: Control propeller thrusts

Figure 7.16 shows the thrusts from the lifting rotors. Note that the thrusts from these rotors to lift and move the vehicle forward are decoupled from this analysis, and thus are not included here. The maximum thrust needed per rotors is not far under 300 N. However, their maximum thrust allocated to control ranges from 2,600 to 5,600 N per rotor, as a result they are largely under-utilised. As such, a recommendation would be to also use these rotors for yaw control (Z-moment), as it is the largest moment, and will reduce the dependency on the control propeller.

Moreover, the low thrust needed means that the system can work with only 70% of the rotors in-operative for the control forces. Finally, note that the thrust used from these rotors greatly reduces around 20 seconds.

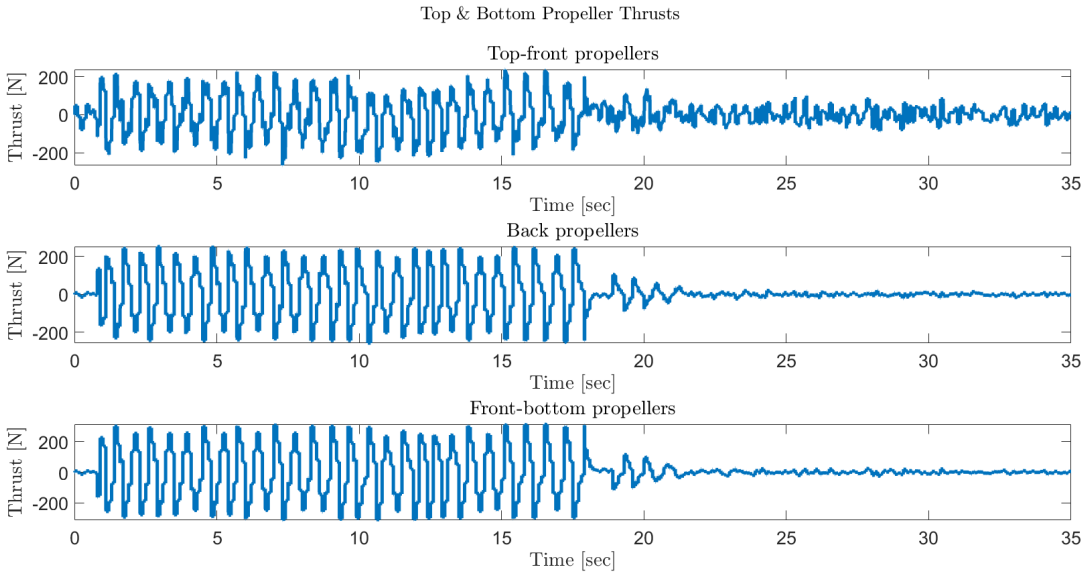

Figure 7.16: Lifting propeller thrusts

In terms of control, the hardest requirements to be met are the comfort requirements. For the linear plane, the

acceleration must be under 0.325 m/s^2, and the maximum deviation may not exceed 1 metre. Figure 7.17 shows the accelerations and the position deviation. The bottom result shows how the total position deviation vector stays well under the 1 m allowed deviation. Meanwhile, the acceleration stays largely under the a_{lim} of 0.325 m/s^2, however there are moments when it is over this value, especially the large peak around 10 seconds. The controller's gains and the forces applied can be altered to try and reduce these, however our analysis suggests these are caused mainly from the time delay, due to the sudden changes the counteracting force is only applied at a delay. To really make the vehicle comfortable, a certain form of deep learning should be applied to the model to make it predictive of the upcoming gust, or LIDAR sensors should be integrated to sense the wind speed before it arrives. One approach was taken to apply a gain to the Kalman filtered signal of the position, this allowed for the acceleration to be reduced many instances below the limit, but the peak was still present. If a data set of the gusts around the Shard was given, or tall buildings in cities, the model could predict the upcoming building wake, and take into account in the model - to allow it to provide a force just before the gust force hits. An example of this is shown in Figure 7.20.

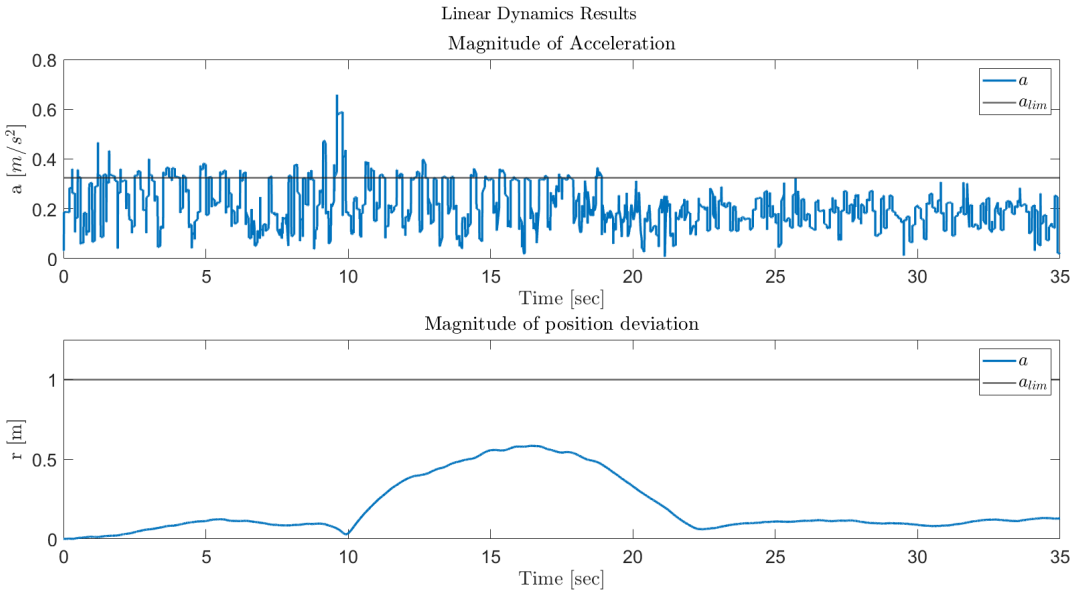

Figure 7.17: Magnitude of linear dynamics results.

Now in terms of the angular plane; the comfort for the angular frame can be quantified as:

$$
\begin{aligned}
|a| =& \sqrt{a_x^2 + a_y^2 + a_z^2} < 0.325 \\
a_x \approx& a_y \approx a_z = \sqrt{\frac{|a|^2}{3}} < 0.1876 \vec{a} = \quad \vec{\alpha} \times r_{cg-\vec{seat}} < 0.325 \\
\begin{bmatrix} \alpha_x \\ \alpha_y \\ \alpha_z \end{bmatrix} =& \begin{bmatrix} 0 & r_z & -r_y \\ -r_z & 0 & r_x \\ r_y & r_x & 0 \end{bmatrix} \cdot \begin{bmatrix} a_x \\ a_y \\ a_z \end{bmatrix} \cdot \frac{1}{r^2}
\end{aligned}
\tag{7.35}
$$

This results in the angular acceleration having a maximum absolute value of 0.0748, 0.2894 and 0.2147 rad/s^2 in the X, Y and Z axes respectively. As a result, Figure 7.18 does meet the angle deviation requirements, however it cannot meet the angular acceleration requirements. Again, partially due to the time-delay involved, predictive control may be able to reduce the angular accelerations to a certain extent. However, as the angular acceleration is far off the desired value, a new design approach should be taken in the next phase to solve this issue:

- Optimizing the position of the centre of gravity; such that it is close to passengers, this will reduce increase the minimum angular acceleration the passengers feel, however it would have to be very close to have a good enough effect.
- Optimize the centre of pressure position such that it is closer to the centre of gravity; this will reduce the aerodynamic moments.
- Pre-tilting the propellers; such that their effect acts instantaneously, counteracting any roll.

- Making the vehicle more symmetric around the z-y plane would also reduce the yaw moment, this could come around from removing the control propellers and using the lifting propellers for yaw control. They would also have to be able to translate in the y-direction, likely through yawing towards the path and moving forward into it.
- Alike to the linear model, apply a learning factor to the controller.
- A better controller design.

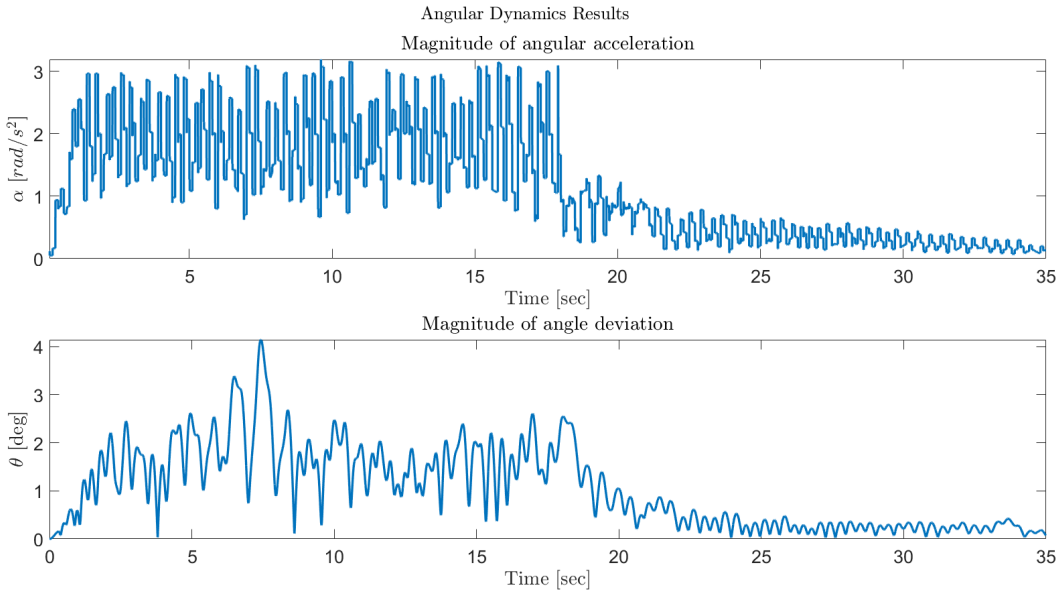

Figure 7.18: Magnitude of angular dynamics results.

The authors in **acc_argument** display the accelerations felt in normal driving, this displays a culmination of their results; so from this perhaps one can argue that the acceleration limit is in fact too low. With 4m/s^2 being comfortable in the lateral direction, this would translate into our vehicle feeling similar to one driving a normal car.

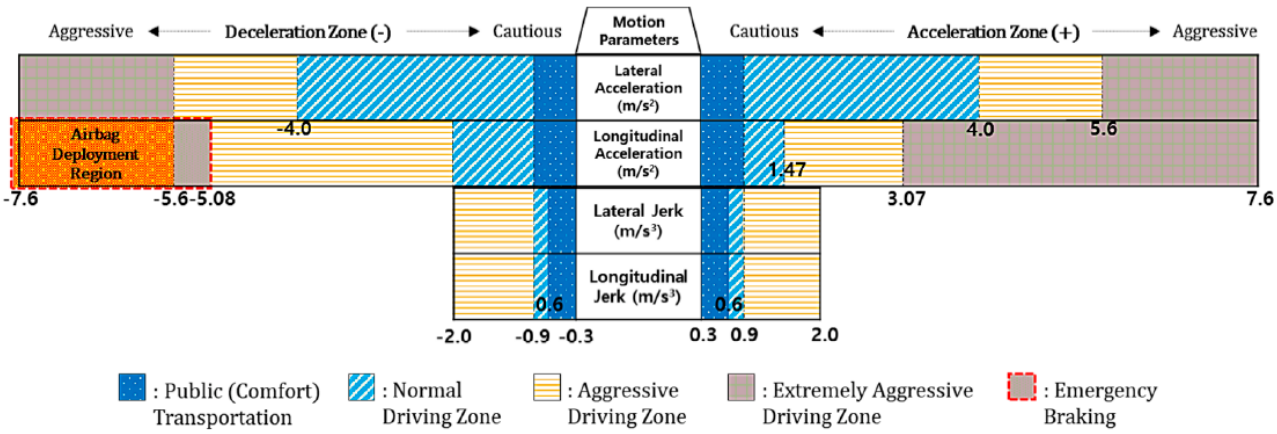

Figure 7.19: Accelerations felt in a car**acc_argument**

7.2.2. Learning results

To make a preliminary analysis into the effects of learning on the model's performance, the linear system was taken into account. Here the Shard case was fed into the aerodynamic module (with an identity as the transformation matrix input and a zero-vector for the vehicle velocity deviation), from here the simulation was run and the resulting aerodynamic forces found. To model the none-100% accuracy of learning techniques, each data point was multiplied by a value, coming from a uniform distribution of 0.5 to 1.0; as a result greatly skewing the data. The data was then interpolated and placed as a look-up table in the Simulink model. The PIDs for

the linear model were tuned with this as an inputting disturbance, and were simulated with the propulsion constraints in and the actual shard and aerodynamic case. The results were rather excellent, as shown by Figure 7.20. The vehicle has a minimal deviation, while meeting the acceleration requirements. Note that, there is no angular model here, but the deviation angles from it are small, and its effect on the linear dynamics system can be neglected. As a result, this shows data of gust should be put into a learning model, to help the controller even better combat the gusts, while keeping the passengers comfortable.

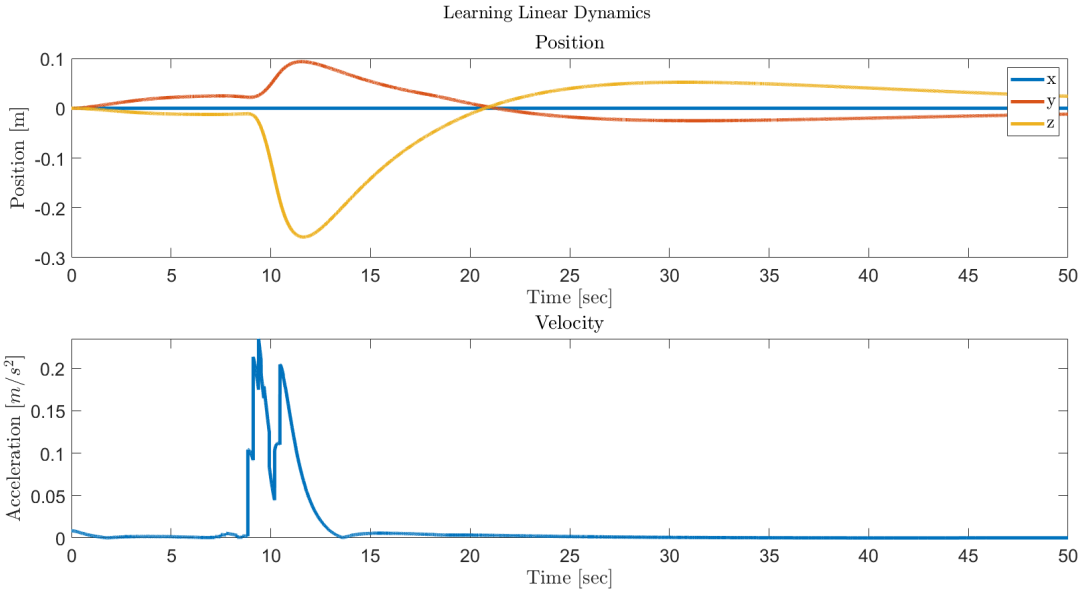

Figure 7.20: Preliminary analysis in the effect of learning on the system's results.

7.2.3. Standard gust profile results

This section models a simple wind gust acting on the vehicle in the Y direction (across the body) for 10.5 seconds, the vehicle is travelling at a nominal cruise speed of 100 km/hr in the X direction (i.e.) is moving forward with respect to the ground. Below, the effects on the linear model and angular model are analysed. Figure 7.21 and Figure 7.22 shows, that the vehicle satisfies all the requirements.

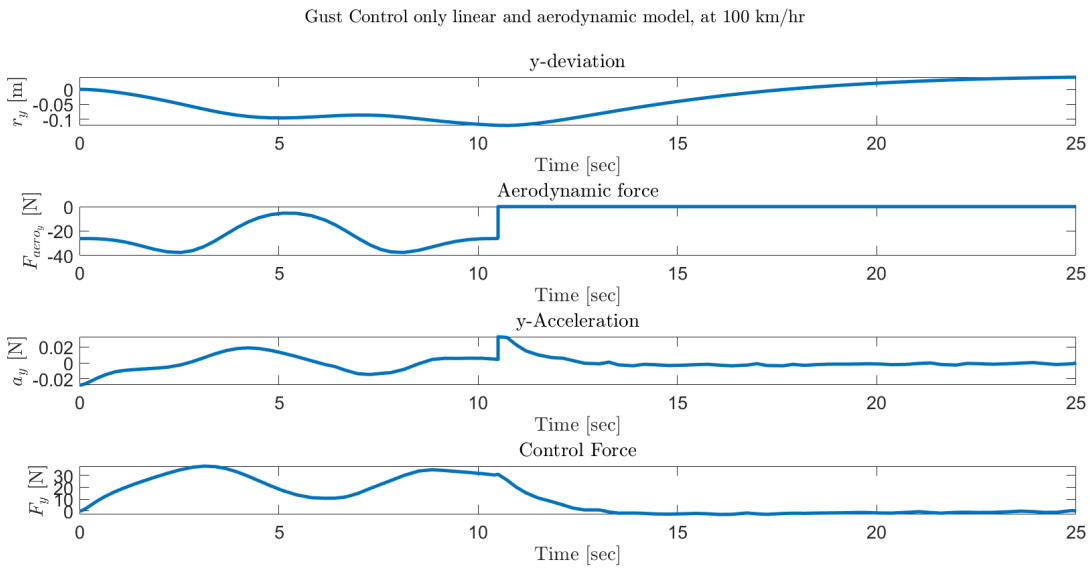

Figure 7.21: Gust control for linear dynamics.

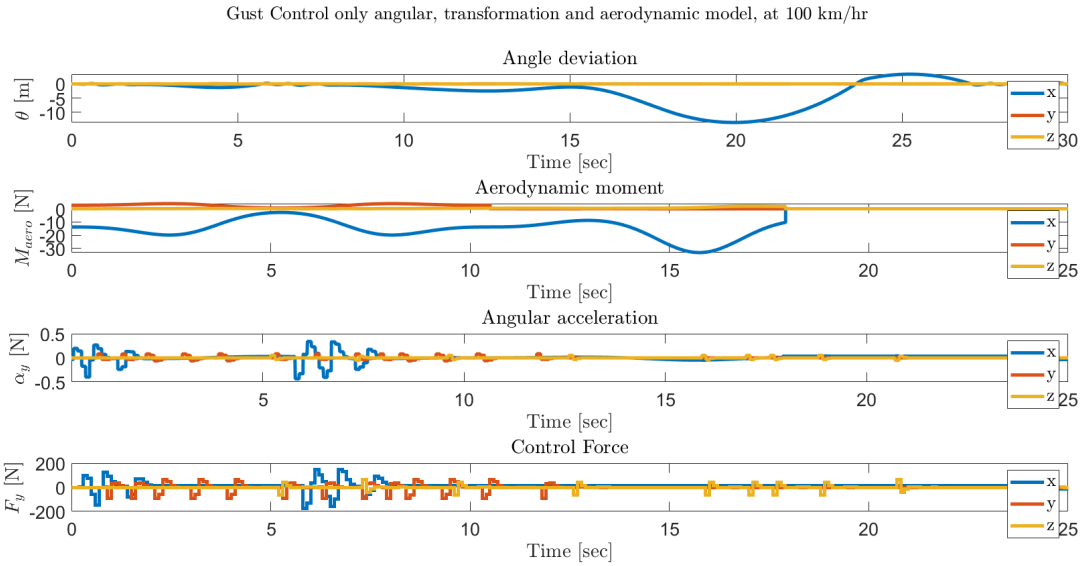

Figure 7.22: Gust control for angular dynamics.

7.2.4. Point mass results

To first quantify the important parameters for control, a point mass model was made, for 1 axis in the linear direction. This modelled the linear Y deviation, with no linear or sensor effects, from the path. Here the wind gust model is used with the first version of the drag model, while the controller is a simple PID.

This model showed C_D, S_{side} and time delay increase the load upon the passengers, control force and deviation from the trajectory increases. While, as C_D and S_{side} increase, so does the load factor, control force and deviation from trajectory. The plots from this are shown in the Midterm report **midterm**, the evaluation from it was: time delay is the most important parameter, but as it increases exponentially: low values are allowed; 0-0.3. Between this range, the results show that the other parameters have a larger effect on the controllability. Moreover, the side surface area and drag coefficients should seek to be as low as possible.

8. Final Structural Design

The final design of the structures of the vehicle is an iterative process. Every time a single component changes in weight, placement or orientation, the loads on certain parts of the vehicle change with it. Due to the changes in loads, the parts will change, and the process starts again from the beginning. All structural parts are designed separately but do impact each other, which is the reason an iterative program has been written, which will be described below. First, the extreme load cases are presented in Section 8.1. Then, the beams connecting the motors to the fuselage are designed in Section 8.2. The cabin is designed in Section 8.3. Next, the fuselage is designed in Section 8.4. In Section 8.5, the crash structures to keep passengers safer during impact are discussed. Section 8.6 discusses the structural aspects of noise reduction inside the cabin. Section 8.7 checks the eigenfrequencies of the structure, to make sure that resonance does not occur. Section 8.8 presents the design of the rotor beams. Section 8.9 shows an overview of the lug joint analysis methods. Section 8.10 and Section 8.11 present the design of the various fuselage joints, and the landing gear attachment. Finally, the material budget is summarized in Section 8.12.

8.1. Load cases

To come up with the structural design, the first step is to know the load cases. There are multiple various load cases. It is very important to find the most critical load cases, because these are the ones sizing the design. However, if a mistake is made in determining the critical load case, it can lead to malfunctioning of the vehicle and safety concerns.

There are 4 main load cases taken into account for the beams and landing gear:

- Take-off
- Standing on the ground
- A gust perpendicular to the beams/landing gear
- Touchdown at landing

At take-off, maximum lift is applied by the rotors. Therefore, this will be a main load case for the beams and the fuselage as well. While standing on the ground, the rotors do not produce any lift and the beam needs to withstand the weight of the beams and the motors. A gust perpendicular to the beams will probably not be as critical, however it will be a load in a different direction and should be taken into account as well. The last load case is in touchdown, this is mainly for the landing gear as the experienced load will be larger than 1g for a short time. All the loads on the beam are displayed in Figure 8.1.

8.2. Beam design

Following from the design of the propulsion system, which is described in Chapter 6, it is given that 8 rotors will be used to propel the vehicle. For every rotor, a beam will connect a rotor to the fuselage. Therefore, 8 of those beams are needed to carry the complete propulsion system.

For the beam, it is required that it will not break under the load cases described in Section 8.1, including a certain safety factor. The first step in designing the beam is to identify all the external forces working on the beam and put them in a Free-Body Diagram (FBD). The beam will be idealized as a cantilever beam. Figure 8.1 shows the FBD. The loadcase from 8.1, which will cause the critical loading on the beam is the take-off loading in which the maximum thrust is working on the beam. This works in the tip of the beam. Also the weight of the beam and the weight of the engine are working in the same loadcase.

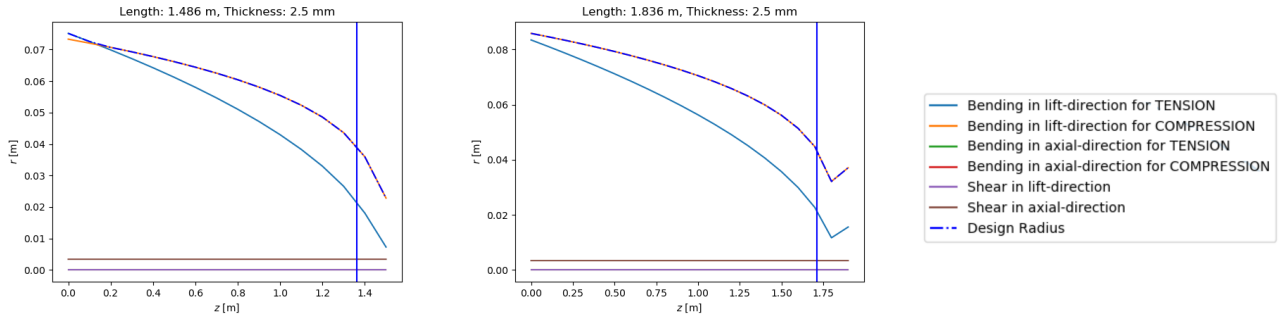

(a) Top&Bottom aft Beam Design **(b)** Bottom Front Beam design

Figure 8.2: Beam Designs, radii required everywhere on the beam span. The vertical line marks the placement of the propeller joint. The dashed line gives the minimum radius required.

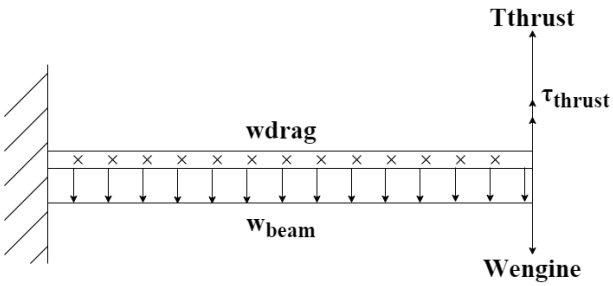

Figure 8.1: Rotor beam free body diagram

In this figure, multiple forces which vary under different load cases are given. The beam carries a rotor with a certain weight and a lift force. The beam itself will be carrying its own load and a drag force.

From the loads which work on the beam, a shear force and a bending moment diagram are derived. The critical loading is the bending stress in compression, due to the thrust of the rotors. For this reason, the diameter of the beam could be increased indefinitely, with a very low thickness. To this end, certain limitations have to be made, such as drag considerations on the overall power efficiency of the vehicle, manufacturability, and buckling. It was decided that the beam would have a root radius of 8.2 cm for the larger beam, and 7.1 cm for the small beam. The rest of the beam had a variable radius, depending on the load at that cross-section. The thickness is kept constant over the span of the beam at 2.5 mm.

8.3. Cabin design and ergonomics

The final thing that needs to be done before the start of the structural design on the design of the fuselage is to make sure all the payload can fit in the vehicle and thus size the fuselage body.

To start off, the passengers will need to sit down into the cabin. The starting point was taken from the initial sizing in the midterm report **midterm**. With the CAD software CATIA, a person with the height of 1.97 m was placed in the Veatle and with the help of ergonomic design he was fitted inside the cabin as comfortable as possible. This length covers the 95th percentile of the length of all male people.

Next up is the remainder of the payload; the suitcases. When people go somewhere they also take luggage with them and this will need to be transported with them inside the vehicle. A special luggage compartment is made. In this luggage compartment, there should be enough space for 2 large sized suitcases and 2 small trolleys, as for the business case the focus is from an airport to the city centre. This will be possible with the luggage compartment which has 0.8 m x 0.5 m dimensions with the width reaching up to the wall, on this constraint the fuselage changed a small amount since it was very tight to include all luggage and still have enough space left to store the batteries behind it.

This was the last big part that had to be stored in the back of the vehicle. This is an advantage for the C.G.-position, to get the C.G. further to the back, this is necessary for the propulsion system, because the propellers are slightly shifted to the back. Also the batteries should be easily accessible for maintenance and battery swapping.

The last things which are fitted in are the control systems and a tablet on which the route of the flight can be

displayed.

8.4. Fuselage design

For the fuselage, different loads are acting on it at various positions. All the loads working on the vehicle during operation are listed below:

- Fuselage weight
- Passenger weight
- Resultant force from beams (Lift and Weight)
- Resultant force from landing gear
- Luggage weight
- Battery weight
- Aerodynamic loads

The fuselage needs to be able to handle these loads. A structural design toolbox was developed to analyse the fuselage loading. For the design, material properties of aluminium are used. For the fuselage to get a shape and a weight estimate, this should give a conceptual design. In a later, more detailed design, the aluminium properties will be replaced for carbon fibre.

8.4.1. Structural design toolbox

For the design of the fuselage, a Python program is created, in which an idealised fuselage is analysed for the stresses and shears which are caused by the forces working on the fuselage. When the fuselage design is initiated, different functions will be executed to find whether the design complies with the requirements or whether different parts need to be iterated.

Initiation

The program is initiated by defining the frames which are needed throughout the length, the z-direction, of the fuselage. This is visible in Figure 8.3. In the toolbox, those frames are different cross-sections of the fuselage. The stringers are initiated by adding them to a certain section between two cross-sections of the fuselage, for those stringers the boom idealisation is used, and those booms do not change throughout a section, except for following the growing cross-sectional area. These booms are also visible in the figure.

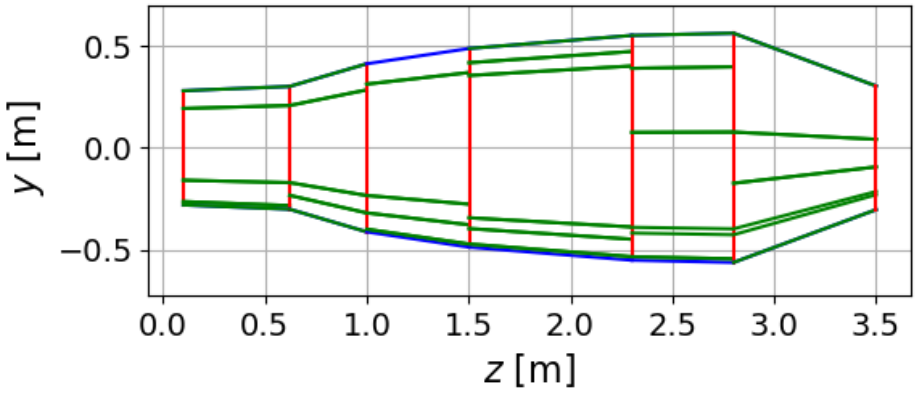

Figure 8.3: Fuselage in toolbox representation seen from the side. The blue lines define the outer edges, the red lines the cross-sections, and the green lines the booms.

The cross-sections and booms are positioned such that requirements and design choices (doors, windows, the cabin, the mounting points to the beams and landing gear) are conveniently introduced into the fuselage structure. This means that cut-outs are also made by removing the skin between cross-sections and booms. The area of the stringer and the skin thickness between two stringers are defined when initiating those cut-outs.

Loading diagrams

The loads during operation need to be as well-defined as possible to analyse the fuselage structure in the end. The shear force and bending moment diagrams for the x-axis and y-axis for maximum thrust and a hard landing are given in Figure 8.4. For the xz-plane, maximum thrust is taken into account for vertical rotors, which is visible in Figure 8.4a and Figure 8.4c.

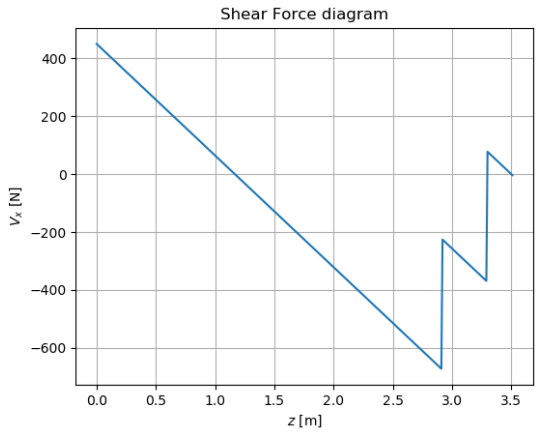

(a) Shear force in x-direction.

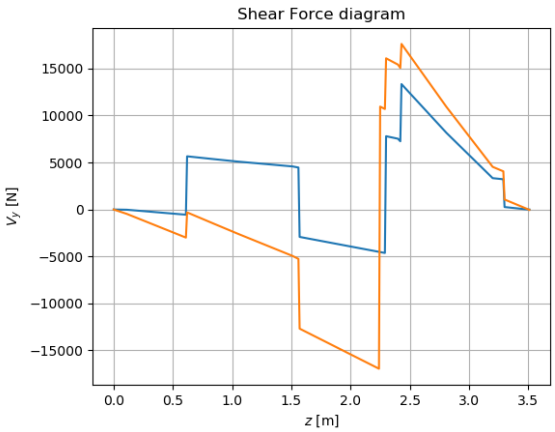

(b) Shear force in y-direction.

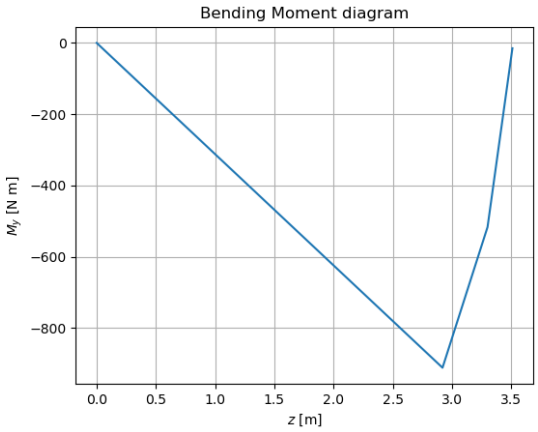

(c) Bending moment in y-direction.

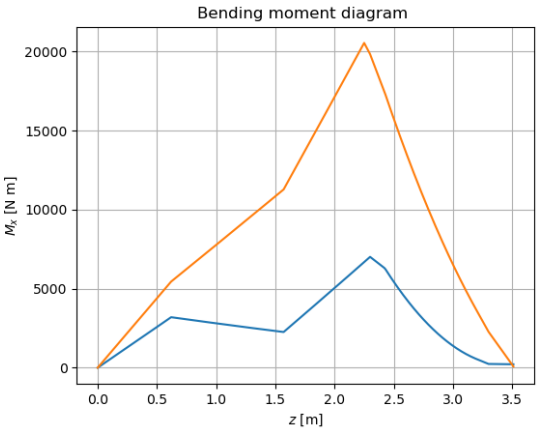

(d) Bending moment in x-direction.

Figure 8.4: Loading diagrams. In blue are the loading diagrams complying with the load case for maximum thrust for all propellers. In orange, the load case for a hard landing is given, which affects the diagrams in the yz-plane.

Normal stress

In the boom idealisation it is assumed that stress only goes through the booms. The thickness of the skin will be set to 0 mm. To compensate for that, a correction is made by adding area in the boom for the analysis, using Equation 8.1 **Magic-Book**.

$$B_i = A_i + \frac{t_D b_d}{6}\Big|_{i\to i+1}\left(2+\frac{\bar{\sigma}_{i+1}}{\bar{\sigma}_i}\right) + \frac{t_D b_d}{6}\Big|_{i\to i-1}\left(2+\frac{\bar{\sigma}_{i-1}}{\bar{\sigma}_i}\right) \tag{8.1}$$

In this equation B_i is the boom area, A_i the stringer area, t_D the skin thickness and b_d the distance between two booms. The stress is an output of the fuselage tool, therefore, it is possible to calcalute the boom area B from the stringer area A, from B to A, when the stress ratios $\frac{\bar{\sigma}_{i+1}}{\bar{\sigma}_i}$ and $\frac{\bar{\sigma}_{i-1}}{\bar{\sigma}_i}$ are known.

After the boom area is estimated, the area moments of Inertia are calculated for every boom, contributing to the total area moments of Inertia of a cross-section. These equations are given in Equation 8.2.

$$\Delta I_{xx_i} = B_i y_i^2 \qquad\qquad \Delta I_{yy_i} = B_i x_i^2 \tag{8.2}$$

Using the area moments of Inertia given in those equations and the bending moments (function of the z-position) from the loading diagram, the direct stress is calculated using Equation 8.3. There are different failure modes for stress. In tension, tensile strength is the limit for carbon fibre, for metals this is the yield strength. In compression, buckling needs to be taken into account. The maximum stress which is allowed in compression is determined using equation 8.4

$$\bar{\sigma}_z = \frac{M_x y}{I_{xx}} + \frac{M_y x}{I_{yy}} \tag{8.3}$$

$$\bar{\sigma}_b = \frac{\pi^2 E}{(l_e/r)^2} \tag{8.4}$$

In this equation E is the E-modulus of the material, $l_e = l \cdot K$ in which l is the length of a stringer and K a value based on the clamping, which is set to 2 due to the fact that the stringers are mounted to the frames.

Shear stress
In the boom idealisation, shear only occurs in the skin panels. Between the booms, the shear flow does not change due to assumption of a constant thickness. Shear is caused by two different type of loads. The first one is the shear force. This is taken from the plot in Figure 8.4a and Figure 8.4b. These shear loads are substituted in Equation 8.6 to get the shear flow $\bar{q}$.

As can be seen from the equation, the shear flow is a summation of the shear flow caused by V_x and by V_y. The shear flow contribution of one of those will be zero on the section which is in line with the axis of the shear force. From there, the $\Delta\bar{q}$ of a boom will be added to the shear flow before the boom.

In addition to this shear force, torsion T on the fuselage will cause a shear flow through the skin. This shear flow is determined using equation Equation 8.6.

In this equation A_{enclosed} is the area of the cross-section enclosed by all the skin. Also, this contribution to the shear flow is equally distributed over the cross-section. This should be added to the shear flow caused by the shear force to have a total shear flow distribution in the cross-section. Now the shear stress is calculated using equation 8.7.

$$\Delta\bar{q} = -\frac{V_x}{I_{xx}} B_i x_i - \frac{V_y}{I_{yy}} B_i y_i \qquad (8.5) \qquad \bar{q} = \frac{T}{2A_{\text{enclosed}}} \qquad (8.6) \qquad \bar{\tau} = \frac{\bar{q}}{t} \qquad (8.7)$$

Design
Using the methods described in the previous sections. It is possible to make a first estimation on what the stringer areas, the stringer positioning and the skin thicknesses need to be. From this, a weight estimation is made. Before this, all values are calculated by using a table with all values. A short version of such a table, is visible in Table 8.1.

Table 8.1: Fuselage cross-section 1 calculations for first for booms

Boom	x [m]	y [m]	B [mm^2]	t_{D} [mm]	ΔI_{xx} [m^4]	ΔI_{yy} [m^4]	$\bar{\sigma}_z$ [MPa]	$\bar{\sigma}_{\text{cr}}$ [MPa]	$\bar{\tau}$ [MPa]	$\bar{\tau}_{\text{cr}}$ [MPa]
1	0.247	0.193	60.0	0.2	$2.23E-6$	$3.65E-6$	8.7	400.0	-39.1	283.0
	0.265	0.207			$2.58E-6$	$4.22E-6$	50.2	400.0	-32.7	283.0
2	0.0	0.28	60.0	0.2	$4.7E-6$	0.0	11.6	400.0	-36.0	283.0
	0.0	0.301			$5.44E-6$	0.0	67.1	400.0	-29.8	283.0
3	-0.247	0.193	60.0	0.2	$2.23E-6$	$3.65E-6$	9.5	400.0	36.8	283.0
	-0.265	0.207			$2.58E-6$	$4.22E-6$	55.0	400.0	32.7	283.0
4	-0.28	-0.159	50.0	0.2	$1.26E-6$	$3.93E-6$	-0.6	-10.1	38.1	283.0
	-0.301	-0.171			$1.46E-6$	$4.54E-6$	-3.3	-10.1	33.2	283.0

From the table above, now the sizing of the stringers and the skins is calculated. There are some parameters from Table 8.1 which need to be taken into account. So the stress and the shear are not allowed to be larger than the critical stress or shear. For stress this is done by keeping the stress $\bar{\sigma}_z$ smaller than the critical stress $\bar{\sigma}_{\text{cr}}$. For different skin panels it is needed to recalculate the shear stress. This is due to the structure around the cutouts, compensating for the cutouts. In the end, the design of the different cross-section is given in Table 8.2, Table 8.3, Table 8.4, Table 8.5, Table 8.6 and Table 8.7. In Figure 8.5 the cross-sections from the different tables are plotted.

Table 8.2: Fuselage design cross-section 1

Boom	A_{str} [m^2]	t_{skin} [mm]	W_{str} [kg]	W_{skin} [kg]
1	[50.1, 50.1]	0.2	0.72	0.47
2	[38.4, 23.8]	0.2	0.45	0.82
3	[36.5, 09.5]	0.2	0.33	0.91
4	[76.4, 69.6]	0.2	1.05	0.78
5	[83.2, 83.2]	0.2	1.19	0.92
6	[89.4, 71.7]	0.2	1.16	0.81
7	[65.7, 94.5]	0.2	1.15	0.46
8	[38.5, 43.1]	0.2	0.59	0.35
Total			6.63	5.52

Table 8.3: Fuselage design cross-section 2

Boom	A_{str} [mm^2]	t_{skin} [mm]	W_{str} [kg]	W_{skin} [kg]
1	[29.5, 29.5]	0.2	0.32	0.38
2	[05.6, 32.8]	0.2	0.21	0.64
3	[54.2, 06.1]	0.2	0.33	0.79
4	[40.5, 46.3]	0.2	0.48	0.69
5	[43.0, 42.9]	0.2	0.47	0.83
6	[59.8, 42.2]	0.2	0.55	0.53
7	[24.0, 81.3]	0.2	0.57	0.44
8	[52.3, 39.8]	0.2	0.5	0.59
Total			3.43	4.9

Table 8.4: Fuselage design cross-section 3

Boom	A_{str} [m^2]	t_{skin} [mm]	W_{str} [kg]	W_{skin} [kg]
1	[90.0, 0.9]	0.0	1.26	0.0
2	[90.0, 0.9]	0.0	1.26	0.0
3	[170.0, 1.70]	0.0	2.38	0.0
4	[101.6, 0.514]	0.2	1.07	2.0
5	[43.2, 0.896]	0.2	0.93	0.96
6	[89.6, 1.664]	0.2	1.79	0.52
7	[210, 2.1]	0.0	2.94	0.0
8	[170, 1.7]	0.0	2.38	0.0
Total			14.02	3.48

Table 8.5: Fuselage design cross-section 4

Boom	A_{str} [mm^2]	t_{skin} [mm]	W_{str} [kg]	W_{skin} [kg]
1	[1.5, 1.5]	0.0	3.3	0.0
2	[1.181, 1.527]	0.2	2.98	1.92
3	[1.335, 0.16]	0.2	1.64	1.8
4	[1.7, 1.7]	0.0	3.74	0.0
5	[1.5, 1.5]	0.0	3.3	0.0
6	[2.0, 2.0]	0.0	4.4	0.0
7	[0.882, 1.668]	0.3	2.81	2.95
8	[1.935, 0.225]	0.3	2.37	2.61
9	[0.227, 2.0]	0.3	2.45	1.24
10	[2.0, 2.0]	0.0	4.4	0.0
11	[2.0, 2.0]	0.0	4.4	0.0
Total			35.81	10.53

Table 8.6: Fuselage design cross-section 5

Boom	$A_{stringer}$ [mm^2]	t_{skin} [mm]	$W_{stringer}$ [kg]	W_{skin} [kg]
1	[69.5, 63.5]	0.2	0.91	0.93
2	[36.6, 35.3]	0.2	0.49	1.17
3	[87.7, 57.6]	0.2	1.0	1.2
4	[04.7, 30.7]	0.2	0.24	1.2
5	[120.0, 120.0]	0.0	1.65	0.0
6	[81.5, 83.3]	0.2	1.13	1.2
7	[84.5, 110.0]	0.2	1.33	1.26
8	[110.8, 77.4]	0.2	1.29	1.16
9	[160.0,160.0]	0.0	2.19	0.0
Total			10.23	8.12

Table 8.7: Fuselage design cross-section 6

Boom	$A_{stringer}$ [mm^2]	t_{skin} [mm]	$W_{stringer}$ [kg]	W_{skin} [kg]
1	[60.0, 60.0]	0.0	1.26	0.0
2	[60.0, 60.0]	0.0	1.23	0.0
3	[22.4, 24.8]	0.12	0.5	0.81
4	[90.6, 11.7]	0.12	1.08	1.48
5	[08.3, 08.4]	0.12	0.17	1.12
6	[13.5, 73.8]	0.12	0.9	0.49
7	[71.3, 62.8]	0.12	1.39	0.66
8	[146.1, 56.4]	0.12	2.13	0.85
Total			8.66	5.42

In the tables, the area has two values. This is the area on one and the other end of the boom. The difference is causes due to the constant boom area which is used to initialise program. The cross-sections are plotted in Figure 8.5. Those values differ in some cases quite a lot. This is caused by some loads which are assumed to be point loads. Due to this point load, stresses change quite rapidly. This behavour is mainly visible in the sections 2, 3, 5 and 6. Because beams are attached here, the landing gear and the batteries, which cause this kind of behaviour. For boom 3 and 4. It is needed to add some booms in places where it is possible. This is a compensation for the places where the door and window cutouts are. These extra booms make it possible to take up some stress, which cannot be handles by the already placed booms in the surrounding cross-sections.

With these results, the total weight of the stringers and skins together is estimated. Summing all weight values gives $W_{FL}, W_{str} + W_{skin} = 78.8 + 38.0 = \mathbf{116.8}$ kg. The estimated weight was 100 kg. With an aluminium structure, the weight will be 116.8 kg. But replacing this with carbon fibre will lead to a weight reduction of 10-20% of the structural weight. With this taken into account, the estimation of 100 kg still holds.

Given those tables, an initial design for the fuselage is made. Still there are locations in the fuselage where a more detailed analysis is required. Those are stated below:

- The booms which represent the beam between the window and the doors need to carry a very large bending moment. They are on the both sides of large cutouts, and therefore it is not possible to place booms nearby.
- This analysis is not representing local effects on stress, some of those local effects are covered in this chapter, in the sections about carbon fibre and hinges.
- The cutouts for the real fuselage are quite large and have hard shapes. Therefore, repositioning of the frames might be needed.

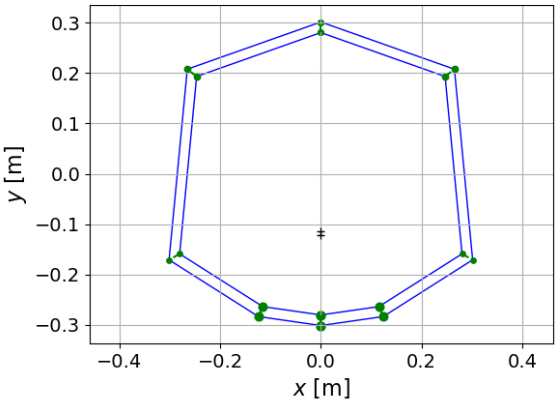

(a) Cross-section 1

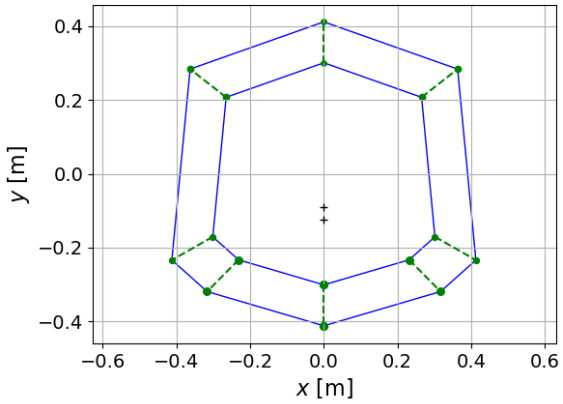

(b) Cross-section 2

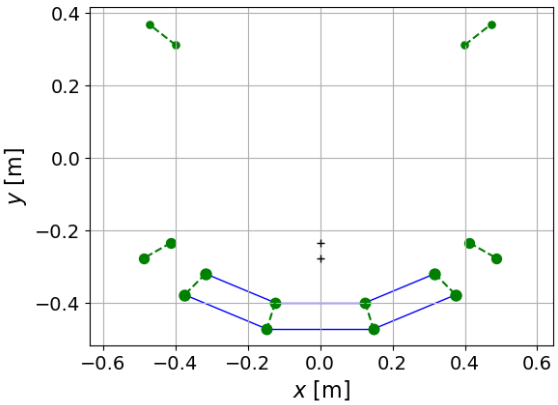

(c) Cross-section 3

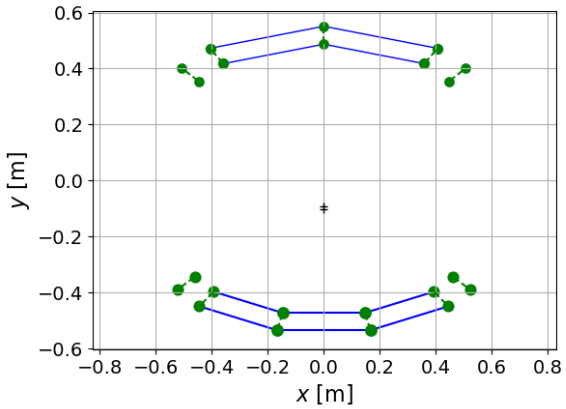

(d) Cross-section 4

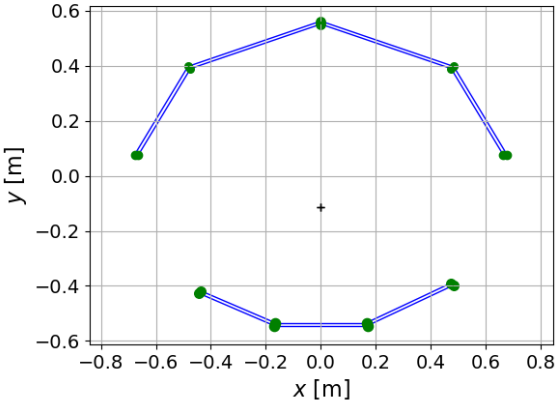

(e) Cross-section 5

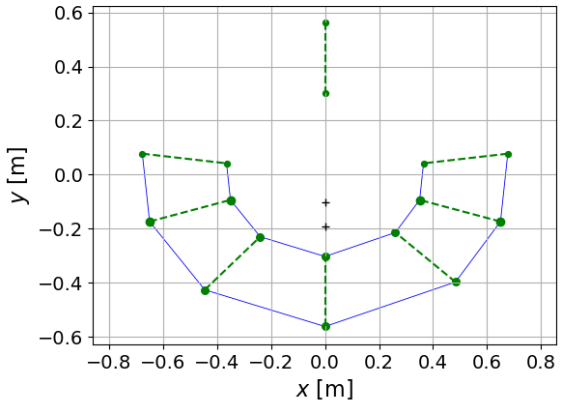

(f) Cross-section 6

Figure 8.5: Cross-sections in fuselage, the positioning of the booms is visible in green. The skins are visible in blue. Those are straight lines in this idealisation.

8.5. Crash structure

This section describes the measures taken to keep the passengers safe during impact. The five main things required to keep passengers safe are: a stiff container which accommodates the passengers, a restraint system to restrain the passengers during impact, an energy absorbing structure, some protection from the local environment and protection from postcrash factors such as fire.

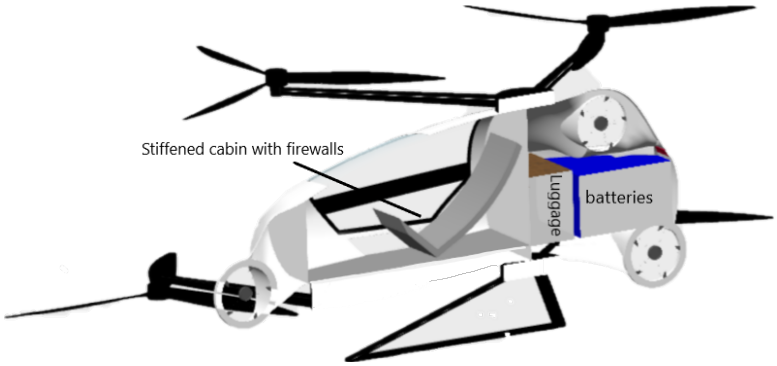

Figure 8.6: Cross-section of the fuselage

Firstly, the container is designed. As can be seen in Figure 8.6, in front of the passenger's feet and behind their back, a wall is installed. This, together with the cabin floor, forms a container which protects the passengers during a crash. Next to forming a container, these walls, in particular the back wall, also serve as a firewall. Postcrash damage due to fire or oil have often led to the death of passengers who survived the initial impact **CrashCREEP**.

To restrain the passengers during impact, the mounting of the chairs and the seatbelts are of uttermost importance. During a crash, the floor of the cabin could potentially deform, therefore, the seats should be mounted in appropriate locations to account for this deformation and still restrain the seat to the fuselage. To restrain the passenger to the chair, seatbelts are necessary. Various options exist on the market today. From single strap seatbelts that are found in commercial aircraft, to full five-point harnesses that can be found in pilot seats. As the single strap seatbelt is not very safe, due to the unrestrained shoulders, the shoulder straps are advisable for the Veatle. The crotch strap, that differentiates the five-point harness from the four-point harness, prevents the passenger from sliding out of the seat. However, helicopters usually use four-point harnesses. Therefore, the passengers in the Veatle will utilise the four-point harness to remain in the seat during a crash.

Even though the passengers are restrained to their seat and the seat is restrained to the cabin floor, the passengers still run the risk of hitting parts of their body on protruding objects in the cabin. Thanks to the minimal interior design, which includes seats and a basic infotainment system, the possibility of hitting the body on dangerous objects within the cabin is minimized as well.

Lastly, during impacts, energy should be absorbed. The impact energy is usually transformed to bending energy for metal structures and in fracture energy for composite structures. This structure would be installed under the floor of the cabin. Five options were recommended by NASA, as presented in Figure 8.7. Additional research should be done for the cabin fuselage crash resistance, as fracture of composite structures can also be dangerous by itself. **NasaCrashFloorStructures**.

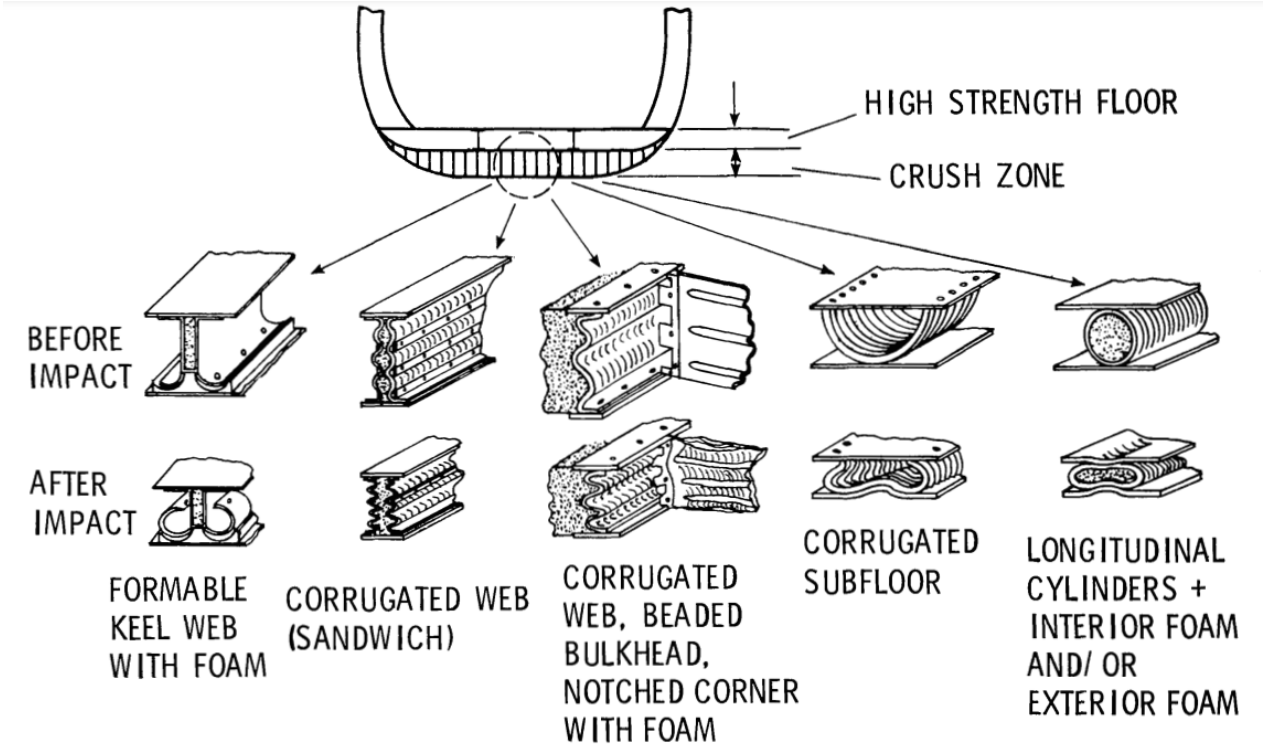

Figure 8.7: Load-limiting, energy-absorbing concepts presented by NASA

It should be noted that the foam core was disregarded during the further analysis of the structures, as it added too much weight for the increase in performance. Next to these structures, the structure of the landing gear is made from carbon fibre, this absorbs energy when it fractures and therefore adds to the crash safety of the passengers.

8.6. Acoustical insulation of the cabin

To provide a sufficient level of passenger comfort, it is likely that the cabin will require some insulation in order to achieve a noise level of < 60 dB(A) **(REQ-PROP-NOI-01)**. NASA has done research into acoustic treatment of a helicopter cabin in the 70s, and they have managed to achieve an approx. 30 dB reduction compared to an untreated case **NASACabin**. They have used 180 kg of insulating material for a MTOW of 18000 kg. With those values in mind, we estimate an additional 10 kg for the cabin insulation in order to achieve the needed cabin comfort. Commercial insulation products are readily available. For the Veatle, 50.8 mm thick POLYDAMP Acoustical Foam will be used for a cabin surface area of 8.0 m^2 leads to 0.40 m^3 volume for a nominal density of 29 kg/m^3 leads to 11.6 kg of insulation material.[1]

8.7. Analysing the eigenfrequencies of the structure

Now that all the design is done, the eigenfrequencies should be checked to make sure that parts of the structures will not suffer from resonance. The lowest eigenfrequency of a system is $f_0 = \frac{1}{2\pi}\sqrt{\frac{k}{m}}$ where f_0 is the frequency, k is the spring constant and m is the mass. For a beam this can also be written as $f_0 = \frac{C_2}{2\pi}\sqrt{\frac{I}{AL^4}}\sqrt{\frac{E}{\rho}}$ where C_2 is a constant, I is the moment of inertia, A is the cross-sectional area, L is the length of the beam, E is the Young's modulus and ρ is the density of the used material. With this formula, the eigenfrequencies of the beams as well as the rotor blades can be calculated.

All these frequencies will be compared to frequencies which can cause resonance, the frequency of the spinning rotors for example. If these frequencies are too close together, a redesign of the blades and beams or a change in rotor RPM is needed to make sure the structure will not fail due to resonance. With these frequencies there has been taken at least a 10% margin, so there will not be very close interaction with the eigenfrequencies.

[1] *https://www.polytechinc.com/products/acoustic-foam[Cited 30/05/2022]*

Table 8.8: Eigenfrequency analysis

Part	Frequencies of the rotation	Natural frequency
Beams	not applicable	60
Rotors	12-15/40-45	121
Propellers	80-100/200-240	278

8.8. Designing the rotor to beam joint

The design for the joint is shown in Figure 8.8a. The key aspect to design the propeller-to-beam joint is the area of the cross-section of the beam connection. This is the critical parameter for this part, because at the joint, the shear loading is the dominant loading. The external loading of this part is shown in the beam design in Figure 8.1. The thickness of this cross-section is varied until a safety factor of 1.5 is reached when using the aluminium AL-7075 alloy. The reason aluminium is chosen over carbon fibre is that the motor is mostly constructed of aluminium, and if it were connected, a greater area would be in contact between the two opposed materials. The critical location for shear is in the red line, where the area is lowest, as shown in Figure 8.8. Another reason for choosing aluminium is the torque generated by the motor. Since the part would be loaded in multiple directions, The fibres in this part would also require resistance in multiple directions, which reduces the weight advantage. Additionally, the cost of designing and manufacturing the part would be prohibitive. The round edges are used to reduce the stress concentration generated in sharp corners, and the cutouts on either side of the joint are used for cooling the motors. The engine is mounted with 6 countersunk bolts to the bottom side of the joint.

(a) Rotor to Beam Joint

(b) Critial Location for Shear Loading

Figure 8.8: Rotor joint views

8.9. Lug joint analysis

The joints of the UAM vehicle are heavily reliant on lug joints. Lug joints are generally used to transfer large loads, and should allow for maintenance and modularity. The trade-off is additional weight, when compared to other methods of joining, such as riveting, which distributes loads more evenly. There are several areas where lug joints are used, for example attaching wings to the fuselage of an aircraft, or attaching the landing gear to the fuselage. For the lug joint analysis, a simplified analysis is performed. There are several modes of failure to take into account, including the tension failure across the net section, shear tear out across two planes, and bearing failure, which are represented in Figure 8.9. The red lines indicate the planes of failure. In this simplified analysis, only the axial load is considered, which is also the critical loading. The reason for this is because of the bending stress in the beam, which is maximum in the edges of the beams.

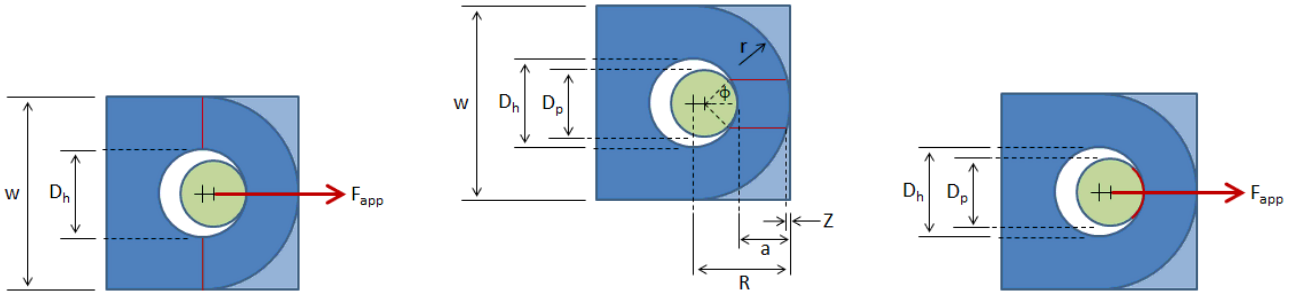

(a) Tensile Failure

(b) Shear tear out failure

(c) Bearing Failure

Figure 8.9: Failure modes of Lug joint in the simplified analysis

For tensile failure, the area of the net section is given by Equation 8.8, and the ultimate tensile load is given by Equation 8.9. The variables for the following equations are shown in Figure 8.9.

$$A_t = (w - D_h)t \tag{8.8}$$

$$P_{tu} = \sigma_{tu} A_t \tag{8.9}$$

For the shear tear out along two planes, where $a = R{-}0.5D_h$, Equation 8.13 gives the ultimate shear load.

$$A_s = 2L_{sp}t \tag{8.10}$$

$$L_{sp} = a + \frac{D_p}{2}(1 - \cos\phi) - Z \tag{8.11}$$

$$Z = r - \sqrt{r^2 - (\frac{D_p}{2}\sin\phi)^2} \tag{8.12}$$

$$P_{su} = \sigma_{su} A_s \tag{8.13}$$

For the bearing failure, the two formulas, 8.14 and 8.15 suffice.

$$A_{br} = D_p t \tag{8.14}$$

$$P_{bru} = \sigma_{bru} A_{br} \tag{8.15}$$

From these three failure modes, it is possible to create a preliminary sizing for the lug joints. From these formulas, possible values for r, D_h, D_p, w and r can be iterated to find the design with the lowest weight. However, the simplified analysis only provides a very rough estimate of the strength of the lug joint. From these initial dimensions, a more accurate design could be achieved using the Air Force Method. The Air Force Method uses empirical curves, accounts for transverse or oblique loading, and considers the connection of the clevis pin. For this method, the overall joint strength could be represented by the Double Shear Joint strength. A convenient calculator is available to manually optimize the design [2]. The calculator is also validated [3]. The analysis starts from the values obtained from the simplified analysis, and altering the dimensions while keeping the overall shape the same, to minimize weight as much as possible.

The general method is as follows. The first step is to calculate the joint strength without pin effects, pin shear strength, and pin bending strength. From these values, it is determined whether the clevis pin is strong in bending, or weak in bending. The pin is strong if the pin is not critical in bending strength. In other words, the pin bending strength is greater than the pin shear strength, or greater than the nominal joint strength. If the pin is strong, it will distribute the load evenly over the lugs, and the lug joint is not affected by unusual behaviour from the clevis pin. In this case, the nominal joint load will be equal to the ultimate joint load. If the pin is weak, the load will not be distributed evenly, and will fail earlier than expected. To account for this, a 'balanced design' joint load will need to be evaluated. For this design, weak pins will not be considered, as they are a poor design choice. Finally, the allowable load is chosen to be the lowest value of either the ultimate joint load or the pin bending strength. This method can be examined in greater detail in **bruhn_1973**.

8.10. Designing the Fuselage Joints

There are three joints which will be connected to the fuselage. The top joint will affix the top four rotor beams to the firewall frame. The bottom joint will attach two of the bottom rotor beams to the same frame, as well as provide a connection point for the four landing gear beams. The front joint will be located on the bottom of the vehicle, attached to the front bulkhead. The top joint is shown in Figure 8.10a.

[2] *https://mechanicalc.com/calculators/lifting-lug-analysis/#divResults [Cited 15/06/2022]*
[3] *https://mechanicalc.com/calculators/lifting-lug-analysis/validation [Cited 15/06/2022]*

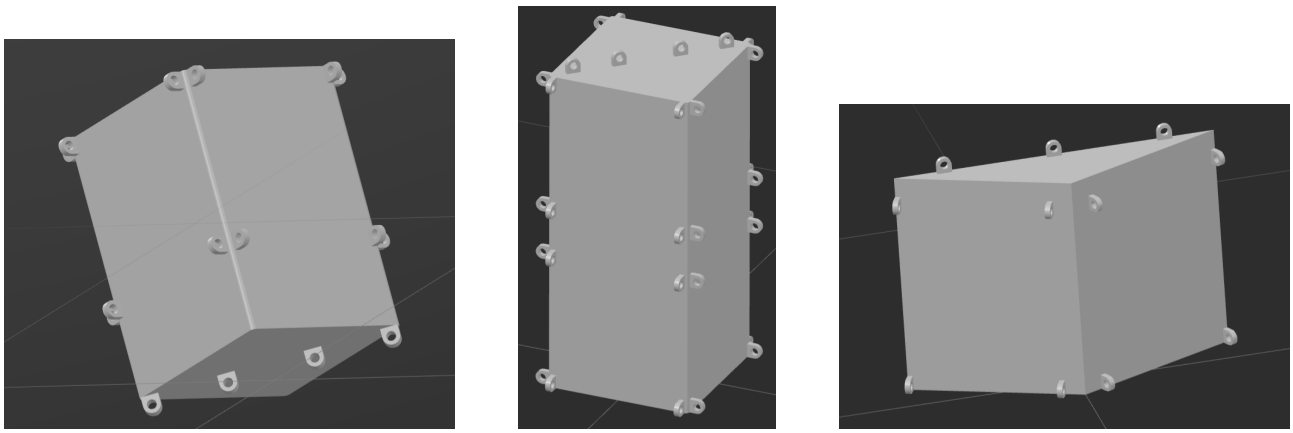

(a) Top Joint View **(b)** Bottom Joint View **(c)** Front Joint View

Figure 8.10: Visual representation of fuselage joints

The method of transferring the loads from the beam to the air frame is done via the use of lug joints. It is attached to each beam with four lug joints, and attached to the frame with four larger lug joints. The frames to which the lug joints will be attached to will be made from aluminium, since carbon fibre is less able to carry concentrated loads. The reason for having four joints is to account for the failure of one lug joint. Otherwise, the failure of one lug joint would result in the failure of the entire vehicle. The critical location for the joint would be the top surface in the figure. This would be the location where the bending moments from all beams would cause the maximum compression. For this reason, the thickness of the joint would need to be at least four times as thick as the beam thickness. The analysis is performed Section 8.9, and the dimensions of the lug joints are shown in Table 8.9. There will also be bushing inside the lug joints to resist abrasion due to the cyclic loading of the vehicle. In addition, the gap between the clevis pin and the inner diameter of the lug will need to be very small, depending on the maximum deflection allowed from the control department. For now, it is assumed to be quite conservative, at approximately 0.2 mm, which comes from the tolerance for an aluminium sheet of 1 cm thick from **rcm industries_2021**. With die casting, the tolerance could be much lower. The small tolerance required would raise the cost of manufacturing, but is necessary to minimise the displacement during loading.

Table 8.9: Top beam lug joint dimensions

Dimensions	Male beam lug joint	Female beam lug joint	Male frame lug joint	Female frame lug joint
R	8.2	8.2	4	4
r	8.2	8.2	4	4
D_p	8	8	4.5	4.5
D_h	8.2	8.2	4.7	4.7
w	15	15	8.5	8.5
t	5.5	2.7	4.2	2.0

For the bottom joint, the design is shown in Figure 8.10b. This joint is similar to the top beam joints, but is extended to include the lug joints for the landing gear beams. The sizing for the dimensions of the lug joints is done in the same manner as in the top joint. The dimensions are summarised in Table 8.10.

The front joint is constructed as shown in Figure 8.10c. The cross-section of the joint will be triangular, with two faces being attached to the beams. Using the same methodology as the top joint, the following lug joint dimensions were created. As explained in the Air-force method, it is important that the critical failure mode is not in the bending of the pin, but either in the shear of the pin, or in one of the three failure modes for the male or female joints described in Figure 8.9.

8.11. Landing gear beam and skid design

When designing a landing gear, it is important that the centre of gravity is never located in front of the most forward point of the landing gear or behind the most aft point of the landing gear, to avoid tipping. Therefore, it is advised to make the landing skids as long as possible. These skids, however, will only endure a relatively

Table 8.10: Bottom beam lug joint dimensions

Dimensions	Male beam lug joint	Female beam lug joint	Male frame lug joint	Female frame lug joint	Male landing beam lug joint	Female landing beam lug joint
R	8.2	8.2	5.1	5.1	7.2	7.2
r	8.2	8.2	5.1	5.1	7.2	7.2
D_p	8	8	5.5	5.5	6.2	6.2
D_h	8.2	8.2	5.7	5.7	6.4	6.4
w	15	15	13.8	13.8	12.0	12.0
t	5.5	2.7	4.8	2.4	5.0	2.6

Table 8.11: Front beam lug joint dimensions

Dimensions	Male beam lug joint	Female beam lug joint	Male frame lug joint	Female frame lug joint
R	8.2	8.2	3.5	3.5
r	8.2	8.2	3.5	3.5
D_p	8	8	4.1	4.1
D_h	8.2	8.2	4.3	4.3
w	15	15	8.0	8.0
t	5.5	2.7	3.8	2.0

small tensional stress and can therefore be kept lightweight. The landing gear design, with dimensions, is shown in Figure 9.3. The landing gear design is similar to the rotor beam design, however, with the loads acting at an angle. The sizing for the thickness of the joint is done in the same manner as in Section 8.2. Thanks to the fact that the landing gear is made out of carbon fibre, it will absorb energy when fracturing in compression, when a crash landing occurs.

8.12. Material budgets

To produce the structures described above, a lot of materials are needed. Most of the structure will be made of carbon fibre, since it is a very stiff material, which also has a strength comparable to metals as aluminium and is super lightweight as well. Carbon fibre will be used, for example for the fuselage, the beams to the motors, the rotor blades and the landing gear.

Also, aluminium and steel will be used. Aluminium will mostly be used in some big parts which are not sufficient to be made out of carbon fibre since they have loading in a lot of different directions, such as the connections between the beams and the rotors. Steel will mostly be used for the little hinges which are quite complex, so it is not easy to make with carbon fibres. These hinges are very small and complex. These parts have a higher change on corroding due to the heat from the engine and the propellers. Therefore, steel is preferred over aluminium.

To come up with how much of the materials are needed, it is first important to know in which efficiency the materials can be used. Studies which are looking into recycling for composites, state that in the aerospace industry, sometimes up to 20-40% of the raw composite materials are going to waste. Since Veatle is aiming at a sustainable production and does not use very complex structures for carbon fibre, the waste of the material will be estimated to be around 20% **Compositewaste**.

For the metals aluminium and steel, almost all the material can be used or recycled. About 5% of those materials is expected to go into waste.

With this, some basic calculations about how much material is needed can be done. The results of these calculations can be seen in Table 8.12

Table 8.12: Materials budget

Material	Amount [kg]
CFRP	126.7
AL7050	20.8
Steel	1
Glass	5.1

9. Preliminary Design Overview

This chapter concludes the design of the vehicle and presents the design to which the team has converged. The vehicle can be seen flying past the Shard in London on Figure 9.1. First, the vehicle is described in Section 9.1, then the weight breakdown is presented in Section 9.2.

9.1. Vehicle description

Figure 9.1: Render of the Veatle flying next to London's Shard

With the preliminary design of Veatle's systems finished, the complete final configuration will be presented. The vehicle's fuselage allows for short comfortable flights for 2 persons and luggage with a total combined weight up to 250 kg and luggage of volume up to 200 l. The Veatle is built for the urban environment and allows for a mission range of up to 20 km plus extra 5 km to account for possible divergence scenarios.

The vehicle has been designed with technology that is already commercially available, which leads to accurate price and weight estimations. The fuselage is mostly made of light weight carbon fibre and is connected to the two joints on the top, each of which is in turn connected to 4 load-carrying beams. At the end of each beam is the propeller, which consists of the EMRAX flux motor, propeller hub and 3-bladed composite propeller with the radius of 1.2 m. The vehicle is designed for safety and can sustain controlled flight even with 2 propellers inoperative. With a maximum take-off weight of around 900 kg, it has low blade loading and has low acoustic signature, which makes it suitable for use in cities. There is also a distributed control propulsion system consisting of 3 5-blade propellers with a radius of 20 cm, which guarantees full control of the vehicle even in the roughest weather conditions with wind speeds up to 20 m/s. Thanks to the configuration of the control propellers, the vehicle can swiftly counteract gusts with minimal rotation, increasing the passengers' comfort. The aerodynamic performance and response of the vehicle body has been computed with the help of computational fluid dynamics. The inside of the vehicle can be seen on Figure 9.2. As can be seen, the vehicle has a stiffened cabin to protect passengers during impact and has a separated compartment for luggage and batteries to protect the passenger in emergencies. At the end of this chapter, the three-view drawing of the vehicle is presented on Figure 9.3.

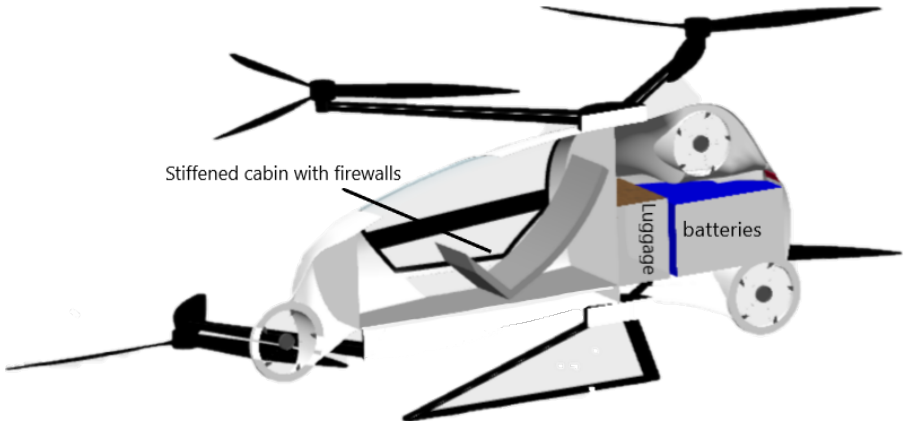

Figure 9.2: The side section of the Veatle

Table 9.1: Design parameters

Characteristic	Design choice/Value	Unit
Configuration	Multirotor	-
Materials	Carbon fibre, aluminium, steel, glass	-
Landing gear	Skids	-
Cabin layout	Seats abreast	-
Control actuators	3 in-plane rotors	-
Unit cost	478k	€
Mass	932	kg
Energy consumption	24	kWh
Battery choice	Li-ion	-
Total battery weight + PDU	325	kg
Frontal drag during cruise	1700	N
Total disk area	36	m^2
Amount of propellers	8	-
Diameter of the rotor	2.4	m
Length engine beams	1.5, 1.8	m
Diameter engine beams	10	cm
Thickness of engine beams	2.5	mm
Force per control rotor	450	N

9.2. Weight breakdown

With the conceptual design of the vehicle finished, the structural thicknesses and material properties for the fuselage, propellers and load-carrying beams are known. Battery design has also been carried out, and some interior cabin design has been done. Most heavy and important parts have been assembled in the CAD drawing, which also provides an overview of masses and inertias. A total mass breakdown for the vehicle is given below in Table 9.2.

Table 9.2: VEATLE Weight Breakdown

Item	**Weight [kg]**
Propulsion Group	
Propeller	3.4 x 8
Connection joint	2.6 x 8
Motor	4.52 x 8
Control propeller + motor + hub	est 4.5 x 3
Total	97.7
Fuselage Group	
Main beams	65.8
Beam to fuselage joints	28.0
Fuselage shell	119.0
Windows	2.3 x 2
Doors	2.0 x 2
Windshield	2.8
Seats	5.3 x 2
Landing Gear	est 12
Avionics	est 10
Total	256.8
Payload Group	
Humans	97 x 2
Luggage	23 x 2
Additional possessions	10
Total	250
Battery Group	
Battery management systems	96.4
Cruise battery cells	73.2
Take-off battery cells	156.3
Total	325.8
Maximum Take-off Weight	
Total	932.2

Note that the given total MTOW is obtained with unrounded numbers, while the numbers given in this table are all rounded for ease of reading. For this reason, the MTOW stated here is slightly different from the results obtained from adding all group's masses shown in the table. The MTOW given at the bottom is the correct value.

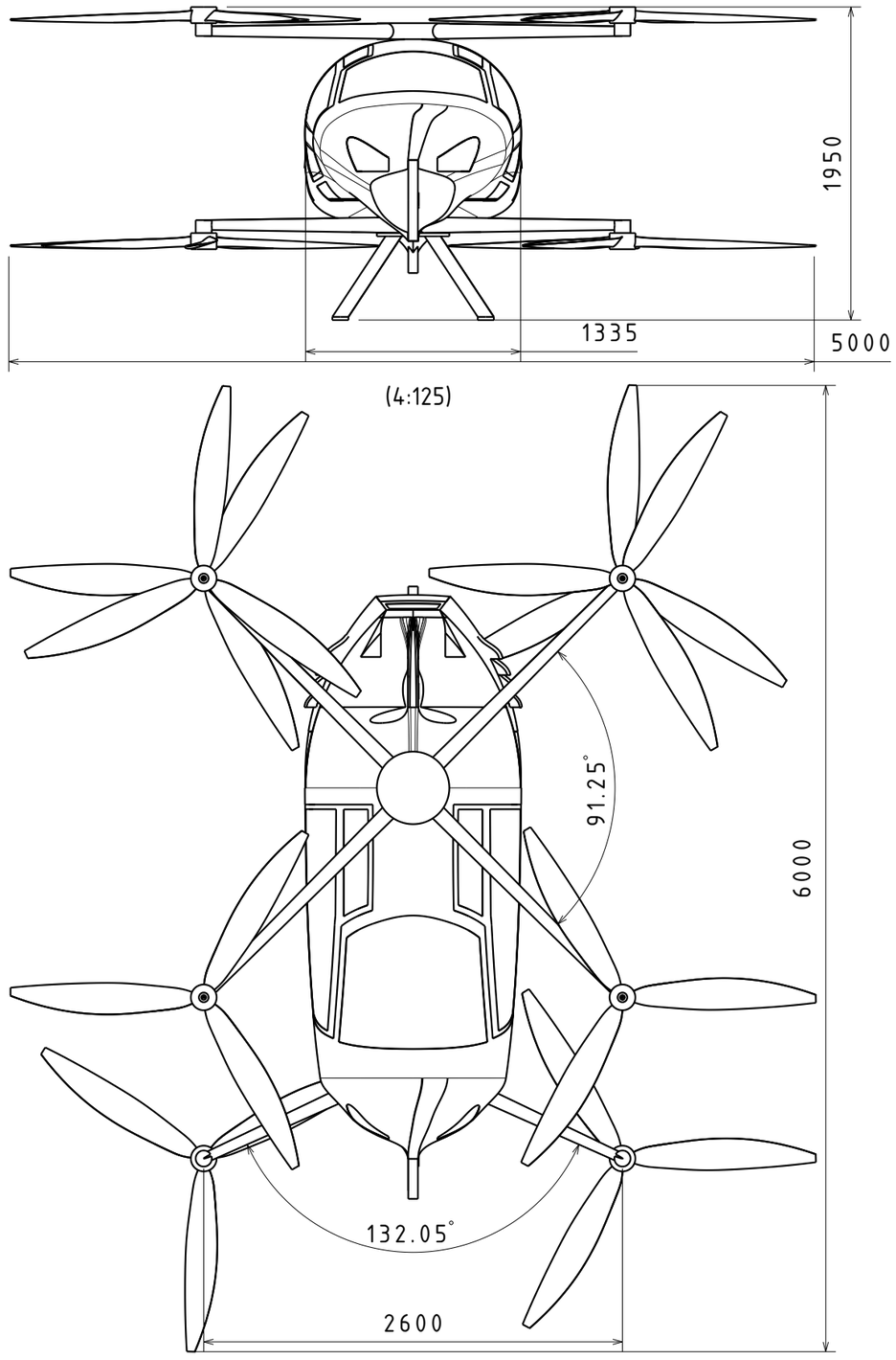

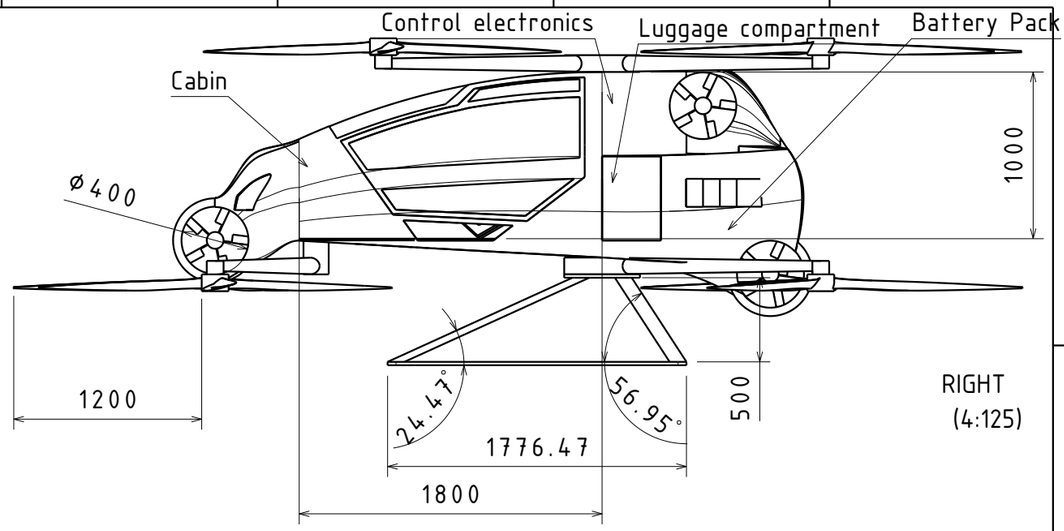

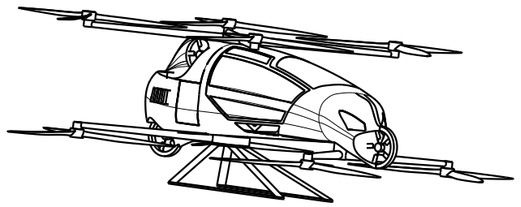

ISOMETRIC
(2:125)

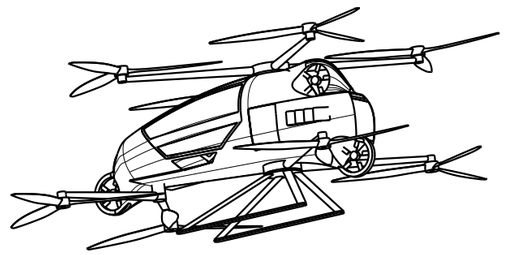

ISOMETRIC
(2:125)

DESIGNED BY: The Veatles DATE: 10/06/2022		Fuselage Assembly, The Veatle	
CHECKED BY: Korneel Van den Berghe DATE: 12/06/2022			
SIZE: A3		group 5, DSE 2022	–
SCALE: 1:250	WEIGHT (kg): 932	DRAWING NUMBER: 01	SHEET: 1/1

This drawing is our property; it can't be reproduced or communicated without our written agreement.

Figure 9.3: 3-view drawing of the Veatle

10. Verification

When designing your own tools, one should aim at verifying all the underlying models and calculations to check the correctness of the calculations. This chapter discusses the assumptions made to design the tools in Section 10.1. Next, the verification of the stability and control tools are discussed in Section 10.5, followed by the structures tools in Section 10.6. Then, the verification of the power and energy storage is elaborated upon in Section 10.4. The aerodynamics tools are verified in Section 10.2. Finally, the propulsion tools developed by the team are verified in Section 10.3.

10.1. Verification of assumptions

In this section, important assumptions behind each department's calculations will be stated and justified.

Assumptions behind the aerodynamic model

ASUMP-AERO-01: The flow around the vehicle is incompressible. *Justification:* The vehicle should not exceed the speed of 200km/h, which corresponds to $\approx 0.15M$, which is within the incompressible regime.

ASUMP-AERO-02: The flow around the vehicle can be simulated by the CFD computation with needed accuracy. *Justification:* At this design stage the aerodynamic response of the vehicle only needs to be approximated within margins of up to 20%. A greater safety margin is taken in the design of control propellers to account for this uncertainty.

ASUMP-AERO-03: The flow inside the urban environment can be simulated by the CFD computation with needed accuracy. *Justification:* The gust profile has also been found from literature about urban flows, in order to provide an independent estimate on possible wind conditions the vehicle can experience. Also, a greater safety margin is taken in the design of control propellers to account for this uncertainty.

ASUMP-AERO-04: The flow around the body is steady. *Justification:* As the aerodynamic model is used for a rough determination of the aerodynamic force coefficients of the vehicle, fluctuations in pressure and velocity are neglected.

ASUMP-AERO-05: The effect of the rotors on the airflow around the fuselage are ignored when determining the aerodynamic response of the fuselage. *Justification:* Taking this into account will significantly increase the complexity of the model.

ASUMP-AERO-06: The velocity at the walls of the enclosure was assumed to be the same as the velocity at the inlet. *Justification:* This could cause flow blockage effects due to the presence of the body. To avoid that, the enclosure is made relatively big and the streamlines near the walls were analysed.

Assumptions behind the propulsion model

ASUMP-PROP-01: The induced velocity is equal throughout the propeller disk area. *Justification:* This is proven to be a valid assumption by Prouty et al. **prouty1995helicopter**.

ASUMP-PROP-02: Radial flow is ignored regarding profile drag. *Justification:* simplification taken from Leishman**HeliPower**.

ASUMP-PROP-03: The flight path angle is small (which has implications on how sin, cos and tan are approached). *Justification:* A equations of motion simplification done by Leishman**HeliPower** for helicopters during forward flight.

ASUMP-PROP-04: The rotor blades are viewed as an infinite wing. *Justificaion:* This is proven to be a valid assumption by Prouty et al. **prouty1995helicopter**.

ASUMP-PROP-05: The wake in the rotor plane is only in the downward direction, neglecting the rotational component of it. *Justificaion:* This is proven to be a valid assumption by Prouty et al. **prouty1995helicopter**.

Assumptions behind the structures and materials model

ASUMP-STRUC-01: The structural design of the fuselage is an idealised boom design which accounts for skin thickness as well as panels and stringers. *Justification:* Verified by expert opinion, Calvin Rans

ASUMP-STRUC-02: The C.G. estimation is based on some estimations such as where the C.G. of a person is located while seating in the vehicle and how the rest of the payload is distributed. *Justification:* The shift in C.G. would be significantly small that it will differ with differ seating positions or getting in and out the vehicle as well, therefore a safety margin is taken into account.

ASUMP-STRUC-03: For the eigenfrequencies, the beams and rotors are all modelled as a cantilever beam *Justification:* They have their own MOI for their respective shape, which is the most important part next to general dimensions.

ASUMP-STRUC-04: The rotor beams are assumed to be Euler-Bernoulli beams. *Justification:* The two assumptions for the Euler-Bernoulli beam theory is that the beam deflection angles are small, and the plane sections remain plane. These two requirements are met, since the deflection of the beam is less than 6 cm.

ASUMP-STRUC-05: The structural design program is made for aluminium and a weight decrease of 15% is used to compensate for using carbon fibre. *Justification:* Verified by expert opinion, Otto Bergsma

Assumptions behind the control model

ASUMP-CON-01: Assume that the body is rigid. *Justification:* The structural design shows that the body has minimal deflection, and thus can be modelled as a rigid body.

ASUMP-CON-02: There is no Coriolis acceleration acting in the angular plane. *Justification:* This was verified by the expert opinion of "Fusion engineering" [1].

ASUMP-CON-03: The transformation order is first around the x-axis, then the y-axis, and finally the z-axis. *Justification:* This is aligned with aerospace standards.

ASUMP-CON-04: The wind gust acts uniform-ally over the body. *Justification:* This makes the problem of first order, to simplify the effect, further analysis should be taken to fully quantify the extra yaw moment exerted from this effect.

ASUMP-CON-05: There are no lasers that disturb the functioning of the Lidar sensor. *Justification:* Such lasers are not common to use and the chance is small that a similar signal is picked up by the Lidar sensor.

10.2. Aerodynamics

In this section, the model used for the aerodynamic analysis is verified. This is done by comparing aerodynamic coefficients, pressure distributions and sensitivity analysis. Also, the noise calculations are verified in this section.

10.2.1. Aerodynamic coefficient check

In order to verify the process of determining the aerodynamic parameters, the side force coefficient is determined in two different ways. One way, is to use the `forceCoeffs` post-processing function and the other way is to use the `paraView` interface. If this aerodynamic force is verified, it can relatively confidently be concluded that the other coefficient are also verified, because the same procedure is used in the calculations of these. Aerodynamic case 2 is considered for this test. Here, a side wind of 20.7 m/s is simulated to the positive Y-direction from the body axis system.

For the calculation of the side force coefficient through the `forceCoeffs` function, the direction of the force coefficient, the airspeed, the reference area and the reference length are put in. Similar to the previously determined aerodynamic coefficients, the reference area is taken to be 1 m^2 and the reference length is taken to be 1 m. For the determination of the side drag coefficient through `paraView`, the following procedure is followed. First, the pressure at each cell of the body is multiplied with the Y-component of the unit surface normal of that cell. Then, the Y-component of the kinematic shear stress is added to this value and it is multiplied with the air density. This results in a total stress per cell. For each cell, this stress is multiplied by its area and these are then summed up to get the total side force on the body. Then, the drag is divided by the dynamic pressure multiplied with the reference area (which is 1 m^2). The results of both procedures are given in Table 10.1.

[1] *https://fusion.engineering/ [Cited: 03/06/2022]*

Table 10.1: Results of the Aerodynamic Coefficient test

Method	Side Force Coefficient [-]
`forceCoeffs`	2.7
`paraView`	2.6

As can be noted, `paraView` gives roughly a 4 % lower force coefficient, which is a small difference.

10.2.2. Comparison of pressure distributions

In order to verify the results of the simulation on the fuselage body, it is compared to a consistent simulation performed on a sphere. All boundary conditions, as well as the meshing procedure and total wetted area are the same. As can be seen in Figure 10.1, the pressure distribution over the body of the fuselage and the sphere shows qualitative and quantitative agreement. Contour map limits are the same across the two cases, and stagnation pressures at the noses of two bodies are approximately 101500 Pa. The wake velocity shown by the slice behind the body in blue also seems to be in some agreement, although the wake of the cylinder is weaker and smaller than for the fuselage, however the distance between the end of the fuselage body to the slice plane is slightly greater than for the sphere.
The drag force on the sphere is 236 N and the drag on the vehicle is 346 N. This can be expected due to the presence of the beams of the vehicle.

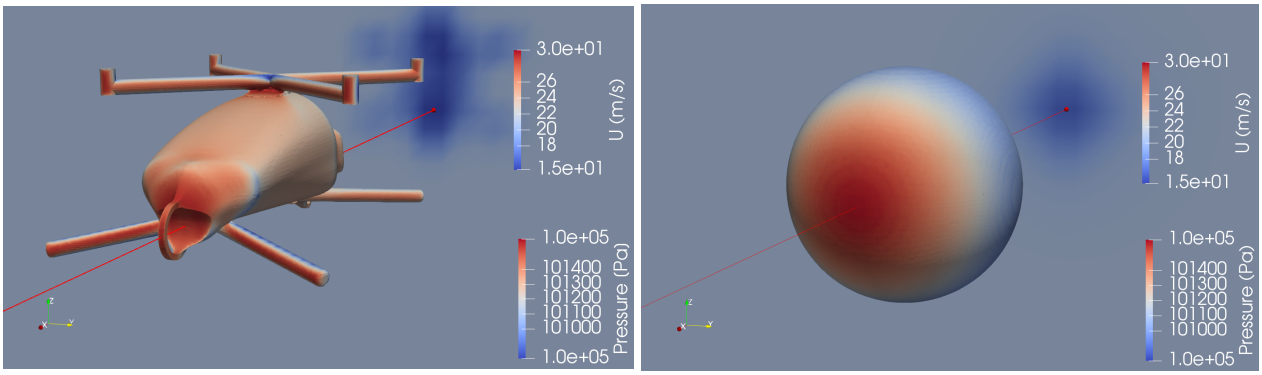

Figure 10.1: Comparison of the fuselage and sphere simulation results in OpenFOAM. Consistent camera position and focal point. Red line indicates the freestream flow direction

10.2.3. Sensitivity analysis

For the sensitivity analysis, changes in aerodynamic parameters (force and moment coefficients) with changing flight conditions (airspeed, angle of attack and side slip) from zero angle of attack and side slip are determined. For this analysis, data from Chapter 5 are used. The analysis of the force and moment coefficients with changes in airspeed is done with cases FrontGust, Front_10 and Front_30 and tabulated in Table 10.2a. For the sensitivity of the force and moment coefficients with changes in angle of attack, cases FrontGust, PitchGust_15 and PitchGust_-15 are used (Table 10.2c). Finally, for the sensitivity of the side slip, cases FrontGust and SideGust_15 are used (Table 10.2b).

Table 10.2: Changes of aerodynamic with changes in velocity, angle of attack and sideslip

(a) Velocity sensitivity table

Coefficient	Front_10	FrontGust	Front_30
C_X [-]	-1.34	-1.32	-1.31
C_Z [-]	-0.19	-0.23	-0.22
C_{m_Y} [-]	$-3.5 \cdot 10^{-2}$	$-1.1 \cdot 10^{-2}$	$-2.8 \cdot 10^{-2}$

(b) Sideslip sensitivity

Coefficient	FrontGust	SideGust_15
C_X [-]	-1.32	-1.46
C_Y [-]	0	0.57
C_Z [-]	-0.23	-0.48
C_{m_X} [-]	0	-0.22
C_{m_Y} [-]	$-1.1 \cdot 10^{-2}$	$5.7 \cdot 10^{-3}$
C_{m_Z} [-]	0	0.56

(c) Angle of attack sensitivity

Coefficient	PitchGust_15	FrontGust	PitchGust_-15
C_X [-]	-1.33	-1.32	-1.48
C_Z [-]	0.55	-0.23	-1.23
C_{m_Y} [-]	-1.14	$-1.1 \cdot 10^{-2}$	1.2

As can be noted in Table 10.2a, with a 50% increase and reduction in windspeed from the gust velocity, the aerodynamic coefficients only change marginally. So, when modelling the controls system with different wind speeds, it is sufficient to use the force and moment coefficients at the gust velocity.
As can be seen in Table 10.2b, the aerodynamic coefficients change significantly with changes in sideslip angle. This means that the coefficients indeed need to be implemented into the control system as a function of sideslip angle. This is as expected due to the change in the shape of the vehicle with respect to the wind.
Finally, changes of aerodynamic coefficients with changes of angle of attack are considered. As can be seen from Table 10.2c, especially the pitch moment and vertical force coefficients vary with changes in angle of attack around zero angle of attack and sideslip. This means that the aerodynamic coefficients indeed also need to be a function of angle of attack.

10.2.4. Noise calculation

Tests were written to verify the code that calculates the produced noise at several angles and distances. The tables in below show the results of these tests. As a starting point, the parameters of the designed vehicle are taken for cruise situations, including its RPM of 600 and sound pressure level of 60 dBA at 500 ft. It must be noted that these are not the conditions at which noise levels are analysed in Section 6.1.4, but they are realistic values which are used as a basis for this verification. Moreover, some of these values were changed for testing purposes, as described in this section.

Unit tests

In order to calculate the noise production by the designed vehicle, a program was written with the dimensions of the propellers and the MTOW as inputs. These inputs are set to 0 in several unit tests to find whether an error is raised. The results are shown in Table 10.3.

Table 10.3: Results of tests T-AERO-NOIS-U

Code	Input	Expected	Outcome	Fail/pass
T-AERO-NOIS-U01	MTOW $= 0$	$SPL = 0$	$SPL \neq 0$	Fail
T-AERO-NOIS-U02	$R_{\text{prop}} = 0$	$SPL = NaN$	$SPL = NaN$	Pass
T-AERO-NOIS-U03	$N_{\text{prop}} = 0$	$SPL = \text{inf}$	$SPL = \text{inf}$	Pass
T-AERO-NOIS-U04	$C_{\text{prop}} = 0$	$SPL = NaN$	$SPL = NaN$	Pass

In order to make the first test pass as well, a check for a valid input of MTOW is added to the code.

Module tests

The code can be divided into four parts: the initialisation of the distance and angle arrays, and the calculation of the rotational noise, vortex noise, and total noise. As the calculations in the last three parts are complicated, these will only be tested using system tests. Therefore, only the following module test was performed.

T-AERO-NOIS-M01: The initialised arrays for the distances and angles were visually checked to make sure the starting values, final values and step sizes were correct. Furthermore, it was checked that the values of the distance and angle at a certain index formed a unique pair. PASS

System tests

Extreme value tests were performed for MTOW and R_{prop}. These extreme value tests also proved that the code is not sensitive to changes in input parameters, and thus the tests were also used as sensitivity analysis. Also, they were used to asserting whether the SPL increases or decreases for the given changes in input.

Table 10.4: Results of tests T-AERO-NOIS-S

Code	Input	Expected	Outcome	Fail/pass
T-AERO-NOIS-S01	MTOW = 10,000 kg	SPL > 60 dBA	SPL = 80 dBA	Pass
T-AERO-NOIS-S02	MTOW = 100 kg	SPL < 60 dBA	SPL = 40 dBA	Pass
T-AERO-NOIS-S03	$R_{\text{prop}} = 10\text{m}, RPM = 50$	SPL < 60 dBA	SPL = 45 dBA	Pass
T-AERO-NOIS-S04	$R_{\text{prop}} = 0.4\text{m}, RPM = 5000$	SPL > 60 dBA	SPL = 70 dBA	Pass

10.3. Propulsion

The tools developed to design the propulsion system are complex and have to be verified before using them for extensive design of the subsystem. First, the blade geometry and rotational velocity tools are verified.

Blade geometry and rotational velocity

Both unit and module tests were implemented to verify the function written for the design of the blade geometry and the rotational velocity. The code is run for several values of linear blade twist, with which the produced lift is calculated per blade element. The main steps in this function are calculation of the local blade pitch angle and the local angle of attack, and determination of the local value of C_l.

T-PROP-BL-U: Unit tests

The unit tests below assert whether the program behaves correctly when the main inputs have a value of 0. The inputs for which this is tested are shown in 10.5, as well as the test results. As unit test T-PROP-BL-U01 initially failed, the program was changed such that a check takes place at the start of the code to assert whether the value of MTOW is valid (MTOW> 0).

Table 10.5: Results of test T-PROP-BL-U

Code	Input	Expected	Outcome	Fail/pass
T-PROP-BL-U01	MTOW = 0	Error	No error	Fail
T-PROP-BL-U02	$R_{\text{prop}} = 0$	Error	Error	Pass
T-PROP-BL-U03	$N_{\text{prop}} = 0$	Error	Error	Pass
T-PROP-BL-U04	$C_{\text{prop}} = 0$	Error	Error	Pass

T-PROP-BL-M: Module tests

For the blade geometry and RPM code, module tests were written for three aspects of the program: the calculation of the local pitch angle, the local angle of attack, and the local lift coefficient. For the local pitch angle, the blade that was used as input was chosen such that the local pitch angle should decrease with 1 deg for each blade element, from 20 deg to 10 deg. The angle of attack at each blade element was checked by changing the vertical velocity component V_v, the horizontal velocity component V_h and the local pitch angle θ_{local}, of which it is a function. Once the local angle of attack is calculated, the lift coefficient for the blade element can be determined. This is done using the lift curve of the chosen airfoil, the NACA 23012. Tests were run for two values of α that are not on the lift curve, and a value of α that is on the lift curve. The expected value of C_l of the latter was taken from **abbott2012theory**. The results of all module tests are shown in 10.6.

Table 10.6: Results of test T-PROP-BL-M01

Code	Input	Expected	Outcome	Fail/pass
T-PROP-BL-M01	Simplified blade, element = 1	$\theta_{\text{local}} = 18\text{deg}$	$\theta_{\text{local}} = 18\text{deg}$	Pass
T-PROP-BL-M02	Simplified blade, element = 4	$\theta_{\text{local}} = 15\text{deg}$	$\theta_{\text{local}} = 15\text{deg}$	Pass
T-PROP-BL-M03	Simplified blade, element = 9	$\theta_{\text{local}} = 10\text{deg}$	$\theta_{\text{local}} = 10\text{deg}$	Pass
T-PROP-BL-M04	$V_v : V_h = 1 : \sqrt{3}, \theta_{\text{local}} = 40\text{deg}$	$\alpha_{\text{local}} = 20\text{deg}$	$\alpha_{\text{local}} = 20\text{deg}$	Pass
T-PROP-BL-M05	$V_v = 0, \theta_{\text{local}} = 10\text{deg}$	$\alpha_{\text{local}} = 10\text{deg}$	$\alpha_{\text{local}} = 10\text{deg}$	Pass
T-PROP-BL-M06	$V_h = 0, \theta_{\text{local}} = 0\text{deg}$	$\alpha_{\text{local}} = 90\text{deg}$	$\alpha_{\text{local}} = 90\text{deg}$	Pass
T-PROP-BL-M07	$\alpha_{\text{local}} = -20\text{deg}$	$C_l = 0$	$C_l = 0$	Pass
T-PROP-BL-M08	$\alpha_{\text{local}} = 20\text{deg}$	$C_l = 0$	$C_l = 0$	Pass
T-PROP-BL-M09	$\alpha_{\text{local}} = 8\text{deg}$	$C_l = 1$	$C_l = 1$	Pass

System tests

For the tests below, the rotational velocities that were taken as a basis to compare new values to are the values corresponding to take-off for the first three tests, and cruise for the final test. The first two system tests assert the behaviour of the program for extreme values of MTOW: values beyond the expected scope. The third and fourth test in Table 10.7 are performed to assess whether the program behaves as expected for slight changes in the main input values, and to see if the program is not too sensitive to this kind of changes.

Table 10.7: Results of tests T-PROP-BL-S

Code	Input	Expected	Outcome	Fail/pass
T-PROP-BL-S01	MTOW= 10,000kg, fixed blade	$RPM >> 800$	$RPM = 2420$	Pass
T-PROP-BL-S02	MTOW= 100kg, fixed blade	$RPM < 800$	$RPM = 730$	Pass
T-PROP-BL-S03	MTOW= 1200kg, fixed blade	$RPM > 800$	$RPM = 900$	Pass
T-PROP-BL-S04	$V_{\text{cr}} = 200\text{km/h}$, fixed blade	$RPM > 800$	$RPM = 800$	Fail

The first test passed as expected: an extremely high value of MTOW causes a significant increase in RPM. The second test was expected to cause a smaller change in the opposite direction, as the blade would stall at RPM far below the initial value. This expectation also turned out to be true. Furthermore, the program is found to be moderately sensitive to changes in MTOW, as a 20% increase of this value causes the RPM to increase to 900. The test for the 20% increase in cruise velocity passed with regard to the expectation, and showed that the program is very sensitive to an increase in cruise velocity. An increase of 11% in cruise velocity caused an increase of 150% in RPM required. This is because the current cruise velocity is already very high for the characteristics of the Veatle, and was therefore expected.

After concluding the above tests, it was decided to run one more test as described below:

T-PROP-BL-S05: This test was run to assess the change in blade geometry in combination with the increase in RPM when the blade geometry is designed for the extreme value of MTOW= 10,000kg. The outcome is that the tip angle changes from $\theta_t = 10°$ to $\theta_t = 4°$, the linear twist from $\theta_l = -38°$ to $\theta_l = -22°$, and the rotational velocity from 800 RPM to 1760 RPM. These changes were as expected, and thus this test passed. PASS

10.4. Power and energy storage

In order to estimate the power and energy required for proper operation of the vehicle, a code was written to calculate this in which the maximum take-off weight is iterated. For this, the weight estimation is used as described in the midterm report, tailored specifically to the final design. A new weight estimation was coded for the control system and the weight of the beams that carry the propellers. To verify the code, the weight and power estimation methods are tested. In this section the verification tests done are described and their results displayed.

10.4.1. Verification of numerical model

Each of the equations and methods used (see Section 6.1.2) have been taken from sources deemed reliable. They have been taken from well known design books like **HeliPower** and **prouty1995helicopter**. The rest of the equations and methods have been taken from research papers. To see exactly where each equation comes from, see Section 6.1.2.

10.4.2. Power required function

The first function tested was the power required function. The results of the main unit tests are shown in Table 10.8. The P_{cr} will not be zero at a MTOW of zero because the rotor drag components will still demand power. For zero RPM the program should give $P_{cr} = \text{NaN}$ since there will be a $0 \cdot \infty$ involved in the calculation. At a V_{cr} of zero the P_{req} will be infinite since μ will be zero and the code involves a division by μ.

Table 10.8: Results of test T-PROP-PREQ-U (unit tests)

Code	Test	Expectation	Result	Pass/Fail
T-PROP-PREQ-U01	MTOW = 0	Low P_{cr} $P_{TO} = 0$	$P_{cr} < 27$kW $P_{TO} = 0$	Pass
T-PROP-PREQ-U02	RPM = 0	$P_{cr} = \text{NaN}$ P_{TO} =normal value	$P_{cr} = \text{NaN}$ $P_{TO} = 332.8$kW	Pass
T-PROP-PREQ-U	$V_{cr} = 0$	$P_{cr} = \infty$ P_{TO} =normal value	$P_{cr} = \infty$ $P_{TO} = 332.8$kW	Pass

The results of the module tests are displayed in Table 10.9. The RPM increase test represents an increase in RPM during cruise, which causes an increase in P_{cr} since there will be more propeller drag. The effect of shortening the blade length on P_{cr} is hard to predict since less lift is produced for the same power, but there is also less rotor blade drag. Furthermore, an interesting observation is that the effect of V_{TO} seems to be very small.

Table 10.9: Results of test T-PROP-PREQ-M (module tests)

Code	Test	Expectation	Result	Pass/Fail
T-PROP-PREQ-M01	MTOW increase (20%)	P_{cr} increase P_{TO} severe increase	P_{cr}: 12% increase P_{TO}: 31% increase	Pass
T-PROP-PREQ-M02	RPM increase (20%)	P_{cr} increase P_{TO} no effect	P_{cr}: 18% increase P_{TO}: no effect	Pass
T-PROP-PREQ-M03	V_{cr} decrease (25%)	P_{cr} decrease P_{TO} no effect	P_{cr}: 23% decrease P_{TO}: no effect	Pass
T-PROP-PREQ-M04	V_{to} decrease (25%)	P_{cr} no effect P_{TO} decrease	P_{cr}: no effect P_{TO}: 0.86% decrease	Pass
T-PROP-PREQ-M05	R_{rotor} decrease (25%)	P_{TO} increase P_{cr} not clear	P_{TO}: 32% increase	Pass

10.4.3. Battery weight estimation function

The battery weight estimation function was changed to incorporate more details. The initial function calculated the energy required and divided this number by a specific energy (in Wh/kg) to get an estimate. The new code also incorporates an algorithm that calculates the amount of cells in series and in parallel needed to actually deliver the required power. The weight is then estimated based on properties of the Sony US18650VTC6 cells (Table 6.7). Simultaneously, it calculates the energy required per flight and checks whether the required capacity is obtained with the cell configuration that the program chooses

The results of the unit tests are given in Table 10.10. With no voltage the theoretically required current will be infinite, and thus the #cells in parallel will be infinite, while the #cells in series is zero. The program thus takes the total amount of cells to be $0 \cdot \infty$, or NaN. #cells in parallel will be zero at an MTOW of zero since the P_{TO} will be zero, and this is what the cell count is based on.

Table 10.10: Results of test T-PROP-BAT-U (unit tests)

Code	Test	Expectation	Result	Pass/Fail
T-PROP-BAT-U01	Voltage = 0	$N_{parallel} = \infty$ $W_{bat} = \text{NaN}$ $(0 \cdot \infty)$	$N_{parallel} = \infty$ $W_{bat} = \text{NaN}$	Pass
T-PROP-BAT-U02	Range $\to \infty$	Code displaying message: 'INSUFFICIENT BATTERY CAPACITY'	'INSUFFICIENT BATTERY CAPACITY'	Pass
T-PROP-BAT-U03	MTOW = 0	$N_{parallel} = 0$	$N_{parallel} = 0$	Pass

The module tests and their results are shown in Table 10.11. The effects on the outcomes of the code are mainly based on increases in P_{TO} since total capacity is not the main challenge anymore, it is providing enough current and voltage to meet the P_{TO} requirement. Increasing the range does not increase weight anymore, but the required capacity might not be met if it is increased too much. Once again it can be concluded that V_{to} has a very small effect on battery mass, but the energy required changes significantly.

Table 10.11: Results of test T-PROP-BAT-M (module tests)

Code	Test	Expectation	Result	Pass/Fail
T-PROP-BAT-M01	MTOW inrease (25%)	$N_{parallel}$ increase E_{req} increase W_{bat} increase	$N_{parallel}$: 38% increase E_{req}: 29% increase W_{bat}: 38% increase	Pass
T-PROP-BAT-M02	Range increase (50%)	Cell counts stay equal Mass stays equal E_{req} increase	Cell count: equal Mass: equal E_{req}: 20% increase	Pass
T-PROP-BAT-M03	V_{TO} decrease (50%)	$N_{parallel}$ decrease W_{bat} decrease E_{req} steep increase	$N_{parallel}$: 4% decrease W_{bat}: 4% decrease E_{req}: 46% increase	Pass
T-PROP-BAT-M04	R_{rotor} decrease (25%)	$N_{parallel}$ increase W_{bat} increase	$N_{parallel}$: 29% increase W_{bat}: 29% increase	Pass

10.4.4. Sensitivity analysis

A sensitivity analysis is interesting to see what parameters influence the results in the strongest way. Several parameters were adjusted to see the effects on the design. The significant effects are displayed in Table 10.12.

Table 10.12: Sensitivity Analysis Power & Battery

Adjusted parameter	Increases	Decreases
MTOW inrease (25%)	P_{TO}: 39%, P_{cr}: 19%, W_{bat}: 38%	DoD: 6.7%
V_{cr} = 100 km/hr (44.4% decrease)	E_{req}: 19%	P_{cr}: 22%
V_{TO} decrease (50%)	DoD: 67%, E_{req}: 59%	W_{bat}: 4.3%, P_{TO}: 1.5 %
R_{rotor} decrease (25%)	W_{bat}: 29%, P_{TO}: 32%, E_{req}: 18%	DoD: 9.4%
Voltage decrease (40%)	DoD: 2.2%	W_{bat}: 2.2 %

The main conclusion is not surprising: an increase in MTOW leads to a severe increase in P_{req} and W_{bat}. V_{cr} and V_{TO} did not show very sensitive behaviour, apart from a steep increase in DoD for a V_{TO} decrease. This is very much undesired since this damages the battery's cycle life. R_{rotor} also has strong negative effects on W_{bat}, which gives more confidence in the design approach taken by the team regarding propulsion (maximising disk area). The voltage has very low impact. Other parameters like RPM, take-off height, and cruise range were found to not have large effects.

10.5. Verification of the controls model

In this section, the control's model of the vehicle is verified. For the models, Matlab code and Simulink configurations were used. First the LiDAR model is verified, followed by the sensor model, and finally each system block pf the 6DOF system.

T-CON-LID-M1:LiDAR sensor model

The following subsection explains the verification of the model of the Lidar used to avoid obstacles.

T-CON-LID-M1-U01: Zero input - The LiDAR model needs to respond correctly if input values of zero are used. The program terminates and does not produce any results if this kind of input is used. Therefore, this first unit test is successful.

T-CON-LID-M1-U02: Input dimensions - For this test, it is checked whether the program terminates if wrong dimensions are used for the input. To perform the test, input vectors are transposed. For every input that is transposed, the program terminates and the following error message is displayed by Matlab. This means that the model will only produce results if the input vectors are in the correct dimensions.

```
Error in port width or dimensions. Expected dimensions for the port must be scalar, vector
or 2-D matrix. However, the port dimension is n-D matrix (n>=3).
```

T-CON-LID-M1-M01: Adding obstacles - This test performs a sanity check for inserting obstacles. Seven random obstacles are created and inserted in the environment. The location, height and width of the buildings are manually compared with the input vectors. The environment is shown in Figure 10.2. All buildings were perfectly inserted by the program and therefore, this test is considered successful.

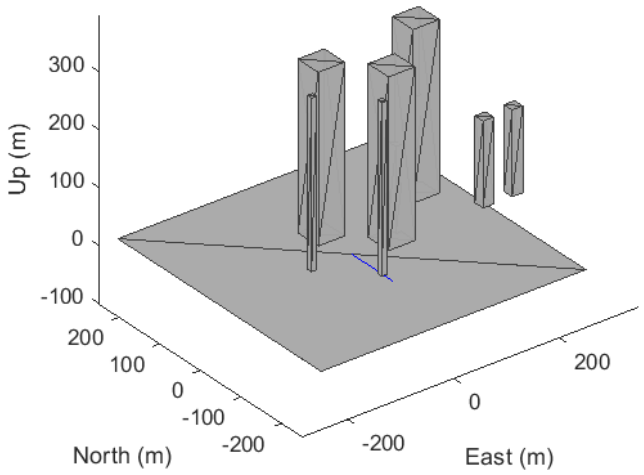

Figure 10.2: T-CON-LID-M1-M01

T-CON-LID-M1-M02: Destination test - This test checks if the destination was correctly implemented by the program. To perform the test, two different waypoints are used. The first one is close to the starting point, 150 meters above it. The waypoint is then [0, 0, 20]. Secondly, a real destination is inputted with values [200, -150, 0], which means 200 meter to the north and 150 to the west of the starting point. The locations are plotted by the program and shown in Figure 10.3.

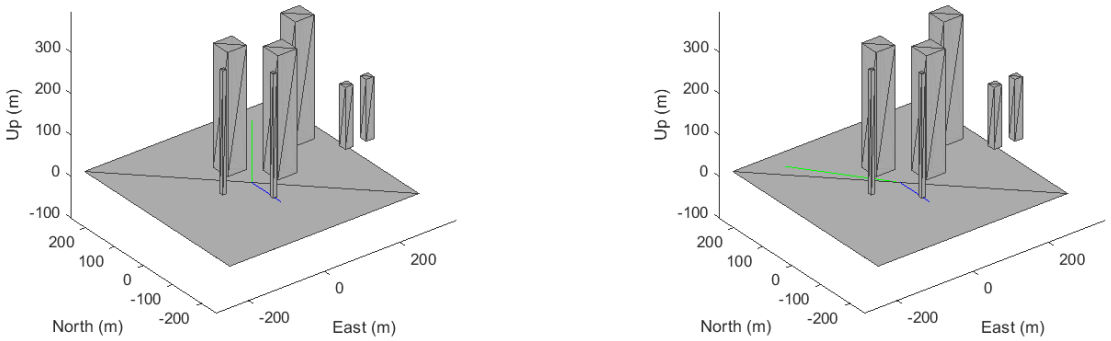

Figure 10.3: T-CON-LID-M1-M02

T-CON-SEN: Accelerometer and Gyroscope sensor models.

T-CON-SEN-U01: Zero noise and bias in the accelerometer model - This test checks if the accelerometer model outputs the same accelerations that are inputted. Without the addition of noise and bias, the values should not change. The test only passes if the values are identical. Three different accelerations with components in x, y and z are inputted. The arrays are compared. The test immediately tests what the program does if a zero input is given. The results are listed in Table 10.13. The program responds correctly to the zero input, however, for non zero values, the exact opposite accelerations are outputted. Therefore, this test is not successful and the model is adjusted accordingly.

Table 10.13: T-CON-SEN-U01

Code	Input	Output	Pass/Fail
T-CON-SEN-U01	[0,0,0]	[0,0,0]	Pass
T-CON-SEN-U02	[1,1,1]	[-1,-1,-1]	Pass
T-CON-SEN-U03	[5,-5,5]	[-5,5,-5]	Pass

T-CON-SEN-U02: Wrong input dimensions for accelerometer model - Inside the six degrees of freedom model, the dimensions of the accelerations can have incorrect dimensions. This test checks whether the program terminates if a wrong vector is inputted. To facilitate the test, the input vector is transposed. Running the test produces the error message below. The test is considered passed.

```
Expected input to be an array with number of columns equal to 3.
```

T-CON-SEN-U03: Zero noise and bias in gyroscope model - This test is identical to T-CON-SEN-U01, but this test is performed on the gyroscope sensor model. Again, no biases are included and no noise is added to the signal. The output values should be identical to the input values. The results are shown in Table 10.14 and demonstrate that the model works correctly and thus this test has passed.

Table 10.14: T-CON-SEN-U03

Code	Input	Output	Pass/Fail
T-CON-SEN-U01	[0,0,0]	[0,0,0]	Pass
T-CON-SEN-U02	[1,1,1]	[1,1,1]	Pass
T-CON-SEN-U03	[5,-5,5]	[5,-5,5]	Pass

T-CON-SEN-U04: Wrong input dimensions for accelerometer model - Inside the six degrees of freedom model, the dimensions of the velocities can have incorrect dimensions. This test checks whether the program terminates if a wrong vector is inputted. To facilitate the test, the input vector is transposed. Running the test produces the error message below. The test is considered passed.

```
Expected input to be an array with number of rows equal to 1.
```

T-CON-SEN-M01: Correct influence of bias and noise - For this test, the bias and noise values explained in Chapter 7 are implemented in the sensor model. A plot is made to check if the signal is still reasonably the same as the input signal. This is done for both the accelerometer and the gyroscope. The inputs are modelled as a sine wave. Then, bias and noise is added to the sine wave. The results of the test are displayed in Figure 10.4. Adding the bias and noise produces the same signal with some small local errors. The test is considered successful.

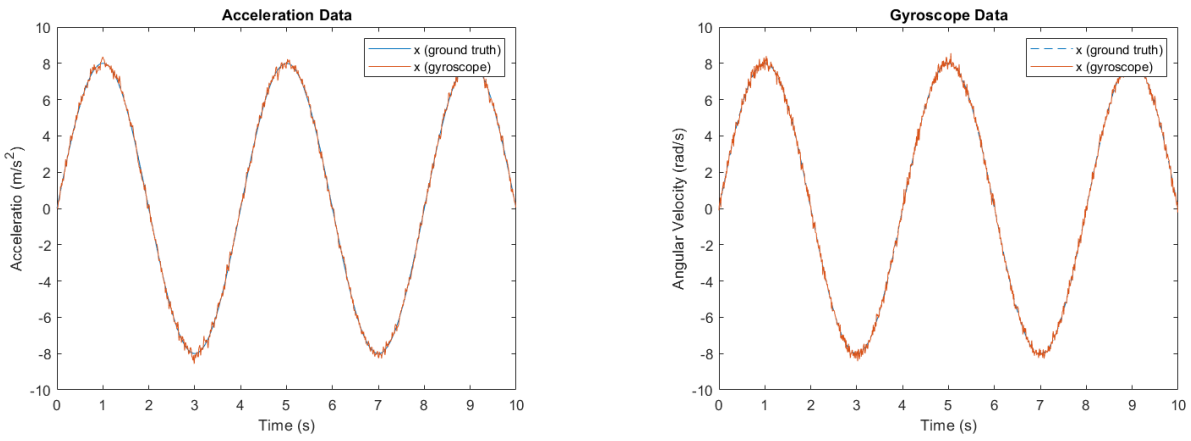

(a) **(b)**

Figure 10.4: Original and simulated sensor signal plots for T-CON-SEN-M01. a) Accelerometer b) Gyroscope

T-SC-SIX-M1: Gust function - The general gust model is verified by plotting the function in Matlab, and verifying it matches the plot produced by both one in Python and *Desmos Graphing Calculator*. PASS

T-SC-SIX-M02: Drag model v1.0

The numerical model is simply the drag equation and as such it can be verified. Table 10.15 performs several unit tests on the drag model, through changing the inputs to the model.

Table 10.15: Results of unit test T-SC-SIX-M02

Code	Input	Expected	Outcome	Fail/pass
T-SC-SIX-M02-U1	v_gust transposed	Error	Error	Pass
T-SC-SIX-M02-U2	$v\_vehicle$ transposed	Error	Error	Pass
T-SC-SIX-M02-U3	rho removed	Error	Error	Pass
T-SC-SIX-M02-U4	S removed	Error	Error	Pass
T-SC-SIX-M02-U5	C_D removed	Error	Error	Pass

Extra unit tests included:

- *T-SC-SIX-M02-U6* : Visual inspection of step function, at time equal to 10.5 seconds the y value should drop from 1 to 0. PASS
- *T-SC-SIX-M02-U7* : A test to check that the Simulink squaring was used correctly, was compared to Matlab wrote. The difference was found equal to zero. PASS

T-SC-SIX-M02-M1 : The module test was concluded by comparing the Simulink result post function to the Matlab function pre step function, the resulting plot below showed that they produce the same results. PASS

Note that during, numerical model verification, a small reference frame error was found and corrected before .

T-SC-SIX-M03: Linear dynamics model

The numerical model is made directly from equations presented in **Dynamics**, as such it can be validated. For the first unit tests, the inputs of the program are set to zero. In Table 10.16, the input parameters are shown. The expected result and the outcome are included as well. Comparing these leads to the conclusion of a fail or pass of the unit test.

Table 10.16: Results of unit test T-SC-SIX-M03

Code	Input	Expected	Outcome	Fail/pass
T-SC-SIX-M03-U1	m	Run error	Division by zero error	Pass
T-SC-SIX-M03-U2	g	Run error	Division by zero error	Pass
T-SC-SIX-M03-U3	τ	Run error	Simulink error	Pass

T-SC-SIX-M03-U4 to U9 : this test is to ensure that the control system responds adequately if empty inputs are given. This is meant to prevent the program from giving results, although inputs are not given correctly. It is expected that the program terminates if any of the inputs is not defined correctly. For every input (including mock inputs coming from other modules), the program terminates and the following error message is shown:

```
Unrecognized function or variable.
```

T-SC-SIX-M03-U10 to U13: these tests set the mock inputs from other systems equal to row vectors instead of column vectors. All tests came up with errors, so all three tests met the PASS criteria.

T-SC-SIX-M03-M1: Without the PID controller feedback, as the aerodynamic force increases the acceleration should increase linearly with force, then the velocity should increase at an increasing rate and the position too. To do this the system was reduced; with the trajectory, feedback, PID and accelerometer error removed, while the aerodynamic force was changed to a ramp function. The results, shown in Figure 10.5, confirm that the test has met the PASS criteria.

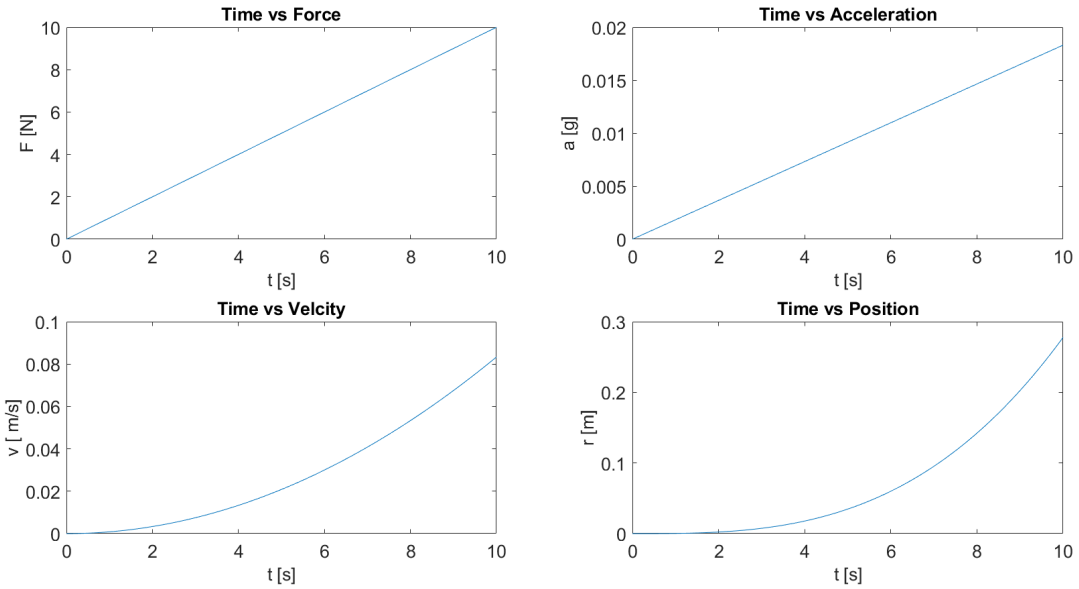

Figure 10.5: Module test: Sanity check for the linear dynamics model

T-SC-M03-M2: Now the PID controllers were tuned via the Simulink tuning procedure, the target trajectory was set to *[5; 4; 3]* in the x, y and z direction respectively. The results were plotted and the target deviation was reached, this shows that this test has met the PASS criteria.

T-SC-SIX-M04: Transformation function

Numerical model verification: The transformation equations are taken from the flight dynamics course (AE3212-I) from TU Delft, they were given from a professor and so are verified.

Due to the high confidence in the numerical model validation, and the simplicity of the code inside it, only standard unit tests where made with random angle inputs in the range of 0 to π.

- *T-SC-SIX-M04-U1*: Test whether the simulator works with a row vector for the disturbed angles - results in an error - PASS
- *T-SC-SIX-M04-U2*: Test whether the simulator works with a row vector for the vertiport angles - results in an error - PASS
- *T-SC-SIX-M04-U3 and U4*: Test whether the simulator works with no disturbed or vertiport angles - results in an error - PASS

T-SC-SIX-M05: Angular dynamics model

Note: For these tests the input-output connection to the gyroscope model and Kalman filter was removed, so the angular velocity flowed directly within the model. Secondly, the control moment, ignores the propulsion module.

After running sanity tests, it was found that three PID controllers were not sufficient to control the system, as the 3 DOF were linked together; thus test criteria: FAIL. As a result, a new controller of an MPC was trialed, this again failed verification, same for an adaptive MPC, the final design of a sigmoid-activated MPC passed verification; the results are shown below.

The following table (Table 10.17), runs unit tests with values in the matlab file are removed from the workspace, before the Simulink is ran.

Table 10.17: Results of unit tests of T-SC-SIX-M05

Code	Input	Expected	Outcome	Fail/pass
T-SC-M06-U1	A	Run error	Simulink Error	Pass
T-SC-M06-U2	B	Run error	Simulink Error	Pass
T-SC-M06-U3	C	Run error	Simulink Error	Pass
T-SC-M06-U4	D	Run error	Simulink Error	Pass
T-SC-M06-U5	I	Run error	Matlab Error	Pass
T-SC-M06-U6	MPC.mat	Run error	Simulink Error	Pass

Tests *T-SC-SIX-M06-U7 to T-SC-SIX-M06-U10* set the steady state matrices A,B,C,D to wrong dimensions, these all resulted in a Simulink error in the varying state-space block. PASS

The modules of this subsystem consist of six different parts: a varying state space, a model predictive controller, a angle error activation for control, a angular velocity direction function, a normalization function and a sigmoid activation function. These will be tested through module tests:

- *T-SC-SIX-M06-M01*: The state space is verified by hand calculations. As the state space matrices are known; they are verified by testing them through a step function, where the slope of the step across them all should be linear and proportional to the relating component on the inverse inertia matrix. PASS
- *T-SC-SIX-M06-M02*: The model predictive controller can be verified on the MPC tune block, where one can see the response of the system. PASS
- *T-SC-SIX-M06-M03*: The angle activation function can be tested by passing a sine wave through it, with the center of the sine-wave equal to the activation function. A clear binary signal should be shown, and can be visually inspected to match with the sine wave. PASS
- *T-SC-SIX-M06-M04*: The angular velocity direction function can be tested the same as the previous test, but the sine wave is centered around 0. PASS
- *T-SC-SIX-M06-M05*: The normalization function is verified, as it's a single Simulink block, which has been verified as correct by Simulink. PASS
- *T-SC-SIX-M06-M06*: The sigmoid function is verified by putting in random 'x' coordinates and then comparing to the result to one calculated on *Desmos graphing calculator*. PASS

For the subsystem test (*T-SC-SIX-M06-S1*), a variety of aerodynamic moments were put in, all the angle errors converged to oscillations around zero. PASS

T-SC-SIX-M06: Shard case implementation in the control model

Numerical model verification:

- The transformation equations are taken from the flight dynamics course (AE3212-I) from TU Delft, they were given from a professor and so are verified.
- The equation for the gradient, and velocity components are from high-school level trigonometry. They have been checked within the team, and due to high experience within the team with this mathematics; these equations can be verified.
- *ASUMP-CON-04*

Unit tests:

T-SC-SIX-M06-U1: Test through visual inspection whether the *csv* file has been read correctly. Then choose random cases, print them and look the value up in the excel version of the csv file, if they match then the criteria is met. PASS

The following table (Table 10.18), runs unit tests with values set to zero.

Table 10.18: Results of unit tests of T-SC-SIX-M06

Code	Input	Expected	Outcome	Fail/pass
T-SC-SIX-M06-U2	u_0	Plot of outputing u_0 straight line equal to 0	Same as expected	Pass
T-SC-SIX-M06-U3	u_1	Plot of outputing u_0 straight line equal to 0	Same as expected	Pass
T-SC-SIX-M06-U4	u_2	Plot of outputing u_0 straight line equal to 0	Same as expected	Pass
T-SC-SIX-M06-U5	Time	Plot of u_0, u_1, u_2 are straight lines	Same as expected	Pass
T-SC-SIX-M06-U6	Time step	Run error	Simulink Error	Pass

The following table (Table 10.19), runs unit tests with values in the matlab file are removed from the workspace, before the Simulink is ran.

Table 10.19: Results of unit tests of T-SC-SIX-M06

Code	Input	Expected	Outcome	Fail/pass
T-SC-SIX-M06-U7	u_0	Run error	Simulink Error	Pass
T-SC-SIX-M06-U8	u_1	Run error	Simulink Error	Pass
T-SC-SIX-M06-U9	u_2	Run error	Simulink Error	Pass
T-SC-SIX-U10	Time step	Run error	Simulink Error	Pass
T-SC-SIX-M06-U11	Transformation matrix	Run error	Simulink Error	Pass

T-SC-SIX-M06-U12: Transformation is a column vector - Simulink error - PASS

Module tests:

- *T-SC-SIX-M06-M01:* Perform a sanity check; test through visual inspection whether the peaks of a plot look alike to data points from the xlsv data file, and the aerodynamic Shard case. PASS
- *T-SC-SIX-M06-M02:* Perform an extreme value test; set the simulation to time greater than the time the gust acts over; the gust velocities should plateau at this time. *Result:* After the gust time (179s), all gust velocities go to 0 instantaneously. *FAIL.*
  The function was changed and the test was re-ran - *PASS.*

T-SC-SIX-M07: Aerodynamic module in the control model

Numerical model verification:

- The normalization equations are simple mathematics.
- The equations for calculating α and β are simply derived from well-known Cartesian-spherical transformation equations.
- The transformation matrix $T_{cg-CATIA}$ was developed by the same procedure as the previously verified transformation equations.
- The coefficients to force equations come from $F = q \cdot C \cdot S$ **flightdynamics**, where C is the coefficient, however the S was set equal to 1 during aerodynamic post-processing and thus drops out.
- The moment equation was first wrote wrong, but after numerical model verification it was corrected. Again, the first part of the equation comes from **flightdynamics**, while the second part from [2].
- The interpolation method was validated by the expert opinion of Prof. Dr. F. Scarano and Dr. A.K. Doan during a review meeting on the review.

Unit Tests:

- *T-SC-SIX-M07-U01:* All coefficients can be interpolated with only the y and z positions, and the coefficient value. PASS.
- *T-SC-SIX-M07-U02:* Use visual inspection to check the values for y and z positions, and the coefficient values; are copied correctly from the aerodynamic data sheet. PASS.

The following table (Table 10.20), runs unit tests with values in the matlab file are removed from the workspace, before the Simulink is ran.

Table 10.20: Results of unit tests of T-SC-SIX-M07

Code	Input	Expected	Outcome	Fail/pass
T-SC-SIX-M07-U3	$\mathcal{T}_{cg-catia}$	Run error	Simulink Error	Pass
T-SC-SIX-M07-U4	$r_{cg-catia}$	Run error	Simulink Error	Pass
T-SC-SIX-M07-U5	$v_{vehicle}$	Run error	Simulink Error	Pass
T-SC-SIX-M07-U6	v_{gust}	Run error	Simulink Error	Pass
T-SC-SIX-M07-U7	TdV	Run error	Simulink Error	Pass
T-SC-SIX-M07-U8	Lookup table for C_X	Run error	Simulink Error	Pass
T-SC-SIX-M07-U9	Lookup table for C_Y	Run error	Simulink Error	Pass
T-SC-SIX-M07-U10	Lookup table for C_Z	Run error	Simulink Error	Pass
T-SC-SIX-M07-U11	Lookup table for C_{m_p}	Run error	Simulink Error	Pass
T-SC-SIX-M07-U12	Lookup table for C_{m_q}	Run error	Simulink Error	Pass
T-SC-SIX-M07-U13	Lookup table for C_{m_r}	Run error	Simulink Error	Pass

[2] *https://engineeringstatics.org/Chapter_04-moments-in-three-dimensions.html [Cited: 08/06/2022]*

One interesting thing found during the unit tests, is that the column vectors can be taken in as row vectors without effecting the running of the system.

Module tests: a sensitivity analysis was conducted against the non-constant items. Figure 10.6 shows how the effect of the gust and vehicle velocity on the magnitude of aerodynamic force, here 1 is x direction, 2 is y and 3 is z. Interestingly this shows that the y direction has the largest effect - this makes sense as it effects the β value.

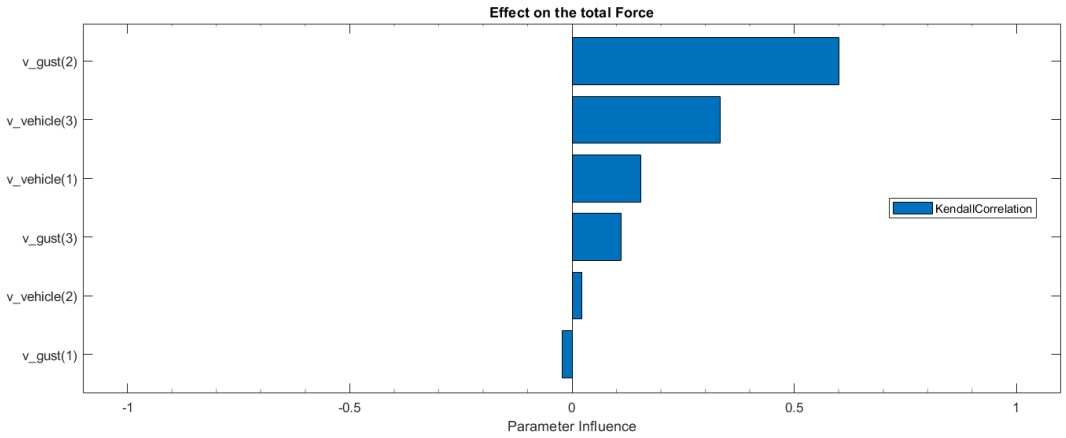

Figure 10.6: Sensitivity analysis for the aerodynamic module

T-SC-SIX-M08: Propulsion module

Numerical model verification: The equation derivation were given through simple free-body diagram methods given in *Engineering Mechanics, Hibbeler*, and so the method to create them can be verified. Whilst the rest, is just simple mathematics.

Unit tests: The following table (Table 10.21), runs unit tests with values in the matlab file are removed from the workspace, before the Simulink is ran.

Table 10.21: Results of unit tests of T-SC-SIX-M08

Code	Input	Expected	Outcome	Fail/pass
T-SC-SIX-M08-U01	$\mathcal{T}_{dV}$	Run error	Simulink Error	Pass
T-SC-SIX-M08-U02	$\mathcal{T}_{Vd}$	Run error	Simulink Error	Pass
T-SC-SIX-M08-U03	$F_c(t-\tau)$	Run error	Simulink Error	Pass
T-SC-SIX-M08-U04	$M_c(t-\tau)$	Run error	Simulink Error	Pass
T-SC-SIX-M08-U05	No saturation limits	Run error	Matlab Error	Pass

The following table (Table 10.22), runs unit tests with values in the matlab file are set to zero, before the Simulink is ran.

Table 10.22: Results of unit tests of T-SC-SIX-M08

Code	Input	Expected	Outcome	Fail/pass
T-SC-SIX-M08-U06	$F_c(t-\tau)$	Zero output force	Zero output force	Pass
T-SC-SIX-M08-U07	$M_c(t-\tau)$	Zero output moment	Zero output moment	Pass

Model tests: The propulsion system consists of six blocks: first transforming the force to the body frame, then turning the forces and moments to propeller thrusts, then limiting the propeller thrusts, then digitising the propeller thrusts through a sample and hold function to model acceleration, then turning the saturated and digitised propeller thrusts back to forces and moments, and finally converting the force to the vertiport frame. The module tests aim to test all of these blocks, although the first and last blocks focus around transformations and have such been verified from verifying the transformation subsystem.

- *T-SC-SIX-M08-M01*: Block 2 and 5 are verified by taking in mock forces and moments, converting them through block 2 to propeller thrusts, then through block 5 back to forces and moments. If these forces and moments are equal then the test is passed. PASS

- *T-SC-SIX-M08-U02*: Block 3 is verified by passing through a sine wave with an amplitude greater than the saturation limit. Visual inspection can clear show if the propeller thrust is limit to it's maximums and minimums. PASS
- *T-SC-SIX-M09-U03*: An extra test is done for Block 2, a degenerate test, as the required forces and moment increase, then all the propeller forces will increase. PASS
- *T-SC-SIX-M10-U04*: Block 4 is verified again through visual inspection, pass through ramp function, and check the positions of the flats and slopes align to the digital signal put into the sample and hold function. PASS

T-SC-SIX-M09: The Kalman filters

For the filtering of the signals, a Kalman filter is used. A built-in Simulink block is used for that. For that reason, only some small unit tests are performed, as it is assumed that the block functions accordingly.

T-SC-SIX-M09-U01: Zero input - This test checks if the Kalman filter outputs values of zero if vectors with zeros are used as input. This is indeed the case. Therefore, this test is successful.

T-SC-SIX-M09-U02: Correct input dimensions - This test checks that the Kalman filter only accepts vectors with the correct dimensions. Both the u and y inputs of the Kalman filter require a 1 by 6 vector. For both inputs, the dimensions are checked. The situations and results are listed in Table 10.23. Using 6 by 1 dimensions does not give an error as was expected. However, this is not seen as a problem as the same data would be used in the Kalman filter. This test has passed.

Table 10.23: T-SC-SIX-M09-U02 to U05

Code	Dimension u	Dimension y	Expected result	Result	Pass/Fail
T-SC-SIX-M09-U02	1x6	1x6	No error	No error	Pass
T-SC-SIX-M09-U03	1x4	1x6	Error	Error	Pass
T-SC-SIX-M09-U04	1x6	1x4	Error	Error	Pass
T-SC-SIX-M09-U05	6x1	6x1	Error	No error	Fail

10.6. Verification of structures

In this section, the codes for the structural design will be verified. The code which needs to be checked is mostly the code for the design of the fuselage. Also, the beam program needs to be verified.

Unit tests

Different unit tests have been performed on the fuselage design. In Table 10.24 the unit tests are stated. Some unit tests were on the amount of items in the input of certain functions. For the cross-section, segments have been defined. So some properties need two values. Therefore, it needs to be tested whether an error occurs when a wrong input is given to a function. Different inputs are NumPy arrays, lists and float variables. Other types of verification are done by checking whether the booms are correctly initiated.

- T-STRUC-FL-U01: Done for the area-, I_{xx}- and I_{yy}-function. A list of 2 items is needed for the function. Only one item is given.
- T-STRUC-FL-U02: Done for the area-, I_{xx}- and I_{yy}-function. A list of 2 items is needed for the function. A single value is given for the function.
- T-STRUC-FL-U03: Checks the amount of items when initialising an instant of a class. This is most important to check whether all items are in the instance.
- T-STRUC-FL-U04: Checks the amount of items when, after initialising an instant of a class, certain methods have run correctly. This is most important to check whether all items are in the instance and that the functions are correctly called.
- T-STRUC-FL-U05: Test the stress and shear equation for dividing by a zero input for I_{xx}.
- T-STRUC-FL-U06: Test the stress and shear equation for dividing by a zero input for I_{yy}.

Table 10.24: Results of wrong length tests T-STRUC-FL-U

Code	Needed input	Input	Expected	Outcome	Fail/pass
T-STRUC-FL-U01	$[i_1, i_2]$	[0]	IndexError	IndexError	Pass
T-STRUC-FL-U02	$[i_1, i_2]$	0	TypeError	TypeError	Pass
T-STRUC-FL-U03	Initiate boom		Boom has 13 items	items = 13	Pass
T-STRUC-FL-U04	Initiate boom		Boom has 17 items	items = 17	Pass
T-STRUC-FL-U05	$I_{xx} > 0$	$I_{xx} > 0$	ZerodivisionError	ZerodivisionError	Pass
T-STRUC-FL-U06	$I_{yy} > 0$	$I_{yy} > 0$	ZerodivisionError	ZerodivisionError	Pass

10.6.1. Sanity check

The sanity check on structures is checking whether strange behaviour is occurring and whether this is unexpected or just erroneous.

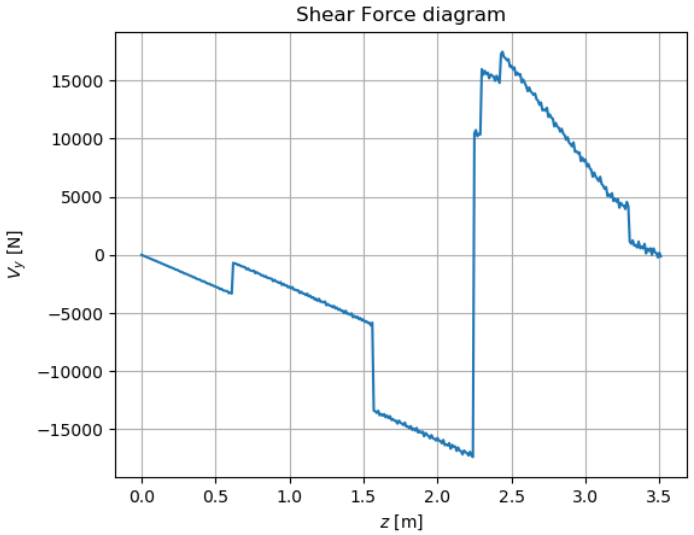

Figure 10.7: Load diagram before checking the code.

- T-STRUC-FL-S01: A function which calculates the total weight, gave values of ±3000 kg per section for skin panels. After checking the equation for a single skin panel, a parenthesis seemed to be in the wrong position. After correction, the panel weight reduced to the order of ±1 kg
- T-STRUC-FL-S02: Visual inspection of the load diagram and prints of cross-section total weights failed, equations should provide smooth behaviour (except for step inputs), but unexpected vibrating behaviour is shown in Figure 10.7. Solved by correcting indenting **return**-statement.
- T-STRUC-FL-S03-S: Final calculations were done for stresses. But strange values came out of that: higher order differences to common values. The reason was quite clear, because it had to do with the stress-ratio for defining the boom area. The critical stresses were used for that, but that leads to those strange ratio's. To solve this, it is chosen to define the boom area, instead of the stringer area, and calculate this stringer area after the analysis is done.

10.6.2. Value testing

A way to test the code if the calculations give reasonable values. This is done by "print" statements and checking by hand calculation. These hand calculations commonly find different errors:

- A variable is called on the wrong location. For example, the stress method, when it is on the wrong location, the right values for the neutral axis, could not be assigned at that point in the code. This gives a small error in the stress distribution.
- A function is called in the wrong location. This could send the wrong value, that is not updated or not even available, into the function.
- Often there is a small mistake in the equation. A factor, a minus sign and a bracket could be in the wrong location. Which affects the magnitude of the value.
- Wrong calling of a list or NumPy item could lead to wrong values or errors in the code.

10.6.3. Sensitivity analysis

Some sensitivity analyses are performed. This is done by increasing the boom area for the first test, and for the second test the skin thickness. In Table 10.25 the outcomes are shown, and test meets the PASS criteria.

Table 10.25: Results from a sensitivity analysis for the fuselage design

Adjusted parameter	Increases	Decreases
T-STRUC-FL-SA01 Cross-section 4 Boom 2 Area $1.5 \cdot B$	 A: 72%	σ_z: 9.5% τ: 7.9%
T-STRUC-FL-SA02 Cross-section 4 Boom 2 Area $1.5 \cdot t$		σ_z: 0% τ: 33.6% A: 21.8%

10.6.4. Verification of the C.G. estimation

For the C.G. estimations, some simple tests are performed. The results of the tests can be seen in Table 10.26

Table 10.26: Results of test T-CG-U

Code	Input	Expected	Outcome	Fail/pass
T-STRUC-CG-U01	All values = 2	C.G.=2	C.G.=2	Pass
T-STRUC-CG-U02	$M_{Total} = 0$	Division by 0	Division by 0	Pass
T-STRUC-CG-M01	Hand calculation	C.G.=1.226	C.G.=1.226	Pass
T-STRUC-CG-M02	Increase battery weight by 10%	C.G. moves aft Total weight increases	C.G. from 2.82 to 2.80 Weight from 803 to 830	Pass
T-STRUC-CG-M03	Battery moved forward y one meter	C.G. moves forward (value increases) Weight stays constant	C.G. from 2.82 to 3.16 Weight from 803 to 803	Pass

10.6.5. Verification of the eigenfrequencies

Just as for the C.G. the eigenfrequencies are based on some standard formula's, so verification is quite easy

Table 10.27: Results of test T-Ef-U

Code	Input	Expected	Outcome	Fail/pass
T-STRUC-EF-U01	L = 0	Division by 0	Division by 0	Pass
T-STRUC-EF-U02	$C2 = 0$	Frequency = 0	Frequency = 0	Pass
T-STRUC-EF-M01	Hand calculation	Frequency = 59.97	Frequency = 59.97	Pass
T-STRUC-EF-M02	Increase C2 by 10%	Frequency increases by 10%	Frequency from 278 to 306 = 10%	Pass

11. Validation

Now that the tools and models used have been verified, it should be checked if they are used to model the correct physical situation. Validation is important to ensure the output of the tools to be valid for the design. First, the aerodynamic tools are validated in Section 11.1. Secondly, the propulsion tools are validated in Section 11.2. The noise analysis is validated in Section 11.3. Then, the battery weight code is validated in Section 11.4. In Section 11.5, the control simulation is validated and finally, in Section 11.6, the fuselage tool is validated.

11.1. Validation of aerodynamic models

In order to know how close the employed aerodynamic models represent the real aerodynamic behaviour of the analysed objects, a couple of tests are done on the models. In Section 11.1.1, the method used to determine the aerodynamic coefficients is validated. In Section 11.1.2, recommendations are given for a more accurate aerodynamic analysis. Finally, in Section 11.1.3, the flow field around the Shard building is validated.

11.1.1. Validation of aerodynamic coefficient estimation

For the validation of the models used for the aerodynamic analysis, a CFD simulation of a simple object is compared with experimental data. For this validation test a sphere is analysed, because there is plenty of experimental data of the airflow around these. The setup of the mesh and the initial conditions are similar to the cases described in Chapter 5.

In this case, only the drag coefficient calculation is validated, as the procedure for the calculation of other aerodynamic coefficients is relatively similar. The drag coefficients are calculated with the `forceCoeffs` function in `OpenFOAM`. In order to validate the results obtained by it, simulations of a sphere with a diameter of 1 meter subject to flows of 0.5, 5 and 50 m/s are used. ISA standard atmosphere conditions are assumed. The reference area was taken to be the projected area of a sphere with the specified diameter. This results in Reynolds numbers of $3.4 \cdot 10^4$, $3.4 \cdot 10^5$ and $3.4 \cdot 10^6$ respectively. From these simulations, drag coefficients of 0.33, 0.18 and 0.14 are obtained respectively. From experiments, it is known that the drag coefficient of a sphere is between 0.4 and 0.5 for Reynolds numbers between 1000 and 200000, as can be seen in Figure 11.1a. At higher Reynolds numbers it drops to roughly 0.1 (the famous drag crisis) and after that it rises up a bit. As can be noted, the drag coefficient at the lowest speed gives a drag coefficient significantly lower than the expected drag coefficient, as it was expected to be between 0.4 and 0.5. The drag coefficient of 0.18 at a Reynolds number of $3.4 \cdot 10^5$ could be slightly underestimated, judging by the plot. Finally, the drag coefficient of 0.14 at a Reynolds number of $3.4 \cdot 10^6$ is underestimated compared to the expected value of roughly 0.2 (Figure 11.1a).

So, it can be concluded that the estimation of the drag is not accurate but gives ballpark values of the expected aerodynamic coefficients. The reason for this could be that the used mesh was relatively coarse. This was done because a significant number of cases was run and not a lot of time was available. For this objective it is acceptable, because most of these values are used for a rough estimation of the aerodynamic response for the controls model.

11.1.2. Recommendations for the aerodynamic coefficient determination

However, in a later stage of the design, it may be beneficial to run some more accurate simulations in order to simulate the response of the vehicle in more detail. Also, the effect of the downwash of the rotors onto the fuselage on the force and moment coefficients can be analysed then.

11.1.3. Quantitative validation of the results by flow visualization

A simple way to detect errors in the numerical solution is to visualise the flow by post-processing and see if the results are physically sensible. An example of this is shown in Figure 11.1b. Three physical phenomena are evident from this figure, which one would expect in the real world:

- Increase in pressure at the front side of the building (flow is coming from the left to right), strong pressure gradient at the corners of the buildings.
- Low-momentum reversed flow region (of helical shape) in the wake of the building.
- Decrease of velocity in streamlines when approaching the building and acceleration when going around it.

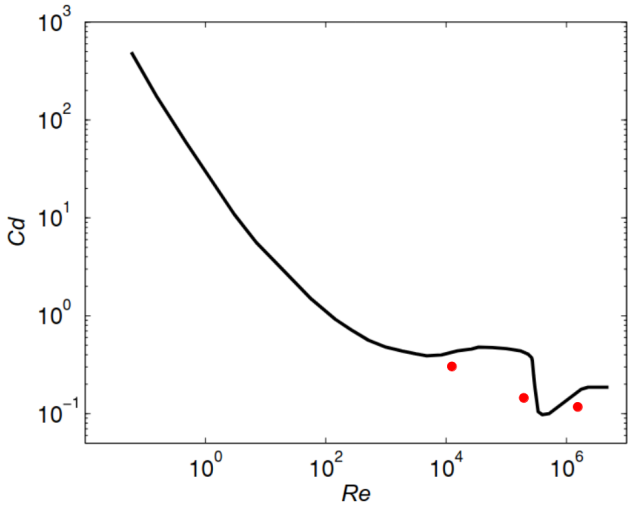

(a) Experimental C_D (black line), OpenFOAM runs (red dots) **spheredragcoefficient**

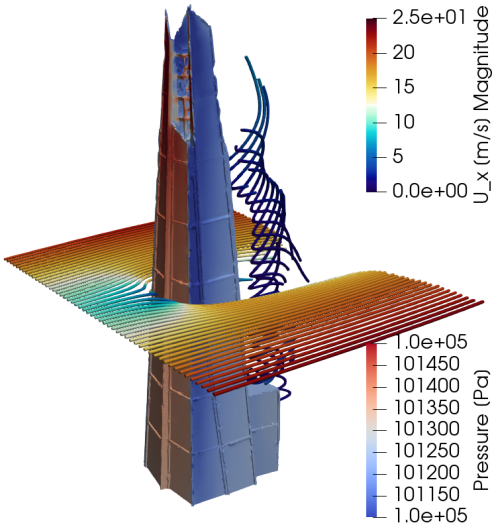

(b) Visual validation of Shard case results. Flow coming from left to right.

.

Figure 11.1

11.2. Validation of the blade geometry and rotational velocity calculations

The calculations performed for both the blade geometry design and the rotational velocity required for each flight phase are presented by Prouty et al. **prouty1995helicopter**. The calculations presented in the book are accompanied by the specifications of 18 different helicopters, which were provided directly by the manufacturers. These specifications include the maximum take-off weight, linear twist, tip radius, chord length and tip speed. It is not specified for which flight phase or other conditions this tip speed is true, and for validation purposes it is assumed that this is the tip speed for hover.

In order to validate the blade geometry and rotational velocity code for the Veatle, a light-weight helicopter was chosen from the article of Prouty to run through the code. Apart from the information on the helicopter given in the article, information on the collective twist (virtual pitch angle at the centre of rotation) is also needed. The only light-weight helicopter in Prouty's database for which this value could be found in literature is the Robinson R22. The value was found in literature to be 14.5 deg [1].

With all the necessary information gathered, the code was run with the specifications of the Robinson R22. The code was validated by providing the blade geometry and rotational velocity as an input, and calculating the generated lift. The order of these steps is reversed with regard to the actual code, but it is a valid method as the same calculations are performed. If the calculated generated lift is close to the value of the required lift, the code is valid.

The calculated lift by the rotor for the specified rotational velocity was compared to the required thrust, which was set at $1.1 \cdot MTOWg$. This showed an error of 13%. The code runs most accurate when a factor of 1.2 is chosen instead of 1.1. In short, it can be concluded that the code calculating the blade geometry and rotational velocity is sufficiently accurate with a relatively small error.

11.3. Validation of noise analysis

The results of the noise analysis in Section 6.1.4 are expressed in dBA, giving the A-weighted sound pressure level. This unit was chosen because it is a good measure of the noise levels as perceived by the human ear, and it was possible to calculate this with the information available. However, the available information for validation is expressed in sound exposure level (SEL), in the units EPNdB. This type of noise level is based on the intensity of the noise, in combination with the duration of the noise. No accurate methods were found to convert dBA to EPNdB with the information given and determined during the design phase. Hence, the only validation that was possible was a qualitative analysis: asserting whether the calculated value in dBA increased with an increase in given EPNdB value of reference aircraft. For the overall noise level, this is the case when comparing

[1] *https://www.pprune.org/archive/index.php/t-101314.html [Cited: 14/06/2022]*

the Bell 407 ($EPNdB = 89.6$ at 500 ft flyover), with the McDonnell Douglas 500E ($EPNdB = 81.0$)[2]. The calculated noise levels indeed showed that the Bell 407 is louder for a longer period during the flyover, thus producing a higher SEL. The McDonnell Douglas 500E has a higher peak noise due to vortices, but the noise level fades more quickly due to low rotational noise. Thus, the SEL of the McDonnell Douglas 500E is indeed calculated to be lower than that of the Bell 407, as also stated in literature. This model is thereby qualitatively validated.

11.4. Validation of battery weight code

The battery code is largely based on the power required code, so this validation will be seen as a validation of both pieces of code. It will be done by comparing it to sample calculations done in other studies (**samplecalc**, **dragpolars**, **tuevtolstats**, **sample3**). These sample calculations are done assuming an eVTOL with a generic mission objective, so requirements such as REQ-HL-03 REQ-HL-12 must not be taken into account when validating the model, as they would lead to an obvious overdesign. The redundancy factors relating to REQ-HL-12 were removed, and the extra energy/power calculations relating to the 3-rotor control system were also removed. The results can be found in Table 11.1.

Table 11.1: Battery code validation

MTOW [kg]	Based on	$W_{\mathbf{bat}}$ report [kg]	$W_{\mathbf{bat}}$ developed code [kg]	Difference
2000	sample	600	707	+18%
1250	sample	475	392	-18%
260	EHang 184	92	53	-42%
1224	KittyHawk Cora	310	353	+14%
1508	Archer Maker	441	489	+11%
1100	Bartini eVTOL	320	389	+22%
900	Volocity Volocopter	278[3]	244	-12%

It can be seen that there is significant deviation for each case, but no obvious bias. The largest deviation is there for the EHang 184. This is a cause for concern since the EHang 184 actually resembles the Veatle the most out of all aircraft tested. This can possibly be explained by the fact that the EHang 184 is really in a different weight class altogether, so the methods used might not be as accurate. The aircraft which yielded results closer to reality are mostly winged concepts, which generally have a smaller portion of their weight allocated to the battery. For that reason, it is a good sign that the weight is moslty overestimated by the program (it would be expected that for a multirotor of a certain MTOW, the battery weight would be higher than for a winged concept). Since there are only a very small number of sufficiently developed eVTOL concepts with a comparable range, validation is a difficult task to perform very accurately. Because of this and the fact that it was sufficiently verified, the code will not be altered at this stage. For the Volocopter Volocity, which was identified as the most direct competitor, the result is not far off from 'reality', but unfortunately it is *under*estimated.

11.5. Validation of the control simulation

The control model cannot be validated sufficiently at this stage of the design. Part of the model already incorporates the propulsion, as well as aerodynamics fuselage and urban turbulence models. These have been validated in the above sections. Meanwhile, the sensor bias and noise levels have been taken from sensor datasheets - so they can be validated by inspection. Apart from this, it is hard to validate the controls model, due to the lack of data available, and the fact that the controller design strongly depends on the characteristics of the vehicle. Most of the validation will have to take place in the later stage of design. A scaled down model of the Veatle should be built and the controller model implemented. Flying the design in a wind tunnel under a known gust speed and direction, will allow for testing of the model. The data generated from this test can be used to validate the model for the aerodynamics, which will directly affect the controllability. Alternatively, an easier approach to validation would be to test the model aboard a pre-made drone, and re-configure the propulsion model to have quadcopter control; however this would take more work to build a new control model for this, and can't valid the Y translation and yaw given from the vertical control propellers.

For the propulsion module, the parametric equations used to allocate the control forces to the top and bottom propellers, have been validated by making a separate model which iterates the propeller combinations until it reaches the minimum cost (total propeller thrust); this iterative process is visualised by Figure 11.2. Running with random combinations of F_z and M_y, the function was validated as it matched the algebraic version, with

[2] *https://www.mdhelicopters.com/files/Models/MD500E_Tech_Desc.pdf [Cited: 14/06/2022]*

some discrepancy, due to the iterative process not being exact. In Figure 11.2, the dashed red lines indicate the maximum rotor thrusts, used for finalising the sizing of the rotors.

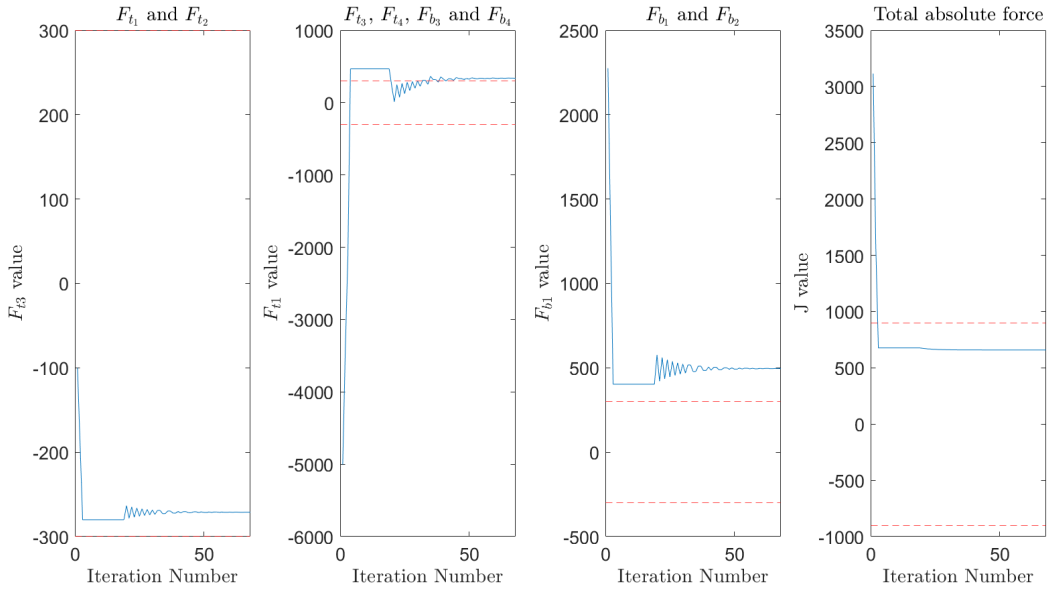

Figure 11.2: The process of iterating to the minimum cost.

11.6. Validation of the structures fuselage tool

To validate the structures tool, a simplified CAD model of one segment of the fuselage is put into a FEM analysis in CATIA. The shape which is used here has a comparable radius to the fuselage. The stringers have areas of $10\,\text{mm}^2$ and a skin thickness of 0.6 mm. A shear load is implemented on one side and the fuselage is clamped on the other side. After that, these stresses are calculated in this part and a render is visible in Figure 11.3.

In the structures tool, a similar analysis has been performed. 161.3, 167.5, 135.0, 76.1, 13.4, -29.2, -35.5, -3.0, 55.9, 118.6 MPa are the values for different booms. It seems that for tension, the values are in the same order of magnitude. But for compression, the values seem to not comply with the model.

The reasons for the difference in the model are listed below:

- The boom idealisation is not completely taking the distribution of the load into account;
- The model is not one to one comparable to the model in the fuselage tool;
- Design assumptions which are made are driving the design too far from reality;
- There are unsolved problems in the tool, which are not found during verification.

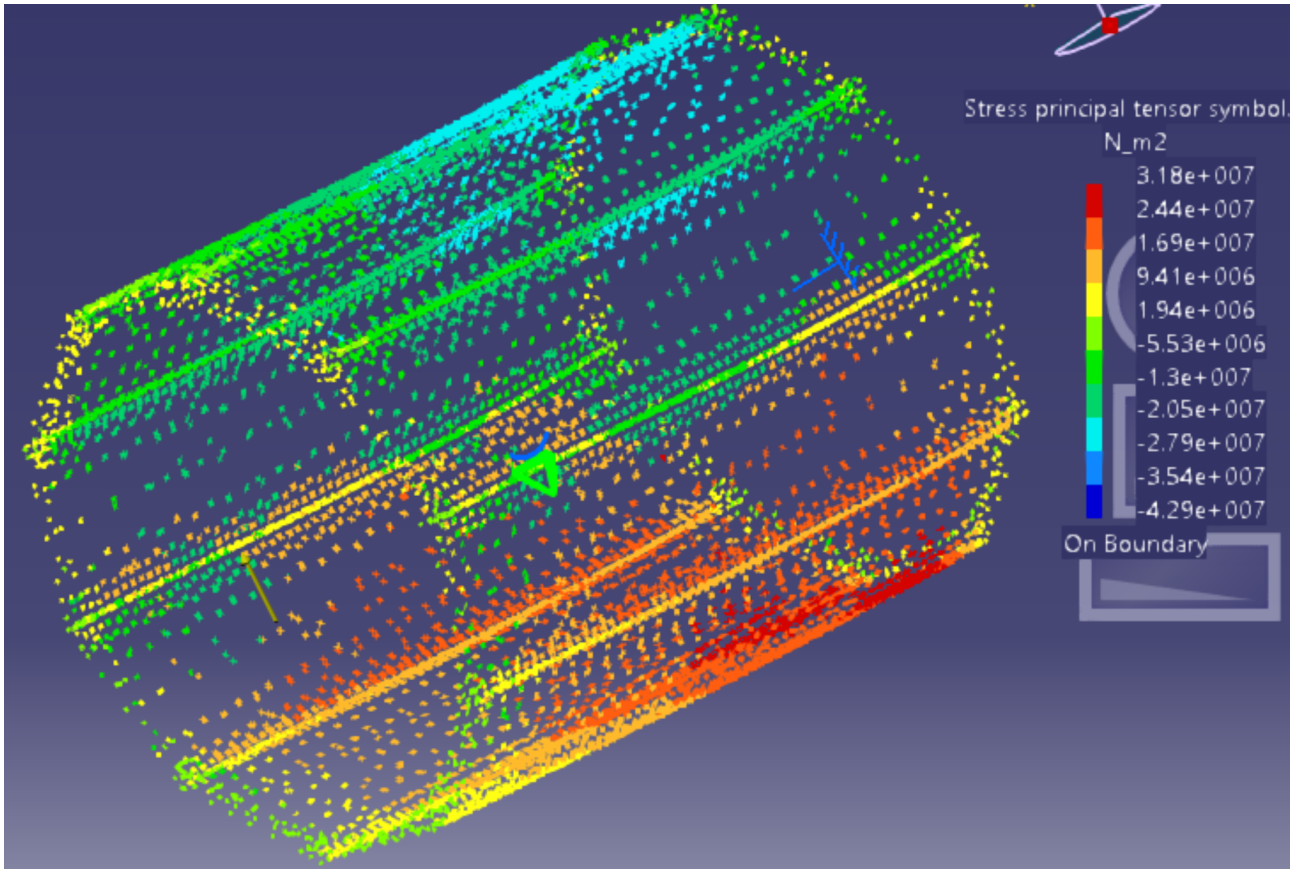

Figure 11.3: Stresses in one simple segment of the fuselage.

12. Operations

In this part of the report, several aspects of the vehicle's operations are described. In Section 12.1, the functional flow diagram and functional breakdown structure are described and displayed. Section 12.2 contains information about the operations during flight, whereas Section 12.3 elaborates on the operations on the ground. Lastly, Section 12.4 includes the internal and external communications of the operations.

12.1. Functional flow diagram and breakdown structure

The main activities concerning the vehicle and operations are split up in six main parts: design, production, operation, maintenance, reuse and recycling of the vehicle. Every main part has activities and subactivities. These are displayed in Figure 12.10 in the form of a functional flow diagram. The components of the diagram have been revised to correspond to the current design. It should be noted that most of the functions remained the same.

The flight performance of the vehicle is split up in five different sections: providing control, providing stability, providing propulsion, maintaining structural performance and providing aerodynamic performance. The vehicle functions have subfunctions. These are displayed in Figure 12.11 in the form of a functional breakdown structure. In the iterated breakdown structure, a function for maintaining structural performance has been deleted, namely changing configuration. The multi-rotor design does not require any change of configuration during flight.

12.2. Flight operations

Operations during flight aim at ensuring a safe and comfortable journey. Urban turbulence and its impact on the vehicle are described in Section 12.2.1. Characteristics of the autonomous flight concept are introduced in Section 12.2.2. Operations during flight must adhere to the requirements set by flight authorities that are summarised in Section 12.2.4. Comfort inside the cabin must be ensured for which environmental control is used, described in Section 12.2.5.

12.2.1. Flight through urban environment

Since the vehicle under development is meant to fly in the urban environment, it has to be sufficiently controllable in order to operate in rough weather conditions inside the urban canopy. Nonetheless, in order to limit the noise and visual disturbance to the city residents, the cruise altitude should be sufficiently high. During take-off and landing, however, the vehicle should be able to safely operate between the top of the buildings and cruise altitude. In rough weather conditions, a wake can develop behind a skyscraper, and the vehicle would have to fly through this wake. For the City of London, which is the business case, the tallest skyscraper is 'The Shard', which has a height of 309.6 m, see **C** in Figure 12.1a [1]. It towers above the city landscape, thus the effect of the surrounding buildings can be neglected. The only relatively tall building in its vicinity is the building of Guy's Hospital, which is the tallest hospital building in the world at 148.65 m. The roof of this building can be seen in Figure 12.1a **A**.

In order to study how this building would affect the air flow around it, a Computational Fluid Dynamics study was set up, with consistent methodology as is described in Chapter 5. The building was put in the centre of the computational domain, with an Standard Triangle Language model found on the Internet [2]. The domain has a surface size of 450 by 450 meters and height of 500 meters.

Consider now that the Veatle has to conduct a take-off manoeuvre from the helipad at the top of Guy's hospital, e.g. point **A**, as shown in Figure 12.1 (a). The height of point A is roughly 140 meters. It will then ascend to 160 meters at point **B** and then fly at some cruise angle to point **D** through point **C**. The horizontal distance between points **B** and **C** is approximately 150 m [3]. Based on the assumption that the vehicle flies in a straight line, that point **C** will be at the height of approximately 200 meters, and point **D** at the height of 240 meters. Assuming that the vehicle will pass 40 meters away from the skyscraper, which is roughly the building width at that height, we can map the **BCD** trajectory from the CFD data, see white arrow in Figure 12.1b.

The velocity along the X-axis, e.g, along the incoming velocity is plotted against the position Y-axis coordinate,

[1] *https://www.tripadvisor.nl/Attraction_Review-g186338-d3539289-Reviews-The_View_from_The_Shard-London_England.html [Cited: 24/05/2022]*

[2] *https://www.ameede.net/the-shard-london-h005315-file-stl-free-download-3d-model-for-cnc-and-3d-printer/ [Cited: 24/05/2022]*

[3] *https://www.google.com/maps/@51.5034456,-0.08567,17.46z [Cited: 24/05/2022]*

see Figure 12.1b. Assuming that the vehicle moves with a velocity of 100 km/h, the crosswind-vs-time plot (in **??**) shows the sideways air velocity that the vehicle would experience when moving in the wake of the vehicle.

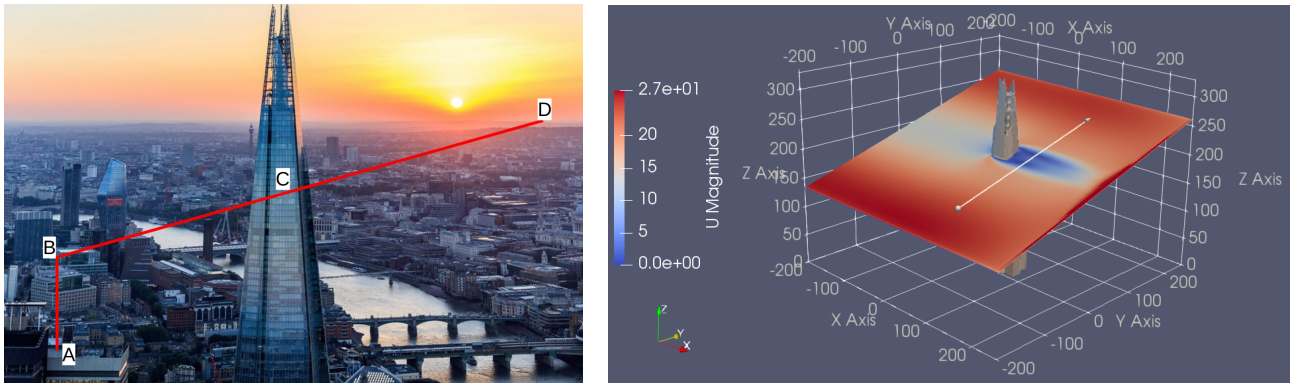

(a) The Shard Tower

(b) CFD domain & results

Figure 12.1

In the urban environment, not only extreme turbulence but also other harsh conditions such as rainfall, lightning strikes and below zero temperatures occur. As the vehicle should be available as much as possible, it should withstand these other weather conditions as well. The coating of the vehicle ensures waterproofness when flying in rainy conditions. As water droplets decrease aerodynamic efficiency, the rotors will have to produce more lift to fly. Thanks to the constraints that the allowable noise levels have put on the propulsion system, enough power is available to ensure flight with decreased aerodynamic performance. Except for raining, icing can also decrease aerodynamic qualities of a vehicle. With winged aerial vehicles, this is a serious issue. Due to the absence of wings, this phenomenon has little impact on the performance of the Veatle. Lastly, the effect of lightning strikes can be prevented by designing a Faradays' cage. As the fuselage is made from carbon fibre, which is conductive, the passengers will be kept safe in case of a lightning strike. One other problem in aerial environment is to avoid birds. A way to keep birds at a safe distance is using bird repelling colours. Next to that, future development could focus on optimizing the structure for impacts by birds.

12.2.2. Autonomous flight and path planning

When developing an urban air mobility vehicle, it is not only important to keep its passengers safe, but also to minimise the possibility of third-party fatalities. Proper path planning allows minimising this. The path planning becomes a trade-off between having the shortest possible path and the safest path. A cost function is presented by Xinyu He et al. **PathPlanning**, which should be minimised, described by Equation 12.1.

$$c = \omega_r \cdot \theta_{risk}(path) + \omega_l \cdot length(path) \tag{12.1}$$

ω_r and ω_l are weights for risk and flight distance, respectively. $\theta_{risk}(p)$ represents the risk for path p and $length(p)$ represents the flight distance for path p. Two main types of risks exist. First, collective ground risks include the number of third party fatalities on the ground. Secondly, individual risk represents the probability that an unprotected person at a certain location is killed. Increasing the risk weight to infinity and the length weight to zero optimises the path for risk. Optimising the path for length requires the opposite. It is found that the increase in number of flights increases both types of risks linearly **PathPlanning**. Optimising for the smallest amount of third party fatalities, however, will lead to certain sparsely populated areas where the risk of fatalities is significantly higher than in other areas, as UAM vehicles will always fly over these areas. However, a good ratio for the weights, allows finding the optimal path where the collective ground risk is relatively small, and no areas with unacceptable high individual risks are present.

By pre-planning all flights in the urban environment, all vehicles can fly coordinated and eliminate the possibility of accidents. Once the route has been pre-planned, the UAM vehicle can use a GPS to track its position, however unforeseen objects may be present during its route. For instance, new construction works and window cleaners, other flying vehicles. As a result, additional information is needed for safety, for example sensors to detect the surroundings. These sensors could be Light Detection and Ranging Sensors (LIDARs); this is commonly used on autonomous cars **ElonMusk_Tesla**, as it allows for a variable range detection. However, a LIDAR needs to be used with other sensors to give a robust dynamic model of the system in real time. An alternative option is optical navigation, while the LIDAR is simpler to use in general flight, the optical navigation technique is useful during parking as it can more reliably detect the parking space; due to simplicity of just detecting the pre-determined parking space when hovering above. Using these sensors allows for object detection in all flight operations **robotics_madrid**, when combined with the sensors from control, commands can be made to manoeuvre around objects. Finally, other sensors commonly used in unison with these devices are radars and ultrasonic sensors; for a more complete object detection procedure. While ultrasonic sensors will not be used on the vehicle, radar can add useful information. One disadvantage of LIDAR is that its laser beams can reflect on raindrops and therefore give inaccurate readings. Here, the radar sensor comes in. A radar sensor is less susceptible to weather conditions, but has a lower accuracy.

To ensure the sensors provide accurate information, filtering will be required. Two main filters are used, first a Kalman filter; which is predominately used for estimation of a linear dynamic system's state, but variations can be used for non-linear systems; as discussed in the literature study of the baseline report. An alternative filter is the particle filter; which is used to estimate the state of a system, which is not constant with time. Both of these filters can be used for three main cases: estimation of position when an inertial navigation system is used (GPS and accelerometers), navigation and target tracking. F.Gustaffasson et al. argue, in **Particle_Filter**, that the particle filter offers better real time performance.

When the UAM vehicle has detected an unpredicted object, it will have to plan a path around it. A Voronoi diagram allows for a maximisation of distance/clearance around the object, if the L2 variant is chosen **path1_madrid**. Another path planning concept is the use of potential graph **path2_madrid**, this is potentials: the goal location generates an attractive potential pulling the UAM vehicle towards the desired trajectory, while the repulsive potential pushes the robot away from obstacles in the path. This method allows planning and control to be coupled, but can cause the UAM vehicle to be trapped at local minima, but is avoided if only using local path planning; for instance only when an unpredicted object arises.

The use of UAM vehicles in the urban environment will cause the airspace to be more congested, as a result the commands from air traffic control will increase. Resulting in a path planning design which can re-route due to commands of air traffic control in flight. Path planning can be done on software such as QGroundControl

To model the memory size needed to autonomously control the vehicle, comparisons can be made to L4 autonomous cars; with their data storage distribution shown in Figure 12.2, also their data generation rate is 1-2 TB/hr from the sensors [4]. However, fully autonomous driving cars (L5) of the future may be more relevant to our problem; but they take a bandwidth of 40 Gb/s; so 20 TB of data sent an hour [5]. Finally, the navigation system shall have access to 5G to allow for faster connections [6].

[4] *https://www.telematicswire.net/autonomous-vehicles-to-boost-memory-requirement/ [Cited: 13/05/2022]*

[5] *https://blog.eurotech.com/en/level-5-autonomous-driving/ [Cited: 13/05/2022]*

[6] *https://www.telekom.com/en/company/details/5g-network-as-foundation-for-autonomous-driving-561986[Cited: 13/05/2022]*

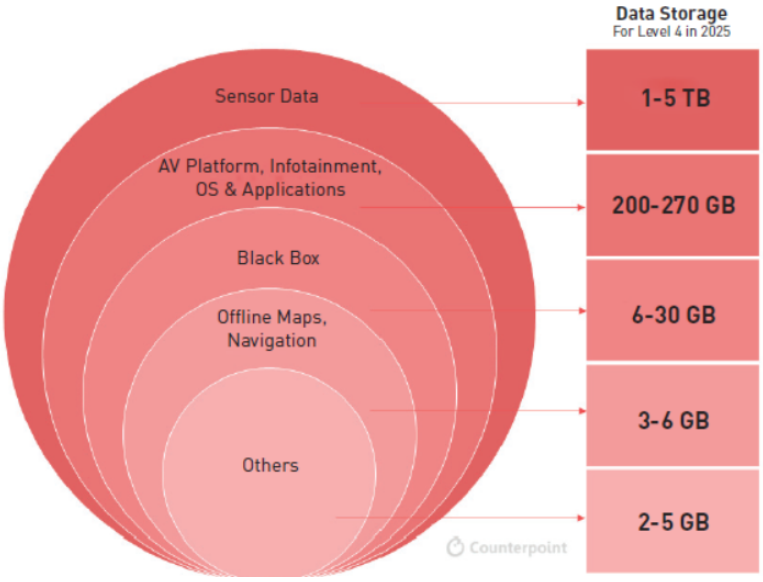

Figure 12.2: The data storage requirements for L4 autonomous cars

The path of a flight from Heathrow Airport to Guy's hospital can be seen in Figure 12.3. A regular flight profile will look similar to this flight. One would take off at one point, fly vertically for around 20 to 50 meters, after which the vehicle climbs in upward angled flight until it reaches 450 metres, after which the cruise phase takes place. When nearing the destination, the vehicle descents in a downward angled flight until it reaches 20 to 50 metres above its landing location. Finally, the vehicle lands vertically on the vertiport. Considering a vertical speed of 6 $\frac{\text{m}}{\text{s}}$, the take-off would take around 10 seconds for the vertical climb phase. Considering a climb angle of 45 degrees, with a speed of around 20 $\frac{\text{m}}{\text{s}}$, the climb phase would take around 30 s. Afterwards, a cruise phase of around 20 km takes place. Considering the cruise speed of 180 $\frac{\text{m}}{\text{s}}$, the cruise phase would take around 7 min. For landing, one can compare to the landing of a helicopter. For helicopters, a downward descend angle of more than 15 degrees is considered a steep descent **FAA_handbook_helis**. Using a similar angled velocity of 20 $\frac{\text{m}}{\text{s}}$, the landing would take around 90 s. For a comfortable landing, the vertical downward speed should not be more than 2 $\frac{\text{m}}{\text{s}}$. Descending the last 50 meters would therefore take 25 s. This leads to a total flight time of around 9.5 min.

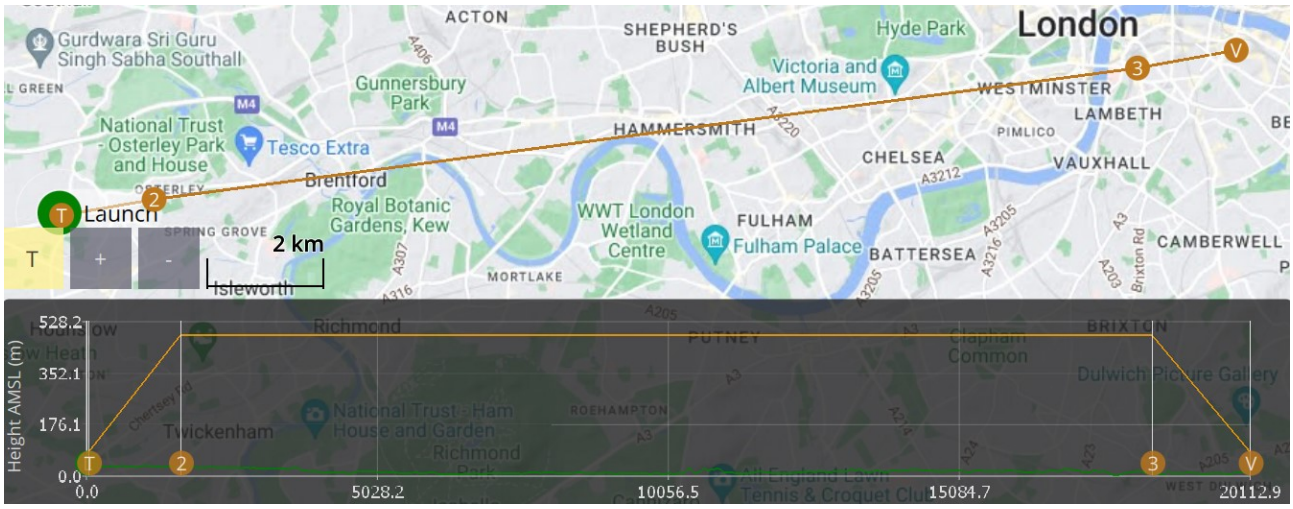

Figure 12.3: Route from Heathrow to Guy's hospital, made in QGroundControl

12.2.3. Mission profile

As explained in Section 3.10, the expected number of flights per day is around 10. Each 20 km flight takes around 10 minutes, and 10 additional minutes are added to the flight time to account for loading and unloading of passengers and luggage. After each flight, the battery is immediately plugged into the charger such that it is ready to fly again as soon as possible. There is also plenty of time allocated throughout the day for maintenance and checkups.

A typical day of operations for the vehicle can be summarised as follows:

- **00:00 - 05:00:** storage, ready for flight checks
- **05:00:** first flight from hub (20 km)
- **06:10:** flight back to hub without passengers (20 km)
- **07:00:** second flight with passengers (20 km)
- **08:00:** battery fully charged again and next flight (20km)
- **08:20:** arrived at destination where next flight is scheduled at 08:30
- **08:20 - 08:30:** battery swapping
- **08:30:** next flight (15 km)
- **08:50 - 10:50:** charging and rest/maintenance
- **10:50:** next flight with only 1 passenger (20 km)
- **11:50:** next flight (20 km)
- **12:20 - 18:00:** scheduled maintenance, no flights
- **18:00:** short flight (10 km)
- **18:45:** next flight (20 km)
- **19:00-19:20:** charging, only up to 80% because final flight is scheduled at 19:25
- **19:25:** final flight (20 km)
- **19:40-00:00:** charging and rest/maintenance

Figure 12.4 shows how the charge level varies throughout the day. Around 19:30, the battery reaches its lowest point of charge ($\approx 28\%$). This shows that even though it is possible to fly without fully charging, the charge level does reach a rather low level. This is in general not desired since it has negative effects on battery life.

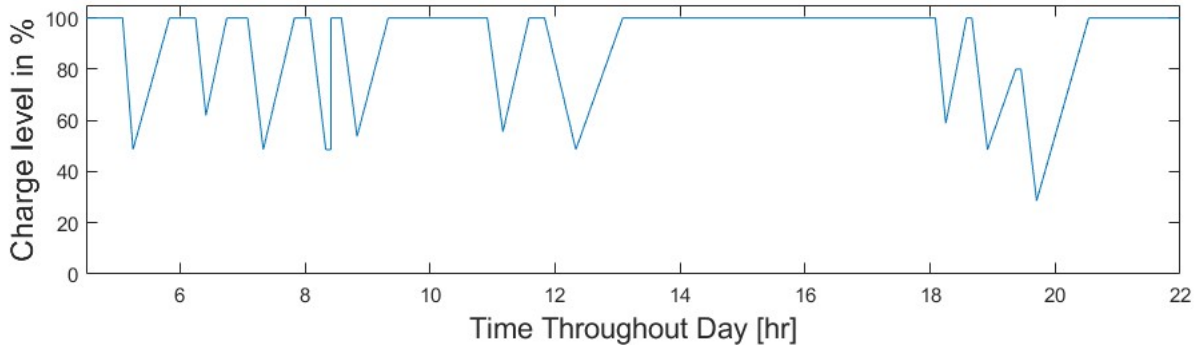

Figure 12.4: Charge level throughout a typical day

Note that the exact timing of flights is not necessarily accurate, this image is mainly to show a possible scenario and display the proportion of the day that flights are being flown and the aircraft being stationary.

12.2.4. Vehicle airworthiness

First, the airworthiness requirements for the vehicle are described. After that, verification methods of these requirements are given.

Airworthiness requirements

EASA has released a recent special condition and Means of Compliance for VTOL, which is used as initial airworthiness requirements for our design, see **easaVTOL**. The rest of this section describes the most important airworthiness requirements for our design as imposed by EASA.

MOC-VTOL.2115 Take-off performance A type-1 reference volume will be used. However, due to operations in a dense urban requirement, we consider a completely vertical take-off and landing for the certification purposes. For this reason, we assume the following take-off procedure:

- Accelerate from $V = 0$ m/s to $V_{TOSS} = 3$ m/s, est. $t = 1$ s.

- Ascend from $h = 0$ m to $h_{TDP} = 20$ m at V_{TOSS}, est. $t = 7$ s.
- We are now at the predetermined **TDP** (take-off decision point) $h_{TDP} = 20$ m. At this point, a decision should be made to either continue take-off or abort.
- Proceed at V_{TOSS} to $h = 30$ m.
- Accelerate from V_{TOSS} to $V_{TOTR} = 7.5$ m/s (take-off transition speed)
- Proceed ascending to $h = 60$ m, est. $t = 6$ s.
- Proceed to $h_{cr} = 300$ m, est. $t = 48$ s.
- Change attitude and continue to cruise.

The landing procedure is in the reverse order of taking off procedure. In total, the take-off procedure is estimated to take approx. 62 seconds. The maximum deflection of the vehicle from its vertical trajectory is given by **REQ-HL-03** and is to be limited to 1 m.

MOC-VTOL.2105 Performance data Under critical wind conditions, EASA prescribes a gust velocity of 9.1 m/s (**CS 27.341**). For our design, the maximal gust velocity is determined to be 20.7 m/s from **REQ-CON-WEA-03**, in combination with the maximum 1 m deflection.

MOC-VTOL.2210 Structural design loads For the VTOL vehicles, structural design requirements are referenced from CS.27:

- **CS 27.301a** Strength requirements are specified in terms of limit loads and ultimate loads, which are limit loads multiplied by a factor of safety.
- **CS 27.303** Unless otherwise provided, a factor of safety of 1.5 must be used.
- **CS 27.337b** The rotorcraft must be designed for any positive limit manoeuvring load factor not less than 2.0 and any negative limit manoeuvring load factor of not less than -0.5.

Based off the above described requirements, the ultimate load factors come out to be $n_{ult} = +3$ g and $n_{ult} = -0.75$ g.

12.2.5. Environmental control

Another important part in the design is the environmental control of the cabin. Some parameters that might need to be regulated are: temperature, pressure, humidity, air quality and light intensity level.
First, in order to regulate the temperature, a desired temperature range is specified based on what is comfortable for passengers and what minimises degradation and failure characteristics of the components. For this, a temperature sensor, a heater and an air conditioner are needed.
A pressure regulator is not included. Because, at the altitudes of operation, the outside pressure will still be comfortable for the passengers.
The humidity of the cabin also is an important factor, because high humidity levels could accelerate degradation of materials and increase the chance of component failure. However, humans are generally comfortable with a relative humidity between 30% and 60% [7]. To regulate this, a humidity sensor, a humidifier and a dehumidifier are needed.
When the aircraft is flying through a city, filters for particulate matter could be used to maintain clean air inside the cabin.
Furthermore, the light intensity in the cabin can also decrease the comfort of the passengers. In order to keep it at a comfortable level, light sensors can be installed at different places throughout the cabin. If the light intensity of a sensor surpasses a predefined threshold for a certain amount of time, a light screen can be lowered at the corresponding side until the light intensity is back in the desired range.
In Figure 12.5, the pressure regulation and temperature regulation are summarised in flowcharts. A similar chart can be made for the light intensity regulation.

[7] *https://www.nationalasthma.org.au/news/2016/indoor-humidity#:~:text=What%20is%20healthy%20humidity%3F,between%2030%20to%2050%20percent.[Cited: 11/05/2022]*

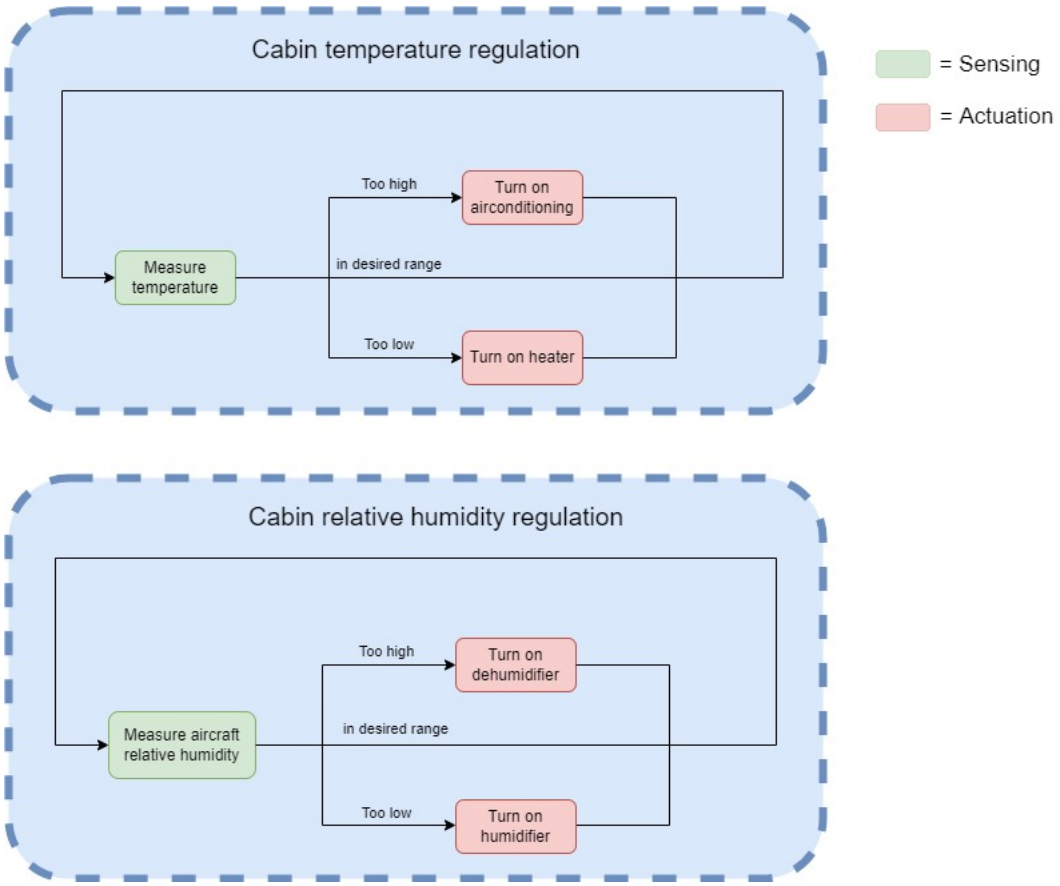

Figure 12.5: Flowcharts of temperature and humidity regulation in the cabin. The colours indicate the type of task performed.

12.3. Ground operations

When the vehicle is not flying, ground operations are crucial to sustain the flow of the process. Smart scheduling, described in Section 12.3.1, is necessary to reach ten flights per day. In order to minimise the time that the vehicle is on the ground, a sophisticated maintenance plan is implemented using a health monitoring system, described in Section 12.3.2. To support all ground operations, an adequate vertiport design must be created, for which the fundamentals are included in Section 12.3.3. Lastly, activities that need to be performed before the first flight are summarised in Section 12.3.4.

12.3.1. Scheduling

In this section, the operational concept of the vehicle is discussed. First, the daily usage is displayed on a timeline in Table 12.1. As can be seen, it is expected that the vehicle will be under heavy use during peak hours, between 6am until 10am and between 3pm until 7pm[8]. During these time slots, the vehicle will be used almost continuously. Therefore, it is important that the operations and logistics are organised well, to minimise time delays. In other words, the goal is to minimise the downtime, which is influenced by the fluency of the disembarking and boarding of the passengers and resupplying the vehicle with energy. This leads to the requirement to make the batteries swappable. Charging the batteries between every flight, with current charging times, would lead to an infeasible downtime. Next to that, charging times are not projected to decrease enough in the near future to accommodate this option. During other time slots, where the demand is relatively low, charging between flights could become a possibility. Therefore, to keep costs low, it is beneficial to only swap batteries when demand is high enough. A charging port should therefore not be discarded. Also, for private purposes, charging the batteries is more viable than swapping the battery pack. When swapping the battery pack, however, a complete loss of power would shut down all systems, which could lead to excessive startup times. Therefore, the vehicle should have a small battery which can keep the communication and navigation systems on idle. Note that the battery swapping will always be done by professionals, or an autonomous system [9].

It is expected that demand between 12pm and 4am will be low enough to perform maintenance and cleaning of

[8] *https://cubetoronto.com/london/what-time-is-rush-hour-in-london-roads/[Cited: 16/05/2022]*
[9] *https://www.ft.com/content/1ce0fa53-3955-4ad3-964c-c991c5e7cde6 [Cited: 13/05/2022]*

the vehicle. The number of flights leaving and arriving at Heathrow Airport can be seen on Figure 12.6. Next to maintenance, this time slot allows for a daily extensive inspection. Most probably, the vehicles will not need big maintenance every day, which allows operators to schedule maintenance of vehicles such that there are always vehicles that can be operated. According to **REQ-RAMS-AVL-01**, for the vehicle to be available for 90 % of the time, maintaining the vehicle every two days, leaves the vehicle available for 44 of the 48 hours. This is a 91 percent availability. If damages exceed certain limits, it could however be necessary to halt operations of the vehicle until damages are repaired.

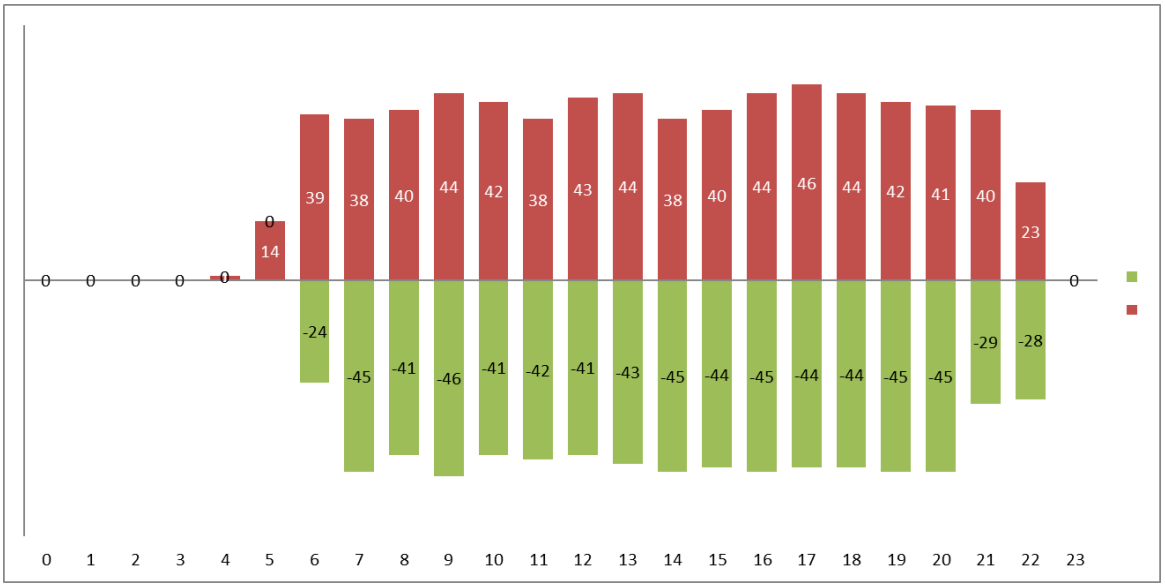

Figure 12.6: Average number of flights leaving and departing in Heathrow Airport in September 2019; Red: arrivals, Green: departures

The planning of this operational concept matches the business case. Although the vehicle is meant to be used by everyone, it is expected that mostly business people will use it, especially at the start of operations. Therefore, the usage is expected to be the highest at the beginning and end of a work day. At night, most vehicles will be in maintenance, however, most countries do not have a lot of flights at night. The United Kingdom, for instance, has restrictions on the number of flights between 23:30 and 06:00. Every trip will be below 20 km of range to increase the number of trips to be performed every day. Next, during peak usage, the battery is swapped to speed up the process. Swapping the batteries is performed by professional mechanics on the vertiport. Changing the battery of the vehicle can be done in less than 10 minutes. According to the battery company, charging the battery takes about 30 minutes, and it will take even longer if it is more discharged due to special manoeuvres or when reserves are used during flight. The charging of the battery is only done if demand for the service is low.

Table 12.1: Timeline of a regular day of the UAM.

Maintenance usage	Low Peak usage	Regular usage	Peak usage	Regular usage	
00:00 - 04:00	04:00-06:00	06:00-10:00	10:00-15:00	15:00-19:00	19:00-00:00

12.3.2. Maintenance and Health Monitoring System

In order to operate the UAM/ Veatle as much as possible, logistics and maintenance need to be very punctual. This increases the revenue of the concept, however, poor maintenance would impair the vehicle to functioning properly. To optimise maintenance procedures, we propose an onboard Aircraft Health Monitoring System (AHMS) for the vehicle.

AHMS uses real time data from multiple sensors that are integrated in the aircraft components to increase safety and reliability. With the use of artificial intelligence, the data can be interpreted and communicated with ground operations. The system detects potential defects inside the vehicle and reports them. The use of such a system will decrease inspection time as it replaces traditional visual inspection techniques such as analysing X-rays. Mainly, two components are present: the airborne health monitoring system and the ground health

diagnostics system. A simplified architecture of AHMS is shown in Figure 12.7 [10].

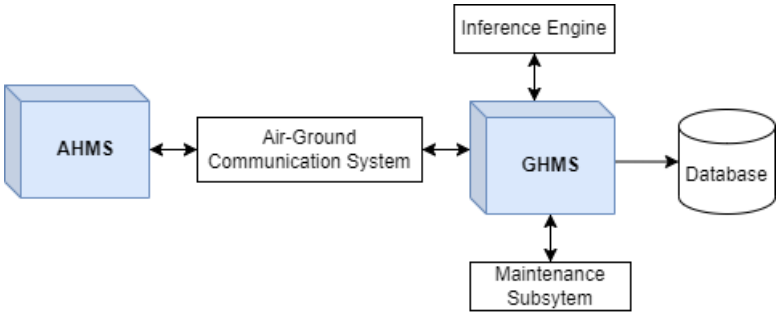

Figure 12.7: Aircraft Health Monitoring System

The AHMS can, for example, include sensors inside the electric motors that monitor the health and trigger manual maintenance checks. Also, the battery life can be closely monitored to predict when it should be replaced. This will allow for efficient storage and logistics of battery components. Other examples are the use of sensors in high loaded sections of the structure and rotors to detect cracks inside the material and analyse vibrations.

To further optimise the maintenance process, components of the vehicle are stored at the location of the vertiports. The least reliable parts are stored in higher amounts, taking into account restrictions on storage capabilities of the vertiports. The number of parts stored is also strictly monitored and replenished. As discussed before, an extensive manual check of the vehicle is done every day. For example, the landing gear and rotors are checked. Before every flight, a small pre-flight check is performed to check if all controls of the vehicle are operational. During this pre-flight check, new passengers could receive the mandatory safety briefing. A basic maintenance plan is presented in Figure 12.8.

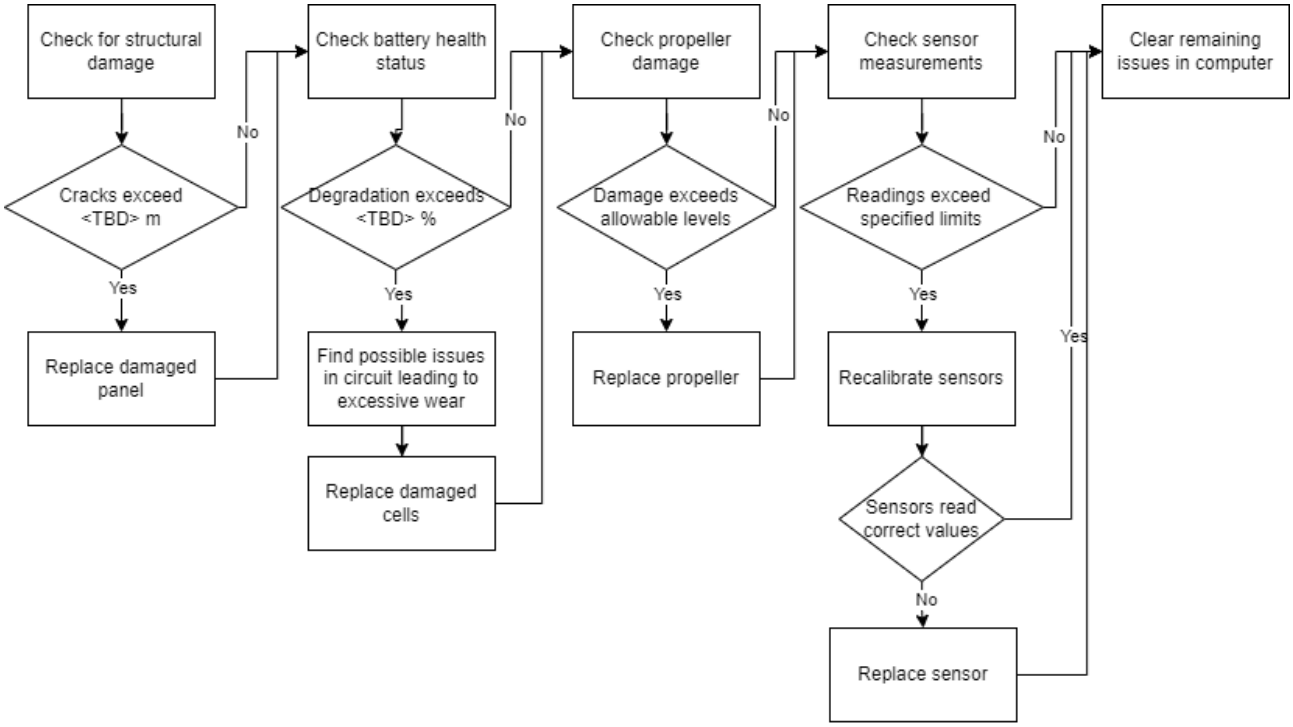

Figure 12.8: Maintenance diagram of the vehicle

12.3.3. Vertiport design

First and foremost, the vehicle will operate in cities from vertiport to vertiport. For safe operations, these vertiports have to suffice to certain requirements. EASA has released a prototype of the technical specifications of such vertiports **VertiportDesignEASA**. They mention certain areas to be required for a vertiport. The

[10] *https://www.einfochips.com/blog/importance-of-health-monitoring-system-for-aircraft/*

areas are: a final approach and take-off area, a touchdown and lift off area, stands (to safely load and unload passengers), a ground taxi route and, finally, an air taxi route. The ground taxi route will not be as relevant as the vehicle uses skids.

Furthermore, the vertiport should accommodate for a battery swapping and charging station which allows users to quickly swap batteries, performed by trained professionals, or to charge their battery for the next flight, if enough time is available. This means that vertiports should have landing pads and allow for taxiing to parking places where a charging and/or swapping service is available.

The final approach and take-off areas should be free of obstacles that are not required to allow the vehicle to operate nominally. Also, it should be of sufficient size to allow the complete vehicle to operate in this zone. This zone should be solid and should withstand the downwash of the vehicle. Around this zone, a safety area should be present to allow the vehicle to safely land when a deviation from the nominal landing area is needed. This area, however, does not need to be solid, but should also be free of obstacles.

12.3.4. Activities before first flight

After the detailed design of the vehicle is finished, further steps are necessary to realise the operations of the vehicle. This section elaborates on the steps to be taken after the final design. There are still some additional phases before the vehicle is actually built and used for a test flight. This section describes the steps until the actual certification of the vehicle. First, a transition between the design and the manufacturing of the vehicle needs to be facilitated. Very detailed 3D technical drawings of the vehicle should be created. All sides of the vehicle need to be visible with the greatest detail. Next to the drawings, a bill of materials should be provided to the manufacturer so that it is clear which material should be used for which part. The drawings and bill of materials are used for the production of the vehicle.

Before the production plan is used to manufacture the vehicle, requested materials and already existing parts need to be collected. The materials for the parts are ordered at a reliable material production company. Materials include aluminium alloys, titanium alloys, stainless steel and composites such as carbon reinforced polymers. Necessary hardware components also need to be ordered and are listed below.

- Battery packs
- Tablet for passenger interaction
- Sensors: accelerometers, gyroscopes, LIDARs, a thermometer and ultrasonic sensors
- GPS and radio systems including antennas
- Central computing system
- Automatic flight control system
- Cables
- Air conditioning elements
- Propellers
- Chairs

After the ordered hardware elements and materials are collected, the production plan can be initiated, which is described in Chapter 13. Following the steps of the production plan yields the first prototype of the Veatle. There are still some necessary steps before the first flight can be operated.

The vehicle needs to be inspected thoroughly to make sure that no mistakes were made during the production plan. All components need to be present, and all hardware components need to be operating. Then, the vehicle's software needs to be uploaded and tested. Tests such as starting and shutting off the vehicle are performed. The remaining steps are to certify the vehicle and transport it to the vertiport for the first flight.

12.3.5. Pre-flight procedures

Boarding a UAM vehicle is slightly more complicated than stepping in a taxi. When the passengers arrive at the vertiport, their luggage is checked for potential dangerous objects. The passengers also pass a short security check. Then, during the ground time of the vehicle, the passengers board the aircraft and the luggage is put in the luggage department. During vehicle checks or battery charging, the passengers are shown a video explaining the safety instructions. Once the door is secured, the vehicle can take off.

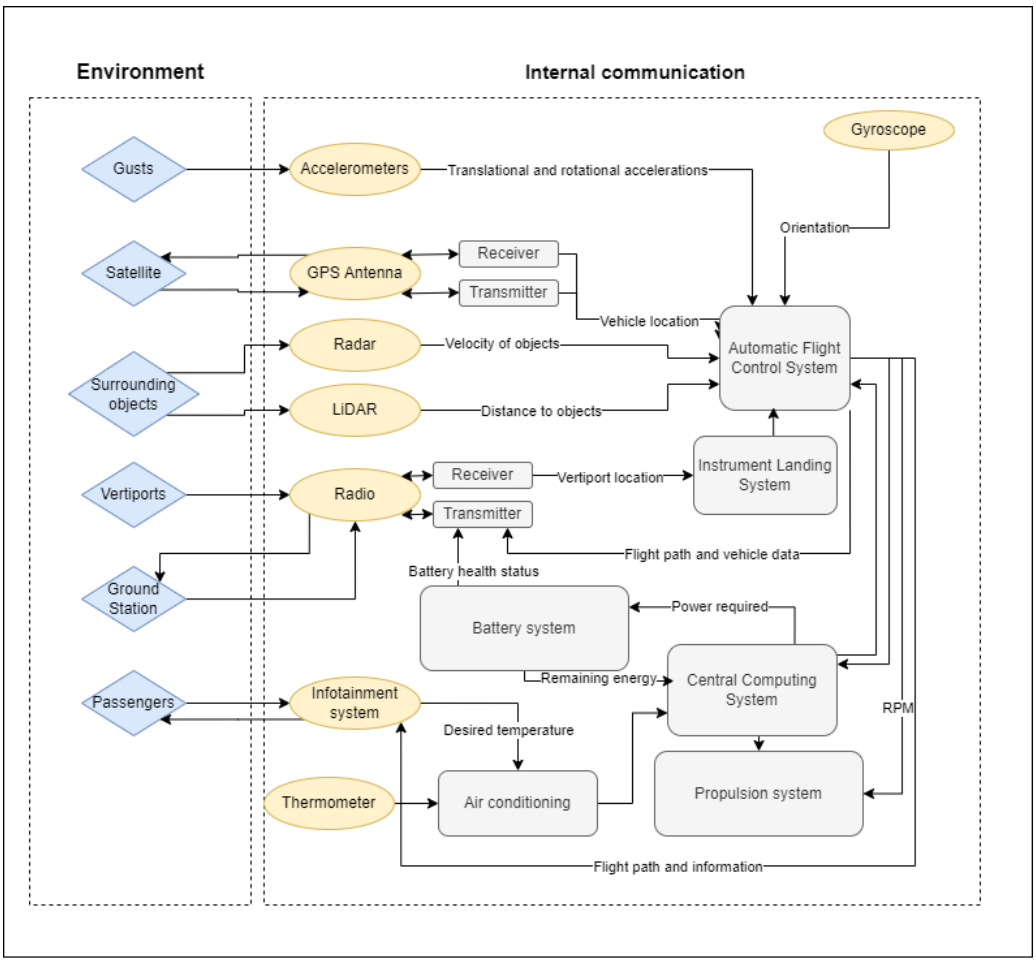

Figure 12.9: Communications flow diagram

12.4. Communications

The communications for the operations are split up in two parts. The internal communication within the vehicle is described in Section 12.4.1. A communications flow diagram is included. The external communications with the ground are explained in Section 12.4.2.

12.4.1. Internal communication

The vehicle will be operable inside an environment. Interactions with the environment need to be accounted and designed for. Figure 12.9 displays the communications flow diagram of the vehicle. It is split up in the environment and internal communication. The blue sections represent communication objects in the environment which are interacted with through sensors in the yellow boxes. The grey boxes are hardware components inside the vehicle. Arrows represent the flows of communication.

12.4.2. External ground communication

In order to facilitate safe, reliable and efficient flight operations, constant wireless communication between the UAM vehicle and the ground is established. This communication is commonly known as the control and non-payload communication (CNPC), defined by the International Telecommunications Union (ITU) **ITU**. The ITU defines three main categories concerning the CNPC:

1. *Communication for UAM Command and Control:* This includes the telemetry report (e.g. flight status) from the UAM vehicle to the ground station. A regular flight command update is sent from the ground station to the UAM vehicle. In the case of autonomous control, this implies the flight trajectory including way points.
2. *Communication for Air Traffic Control (ATC) Relay:* Considering the business case, the vehicle will be flying through airspace where other aircraft may be present. ATC needs live locations of all UAM vehicles to ensure safety in the airspace.
3. *Communication Supporting 'Sense and Avoid':* This type of communication could be directly between

UAM vehicles or via the ground. Awareness of surrounding airborne vehicles could improve safety.

This section will focus on the communication with the ground and mostly regards the first two types of communication. Besides, the ground station will is also assumed to be the air traffic control centre. There is communication in both directions. Y. Zeng et al. **UAVcomm** investigate the latest advances in Unmanned Aerial Vehicle (UAV) communications. The command and control of these vehicles can be strongly compared to the command and control of UAM vehicles. Based on the findings in the report, a simple link budget can be created, which is described in Table 12.2. Only a command control uplink and downlink are considered. The UAM vehicle has no payload data to be sent, so this is not included.

Table 12.2: Link budget for ground communication

	Data Type	**Data Rate**	**Reliability**	**Latency**
Downlink (UAM to ground)	Command and control	$60 - 100$ Kbps	10^{-3} packet error rate	50ms
Uplink (ground to UAM)	Command and control	$60 - 100$ Kbps	10^{-3} packet error rate	-

There are several types of communication that can be used. Foremost, there is the direct link, which is direct communication between the UAM vehicle and the ground station. Advantages are low cost and simplicity, however, it is only possible for limited range and low data rates. As the range and data rates will be small, this is a feasible option. Secondly, a satellite can be used as an intermediate component. There is global coverage, however, this is expensive and has a higher energy consumption. As global coverage is not necessary and energy needs to be conserved, this option is not really feasible. Thirdly, a cellular network can be used. Advantages are that this is cheap and has high performance. An important disadvantage is the reliability, as terrestrial communication also uses cellular networks. Because of the risk of hacking, this option is not safe and will therefore not be used. Taking into account all three options, the first option of a direct link is chosen.

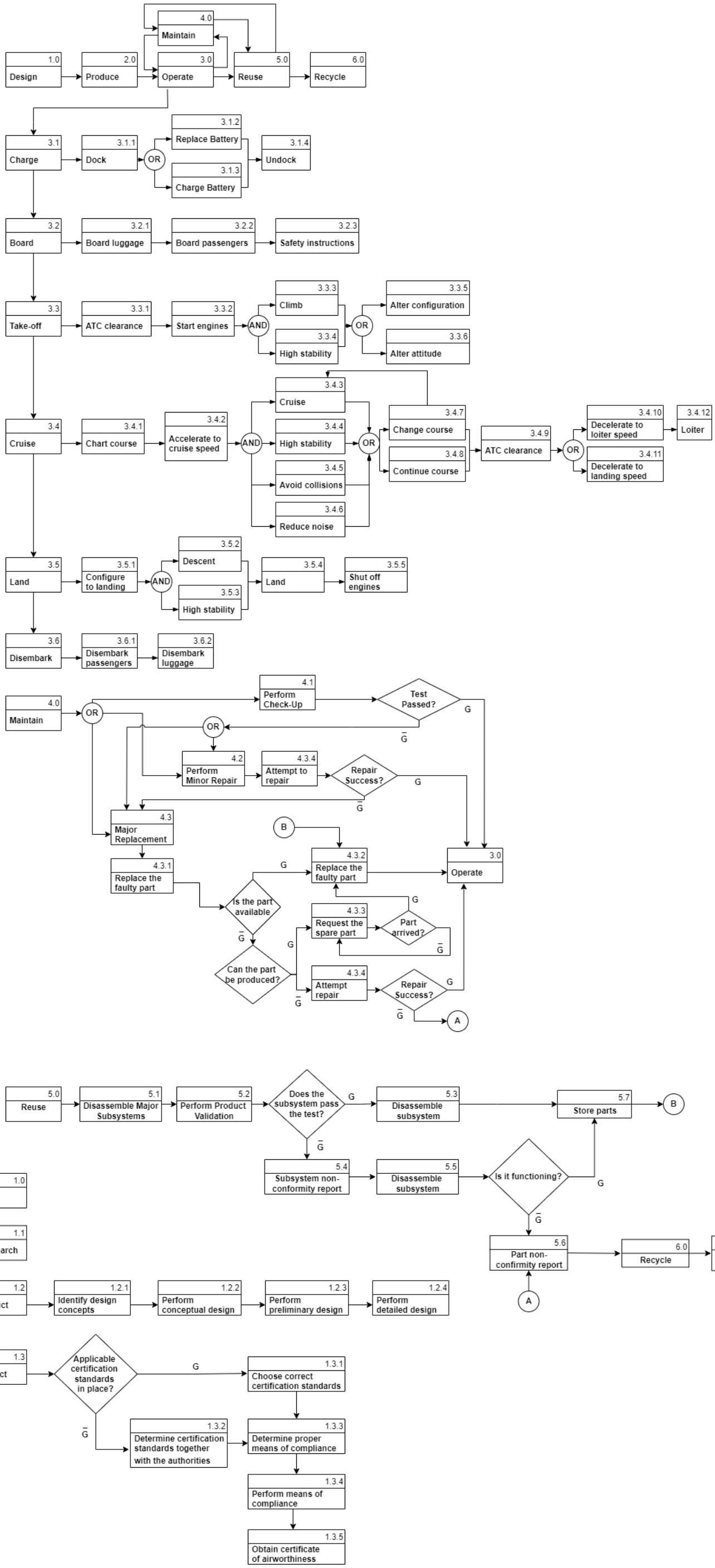

Figure 12.10: Functional Flow Diagram

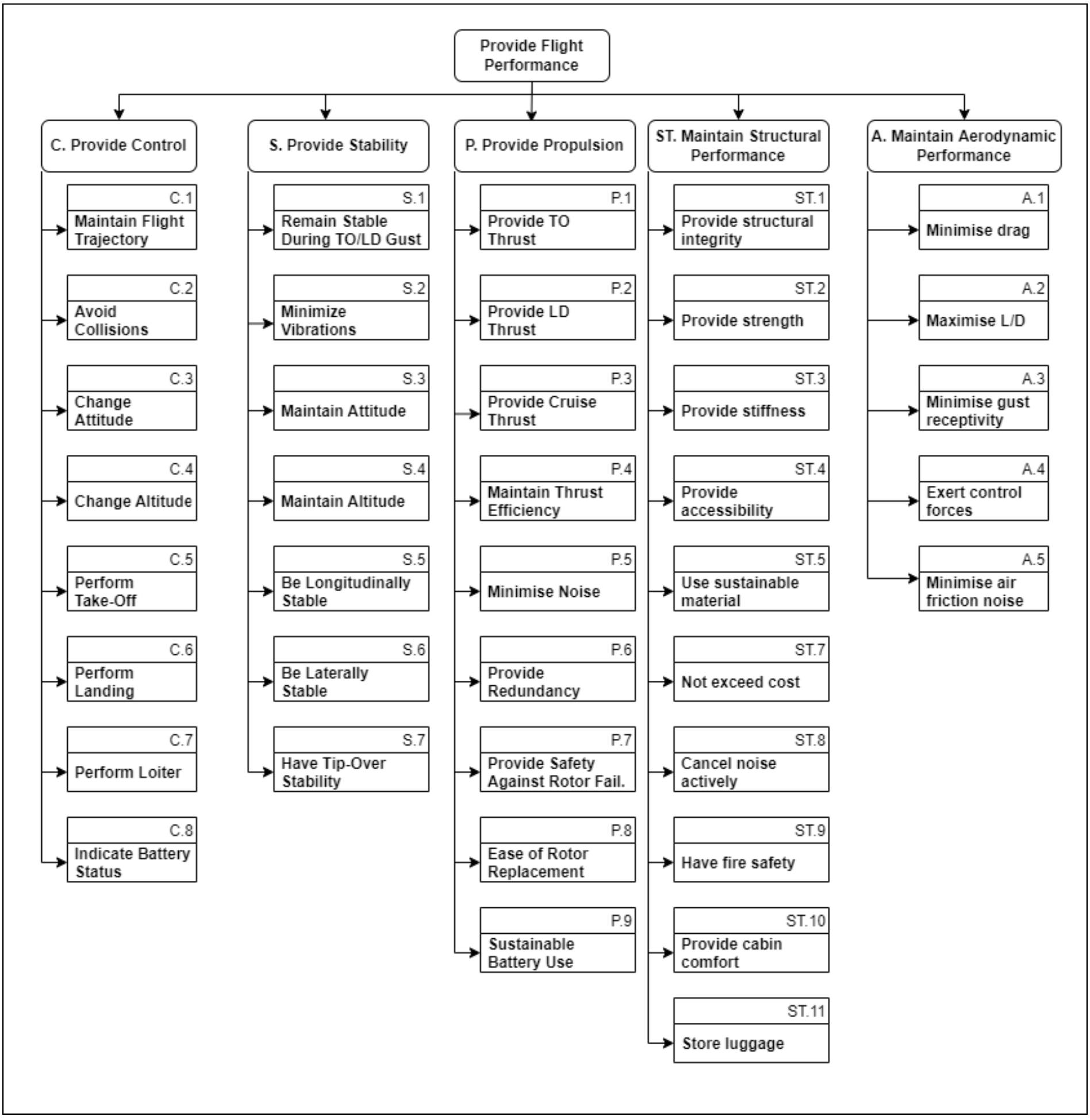

Figure 12.11: Functional Breakdown Structure

13. Production Plan

Since eVTOL vehicles are currently not mass-produced, the production plan is still unknown. Therefore, other types of production lines need to be taken as an initial reference. The production process will be compared to both the aircraft, and automotive industries, because of the product similarity and scale of production **eVTOLmassproduce**. In the future, the product series could be expected to be between that of general aviation aircraft and automobiles.

This chapter is divided into multiple sections. First, an outline of the actual planning is given in Section 13.1. Next, in Section 13.2, the manufacturing plan is given. The assembly plan follows in Section 13.3. In Section 13.4, the integration plan is discussed, and in Section 13.5 the materials for a minimum structure are outlined. Finally, in Section 13.6 the production flow chart is presented.

13.1. Preliminary planning

For a new product such as this eVTOL vehicle, the following steps need to be taken during the preliminary planning of the product **preplanning**:

- Collect the right design documentation to prepare for manufacturing and assembly;
- Plan blank manufacturing;
- Analyse manufacturing tasks;
- Select a manufacturing system;
- Select the optimal manufacturing variant;
- Estimate costs and time data.

13.2. Manufacturing plan

The manufacturing of the vehicle begins by collecting the raw materials. In the case of the Veatle, this will predominantly be carbon fibre and some amount of aluminium and steel. After all the materials are gathered, the components and parts can be manufactured. The biggest part to be produced is the body or fuselage of the eVTOL vehicle. If most parts are produced, the assembly can begin. The assembly of the parts will be done around the fuselage. The relevant parts will be brought together with the fuselage. When this is done, the first layer of coating will be placed on the vehicle. Throughout the design, some quality control will be required. This starts at the part design, to make sure that if a single part does not meet the requirements, it is the only part which needs to be replaced or changed, instead of the entire assembly of the vehicle. The last quality checks will be done on the full assembly. If these checks are completed successfully, the outside of the vehicle will be painted in the desired colour for the customer, and the interior assembly can begin. The vehicle will be finished with the landing gear, batteries and other parts. Last but not least, overall quality control and validation need to be performed on the whole vehicle.[1][2]

13.2.1. Tolerances

Tolerances on different parts and sub-assemblies are important to consider during analysis of the manufacturing methods and cost analysis: the manufacturing method should have a certain precision and yet it should not be too expensive or have unnecessary costs. Tolerances are crucial to implement in the design. If different parts do not fit or do not move in the way they are supposed to do, they need to be repaired or replaced. Consequently, time, money and materials are wasted.

13.2.2. Pretreatment

Pretreatment of the materials can be done for a lot of reasons. Materials can be treated to be more heat or current resistant. Pretreatment can also be used as an important factor for reducing the probability of failure, which could delay the production process a lot. Also, for all materials pretreatment makes it possible to have coatings on the material's surface if needed for example to stop corrosion. For the chosen materials, some pretreatment methods are performed.

Firstly, for aluminium, pretreatment entails cleaning to remove residual oil, oxide films and mechanical disturbed layers [3]. This is done chemically or electrically. Secondly, for carbon fibre, the pretreatment consists of heating and coating. This is meant to give the fibres thermal stability. Still, the tensile strength will decrease to between only 50 and 80% of the initial strength. Without coating, this will even be only 37%. The E-modulus actually increases by between 30 and 75% **precarbon**. Finally, the pretreatment of stainless steel is done to acquire smooth surfaces and a high hydrophilicity. This is done by chemical, plasma electrolytic or CO_2 cryoblasting techniques **NIEMI20102424** [4].

Lastly, in the design, there are some direct connections from aluminium to CFRP. Due to the specifications of the two materials, galvanic corrosion is a problem. However, there are some coatings which can be used to reduce this form of corrosion. From new studies where "plasma electrolytic oxidation treatment" is used, the corrosion can be reduced by more than 90% **Galvanic**. By using these kinds of treatments, the aluminum-CFRP bonds are prepared and are only used in easily interchangeable parts if necessary.

13.2.3. Part manufacturing processes

There are a lot of different part manufacturing processes. The main difference for the eVTOL vehicle in type of parts is the size of all the different parts, from a full fuselage to a small hinge they all have their own level of detail. Additionally, some of these parts will be made of composite materials and others of metal. This already gives huge differences for the production processes.

There are different methods for the production of a carbon fibre structure. The three most common processes are wet lay-up, vacuum infusion and prepreg. For the most efficient structure prepreg carbon fibre needs to be used. This is carbon fibre which has the optimum amount of resin already in the material. It should be cooled in the freezer and when it goes into the process of stacking up carbon fibre layers, it should be out of the freezer for a couple of hours to warm up. After the carbon fibre layers are stacked in the mould, the product needs to have an autoclave treatment to harden out.

For aluminium parts casting is a common method in industry. There are quite some advantages of aluminium casting. The main advantages are that it is easy to produce many parts in a short amount of time and that the finishing process is limited. The low cost, the easy manufacturability and light weight make aluminium an attractive material in the aviation industry. Still, the even lighter weight of carbon fibre puts a limit on the use of aluminium for this type of vehicle.

The production of stainless steel parts will be different from the production of aluminium parts. For steel, the parts will mainly be produced with a CNC machine, due to high complexity of small steel hinges and connectors [5].

The vehicle will be built up from different parts joined together. Some of these parts are quite large. For example, the fuselage will be made in 2 separate parts, so that it can be removed from the mould easily, since it is a closed structure. Smaller parts will be in places where the loads differ quite much during the flight, for example the places where the rotors are mounted to beams. These parts are most probably made of metals.

13.2.4. Post-manufacturing processes

After all the parts are produced, the post-manufacturing process starts. Post-manufacturing focuses mostly on acquiring the essential surface characteristics such as water and heat resistance, roughness, improving aesthetics, geometric accuracy and mechanical properties.

The most important post-manufacturing processes in the production of the VTOL are:

- Heat treatments
- Coating
- Surface finishing processes
- Inspecting

The heat treatments and coating will make sure that the material will be resistant to all kinds of weather it will encounter during the life cycle. The parts will be waterproof as well as heat and ice resistant. The surface finishing process makes sure the surface is smooth enough to provide sufficient aerodynamic performance. Lastly, the inspection of the components is very important. This will be first done by people to see if the parts are manufactured correctly and afterwards will be done by computed tomography or other scanning methods to make sure the parts are validated without the need to destruct them. This inspection of the elements with sensors will be the most important part in validation for the part manufacturing side, since it is able to measure slight variations in wall thickness, or detect small cracks. Lastly, it verifies that no remainders of the manufacturing process such as dust or powder will stay in the parts [6].

13.3. Assembly plan

After all parts are produced, a full product is constructed. The assembly is done with the fuselage as a starting point. The fuselage will be constructed and after this, the beams are fixed to the rotors. Then the doors, motors,

[5] *https://www.cnclathing.com/cnc-machining-services?gclid=CjOKCQjwpv2TBhDoARIsALBnVnnHeUG_-X7mlnaFTeUosDNLuYW4yp6efHpIbTg6Hp9xU_TcQewG17QaAnGKEALw_wcB [Cited 14/05/2022]*

[6] *https://3dadept.com/post-processing-the-last-step-in-the-manufacturing-process/ [Cited 09/05/2022]*

landing gear will be placed at their specific location. When all this is done, some quality control needs to be done again to make sure parts are correctly assembled.

13.3.1. Assembly jigs

When the parts will be put together, it is crucial that they will stay in their place. A small deviation in position can lead to a misplacement of another part, which can cause malfunction of the product. Therefore, assembly jigs will be designed to hold all parts at their exact desired place. It not only provides the required accuracy, but also improves the ease of the repeatability. From these jigs the assemblies will be made.

The main part where an assembly jig needed is the fuselage, the starting point of the assembly. Other important parts that might need their own assembly jigs are the beams and the motors.

The assembly jigs will be made of mild steel. It is the most suitable and economically efficient option to use **Designjigs**. Also, it is very sustainable and can be used for a very long time. Next to this, the material is not brittle, which is needed for the jigs [7].

13.3.2. Joining methods

There are different types of fasteners: [8]

- Mechanical fasteners or pins: bolts, screws, nuts, etc. Great for non-permanent joining;
- Weld assembly: fusing metal parts together. Great for robust permanent joining;
- Adhesive bonding: no stress concentration, high joining efficiency.

For joining it is decided whether a part should be removable somewhere during the lifespan and whether the fastener meets the structural integrity requirement, because some joints give high stress concentrations. Also, for the fuselage skin, aerodynamic properties and being watertight also play a role.

For example for the doors, mechanical joints and fasteners will be used. However, for parts such as joining the beam in the joints, adhesive bonding will be used to limit the CFRP aluminium connection.

13.3.3. Non-destructive quality control

Just as for the part manufacturing some quality control needs to be done. Especially in the assembly phase, it is needed to have a non-destructive way of controlling since a lot of parts might become useless if one part breaks.

The first way of quality control, inspection, was already specified in the manufacturing plan. Inspection is one of the mostly used forms of quality control. Computed tomography is used to detect cracks, openings between the assembly or variances in thickness etc. With this, mistakes can be spotted early before doing other tests.

Next to this, a leak test should be performed to make sure the structure of the vehicle is free of manufacturing mistakes which lead to holes or cracks. A sniffer method leak test is preferred as the exact place of the leakage can be determined. The vehicle will be filled with a gas and if it escapes the vehicle it will be noticed by the sniffer probe which can be moved both manually or automatically. Since it is moving alongside the vehicle it is better to detect the position of the leaks and weaknesses [9].

13.4. Integration plan

The last step in the production is the integration of all parts. First the interior of the cabin will be constructed. After this the cable integration will be fixed and the last part will be the integration of the battery and starting the vehicle.

For the interior of the cabin there are just a few things to be done. Since the eVTOL vehicle is fully autonomous, besides the passengers it only contains seats and a luggage department. For the air taxis without predefined locations, a navigation pad is needed as well. This will just be a tablet design where users can insert their location within the range of the VTOL. On the outside of the vehicle other subsystems which are not included yet, such as the motors, will be placed.

As mentioned before, the next thing is the cable integration. Since the product is still in the first design stage, this will not be described in great detail. However, some basic rules could be stated already. This includes that the cables should not interfere with the passengers and that they should not have any disturbance while

[7] *https://pediaa.com/difference-between-mild-steel-and-stainless-steel/ [Cited 10/05/2022]*
[8] *https://www.vista-industrial.com/blog/types-of-joining-and-assembly-in-metal-manufacturing/ [Cited 10/05/2022]*
[9] *https://www.inficon.com/v1/attachment/Leak-Testing-in-the-automotive-industry [Cited 10/05/2022]*

boarding and disembarking the vehicle. Therefore most cables will probably be going around the side, top or bottom of the cabin or, if possible, under or over the floor or roof of the cabin.

The last thing that needs to be done before the vehicle is able to fly is integrating the battery. The battery will be in the back of the fuselage for stability reasons. For safety, the battery should have a sufficient housing which withstands the loads and is electricity and heat resistant. This part should already be done in the manufacturing phase. The batteries should be able to connect to the subsystems and preferably be able to charge within its case.

After all the integration is done, it is time for the last inspection and checks to make sure everything is connected properly. When these checks are done, the eVTOL vehicle is ready to start the engines and perform a test flight.

13.5. Properties and production of materials

There are different materials which are needed for the manufacturing. For the vehicle's structure, the following materials are most common in aircraft industry:

- Carbon fibre
- Aluminium alloys
- Stainless steel

Those materials all have different properties and therefore different purposes for the vehicle. Carbon fibre is very lightweight, strong and stiff, but it is not easily recyclable. For the production of carbon fibre parts, moulds should be made. The moulds are made of different materials, depending on the costs and the amount of times a mould should be reused. On the latter, it depends on whether it is expensive and time-consuming to restore the mould from small damages. After making the mould, the carbon fibre layers will be laid up into it. Different methods are available for this stack up of carbon fibre. This has effects on the final mass, but mostly on the time it takes for the production.

From metals, aluminium is known to be lightweight, cheap and has good strength and stiffness properties. For manufacturing, it is easy and cheap to produce a huge amount of parts by die casting and the finishing process is limited. Currently, it is much less used in aircraft industry, because aluminium is not optimal for extreme temperatures and chemicals [10]. These temperature differences are not problematic on the altitude the eVTOL will fly, so parts made of this material will be in the design. In aerospace industry, the aluminium alloy 7000 series is most common, because of its high strength on low corrosion properties. In addition, fatigue is also a very important issue for aluminium. This is less of an issue for carbon fibre, which does not have a metallic, crystalline structure. This fatigue would need to be inspected in the joints during the weekly maintenance. Carbon fibre also experiences fatigue, to a lower extent. Inspection for fatigue is also more difficult, since damage occurs internally, when compared to metals, where cracks mainly propagate from the surface. Some acoustic analysis or radiography analysis could be done during maintenance, or a dry cloth could be run across the surface to catch any exposed fibres and detect failure for fail-safe carbon fibre parts.

Stainless steel has good strength, stiffness and corrosion capabilities. Still, it is quite heavy. Therefore, it will only be used in hinges and other places where limited degradation and high strength is needed.

13.6. Production flow chart

In Figure 13.1 the production flow diagram is given. In this flow diagram the full outline of the production process as described in this chapter is broken up into blocks. It starts with the concept generation. After that, the set-up of the manufacturing process, the part manufacturing and the assembling and integration until the end product are given. Finally, the validation process is given.

[10] *https://www.marlinwire.com/blog/aluminum-vs.-stainless-steel-stainless-steel-in-aviation [Cited 09/05/2022]*

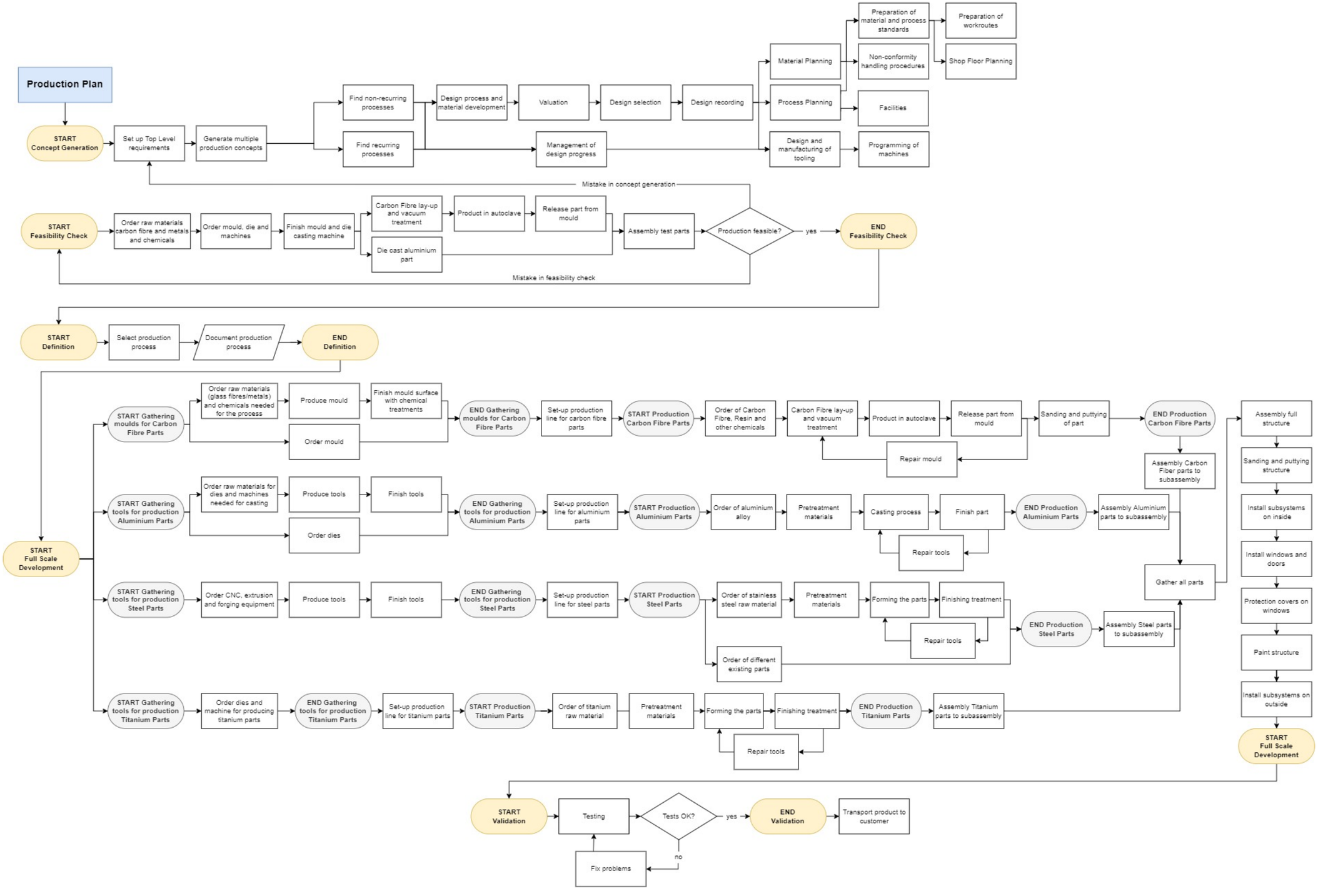

Figure 13.1: Production flow diagram

14. Block Diagrams

In this chapter, some block diagrams that clarify the functioning of the vehicle are displayed. In Section 14.1, the hardware block diagram shows some important physical components of the vehicle. In Section 14.2, a very simplified representation of the control software is shown. The electrical block diagram containing information about the charger, batteries, power distribution and different energy compartments is included in Section 14.3.

14.1. Hardware block diagram

Figure 14.1 shows the hardware block diagram of the vehicle. It is split up in components inside the vehicle and components outside the vehicle. The central computing system produces commands for other subsystems and monitors the software. The automatic flight control system is in control of the stability of the aircraft and maintaining its trajectory. It is assisted by the instrument landing system. The flight control system actuates the motors that drive the rotors. On the left side of the diagram, the sensors are displayed which are connected to the environment. The tablet and air conditioning are the only two systems that the passenger interacts with. Electricity from the battery is managed by the power management system. Finally, the health monitoring system indicates necessary maintenance and critical flight data is stored in the black boxes. The Simulink control system would be directly uploaded on the flight computer hardware block.

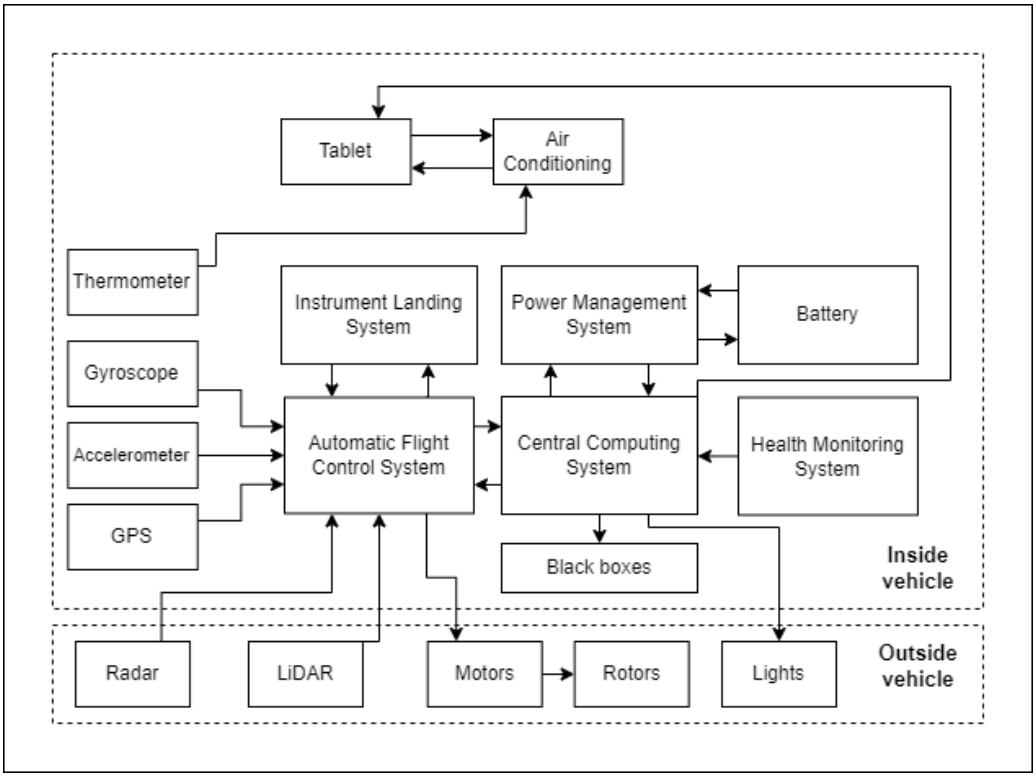

Figure 14.1: Hardware block diagram

14.2. Software block diagrams

Software of the vehicle is mostly included in the control system design. The flight computer will have this software. The simplified block diagrams for this software are present in Chapter 7. These block diagrams represent the Simulink model used.

14.3. Electrical block diagram

The electrical block diagram is shown in Figure 14.2. The battery compartment is split up in two different batteries, one for take-off and landing purposes and one for cruise purposes. Power to and from the battery is managed by the power distribution module. The on-board charger transfers power from the vertiport to the batteries. An auxiliary battery is included to support flight computers and other hardware components when the batteries are swapped. Energy is transferred to three different compartments. The control module contains most electrics and software. In yellow, miscellaneous hardware components are grouped together. The propulsion module also has a separate group and requires the most power during flight.

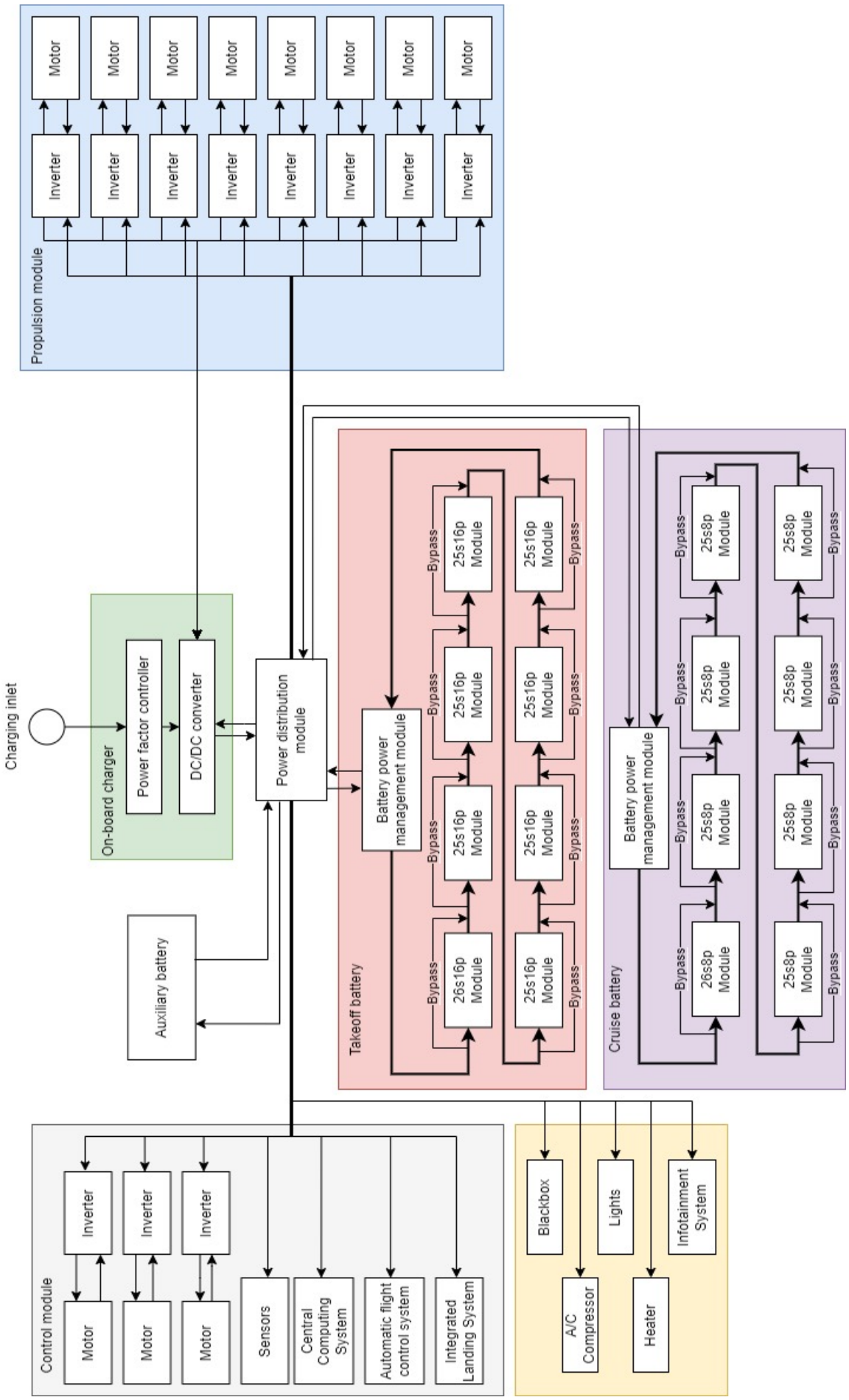

Figure 14.2: Electrical block diagram

15. Sustainability Analysis

A factor that weighs into the transportation industry now more than ever is sustainability. From the conceptual design phase all the way through to the operation of the vehicle, sustainability should be considered at every step of the process. There are three main pillars of sustainability that are crucial to take into account, and thus these are analysed for the Veatle in this chapter. The environmental impact of the final design is elaborated upon in Section 15.1, followed by the projected impact of the Veatle on society in Section 15.2. The final pillar, the economical sustainability, is analysed in Section 15.3.

15.1. Environmental sustainability

The environmental impact of the Veatle can be determined by analysing its carbon footprint and the Cumulative Energy Demand (CED). The total carbon footprint of the vehicle depends on three stages of its life cycle: production, operations and end-of-life (EOL). These aspects of the Veatle's carbon footprint are worked out in Section 15.1.1, Section 15.1.2 and Section 15.1.3 respectively.

15.1.1. Production environmental impact

The environmental impact of the production of the vehicle is dependent on the type of materials used in the vehicle, the mass of these materials, and the methods in which the parts are manufactured and then assembled.

The main material used in the vehicle is a carbon fibre reinforced polymer (CFRP). The use of this material is necessary for UAM applications, as other materials with sufficient strength are too heavy for these vehicles. However, according to the Idemat 2022 index, a common CFRP existing of 25% carbon fibre has a carbon footprint per kg material of 23.64 kg CO_2. This is significantly higher than aluminium and steel, common materials for other means of transportation, which have equivalent CO_2 weights of 8.82 and 0.96, respectively. This high carbon footprint of CFRP is mainly due to the high efforts that are required for the manufacturing of CFRP sheets: the preheating and autoclave processes are the source of significant carbon emissions. Research is being conducted to find less energy-intensive methods of forming CFRP, but none of these methods have been proven to be effective enough to seriously challenge the status quo.

The third column in Table 15.1 shows the carbon footprint of each material in the Veatle. The other columns provide information on the quantity of the material per vehicle, the total energy required to produce this amount of material (CED), and the impact of this amount of material on the human health using the DALY index. The latter is not factored into this pillar of sustainability, but is analysed further in the social sustainability analysis in Section 15.2.

Table 15.1: Carbon footprint of materials in the vehicle

Materials	**Quantity**	**Carbon footprint** kg CO_2	**CED** MJ	**Human health impact** DALY
CFRP 25%	126.7 kg	2995.5	47073.5	86.4
Aluminium	20.8 kg	183.5	3028.6	5.4
Steel	est 1.0 kg	1.0	10.3	0.0
Glass	5.1 kg	10.2	154.6	0.3
Polyurethane	4 kg	12.1	534	0.3
Total	-	3203.3	5081.4	92.5

The total of the quantity is not displayed in the table, as it does not contribute to the analysis. The table above clearly shows that the CFRP used for the Veatle has the biggest impact on the carbon footprint, as elaborated on previously in this section. Another concerning property of CFRP is the impact on the human health, as this amount of CFRP has a total DALY index of 86.4.

Aside from materials used for mostly structural purposes, there are also key products that are integrated in the Veatle like batteries, electric motors etc. An overview of these products is shown in Table 15.2. The exact types of products were not found in the Idemat database, so products were chosen that resemble the integrated products as closely as possible.

Table 15.2: Carbon footprint of materials in the vehicle

Products	**Quantity**	**Carbon footprint** kg CO_2	CED MJ	Human health impact DALY
Li-ion batteries	218.5 kg	13290.8	207305.1	423.0
Electric cord + PDS	90.7 kg	14.5	450.0	0.4
Printed Circuit Board	est 1 kg	475.0	7215.4	13.9
Electric motor	62.4 kg	181.8	2990.2	7.0
Led light bulb	14 pieces	206.4	3235.4	6.0
Total	-	14168.5	221195.8	450.3

It is clear from the table above that certain products, like the circuit board and batteries, have a high carbon footprint due to energy intensive production methods.

Combining the information in Table 15.1 and Table 15.2, the total carbon footprint of the materials and products integrated into the Veatle is calculated to be 17,370.8 kg CO_2, the total energy needed to produce the materials and products is 226,277.2 MJ, and the human health impact is 542.8 DALY. An important factor that has not been taken into account is the production of specific structural parts of the Veatle, as the Idemat index does not provide information on this. However, it can thus be assumed that the values presented in this paragraph are higher in reality.

The conclusion that can be taken from this analysis of the production of the Veatle with regard to the environmental impact is that the carbon footprint in the order of 10^5 kg CO_2, which is mainly due to the use of close to 130 kg of CFRP and 220 kg of Li-ion batteries. As of now, there are no alternatives for CFRP and Li-ion batteries that would reduce the carbon footprint, while performing well enough for an eVTOL vehicle to fly as specified in the requirements.

15.1.2. Operations environmental impact

The Veatle's environmental impact due to operations mainly comes down to the energy required per flight, which is 234 kWh for a flight of 20 km. The predictions for operations assume an average of 10 flights a day. As the business case assumes London as operational area, the values in the Idemat database are used for electricity in the UK. The results of the analysis for this business case is shown in Table 15.3.

Table 15.3: Carbon footprint of materials in the vehicle

Time interval	**Quantity**	**Carbon footprint** kg CO_2	**CED** MJ	**Human health impact** DALY
Per flight	23.4 kWh	6.6	137.4	1.5
Per day	234 kWh	66.4	1,374.4	14.6
Per year	85,410 kWh	24,252.0	501,671.6	5,320.0

It has to be noted that this analysis assumes modern-day values of the carbon footprint of British electricity. It is expected that in the future, when the Veatle is operational, a larger part of electricity in the UK is generated through green sources. Sweden, for example, has a carbon footprint per MJ of electricity that is eight times lower than that of the UK. It is reasonable to assume that the electricity generation in the UK will also be moving in this direction going forward.

15.1.3. End-of-life environmental impact

As mentioned in Section 15.1.1, the vehicle mainly consists of carbon fibre. An advantage of this design choice is that carbon fibre generally has a longer lifetime than metal alloys: it experiences close to no fatigue, and it does not corrode. However, recycling carbon fibre is not as simple as recycling metals. When recycling a CFRP, the fibres that result from the process are discontinuous and not necessarily of a size that allows for reuse **dauguet2015recycling**. In order to ensure the EOL of the Veatle to have a low carbon footprint, either the recycling process for CFRP should be improved in order to produce carbon fibre that can be reused for UAM, or applications should be sought for shorter, discontinuous carbon fibres.

Another recyclability challenge is that of the lithium-ion batteries used in the vehicle. The minimum expected lifetime of these modules is 5 years, after which they should be recycled in order to reduce the carbon footprint. However, in 2019, only 5% of the Li-ion batteries used in cars in Europe were recycled, with the other 95% ending up in landfills. Even though recyclability is possible, there are often technical, economical, and regulatory factors that cause the batteries not to be recycled.[1] The high total carbon footprint of the batteries in the

[1] *https://cen.acs.org/materials/energy-storage/time-serious-recycling-lithium/97/i28 [Cited: 13/06/2022]*

Veatle 13290.8 kg CO_2 makes it crucial to recycle these batteries in order to be sustainable.

Other materials used in the Veatle are less problematic regarding recyclability. Aluminium and steel can both be recycled without negatively impacting its properties. Also, recycling these metals is usually cheaper than creating new material out of raw materials. The parts made of aluminium and steel are thus not expected to be a problem for the end-of-life contribution to the carbon footprint of the vehicle.

15.2. Social sustainability

The environmental sustainability of the Veatle will be crucial for the acceptance of the vehicle by the public. However, there are more factors that weigh into the public perception of the Veatle. Section 15.2.1 analyses the impact of the Veatle on the human health, after which Section 15.2.2 reviews the noise produced in the urban environment and its impact on social acceptance of the Veatle.

15.2.1. Health impact and social sustainability

An important aspect that must be taken into account is the DALY index, already touched upon in the previous section. This index is used to quantify the effect of a process or product on the health of people, with the DALY number representing the total years of life lived with diseases or disabilities and years of life lost with respect to the initial life expectancy of a person. From the tables in the previous section, it can be concluded that the total health impact caused by production is 542.8 DALY. This is a high number for the DALY index. However, for the acceptance of the public, it is important who suffers from this impact on the human health. A large factor of the DALY index is due to the carbon fibre and the batteries.

The contribution of carbon fibre to the total DALY index is mainly due to toxicity problems during production of the material. When forming CFRP sheets, toxic vapours are produced by the resin in which the fibres are to be laid. This can be harmful for the people working on the sheet if they do not wear protective equipment. Also, while cutting the carbon fibres to their ideal sizes, very small parts of it can break off and go into the air. When breathed in, this can also negatively affect one's health. Thus, a large part of the 86.4 DALY is expected to be specific to the people who work on the manufacturing of the CFRP sheets, and can be decreased by wearing protective gear.

The same goes for Li-ion batteries. These batteries contain materials that can be toxic to humans, like copper, nickel, lead, and organic chemicals in the electrolytes [2]. So similar to the CFRP sheets, the high DALY index of Li-ion batteries is mostly meant for the production workers, and can be decreased by taking protective measures. However, a danger regarding Li-ion batteries is that they are flammable. If a fire occurred due to battery failure, the harmful toxins mentioned previously should not be allowed to enter the passenger cabin, in order to prevent them from experiencing a negative impact on their health.

15.2.2. Impact of noise on social sustainability

An elaborate analysis of the noise produced by the Veatle is presented in Section 6.1.4. For most of the urban environment in which the Veatle will be operated, the noise generated by the vehicle is at the same level as the urban background noise. As such, the increase in overall noise level will only be 3.5 dBA. This is a minimal increase in noise and is not expected to negatively impact the social sustainability of the vehicle.

The noise generated during take-off on the other hand is more significant. The noise emissions are 70 dB when the Veatle flies at a height of 50 m and the observer is on the ground at an angle of 45 degrees from the vehicle. This means that living around vertiports is expected to cause similar complaints in the community as living around airports or windmills.

The negative impact of the high noise levels during take-off and landing on the social sustainability can be mitigated by two countermeasures. One of these measures is to place the vertiports in business districts, as the business case of the Veatle prescribes. This way, the effect of high noise emissions does not disturb people in their residential homes. Furthermore, the background noise in these busy business districts is already high, masking the sound pressure levels of the Veatle during take-off. The other countermeasure is to ensure subsidies for the residents that are in the area of the vertiports despite the previously explained countermeasure. This subsidy can be used for higher quality of insulation in residencies, thus reducing the perceived noise levels inside of homes. This measure is already implemented for residents that are hindered by the expansion of airports, for example in the area of Amsterdam Airport Schiphol [3].

[2] *https://www.ncbi.nlm.nih.gov/pmc/articles/PMC5920515/#:~:text=Lithium%20batteries%20contain%20potentially%20toxic,LiBF4%2C%20and%20LiPF6. [Cited: 13/06/2022]*

[3] *https://leefomgevingschiphol.nl/ [Cited: 14/06/2022]*

15.3. Economical sustainability

The final form of sustainability that is important to be analysed is the economical sustainability. For the standard business case as presented in Chapter 3, a company will make a significant investment of around half a million euros to acquire a Veatle, or probably more than one. It is crucial for this party that it will earn back its investment plus profit within a certain time period. For this, the Veatle must be long-lasting with minimal operational expenses and must provide passengers with a pleasant experience as to create and maintain demand. Whether the Veatle is economically stable depends on its required operational expenses. These costs will be mainly dictated by charging and maintenance.

15.3.1. Charging expenses

On an average flight, the energy consumption will be around 24 kWh, as mentioned in Chapter 9. Effort has been made to minimise the energy consumption, as energy is expensive on average and events elsewhere in the world can lead to sudden increases in its price, for example during the Russian-Ukranian war in 2022[4]. In these cases where prices for energy are high, the Veatle must still be able to operate while being profitable for the client. Other expenses related to charging are buying charging equipment like a cable and an external charging station for during peak hours, and salaries for the workers that charge and swap the batteries.

15.3.2. Maintenance expenses

While maintaining high safety standards, the maintenance costs are optimised by designing for ease of maintenance, performing autonomous checks on the health status of parts, and ensuring parts to have a long lifetime in order to minimise part replacements.

The rotors, for example, are placed in an open configuration rather than ducted, and the batteries are easily taken out of the vehicle for check-ups. Furthermore, the AHMS, as elaborated upon in Chapter 12, allows the vehicle to monitor the state of its batteries, electric motors and heavily loaded structural sections continuously in order to minimise the number of check-ups needed. Reducing the frequency at which parts need to be replaced has also been taken into account during the design phase. The depth of discharge of the batteries is set at 50%, to maximise its lifetime. Moreover, as explained in Section 15.1, most of the structural parts of the Veatle are made out of CFRP, which has a long lifetime compared to other materials used in vehicle structures like aluminium, due to the minimal effect of fatigue on this material and its resistance to corrosion.

16. Ethics

Emerging new technologies often introduce interesting ethical topics. For instance, deepfake technology poses some very serious and dangerous ethical debates. Nowadays, technology can develop so fast that sometimes the ethical consequences are not properly considered. A key question is whether engineers can be held responsible for the consequences of their creations. Urban Air Mobility also introduces some ethical considerations, which are briefly discussed in this short chapter.

The use of the Veatle involves an important field of technological ethics: autonomous flight. Autonomous flight in Urban Air Mobility touches this field in two different ways, which can be formulated by two questions: how safe are the passengers in the autonomous vehicle and how safe are the surroundings of the vehicle? For both ethical problems, an ethical framework is used to formulate some rules and guidelines for the use of the Veatle.

Firstly, the safety of the passengers inside the Veatle is considered. Although autonomous flight technology is already very advanced, incidents can always occur and need to be accounted for. If one of the vehicles crashes, who is responsible for the crash? For this question, the ethical framework of deontology **deontology** is introduced. Deontology is an ethical theory that says actions are good or bad according to a clear set of rules. Rules need to be set to come to an agreement of the safe use of the vehicle. A document will be released containing all safety procedures and activities that make sure that the vehicle is as safe as possible. If one understands the possible dangers and has been warned about them, the use of the vehicle as at their own risk. Besides, an extra measure will be taken. To increase the safety and confidence of passengers, remote pilots will be present at coordination centres to take over the vehicle's control in case of the autonomous system malfunctioning.

The other case involves the safety of the surroundings of the vehicle. People in cities are already exposed to many dangers; cars and busses for example, but also crashing helicopters and airplanes. Veatles flying around will pose another danger to the people on the ground. If the vehicle falls from the sky, sometimes it is still

[4] *https://www.dnb.nl/algemeen-nieuws/2022/hoe-we-economisch-geraakt-worden-door-de-oorlog-in-oekraine/#:~:text=De%20stijging%20van%20de%20energieprijzen,schoot%20bijna%2030%20procent%20omhoog. [Cited: 14/06/2022]*

controllable. The ethical problem introduced: is the safety of the passengers or the safety of the people on the ground prioritised? For this, the ethical framework of utilitarianism **utili** is used. The right choice under utilitarianism is one in which the greatest good is achieved for the greatest number of people. Therefore, if the vehicle can still react, the number of fatalities should be minimised. This means that one person on the ground would be sacrificed for the safety of two passengers.

17. Conclusion

The future of urban transportation is getting closer each day, with new concepts of urban air mobility vehicles being launched at a higher frequency than ever before. Even though these concepts are designed to avoid several safety issues by adding propulsive redundancies and extra energy storage, little attention is given to the effects of turbulence in urban areas. Not only can urban turbulence cause discomfort for UAM passengers, but it can also lead to unsafe situations. So the question arises, can the effects of urban turbulence on UAM be mitigated by integrating countermeasures in the design of an eVTOL vehicle?

For this problem, the Veatle design is proposed. This new eVTOL vehicle concept challenges all existing ones by being the first to actively respond to the problem of urban turbulence. It has three control propellers that can provide thrust in the lateral direction of the vehicle, specifically designed to counteract gusts coming from both sides. The propeller hubs are equipped with a variable-pitch mechanism. This way, the rotors can spin throughout the flight, adjusting pitch if thrust must be generated in the direction opposite of sudden gust loads. This mechanism is able to generate control forces of high magnitude, sufficient to counteract urban gust loads during harsh wind forces of up to 8 Beaufort. Its reaction time is low enough for the Veatle to stay on its trajectory with a deviation of no more than 1 m. The three control propellers are placed such that they can counter lateral displacements of the vehicle, as well as rotation around the Veatle's x-axis and z-axis.

These control propellers are coupled to a cutting edge control system. The control system uses three PID controllers and an MPC coupled with sigmoid activation, in order to provide complete 6DOF control. Two tests cases were considered: counteracting a gust profile with a 24 m/s peak and a wake from the Shard building in London. The result from the first case showed that the vehicle was able to provide the passengers with a comfortable flight, with a maximum deviation of 0.15 m and a 12° roll degree. The latter case gave a maximum deviation not far over 50 cm, but the acceleration slightly overshot the comfort requirements. However, a preliminary analysis of a learning model for the linear controller decreased the maximum deviation and kept the passenger comfortable. Although the angle is also kept within comfortability constraints (under 4°), the angular acceleration makes it uncomfortable for the passengers. Several recommendations have been presented to improve on the passenger comfortability in the design stage, for instance by designing a more optimal controller or optimizing the centre of pressure position to minimise the aerodynamic moments.

The unique control and quick response propulsion systems of the Veatle are the main aspects that set this vehicle apart from any other in the UAM industry. However, the Veatle is also designed such that other properties are preferable over modern-day eVTOL concepts. Special attention was given to the public acceptability of the Veatle, in order for the vehicle to be embraced by the local community once it enters into service in urban areas. The main rotors were designed to maximise the disk area while complying to the maximum dimension requirements of 6 x 5 x 2 m, which results in a total disk area of 36.2 m^2. This was maximised in order to decrease both the noise inside the passenger cabin, as the noise for observers in the urban area. For the same reason, the choice was made for three blades per rotor to decrease noise generation while still flying efficiently. The calculated noise levels as perceived by observers on the ground are 51 dBA during cruise and 68 dBA during take-off. These are noise levels that do not exceed those of urban background noise and classroom chatter, respectively, and will thus not have a negative impact on the community embracing the Veatle.

Reflecting on the design, the Veatle meets the requirements set by the customer to support the best design possible. Most important of all, the vehicle is weather-rugged and is able to fly in very strong winds of 8 Beaufort. This is really exceptional for this kind of vehicle. To further fit in the urban environment, noise levels have been kept below critical values. This encourages people in the city to accept the use of urban air taxi's. Furthermore, the comfort of the passengers was considered. The motion is assumed comfortable if accelerations are below 0.325 m/s^2 and are of a frequency above 0.5 Hz. The control system of the Veatle complies with these requirements. Lastly, the carbon footprint of the vehicle and its manufacturing has been minimised to contribute to the sustainable development of the modern world. The safety of the Veatle also has been maximised to further encourage the use of its service. The propulsion system is 75% redundant, a fire wall is included, and a remote pilot is available to take over if the control system fails.

To conclude this report, some recommendations are made to encourage the future development of urban air mobility. Foremost, it is of the uttermost importance to keep improving the safety of the passengers. Therefore, it is recommended to design a bird proof design. A lot of birds are in urban areas, which could damage the rotor blades and can pose a problem to the continuity of the vehicle's operation. Secondly, it is proposed to use the main rotors for yawing motion, whereas now the control propellers are used to turn the vehicle. This

will be more energy efficient and can be designed for. Next, the crash structure explained in the report needs to be designed in a quantitative way. Now, the concept is only explained without the actual design of the structure. If the vehicle crashes, a solid crash structure may save the lives of the passengers. Furthermore, the improvements in battery technology could open new opportunities and make the vehicle even lighter. This should therefore be monitored carefully, to ensure an optimal design. To make it even more sustainable, the use of other composites instead of CFRP should be considered, since carbon fibre is adding a big part of the carbon footprint. Furthermore, more elaborate research could be performed regarding the noise impact of eVTOLs using rotors in cities. It is paramount in the acceptance of UAM with the public that these vehicles do not disturb the daily life in a city. Lastly, tests should be run to quantify the efficiencies of the main rotors in the current configuration, simulating the effects of blade-vortex interactions and induced velocities caused by other rotors. These values can then be integrated into the propulsive analysis of the Veatle.
So, with the Veatle, the concept of a low noise, weather rugged urban air mobility vehicle is proven. This will help with the introduction of UAM vehicles into the society.

18. Acknowledgements

After spending the last ten weeks on trying to get one step closer to Urban Air Mobility, we are proud with what we have been able to achieve in a relatively short timespan. This design is a result of enthusiastic team work, creativity and dedication (and coffee) and leads to the end of our Bachelors in Aerospace Engineering at the Delft University of Technology.

We would like to thank our tutors Fulvio Scarano and Anh Khoa Doan for their guiding, availability and expertise throughout the project. We also want to thank our coaches Victor Poorte and Wenhua Qu for their help and being so open throughout the project. Thanks to the approachability of our incredible tutors and coaches, we were able to keep a very enjoyable, yet productive work environment the past ten weeks. Next to the tutors and the coaches, we would like to thank Juliana Carolina Kiraly Thomaz Rodrigues for the help with the business aspects of operating eVTOLs and for her feedback on our reports and presentations.

We also want to thank Daniele Ragni for being available for questions regarding the propulsion system and to help us with our doubts about noise levels. When we were aiming at improving the aesthetics of our design, Elmer van Grondelle was available and gave us very helpful tips in making the vehicle more visually appealing. Next to TU Delft staff members, Robert Crone of Fusion Engineering was so kind to offer us help with sensor and control modelling tips, which we are thankful for.

Next, we would like to thank all the inspirational teachers we have met at TU Delft for motivating us and for teaching us about their field of expertise. Without all of them, this design would never have converged to anything that has the potential to fly. Lastly, we want to thank all previous engineers working on the topic of UAM for the work they reported in previous projects, on which we have built further.

To conclude this report, we would like to thank each other for the dedication, the profound conversations, the nice coffee breaks and the team building sessions at Bouwpub. Not only did this report result in the end of our B.Sc. in Aerospace Engineering, it also led to a new, close group of friends.

The Veatles

A. Gantt chart

Flying Through Urban Turbulence

Turbulence Resistant Urban UAM

Group 5

Project Start Date: 17/04/2022

Scrolling Increment: 2

Legend: Completed | In Progress | Behind of Schedule | Ahead of Schedule | Overtime

Identifier	Milestone description	Category	Completed to	Progress	Start	Days	End
Project plan	Deadline: 22 April			100%			
Baseline report	Deadline: 29 April			100%			
Mid-term report	Deadline 16 May			100%			
Final Report	Deadline: 15 June			100%			
F.1	***Analyse business case***	Completed	R.H.	100%	09-Jun	2	10-Jun
F.1.1	Check Roland Berger methods for pilot/autonomous	Completed	R.H.	100%	09-Jun	1	09-Jun
F.1.2	Explain why our concept is new (differentiate)	Completed	R.H.	100%	09-Jun	1	09-Jun
F.1.3	Allocate resources and breakdown budget	Completed	R.H.	100%	09-Jun	1	09-Jun
F.1.4	Make Cost Breakdown Stucture	Completed	T.E.	100%	09-Jun	1	09-Jun
F.1.5	Find beachhead market and expansion possibilites (eg retrofit)	Completed	R.H.	100%	09-Jun	1	09-Jun
F.2	***Design operations***	Completed	Everyone	100%	17-May	4	20-May
F.2.1	Describe operations and logistic concept	Completed	T.E., K.V.d.B.	100%	03-Jun	1	03-Jun
F.2.1.1	Explain operational window (see midterm)	Completed	T.E., K.V.d.B.	100%	03-Jun	1	03-Jun
F.2.1.2	Match operational concept to business concept	Completed	T.E., K.V.d.B.	100%	03-Jun	1	03-Jun
F.2.1.3	Estimate time of swapping vs charging	Completed	T.E., K.V.d.B.	100%	03-Jun	2	04-Jun
F.2.2	Describe RAMS characteristics	Completed	O.K., J.V.	100%	25-May	1	25-May
F.2.3	Analyse performance	Completed	S.K., O.d.K.	100%	08-Jun	1	08-Jun
F.2.3.1	Make flight profile diagram	Completed	O.d.K	100%	08-Jun	1	08-Jun
F.2.3.2	Charge - flight diagram	Completed	S.K.	100%	09-Jun	1	09-Jun
F.2.3.3	Charge - day of use diagram	Completed	S.K.	100%	09-Jun	1	09-Jun
F.2.4	Analyse noise characteristics and emissions	Completed	S.K., O.d.K	100%	07-Jun	1	07-Jun
F.2.5	Develop project design & development logic	Completed	Multiple Teams	100%	01-Jun	1	01-Jun
F.2.5.1	Identify tasks for certification	Completed	O.V., O.K, J.V.	100%	01-Jun	1	01-Jun
F.2.5.2	Identify facilities required for manufacturing	Completed	M.L., R.H.	95%	01-Jun	1	01-Jun
F.2.5.3	Identify facilities needed to perform operations	Completed	T.E., J.v.Z, K.V.d.B.	95%	01-Jun	1	01-Jun
F.2.5.4	Identify activities required for first flight	Completed	T.E., J.v.Z, K.V.d.B.	100%	01-Jun	1	01-Jun
F.2.6	Analyse safety	Completed	M.L., R.H.	100%	19-May	1	19-May
F.2.6.1	(dropped)	Completed	M.L., R.H.	100%	19-May	1	19-May
F.2.6.2	Analyse failure safety	Completed	K.V.d.B	100%	30-Jun	1	30-Jun
F.2.7	Analyse one turbulence case	Completed	M.L., R.H.	100%	12-Jun	1	12-Jun
F.2.7.1	Find Wind profile	Completed	J.V., O.K.	100%	12-Jun	1	12-Jun
F.2.7.2	Estimate control reactions	Completed	J.v.Z.	100%	12-Jun	1	12-Jun
F.2.7	Design cabin	Completed	O.V.	100%	01-Jun	1	01-Jun
F.2.8	Perform trajectory mapping	Completed	K.V.d.B.	100%	02-Jun	1	02-Jun
F.2.9	Maintenance/ Cleaning	Completed	T.E.	100%	03-Jun	1	03-Jun
F.3	***Design propulsion subsystem***	Completed	S.K., O.d.K	100%	17-May	6	24-May
F.3.1	Analyse requirement/ compliance	Completed	S.K., O.d.K	100%	31-May	1	31-May
F.3.2	Design power storage subsystem	Completed	S.K., O.d.K	100%	25-May	2	26-May
F.3.2.1	Size batteries	Completed	S.K., O.d.K	100%	25-May	1	25-May
F.3.2.2	Design power management subsystem	Completed	S.K., O.d.K	100%	30-May	2	31-May
F.3.2.3	Design power control and distribution unit	Completed	S.K., O.d.K	100%	31-May	1	31-May
F.3.2.4	Determine optimal battery locations (swappable!)	Completed	S.K., O.d.K	100%	31-May	1	31-May
F.3.3	Create propulsion budgets	Completed	S.K., O.d.K	100%	02-Jun	1	02-Jun
F3.3.1	Determine motors to be used	Completed	O.d.K., S.K.	100%	02-Jun	1	02-Jun
F3.3.2	Choose propellers	Completed	O.d.K., S.K.	100%	02-Jun	1	02-Jun
F.3.4	Analyse acoustic effects	Completed	S.K., O.d.K	100%	07-Jun	2	08-Jun
F.3.5	Determine propeller configuration	Completed	O.d.K., S.K.	100%	20-May	3	22-May
F.3.5.1	Select mumber of rotors	Completed	O.d.K., S.K.	100%	20-May	1	20-May
F.3.5.2	Meet Daniele Ragni	Completed	O.d.K., S.K.	100%	23-May	1	23-May
F.3.5.3	Determine rotor positioning	Completed	O.d.K., S.K.	100%	24-May	1	24-May
F.3.6	Perform sensitivity analysis	Completed	O.d.K., S.K.	100%	09-May	4	12-May
F.4	***Design structures***	Completed	R.H., M.L., K.V.d.B., O.V., O.K., J.V.	100%	19-May	12	03-Jun
F.4.1	Analyse sizing load cases	Behind Schedule	M.L.	100%	19-May	1	19-May
F.4.2	Select materials	Completed	M.L., R.H.	100%	19-May	1	19-May
F.4.3	Design structure	Completed	R.H., M.L., O.V.	100%	20-May	3	24-May
F4.3.1	Iteration of beam design	Completed	M.L	100%	20-May	3	22-May
F4.3.2	Fuselage Structure Literature Study	Completed	O.V.	100%	20-May	1	20-May
F4.3.3	Find buckling modes	Completed	R.H.	100%	30-May	2	31-May
F4.3.4	Design joint beam with fuselage	Completed	O.V.	100%	23-May	3	25-May
F4.3.5	Design Landing Gear	Completed	M.L.	100%	23-May	2	24-May
F4.3.6	Design Fuselage	Completed	O.V., M.L.	100%	30-May	3	01-Jun
F.4.4	Draw CAD model	Completed	K.v.d.B	100%	30-May	5	03-Jun
F.4.4.1	Draw parts	Completed	K.v.d.B	100%	30-May	2	31-May
F.4.4.2	Draw technical drawings	Completed	K.v.d.B	100%	31-May	1	31-May
F.4.4.3	Make assembly	Completed	K.v.d.B	100%	01-Jun	1	01-Jun
F.4.4.4	Make assembly drawing and exploded view	Completed	K.v.d.B	100%	02-Jun	1	02-Jun
F.4.4.5	Make physical model (3D printed?)	Completed	K.v.d.B	100%	10-Jun	1	10-Jun
F.4.5	Analyze eigenfrequencies	Completed	R.H.	100%	03-Jun	1	03-Jun
F.4.6	Analyze fatigue life	Completed	O.V.	100%	07-Jun	1	07-Jun
F.4.7	Iterate production plan	Completed	R.H.	100%	07-Jun	2	08-Jun
F.4.7.1	Iterate manufacturing plan	Completed	R.H.	100%	02-Jun	1	02-Jun
F.4.7.2	Iterate assembly plan	Completed	R.H.	100%	07-Jun	2	08-Jun
F.4.7.3	Iterate integration plan	Completed	R.H.	100%	07-Jun	1	07-Jun
F.5	***Perform system Engineering***	Completed	Everyone	100%	19-May	5	25-May
F.5.1	Iterate planning	Completed	T.E., K.V.d.B.	100%	19-May	1	19-May
F.5.1.1	Make functional flow and breakdown diagrams	Completed	T.E.	100%	23-May	1	23-May
F.5.1.2	Make organogram	Completed	T.E.	100%	23-May	1	23-May
F.5.1.3	Iterate Gantt chart	Completed	K.V.d.B.	100%	23-May	1	23-May
F.5.2	Perform risk assessment	Completed	J.V.	100%	08-Jun	1	08-Jun
F.5.2.1	Iterate risk map	Completed	J.V.	100%	08-Jun	1	08-Jun
F.5.2.2	Technical risk assessment	Completed	J.V.	100%	08-Jun	1	08-Jun
F.5.2.3	Organizational risk assessment	Completed	J.V.	100%	08-Jun	1	08-Jun
F.5.3	Final design	Completed	Everyone	100%	20-May	4	25-May
F.5.3.2	Configuration and layout	Completed	Everyone	100%	20-May	1	20-May
F.5.3.3	Revisit system requirements	Completed	J.V.	100%	08-Jun	1	08-Jun
F.5.3.4	Revisit Class I and II estimations	Completed	O.K.	100%	08-Jun	2	09-Jun
F.5.3.5	Make N2 chart and converge design	Completed	O.V., O.K., J.V	100%	08-Jun	2	09-Jun
F.5.3.6	Create technical budgets	Completed	Everyone	100%	08-Jun	1	08-Jun
F.5.4	Design subsystem integration	Completed	T.E., J.v.Z., K.V.d.B.	100%	21-May	1	21-May
F.5.4.1	Make hardware block diagram	Completed	T.E., K.V.d.B.	100%	21-May	1	21-May
F.5.4.2	Make software block diagram	Completed	T.E., J.v.Z.	100%	21-May	1	21-May
F.5.4.3	Make electrical block diagram	Completed	O.d.K, S.K.	100%	21-May	1	21-May
F.5.4	Iterate requirements	Completed	Everyone	100%	30-May	1	30-May
F.5.4.1	Iterate control requirements	Completed	J.v.Z., T.E.	100%	30-May	1	30-May
F.5.4.2	Iterate operations requirements	Completed	K.V.d.B.,O.V.	100%	30-May	1	30-May
F.5.4.3	Iterate structures requirements	Completed	R.H., M.T.	100%	30-May	1	30-May
F.5.4.4	Iterate aerodynamic requirements	Completed	J.V., O.K.	100%	30-May	1	30-May
F.5.4.5	Iterate power and propulsion requirements	Completed	S.K., O.d.K	100%	30-May	1	30-May

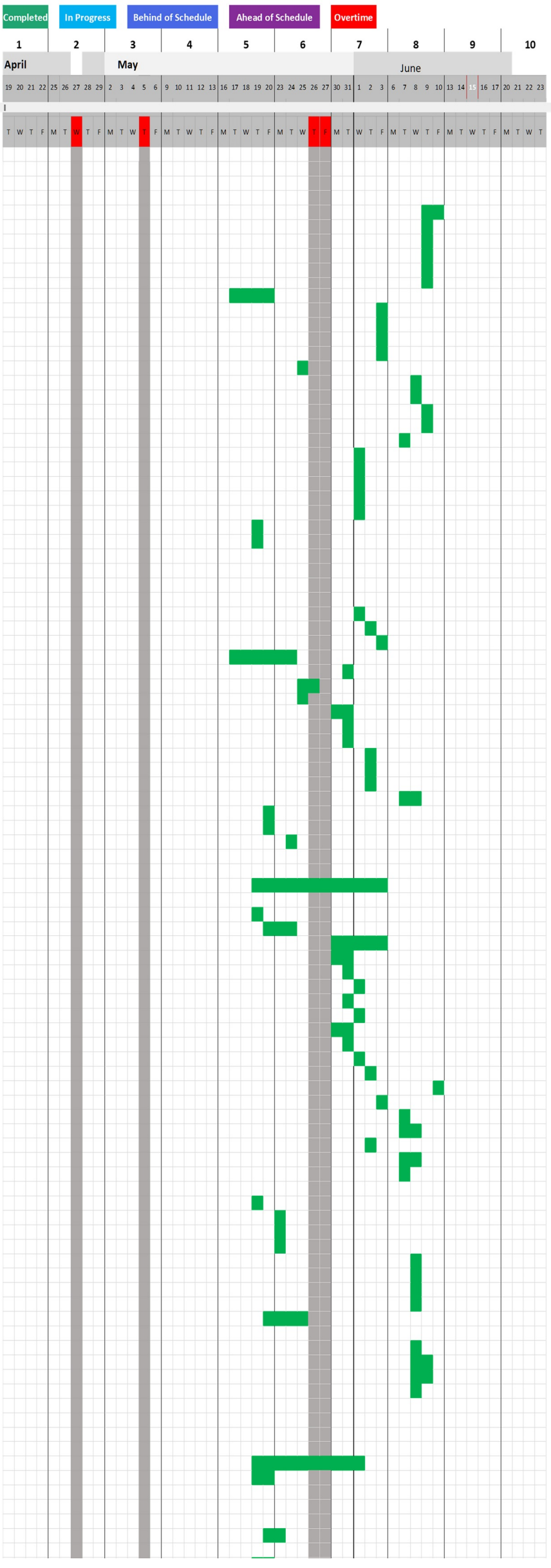

Figure A.1: Gantt chart part 1

F.6	***Analyse control and stability***	Completed	T.E, J.v.Z.	100%	19-May	10	01-Jun
F.6.1	Define stability characteristics	Completed	T.E., J.v.Z.	100%	19-May	2	20-May
F.6.1.1	Estimate behavior model for forward flight	Completed	J.v.Z.	100%			#######
F.6.1.2	Estimate behavior model for lateral flight	Completed	J.v.Z.	100%			#######
F.6.2	Define control characteristics	Completed	T.E., J.v.Z.	100%	20-May	2	23-May
F.6.4	Perform control system design	Completed	T.E., J.v.Z.	100%	26-May	3	30-May
F.6.4.1	Design 6 DOF controller	Completed	J.v.Z.	100%	24-May	2	25-May
F.6.4.2	Design actuators (for eg flaps)	Completed	O.K.	100%	25-May	2	26-May
F.6.4.3	Perform trajectory mapping	Completed	K.VdB	100%	25-May	2	26-May
F.6.5	Communications with Ground	Completed	T.E.	100%			#VALUE!
F.6.6	Design sensor model	Completed	T.E., K.V.d.B.	100%	20/05/2022	6	25-May
F.6.6.1	Perform literature study	Completed	T.E., K.V.d.B.	100%	20/05/2022	1	20-May
F.6.6.2	Model IMU	Completed	T.E.	100%	23/05/2022	2	24-May
F.6.6.3	Model for LiDAR, Radar, Cameras...	Completed	K.V.d.B.	100%	23/05/2022	2	24-May
F.6.7	Filtering signals from sensors	Completed	J.v.Z., T.E., K.V.d.B.	100%			#######
F.6.7.1	Perform literature research on filters	Completed	J.v.Z., T.E., K.V.d.B.	100%			#######
F.6.7.2	Model filters in MatLab	Completed	J.v.Z., T.E., K.V.d.B.	100%	03-Jun		02-Jun
F.7	***Verification***	Completed	Everyone	100%	01-Jun	4	06-Jun
F.7.1	Verify code	Completed	T.E., J.v.Z., K.V.d.B.	100%	02-Jun	3	06-Jun
F.7.1.2	Verify 6DOF	Completed	J.v.Z.	100%	02-Jun	2	03-Jun
F.7.1.3	Verify filtering model	Completed	J.v.Z.	100%	02-Jun	2	03-Jun
F.7.1.4	Verify Sensor model	Completed	T.E.	100%	02-Jun		01-Jun
F.7.1.5	Verify rotors model	Completed	O.d.K., S.K.	100%	02-Jun		01-Jun
F.7.1.6	Verify battery model	Completed	S.K.	100%	02-Jun		01-Jun
F.7.1.7	Verify emission and noise	Completed	J.V.	100%	09-Jun		08-Jun
F.7.3	Write V&V plan	Completed	J.v.Z.	100%	03-Jun	2	06-Jun
F.7.4	Verify legal requirements	Completed	O.K.	100%	01-Jun	1	01-Jun
F.7.5	Verify integration of subsystems	Completed	Everyone	100%	02-Jun	1	02-Jun
F.7.5.1	Verify assembly in CAD	Completed	K.V.d.B.	100%			#######
F.7.5.2	Verify integration of code	Completed	Everyone, but people above	100%			#######
F.8	***Validation***	Completed	Everyone	100%	03-Jun	2	06-Jun
F.8.1	Analyse system accuracy	Completed	Everyone	100%	08-Jun	2	09-Jun
F.8.2	Validate structural analysis using CAD	Completed	M.L.	100%	08-Jun	2	09-Jun
F.8.3	Validate code and tools developped	Completed	Everyone	100%	03-Jun	2	06-Jun
F.8.4	Validate control system	Completed	J.v.Z.	100%	08-Jun	2	09-Jun
F.9	***Write report***	Completed	Everyone	100%	31-May	10	13-Jun
F.9.1	Write introduction	Completed	O.V.	100%	09-May	1	09-May
F.9.2	Write conclusion	Completed	O.d.K., R.H., J.v.Z.	100%	09-Jun	1	09-Jun
F.9.3	Proofread	Completed	Everyone	100%	13-Jun	2	14-Jun
F.9.3.1	Check consitency	Completed	Everyone	100%	13-Jun	1	13-Jun
F.9.3.2	Check text	Completed	Everyone	100%	13-Jun	1	13-Jun
F.9.3.3	Check figures and layout	Completed	Everyone	100%	13-Jun	1	13-Jun
F.9.3.4	Check compliance with requirements	Completed	Everyone	100%	13-Jun	1	13-Jun
F.10	**Perform aerodynamic design**	Completed	O.V., J.V., O.K.	100%	23-May	8	01-Jun
F.11	***System Engineering***	Completed	Everyone	100%			#NUM!
F.11.1	Find Preliminary code architectures	Completed	Everyone	100%	15-May	1	15-May
F.11.1.1	Find operations code architecture	Completed	K.V.d.B.	100%	15-May	1	15-May
F.11.1.2	Find structures code architecture	Completed	R.H., M.L.	100%	15-May	1	15-May
F.11.1.3	Find propulsion code architecture	Completed	S.K.,O.V.	100%	15-May	1	15-May
F.11.1.4	Find aerodynamics code architecture	Completed	O.V., J.V., O.K.	100%	15-May	1	15-May
F.11.1.5	Find control code architecture	Completed	J.v.Z.	100%	15-May	1	15-May
F.11.2	Iterate N2 Charts	Completed	O.K.	100%	16-May	1	16-May
Poster	Deadline: 15 June						
Jury Summary	Deadline: 8 June						
J.1	**Describe mission**	Completed	Everyone	100%	07-Jun	1	07-Jun
J.2	**Describe solution**	Completed	Everyone	100%	07-Jun	1	07-Jun
Red Booklet	Deadline: 22 June						
R.1	**Describe mission**	Assigned	Everyone	0%	21-Jun	1	21-Jun
R.2	**Describe trade-offs and solution**	Assigned	Everyone	0%	21-Jun	1	21-Jun
R.3	**Make 3-view drawing**	Assigned	Everyone	0%	21-Jun	1	21-Jun
Presentation	Symposium: 23 June						
PR.1	**Decide on content**	Assigned	Everyone	0%	21-Jun	2	22-Jun
PR.2	**Make task division**	Assigned	Everyone	0%	21-Jun	2	22-Jun
PR.3	**Make Slides**	Assigned	Everyone	0%	21-Jun	2	22-Jun
PR.4	**VR experience**	Assigned	Everyone	0%	21-Jun	1	21/Jun
Final Review	Review: 20 June			0%			
FR.1	**Decide on content**	Assigned	Everyone	0%	17-Jun	2	20-Jun
FR.2	**Make task division**	Assigned	Everyone	0%	17-Jun	2	20-Jun
FR.3	**Make Slides**	Assigned	Everyone	0%	17-Jun	2	20-Jun
FR.4	**Invite RHIA,... on symposium**	Assigned	Everyone	0%	18-Jun	1	

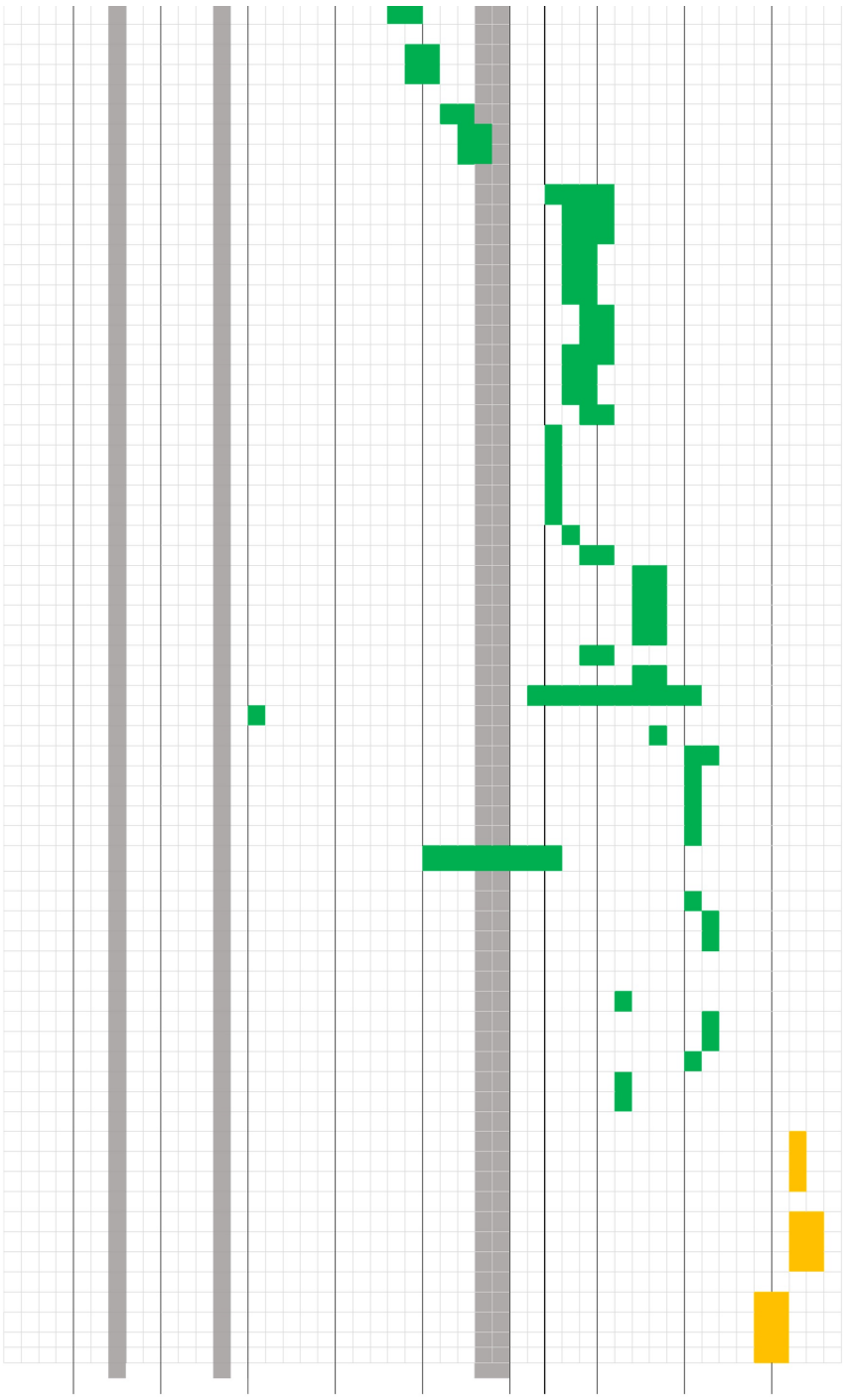

Figure A.2: Gantt chart part 2